

**APPLICATIONS OF LARGE AMPLITUDE FOURIER
TRANSFORMED ALTERNATING CURRENT VOLTAMMETRY
FOR THE DETERMINATION OF FAST HETEROGENEOUS
ELECTRODE KINETICS**

A Thesis Submitted by

Kiran Bano

In partial fulfillment of the requirements for the degree of

Doctor of Philosophy to the

School of Chemistry,

Monash University, Clayton, VIC, Australia

Notice 1

Under the Copyright Act 1968, this thesis must be used only under the normal conditions of scholarly fair dealing. In particular no results or conclusions should be extracted from it, nor should it be copied or closely paraphrased in whole or in part without the written consent of the author. Proper written acknowledgement should be made for any assistance obtained from this thesis.

TABLE OF CONTENTS

Table of Contents	i
Abstract	iii
Symbols and Notations	vi
General Declaration	viii
Acknowledgements	x
Chapter 1. INTRODUCTION	1
1.1. Conventional Methods of Electrode Kinetic Measurement.....	2
1.2. Problem Statement.....	5
1.3. AC Voltammetry	6
1.4. Scopes of Large Amplitude FT AC Voltammetry	7
1.5. Thesis Objectives	9
1.6. Thesis Outline	10
CHAPTER 2. AC VOLTAMMETRY: EXPERIMENTS AND SIMULATIONS.....	17
2.1. Introduction.....	18
2.2. Instrumentation	18
2.3. FT Inverse FT Protocol of Data Analysis	21
2.4. Simulations	21
CHAPTER 3. ELECTRODE KINETICS STUDIES AT MACRODISK ELECTRODES: LOW FREQUENCY FT AC VOLTAMMETRY	25
Declaration of Thesis Chapter 3	26
Thesis Chapter 3	27
CHAPTER 4. ELECTRODE KINETICS STUDIES AT ROTATING DISK ELECTRODES: LOW FREQUENCY FT AC VOLTAMMETRY	51
Declarations of Thesis Chapter 4	52
Thesis Chapter 4	53
CHAPTER 5. ELECTRODE KINETICS STUDIES AT MACRODISK ELECTRODES: HIGH FREQUENCY FT AC VOLTAMMETRY	69
Declarations of Thesis Chapter 5	70
Thesis Chapter 5	71

CHAPTER 6. INVESTIGATION OF FAST ELECTRODE KINETICS AT MICRODISK ELECTRODES: HIGH FREQUENCY FT AC VOLTAMMETRY TO STUDY THE EFFECT OF VISCOSITY	96
Declarations of Thesis Chapter 6	97
Thesis Chapter 6	98
CHAPTER 7: ELECTRODE KINETICS STUDIES AT MICROELECTRODES IN CONVENTIONAL SOLVENT: HIGH FREQUENCY FT AC VOLTAMMETRY ..	140
Declarations of Thesis Chapter 7	141
Thesis Chapter 7	142
CHAPTER 8. EFFECT OF DENSITY OF STATES AND ADIABATICITY IN ELECTRODE KINETICS STUDIES.....	162
Declarations of Thesis Chapter 8	163
Thesis Chapter 8	164
CHAPTER 9. CONCLUSIONS AND FUTURE WORK	205
Conclusions.....	206
Future Works	208
APPENDIX.....	209
Declaration of Thesis Appendix	210

ABSTRACT

The aim of this research is to demonstrate achievements and difficulties of using large amplitude Fourier transformed (FT) alternating current (AC) voltammetry for measurement of the electrode kinetics of fast electron transfer processes. Research is focussed on study of outer-sphere electron transfer processes at electrode/solution interface. Electrode kinetics of these processes have been investigated by varying the electrode size from macro to microdisk electrodes, increasing AC frequency to enhance the sensitivity of the method for determination of electrode kinetics and rotating the electrode.

Large amplitude FT AC voltammetry provides access to higher harmonics AC components at macrodisk electrodes that are more sensitive to the electrode kinetics than the fundamental harmonic. Low frequency FT AC voltammetry is used to determine the heterogeneous electron transfer kinetics (k^0 value) of electron transfer processes involving reduction of 7,7,8,8-tetracyanoquinodimethane (TCNQ), oxidation and reduction of $\text{TCNQ}^{\bullet-}$ and oxidation of TCNQ^{2-} in acetonitrile. k^0 values are determined by comparison of the experimental data with simulations that take into account the effect of uncompensated resistance and double layer capacitance. Values of $0.30 \pm 0.05 \text{ cm s}^{-1}$ are obtained at platinum (Pt) and glassy carbon (GC) electrodes for both $\text{TCNQ}^{0/\bullet-}$ and $\text{TCNQ}^{\bullet-/2-}$ processes.

Macrodisk electrode studies for kinetics determination are then extended to the rotating disk electrode; applications and theory of large amplitude FT AC voltammetry at a rotating disk electrode (RDE) are described. Resolution of time domain data into DC and AC harmonic components reveals that the mass transport for DC component is controlled by convective-diffusion, while the background current free higher order harmonic components are flow rate independent and governed by linear diffusion. The large amplitude AC voltammetry with RDE methodology is used to demonstrate that kinetics and diffusion coefficient information

can be extracted from a single experiment. Large amplitude FT AC voltammetry at the RDE has a similar sensitivity for kinetics estimation as at stationary electrodes, however, it has potential for applications where the use of DC Voltammetry encounters some difficulties: i.e. voltammetry of surface confined proteins and catalytic reaction coupled with electron transfer processes.

Large amplitude FT AC voltammetry at high frequency is then applied to study the electrode kinetics of tetrathiafulvalene (TTF), its radical cation $\text{TTF}^{\bullet+}$ and that of dication TTF^{2+} in acetonitrile (0.1 M Bu_4NPF_6). AC frequency (f) = 233 Hz is used at GC and platinum Pt macrodisk electrodes to enhance the kinetic sensitivity and hence upper limit of measurable heterogeneous charge transfer rate constant. k^0 values for $\text{TTF}^{0/\bullet+}$ and $\text{TTF}^{\bullet+/0}$ are found to be $\geq 1.0 \text{ cm s}^{-1}$ and regarded as reversible under the AC conditions used. However, the significantly slower / quasi-reversible behavior is observed for the $\text{TTF}^{\bullet+/2+}$ redox couple, with k^0 being $0.30 \pm 0.05 \text{ cm s}^{-1}$.

High frequency (1.23 kHz) large amplitude (80 mV) FT AC voltammetry is then employed at carbon fiber and Pt microdisk electrodes to probe the fast electron transfer kinetics associated with the reduction of 2,3,5,6-tetrafluoro-7,7,8,8-tetracyanoquinodimethane (F_4TCNQ) in ionic liquids (ILs). The limitations encountered in the ILs are discussed and data are compared with kinetic studies at macrodisk in the conventional molecular solvent acetonitrile (MeCN) at high frequency. In most of the cases, k^0 values relate to the viscosity of the solvent, however, in some ionic liquids other factors may also influence the electron transfer kinetics.

For kinetics measurement of $\text{TTF}^{0/\bullet+}$ process, large amplitude FT AC voltammetry was employed at microelectrodes, where mass transport for DC component obeys radial diffusion. Pros and cons of using high frequency at microelectrodes are discussed in detail for the extraction of kinetic and thermodynamic parameters under the experimental conditions.

Simulations of results at a microelectrode give k^0 values for the $\text{TTF}^{0/+}$ process as 2.5 cm s^{-1} , while $\text{TTF}^{+/2+}$ process is found to be slower ($k^0 = 0.4 \text{ cm s}^{-1}$) as determined previously in macroelectrodes measurements.

For some outer-sphere electron transfer processes, the dependence of the standard electrochemical rate constant of the electrode material is studied at carbon electrodes (boron doped diamond (BDD) and GC electrodes) and results are compared with metal electrodes (Pt and gold (Au)) electrodes. A comprehensive discussion is provided about the effect of the density of states on measurement of electrode kinetics and adiabaticity of the system. The effect of density of states was found with electron transfer kinetics for ruthenium hexamine $[(\text{Ru}(\text{NH}_3)_6)]^{3+}$ and silicone tungstate $[\alpha\text{-SiW}_{12}\text{O}_{40}]^{4-}$ reduction in aqueous medium where slow kinetics were observed at BDD. However, in case of TCNQ, TTF and TTF^{*+} , their electrode processes appear to be adiabatic and independent of the low density of states of BDD

NOMENCLATURE/NOTATIONS

FT	Fourier Transform
AC	Alternating Current
BAS	BioAnalytical System
iR_u	Ohmic Drop
C_{dl}	Double Layer Capacitance
GC	Glassy Carbon
Pt	Platinum
Au	Gold
BDD	Boron Doped Diamond
RDE	Rotating Disk electrode
C	Concentration
d	Diameter of the electrode
r	Radius of the electrode
f	Frequency
ΔE	Amplitude
F	Faraday's Constant
T	Temperature
I_p	Peak Current
I_{lim}	Limiting Current
E^0	Standard Redox Potential
A	Electrode Area
ω	AC frequencies for harmonic components
ω^*	RDE rotation velocity
ν	DC Scan Rate

ν_k	Kinematic Viscosity
ΔE_p	Peak Separation in Cyclic Voltammogram
A	Area of the Electrode
k^0	Electron Transfer Rate Constant
D	Diffusion Coefficient
$TCNQ$	7, 7, 8, 8-Tetracyanoquinodimethane
Fc	Ferrocene
F_4TCNQ	2, 3, 5, 6,-tetrafluoro-7,7,8,8-tetracyanoquinodimethane
TTF	Tetrathiafulvalene
MeCN	Acetonitrile
S	Schmidt Number

GENERAL DECLARATION

Declaration for thesis based or partially based on conjointly published or unpublished work

In accordance with a Monash University Doctorate Regulation 17.2 Doctors of Philosophy and Research Master's regulations the following declarations are made:

I hereby declare that this thesis contains no material which has been accepted for the award of any other degree or diploma at any university or equivalent institution and that, to the best of my knowledge and belief, this thesis contains no material previously published or written by another person, except where due reference is made in the text of the thesis.

This thesis includes three original papers published in peer reviewed journals and three unpublished publications. The core theme of the thesis is the measurement of electrode kinetics of fast processes. The ideas, development and writing up of all the papers in the thesis were the principal responsibility of myself, the candidate, working within the School of chemistry under the supervision of Dr. Jie Zhang and Prof. Alan M.Bond.

The inclusion of co-authors reflects the fact that the work came from active collaboration between researchers and acknowledges input into team-based research..

In the all chapters of this thesis, my contribution to the work involved the following:

Thesis chapter	Publication title	Publication status*	Nature and extent of candidate's contribution
3	Electrode kinetics Associated with Tetracyanoquinodimethane (TCNQ), $\text{TCNQ}^{0/\bullet-}$, TCNQ^{2-} Redox Chemistry in Acetonitrile As Determined By Analysis of Higher Harmonic Components Derived from Fourier Transformed Large Amplitude AC Voltammetry	Published	Initiation, Key Ideas, Experimental Work, Writing up

4	Large Amplitude Fourier Transformed AC Voltammetry at a Rotating Disk Electrode: A Versatile Technique for Covering Levich and Flow Rate Insensitive Regimes in A Single Experiment	Published	Initiation, Key Ideas, Experimental Work, Writing up
5	Fourier Transformed Large Amplitude AC Voltammetric Study of Tetrathiafulvalene (TTF): Electrode Kinetics of the $TTF^0/TTF^{\bullet+}$ and $TTF^{\bullet+}/TTF^{2+}$ Processes	Published	Initiation, Key Ideas, Experimental Work, Writing up
6	Investigation of Fast Electrode Kinetics at Microdisk Electrodes: High Frequency FT AC Voltammetry to Study the Effect of Viscosity	Draft	Initiation, Key Ideas, Experimental Work, Writing up
7	Electrode Kinetic Measurements Using High Frequency Large Amplitude Fourier Transformed AC Voltammetry at Microelectrodes in Conventional Solvents	Draft	Initiation, Key Ideas, Experimental Work, Writing up
8	Dependence of Heterogeneous Electron Transfer Rate Constant on Electrode Materials: The Effect of Density of States and Adiabaticity	Draft	Initiation, Key Ideas, Experimental Work, Writing up

Signed:



Date:

.....28-11-2013.....

ACKNOWLEDGEMENTS

It is a great pleasure to thank many people and organizations that have helped me to complete my Ph. D studies at Monash university.

At first I would like to express my gratitude to my M.Phil supervisor Dr. Inam-ul-Haque for introducing Prof. Alan M. Bond to me so that I may work with this group for six months. I thankfully acknowledge the award from the Monash University Faculty of Science Dean's International Postgraduate Research Scholarship Scheme that provides my tuition fees and other allowances. In particular, I gratefully acknowledge my supervisors Dr. Jie Zhang and Prof. Alan M. Bond for giving me a top-up stipend scholarship that made my life easier.

I would appreciate my extremely kind and enthusiastic supervisors who have always encouraged me and not only provided me with good ideas but also mentored my way of thinking about a research project. I extremely thankful to them for giving me the time or discussion of my experimental results and assistance with writing papers for publications as well as this thesis.

I would also like to thank my group members and visitors of Alan Bond and Jie Zhang's group. I am extremely grateful to Dr. Sixuan Guo, Dr. Chong Yong Lee, Dr. Ayman Nafady, Dr. Muhammad J. A Shiddiky, Ms. Yuping Lu, Dr. Shufeng Zhao, Dr. Alexander Simanov and Dr. Shaimaa Ahmad for their help with experimental techniques and theory. I sincerely thank Dr. Stephen Feldberg and Dr. Gareth Kennedy for helpful discussions about using simulation softwares used in this thesis. I would also like to appreciate the support extended by my colleagues and friends in difficult times i had in Australia.

Finally and most importantly, I am deeply indebted to my whole family for their encouragement, support and help. For my parents who have raised me and always

encouraged me to study at as high level as possible. Most of all my husband who has been very much understanding and supportive during my Ph.D studies.

Overall, I feel very blessed to have all these people in my life without whom I could not achieve this milestone.

CHAPTER 1

INTRODUCTION

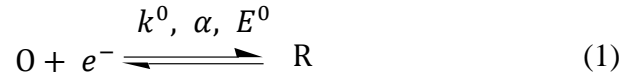
CHAPTER 1

INTRODUCTION

1.1. Introduction

A simple electron transfer reaction at an electrode surface can be represented by equation (eq.)

1



Voltammetric characteristics of the electron transfer between an electrode and the redox specie as represented in this equation are described in terms of reversible standard/formal potential (E^0), heterogenous charge transfer rate constant (k^0) and charge transfer coefficient (α).¹ E^0 (V, versus (vs.) reference electrode) is an important thermodynamic parameter related to Gibbs free energy (ΔG)¹⁻⁴

$$\Delta G = -nF\Delta E^0 \quad (2)$$

where n is number of electrons transferred in the reaction and F is Faraday's constant. The electrode kinetics or heterogenous charge transfer rate constant k^0 (cm s^{-1}) is measured at E^0 . A reversible system is at equilibrium and hence obeys the Nernst equation (3)¹

$$E = E^0 + \frac{RT}{F} \ln \left(\frac{C_O}{C_R} \right) \quad (3)$$

where E^0 is the potential of the electrochemical cell and C is the bulk concentration of O or R . For a kinetically controlled system, k^0 is related to k_f (rate of the forward reaction) and k_b (rate of the backward reaction) as per Butler-Volmer theory⁵ is described by eq. (4) and (5)

$$k_f = k^0 e^{-\alpha \frac{F}{RT} (E - E^0)} \quad (4)$$

$$k_b = k^0 e^{(1-\alpha) \frac{F}{RT} (E - E^0)} \quad (5)$$

The current and its relationship to E^0 , k^0 and α is represented by eq. 6⁵

$$i = nFAk^0 [C_O(0,t)e^{-\alpha F/RT(E-E^0)} - C_R(0,t)e^{(1-\alpha)F/RT(E-E^0)}] \quad (6)$$

The charge transfer rate coefficient, α is a dimensionless parameter and it defines the shape of the reaction co-ordinates. Alternatively, Marcus-Hush theory⁶⁻¹¹ can be used to describe the electrode kinetics but the quasi-reversible electron transfer processes studied in this thesis are treated by the Butler-Volmer theory.

Electrode kinetics have been studied by many methods; initially, Tafel plots^{1,12} have been employed to derive the exchange current i_0 which is directly related to k^0 as shown in eq. 7

$$i_0 = FAk^0 C_O^{(1-\alpha)} C_R^\alpha \quad (7)$$

Aided by the development of transient DC (linear sweep and cyclic) voltammetry, Nicholson and Shain's method^{13,14} was introduced for the measurement of rapid electron transfer kinetics. In DC cyclic voltammetry, a ramped waveform of known scan rate is applied to the working electrode and the resulting current is recorded as a function of applied potential with respect to the reference electrode. Nicholson's method uses the ΔE_p (difference in the reduction (E_p^{red}) and oxidation (E_p^{ox}) peak potentials) as a function of scan rate to measure k^0 value. However, this method suffers from the limitation caused by very large background capacitive current observed at high scan rate that contributes to the non-faradaic time constant^{1,5} (τ) of the cell

$$\tau = R_u C_{dl} \quad (8)$$

where R_u is the uncompensated solution resistance and C_{dl} is the double layer capacitance. Uncompensated solution resistance also increases the peak separation in a similar manner to slow kinetics and considerable care is needed in interpreting the data. In particular, care needs

to be taken to ensure that the effect of uncompensated resistance and double layer capacitance are considered, especially in non-aqueous solvents.

In hydrodynamic voltammetry, some of the limitations associated with the transient DC voltammetry are avoided by using rotating disk, channel or wall jet electrodes.¹⁵⁻²⁵ In these cases, steady state can be achieved at sufficiently slow scan rates because the mass transport rate towards the electrode is enhanced by convection. In the hydrodynamic steady state methods, double layer charging current is avoided. For kinetic measurements, steady state voltammograms are obtained over a wide range of convection rates. The time variable (scan rate in transient DC technique) is now introduced in the form of electrode rotation rate or solution velocity.¹ Kinetic parameters are extracted from the differences in the half wave potential $E_{1/2}$ and quartile potential $E_{1/4}$ (or $E_{3/4}$) from the reversible potential.¹ Provided the hydrodynamics are well defined, then this method is readily treated theoretically. Analytical and mechanistic studies of simple redox, catalytic and biological processes have been widely undertaken at rotating disc electrodes (RDEs).^{18,26-31} For kinetic measurements, macrosized rotating disc electrodes still have the same advantages over use of macro sized stationary electrodes. Thus, the steady state limiting current is unaffected by slow electron transfer kinetics and uncompensated resistance so the diffusion coefficients are easily determined by this parameter and use of the Levich equation.¹⁵ However, this method also suffers some disadvantages. In particular, problems are still encountered from the influence of R_u when the measurement of the half wave potential is needed to quantify the electrode kinetics. Channel and jet electrodes³²⁻³⁸ are potentially attractive for the measurement of the fast electron transfer kinetics but there are constraints when working with high viscosity solvents or under high pressure and experiment and electrode designs are demanding.

In order to obtain meaningful fast scan rate transient voltammetric data, the ohmic drop should be reduced as far as possible and experimental time scales should be 5-10 times the

cell time constant (RC time constant). This can be aided by decreasing the electrode size to study very fast electron transfer kinetics, microelectrodes or even nanoelectrodes may be used in order to minimize the impact of iR_u (ohmic) drop. Microelectrodes, due to their reduced size possess advantageous properties like fast double layer charging and high mass transport rates with reduced iR_u drop at short time scales (high scan rate); these characteristics reduce the cell time constant and extend applications of transient voltammetry to the study of faster electrode kinetics ($k^0 > 0.1 \text{ cm s}^{-1}$).³⁹⁻⁴⁶ The use of these electrodes also provide enhanced mass transport rate from radial diffusion and can also be operated under transient conditions. Microelectrodes have been widely used for the fast electrode kinetic measurements under steady state or transient (fast scan) conditions. In the second case, a three-point analysis method is often used based on the differences of quartile and half wave potentials and advantages and disadvantages are similar to Nicholson's ΔE_p method. Nanoelectrodes have some limitations due to possible uncertainties in electrode geometries.

Electrode kinetic also have been determined by using probe techniques like scanning electrochemical microscopy (SECM)⁴⁷⁻⁴⁹ that records an approach voltammogram when the tip of an ultra micro or nano electrode⁵⁰⁻⁵³ is close to a substrate. Small tips allow fast mass transport and kinetics of fast electron transfer processes are determined without interference from uncompensated resistance effects.

1.2. Problems / shortcomings in DC voltammetry

In many voltammetric studies, the effect of uncompensated resistance has been neglected in the theory. Ideally, the effect of iR_u should be taken into account in the development of the theory. However, as pointed out by Nicholson in his theoretical studies of transient DC voltammetry,^{13,54} there are limitations with this approach because the uncompensated resistance and slow kinetics have a similar effect on peak positions and other characteristics. Even if, problems that arise from the uncompensated resistance effect are overcome, an

extensive series of experiments still need to be undertaken, while maintaining the electrode in a reproducible state. Moreover, the Faradaic to background capacitance current ratio becomes less favorable in the higher scan rate regime since capacitance current increases faster with scan rate than does the Faradaic current. These factors make DC transient cyclic Voltammetry at a macrodisk electrode problematic for the measurement of fast electrode kinetics. Limitations with nanoelectrodes arise from imperfections in disk geometry and the need to obtain data from a set of experiments with different electrode radii

1.3. AC voltammetry for kinetics measurement

After the invention of AC voltammetry (polarography)⁵⁵⁻⁶⁰ in the 1950s the method has been extensively developed by Smith and co-workers.⁶¹⁻⁷³ In AC voltammetric/polarographic techniques, an alternating potential of known frequency is superimposed onto the DC waveform and the AC response is used to measure the kinetics and thermodynamics information of fast electrode process.⁷⁴⁻⁸² AC voltammetry allows high-precision measurements because it probes a very thin layer close to the electrode surface and allows measurement over a wide time (or frequency) range. The theory and advantages of applying small amplitude AC cyclic voltammetry are well known^{78,79,81-87} Data analysis may utilize the equivalent-circuit method^{88,89} of impedance for the extraction of kinetics parameters along with the solution resistance, the double-layer capacitance and the mass transport impedance from a single experiment. Small amplitude AC voltammetry is a useful quantitative technique for the study of fast reactions. However, under a small-amplitude, nonlinear regime second and higher order AC components are very small and therefore difficult to measure. This continues with the difficulty of data processing, hence the applications in the electrode kinetics has been limited.

1.4. Large amplitude FT AC voltammetry

Breakthroughs in practical applications of large amplitude AC voltammetry have been encouraged^{90,91} by the availability of fast numerical simulation techniques based on the implicit Richtmyer modification (FIRM) method and data analysis with the Fourier transformation method have given access to a great deal of information on higher harmonics which may otherwise not be available.

Large amplitude FT AC voltammetry applied to surface confined processes such as surface-bound azurin at a paraffin-impregnated graphite electrode⁹⁴ and heme and myoglobin molecules incorporated into a didodecyldimethylammonium bromide (DDAB) film adhered to a pyrolytic graphite electrode gives information about their redox processes.⁹⁵ This method produces a detailed understanding of the reactions involving surface-confined redox proteins exhibiting multiple electron-transfer processes as found in cytochrome C peroxidase⁹⁶ and the free-base porphyrin, 5,10,15,20-tetrakis(1-methyl-4-pyridyl)-21H,23H-porphine (H2TMPyP).⁹⁷ Large amplitude AC voltammetry has also found its applications in a study of surface-confined redox proteins having multiple redox centers as shown for Ferredoxin I from *Azotobacter vinelandii* at pyrolytic graphite electrodes.⁹⁸ Surface confined protein film voltammetry methods using large amplitude FT AC voltammetry have helped to understand the electron transfer processes of biologically important systems via the employment of kinetically sensitive, but background devoid, higher harmonic components. For the DC and fundamental harmonic cases, the background current dominates the voltammetry. In contrast, the capacitive current does not contribute to the second and higher harmonic voltammograms. Furthermore, the higher harmonic faradaic currents are greatly amplified when large amplitude sinusoidal perturbations are employed as an alternative to the traditionally used small amplitude AC methods. Any contribution from heterogeneity in the adsorbed layer and complexities in the reaction mechanism under conditions of large-amplitude FT AC cyclic

voltammetry can be more readily identified as compared to conventional DC cyclic voltammetry.

Use of large amplitude square wave superimposed onto the traditional triangular voltage used in DC cyclic voltammetry also provides a new form of data analysis for kinetics studies of the blue copper protein azurin, immobilized on polycrystalline gold electrodes modified with self-assembled monolayers of different length alkanethiols.⁹⁹ Even harmonics are used in this case for kinetic evaluation of electron-transfer processes because they are highly selective to quasi-reversible behaviour and insensitive to reversible or irreversible processes and almost devoid of background charging current. Surface heterogeneity of the electrode can be readily identified as observed in the case with large amplitude FT AC Voltammetry. Estimates of the percentage of edge plane defect sites are deduced from capacitance (fundamental harmonic AC component) and higher harmonics. AC Faradaic currents are considered to provide a more reliable estimation of kinetic than available for analysis of DC aperiodic component or conventional DC cyclic voltammograms.¹⁰⁰ This kinetic selectivity also facilitates the measurement of chemical kinetics of homogeneous chemical reactions coupled with electron transfer,¹⁰¹ particularly under Fourier transform analysis of electrode kinetics. Thus, application of an advanced AC electroanalytical technique has enhanced the understanding of the charge transfer processes involved in electrocatalysis.¹⁰²⁻¹⁰⁴

In addition to applications of large amplitude AC Voltammetry to understand the mechanisms of surface confined biological active compounds, applications for the study of electrode processes where the redox active system is dissolved in the electrolyte medium have been reported. General numerical simulations for this situation are available based on separation of harmonics by FT method. Thus, if a large amplitude FT AC cyclic voltammetric experiment is undertaken; (a) the DC cyclic component provides an estimate of E° (because the R_u and k^0 effects are minimized); (b) the fundamental harmonic provides an estimate of C_{dl} (because it

has a high capacitance-to-faradaic current ratio); and (c) the second harmonic provides an estimate of R_u , k^0 , and α (because the C_{dl} effect is minimized). Methods of refining the initial estimates are then implemented. As a check on the reliability of the parameters (estimated on the basis of an essentially heuristic approach that solely utilizes the DC, fundamental, and second harmonic voltammograms), comparison of the predicted simulated and experimental third (or higher) harmonic voltammograms can be used to provide new details as to verify that agreement between theory and experiment has been achieved at a predetermined level.¹⁰⁵ Advantages of using higher harmonics not available in conventional small amplitude AC or DC cyclic voltammetric methods are now well known.^{106,107} Importantly, random and systematic experimental errors in higher harmonics can be removed by use of FT AC voltammetry. Data analysis in frequency domain can be used to reduce the magnitude of random (Gaussian) noise and systematic errors introduced by mains frequency. Even the eighth harmonic for a fast process can be detected in the presence of very significant noise levels,¹⁰⁸ where the effect of uncompensated resistance and kinetics can be distinguished in higher AC harmonics.¹⁰⁹ These aspects of large amplitude FT AC voltammetry facilitate to determine the electrode kinetics associated with the fast processes.

1.5. Thesis Objectives

The primary aim of this thesis is to investigate the electron transfer kinetics of some outer sphere electron transfer processes by using large amplitude FT AC voltammetry under a range of conditions and to explore new methods for the determination of fast electron transfer kinetics.

1.6. Thesis Outline

- i. **Chapter 1** reviews the background of electrode kinetic studies
- ii. **Chapter 2** describes the theory of large amplitude FT AC voltammetry and simulation softwares used in this thesis
- iii. **Chapter 3** provides the electrode kinetics associated with TCNQ, $\text{TCNQ}^{\bullet-}$ and TCNQ^{2-} (TCNQ = 7,7,8,8-tetracyanoquinodimethane) redox chemistry in acetonitrile at macrodisk electrodes: A low frequency study.
- iv. **Chapter 4** focuses on the attributes of large amplitude FT AC voltammetry at a rotating disk electrode for electrode kinetics determination.
- v. **Chapter 5** provides a high frequency large amplitude FT AC voltammetric study of tetrathiafulvalene (TTF): Electrode kinetics as reported for the $\text{TTF}^0/\text{TTF}^{*+}$ and $\text{TTF}^{*+}/\text{TTF}^{2+}$ processes
- vi. **Chapter 6** describes the investigation of fast electrode kinetics in ionic liquids using large amplitude FT AC voltammetry: A high frequency study
- vii. **Chapter 7** focuses on the electrode kinetics measurement using large amplitude FT AC voltammetry at microelectrodes in conventional solvents
- viii. **Chapter 8** discusses the dependence of heterogeneous electron transfer rate constant on electrode materials in terms of density of states and adiabaticity.
- ix. **Chapter 9** provides the summary of the main findings of the thesis together with suggestions for future work

References:

- (1) Bard, A. J.; Faulkner, L. R. *Electrochemical methods: fundamentals and applications*; John Wiley: New York, **2001**.
- (2) Bond, A. M. *Modern polarographic methods in analytical chemistry*; Marcel Dekker: New York, **1980**.
- (3) Compton, R. G.; Sanders, G. H.; Oxford: New York, **1996**.
- (4) Bond, A. M. *Broadening electrochemical horizons: principles and illustration of voltammetric and other techniques*; Oxford University press, **2002**.
- (5) Zoski, C. G. *Handbook of electrochemistry*, **2007**.
- (6) Marcus, R. A. *J. Chem. Phys.* **1956**, 24, 966.
- (7) Silverstein, T. P. *J. Chem. Educ.* **2012**, 89, 1159.
- (8) Clegg, A. D.; Rees, N. V.; Klymenko, O. V.; Coles, B. A.; Compton, R. G. *Chemphyschem.* **2004**, 5, 1234.
- (9) Clegg, A. D.; Rees, N. V.; Klymenko, O. V.; Coles, B. A.; Compton, R. G. *J. Am. Chem. Soc.* **2004**, 126, 6185.
- (10) Clegg, A. D.; Rees, N. V.; Klymenko, O. V.; Coles, B. A.; Compton, R. G. *J. Electroanal. Chem.* **2005**, 580, 78.
- (11) Feldberg, S. W. *Anal. Chem.* **2010**, 82, 5176.
- (12) Rao, G. P.; Rangaraj, S. K. *J. Electroanal. Chem.* **1974**, 55, 151.
- (13) Nicholson, R. S. *Anal. Chem.* **1965**, 37, 1351.
- (14) Nicholson, R. S.; Shain, I. *Anal. Chem.* **1964**, 36, 706.
- (15) Alden, J. A.; Hakoura, S.; Compton, R. G. *Anal. Chem.* **1999**, 71, 806.
- (16) Aoki, K.; Tokuda, K.; Matsuda, H. *J. Electroanal. Chem.* **1985**, 195, 229.
- (17) Booth, J.; Compton, R. G.; Cooper, J. A.; Dryfe, R. A. W.; Fisher, A. C.; Davies, C. L.; Walters, M. K. *J. Phys. Chem.* **1995**, 99, 10942.

- (18) Kanzaki, Y. *Denki Kagaku* **1985**, 53, 560.
- (19) Kanzaki, Y.; Bruckenstein, S. *J. Electrochem. Soc.* **1979**, 126, 437.
- (20) Macpherson, J. V. *Electroanal.* **2000**, 12, 1001.
- (21) Pungor, E.; Feher, Z.; Varadi, M. *CRC Cr. Rev. Anal. Chem.* **1980**, 9, 97.
- (22) Rees, N. V.; Compton, R. G. *Russ J. Electrochem.* **2008**, 44, 368.
- (23) Tokuda, K.; Aoki, K.; Matsuda, H. *J. Electroanal. Chem.* **1977**, 80, 211.
- (24) Tokuda, K.; Bruckenstein, S. *J. Electrochem. Soc.* **1979**, 126, 431.
- (25) Tokuda, K.; Matsuda, H. *J. Electroanal. Chem.* **1973**, 44, 199.
- (26) Bidwell, M. J.; Alden, J. A.; Compton, R. G. *J. Electroanal. Chem.* **1996**, 417, 119.
- (27) Costa, C.; Doche, M. L.; Hihn, J. Y.; Bisel, I.; Moisy, P.; Leveque, J. M. *Ultrasonics* **2010**, 50, 323.
- (28) Suzuki, J. *B Chem. Soc. Jpn.* **1969**, 42, 3487.
- (29) Suzuki, J. *B Chem. Soc. Jpn.* **1970**, 43, 755.
- (30) Velicky, M.; Tam, K. Y.; Dryfe, R. A. W. *J. Electroanal. Chem.* **2012**, 683, 94.
- (31) Wan, Z.; Chen, Q. *Talanta* **1987**, 34, 657.
- (32) Fisher, A. C.; Compton, R. G. *J. Appl. Electrochem.* **1992**, 22, 38.
- (33) Compton, R. G.; Unwin, P. R. *J. Electroanal. Chem.* **1988**, 245, 303.
- (34) Compton, R. G.; Unwin, P. R. *J. Electroanal. Chem.* **1986**, 205, 1.
- (35) Compton, R. G.; Unwin, P. R. *J. Electroanal. Chem.* **1986**, 206, 57.
- (36) Compton, R. G.; Laing, M. E.; Unwin, P. R. *J. Electroanal. Chem.* **1986**, 207, 309.
- (37) Compton, R. G.; Fisher, A. C.; Wellington, R. G.; Dobson, P. J.; Leigh, P. A. *J. Phys. Chem.* **1993**, 97, 10410.

- (38) Compton, R. G.; Dryfe, R. A. W.; Alden, J. A.; Rees, N. V.; Dobson, P. J.; Leigh, P. A. *J. Phys. Chem.* **1994**, 98, 1270.
- (39) Vijaikanth, V.; Li, G. C.; Swaddle, T. W. *Inorg. Chem.* **2013**, 52, 2757.
- (40) Amatore, C.; Fosset, B.; Bartelt, J.; Deakin, M. R.; Wightman, R. M. *J. Electroanal. Chem.* **1988**, 256, 255.
- (41) Amatore, C. A.; Fosset, B.; Deakin, M. R.; Wightman, R. M. *J. Electroanal. Chem.* **1987**, 225, 33.
- (42) Amatore, C.; Deakin, M. R.; Wightman, R. M. *J. Electroanal. Chem.* **1987**, 225, 49.
- (43) Deakin, M. R.; Wightman, R. M.; Amatore, C. A. *J. Electroanal. Chem.* **1986**, 215, 49.
- (44) Amatore, C. A.; Deakin, M. R.; Wightman, R. M. *J. Electroanal. Chem.* **1986**, 206, 23.
- (45) Ito, C. R.; Asakura, S.; Nobe, K. *J. Electrochem. Soc.* **1972**, 119, 698.
- (46) Ito, C.; Asakura, S.; Nobe, K. *J. Electrochem. Soc.* **1970**, 117, C118.
- (47) Amemiya, S.; Bard, A. J.; Fan, F. R. F.; Mirkin, M. V.; Unwin, P. R. *Annu. Rev. Anal. Chem.* **2008**, 1, 95.
- (48) Gewirth, A. A.; Niece, B. K. *Chem. Rev.* **1997**, 97, 1129.
- (49) Lu, X.; Wang, Q.; Liu, X. *Anal. Chim. Acta* **2007**, 601, 10.
- (50) Arrigan, D. W. M. *Analyst* **2004**, 129, 1157.
- (51) Cox, J. T.; Zhang, B. *Annu. Rev. Anal. Chem.* **2012**, 5, 253.
- (52) Sun, P.; Mirkin, M. V. *Anal. Chem.* **2006**, 78, 6526.
- (53) Wu, Y. H.; Hu, S. S. *Ind. J. Chem. A* **2005**, 44, 891.
- (54) Nicholson, R. S.; Shain, I. *Anal. Chem.* **1964**, 36, 1212.
- (55) Breyer, B.; Gutman, F.; Hacopian, S. *Aust. J. Sci. Res. Ser. A* **1950**, 3, 567.

- (56) Breyer, B.; Hacobian, S. *Aust. J. Sci. Res. Ser. A* **1951**, 4, 610.
- (57) Breyer, B.; Hacobian, S. *Aust. J. Chem.* **1954**, 7, 225.
- (58) Breyer, B.; Bauer, H. H.; Hacobian, S. *Aust. J. Chem.* **1955**, 8, 312.
- (59) Okuda, M.; Tachi, I. *Bull. Chem. Soc. Jpn.* **1955**, 28, 37.
- (60) Senda, M.; Tachi, I. *Bull. Chem. Soc. Jpn.* **1955**, 28, 632.
- (61) Brown, E. R.; Smith, D. E.; Deford, D. D. *Anal. Chem.* **1966**, 38, 1130.
- (62) Delmastr.Jr; Smith, D. E. *J. Electroanal. Chem.* **1967**, 14, 261.
- (63) Hayes, J. W.; Ruzic, I.; Smith, D. E. *J. Electroanal. Chem.* **1974**, 51, 269.
- (64) Hayes, J. W.; Ruzic, I.; Smith, D. E. *J. Electroanal. Chem.* **1974**, 51, 245.
- (65) Hayes, J. W.; Smith, D. E. *J. Electroanal. Chem.* **1980**, 114, 293.
- (66) Hayes, J. W.; Smith, D. E. *J. Electroanal. Chem.* **1980**, 114, 283.
- (67) Mccord, T. G.; Brown, E. R.; Smith, D. E. *Anal. Chem.* **1966**, 38, 1615.
- (68) Mccord, T. G.; Smith, D. E. *Anal. Chem.* **1968**, 40, 289.
- (69) Mccord, T. G.; Smith, D. E. *Anal. Chem.* **1969**, 41, 1423.
- (70) Bond, A. M. *J. Electroanal. Chem.* **1972**, 36, 235.
- (71) Bond, A. M. *Talanta* **1974**, 21, 591.
- (72) Bond, A. M.; Blutstein, H.; Ohalloran, R. J. *Abstr. Pap. Am. Chem. Soc.* **1975**, 61.
- (73) Bond, A. M.; Waugh, A. B. *Electrochim. Acta* **1970**, 15, 1471.
- (74) Abouelenien, G. M. *J. Electroanal. Chem.* **1993**, 345, 147.
- (75) Bond, A. M. *J. Electroanal. Chem.* **1974**, 50, 285.
- (76) Bond, A. M.; Ohalloran, R. J.; Ruzic, I.; Smith, D. E. *J. Electroanal. Chem.* **1978**, 90, 381.
- (77) Curran, D. J.; Kingsley, E. D. *Abstr. Pap. Am. Chem. Soc.* **1982**, 183, 14.
- (78) Garai, T.; Szepesvari, I.; Guti, Z. *Magy. Kem. Foly.* **1983**, 89, 241.

- (79) Garai, T.; Szepesvari, I.; Guti, Z. *Acta Chim. Hung.* **1984**, *115*, 137.
- (80) Henderson, D.; Gordon, J. G. *J. Electroanal. Chem.* **1980**, *108*, 129.
- (81) Kanazawa, K. K.; Diaz, A. F. *J. Electrochem. Soc.* **1978**, *125*, C170.
- (82) Rashwan, F.; Mohran, H. *B Chem. Soc. Jpn.* **1993**, *66*, 1871.
- (83) Muzikar, M.; Fawcett, W. R. *Anal. Chem.* **2004**, *76*, 3607.
- (84) Brevnov, D. A.; Finklea, H. O.; Van Ryswyk, H. *J. Electroanal. Chem.* **2001**, *500*, 100.
- (85) Rosvall, M. *Electrochem. Commun.* **2000**, *2*, 791.
- (86) Brevnov, D. A.; Finklea, H. O. *J. Electroanal. Chem.* **2000**, *488*, 133.
- (87) Los, P.; Zabinska, G.; Kiszka, A.; Christie, L.; Mount, A.; Bruce, P. G. *Phys. Chem. Chem. Phys.* **2000**, *2*, 5449.
- (88) Hirose, S.; Yamayoshi, Y.; Taga, M.; Shimizu, H. *Jpn. J. Appl. Phys. Part 1* **1991**, *30*, 117.
- (89) Zhang, Z. L.; Li, Y. L.; Xu, Z. S.; Zhu, X. L.; Kang, Q.; Shen, D. Z. *Int. J. Electrochem. Soc.* **2013**, *8*, 3357.
- (90) Gavaghan, D. J.; Bond, A. M. *J. Electroanal. Chem.* **2000**, *480*, 133.
- (91) Engblom, S. O.; Myland, J. C.; Oldham, K. B.; Taylor, A. L. *Electroanal.* **2001**, *13*, 626.
- (92) Rosvall, S. J. M.; Sharp, M.; Bond, A. *J. Electroanal. Chem.* **2002**, *536*, 161.
- (93) Gavaghan, D. J.; Elton, D.; Oldham, K. B.; Bond, A. M. *J. Electroanal. Chem.* **2001**, *512*, 1.
- (94) Fleming, B. D.; Zhang, J.; Elton, D.; Bond, A. M. *Anal. Chem.* **2007**, *79*, 6515.
- (95) Lee, C. Y.; Bond, A. M. *Langmuir* **2010**, *26*, 5243.
- (96) Stevenson, G. P.; Lee, C. Y.; Kennedy, G. F.; Parkin, A.; Baker, R. E.; Gillow, K.; Armstrong, F. A.; Gavaghan, D. J.; Bond, A. M. *Langmuir* **2012**, *28*, 9864.

- (97) Fleming, B. D.; Bond, A. M. *Electrochim. Acta* **2009**, *54*, 2713.
- (98) Lee, C. Y.; Stevenson, G. P.; Parkin, A.; Roessler, M. M.; Baker, R. E.; Gillow, K.; Gavaghan, D. J.; Armstrong, F. A.; Bond, A. M. *J. Electroanal. Chem.* **2011**, *656*, 293.
- (99) Fleming, B. D.; Barlow, N. L.; Zhang, J.; Bond, A. M.; Armstrong, F. A. *Anal. Chem.* **2006**, *78*, 2948.
- (100) Lee, C. Y.; Fleming, B. D.; Zhang, J.; Guo, S. X.; Elton, D. M.; Bond, A. M. *Anal. Chim. Acta* **2009**, *652*, 205.
- (101) Lee, C. Y.; Bullock, J. P.; Kennedy, G. F.; Bond, A. M. *J. Phys. Chem. A* **2010**, *114*, 10122.
- (102) Lee, C. Y.; Bond, A. M. *Langmuir* **2010**, *26*, 16155.
- (103) Lee, C. Y.; Guo, S. X.; Murphy, A. F.; McCormac, T.; Zhang, J.; Bond, A. M.; Zhu, G.; Hill, C. L.; Geletii, Y. V. *Inorg. Chem.* **2012**, *51*, 11521.
- (104) Shiddiky, M. J. A.; O'Mullane, A. P.; Zhang, J.; Burke, L. D.; Bond, A. M. *Langmuir* **2011**, *27*, 10302.
- (105) Sher, A. A.; Bond, A. M.; Gavaghan, D. J.; Harriman, K.; Feldberg, S. W.; Duffy, N. W.; Guo, S. X.; Zhang, J. *Anal. Chem.* **2004**, *76*, 6214.
- (106) Zhang, J.; Guo, S. X.; Bond, A. M.; Marken, F. *Anal. Chem.* **2004**, *76*, 3619.
- (107) Sher, A. A.; Bond, A. M.; Gavaghan, D. J.; Gillow, K.; Duffy, N. W.; Guo, S. X.; Zhang, J. *Electroanal.* **2005**, *17*, 1450.
- (108) Gavaghan, D. J.; Bond, A. M. *Electroanal.* **2006**, *18*, 333.
- (109) Zhang, J.; Guo, S. X.; Bond, A. M. *Anal. Chem.* **2007**, *79*, 2276.

CHAPTER 2

AC VOLTAMMETRY: EXPERIMENTS AND SIMULATIONS

CHAPTER 2

AC VOLTAMMETRY: EXPERIMENTS AND SIMULATIONS

2.1. Introduction

Voltammetric experiments are generally conducted in a three electrode cell using a potentiostat containing the redox active specie dissolved in the electrolyte solution. A supporting electrolyte concentration ≥ 0.01 M is usually used in voltammetric experiments to establish a well defined double layer and to minimize the solution resistance and migration effects. In this arrangement, reactions of interest occur at the working electrode while the current is passed between the working and counter electrode. The potential of the working electrode is compared with that of the reference electrode. In addition, the reference electrode is placed as close as possible to the working electrode surface to minimize the effect of iR_u / ohmic drop. The cell has an inlet and an outlet for purging with an inert gas to displace any illustrative oxygen present in the solution.

In cyclic voltammetric experiments, the potential of the working electrode is usually swept between initial and switching potential at a certain scan rate and then sweep direction is reversed and the potential returns to its initial value.

This chapter describes the basis of large amplitude FT AC voltammetry and simulation softwares used in this thesis.

2.2. Large amplitude FT AC voltammetry Instrumentation

Figure 1 summarizes the key features in low-cost instrumentation needed to achieve a unified approach to FT voltammetry. A 2.5-GHz Pentium 4 desktop computer can be used for data analysis and instrument control. The FT AC voltammetric instrumentation is based on a conventional three-electrode potentiostat driven by a sigma digital-to-analog converter (DAC)

and a DAC Software compensates for the time delay introduced through the ADC and DAC devices (~33 samples each). Stereo hardware limits the upper sampling rate to ~40 kHz. This implies that the upper usable frequency is 20 kHz, because Nyquist's theorem requires the sampling rate to be at least twice the highest frequency component of the signal being analyzed. This DAC can produce a DC ramp with a potential range of ± 3 V.

The AC experiments carried out using instrumentation in conjunction with frequency analyser offer considerably increased sensitivity for mechanistic and kinetic estimation. An AC voltammetric measurement is usually performed in an electrochemical cell where diffusion is the dominant mode of transport. Typically, an amplitude higher than 40 mV is normally employed in large amplitude FT AC measurements. This perturbation ensures that only slight changes in concentrations occur close to the electrode surface and allows mathematical analysis to assume that the effect on the electrode kinetics can be calculated in a linear manner, even though the electrode kinetics strictly have an exponential dependence on the applied voltage. The maximum change in AC current is seen to occur at E^0 as this is the region where the electrode kinetics are most sensitive to voltage changes, whereas at the two extremes of the voltage range there is no variation since the electrode kinetics are insignificantly affected and so the current doesn't vary.

Consequently, the potential at time t , $E(t)$ is given by eq 1

$$E_{app}(t) = E_{DC}(t) + E_{AC}(t) \quad (1)$$

$$E_{DC}(t) = E_{start} - vt; 0 \leq t \leq t_s \quad (2)$$

$$E_{DC}(t) = E_{start} - 2vt_s + vt; t_s \leq t \leq 2t_s \quad (3)$$

$$E_{AC}(t) = \Delta E \sin(2\pi ft); 0 \leq t \leq 2t_s \quad (4)$$

Figure 2 illustrates the waveform used for the linear sweep voltammetry case, and the output when total current is plotted against time in the linear sweep form of the experiment.

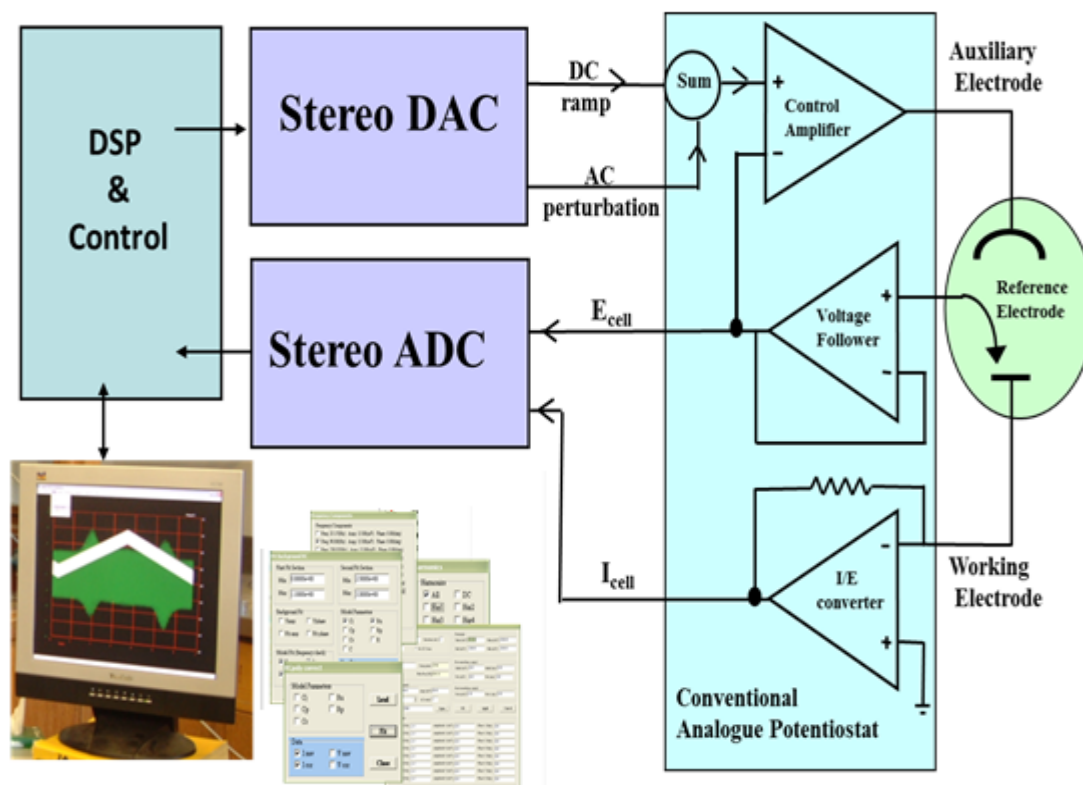


Figure 1: Shows the instrumentation details of an AC potentiostat reproduced from reference (6)

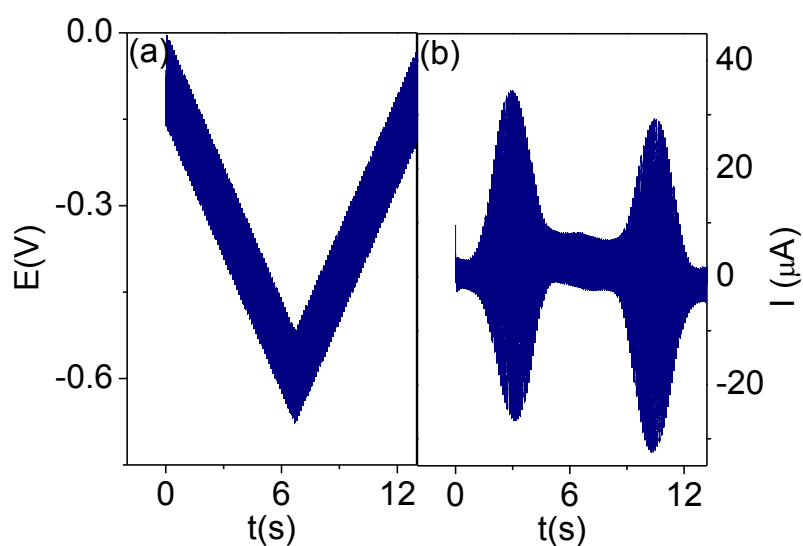


Figure 2: (a) Sine wave employed in AC cyclic voltammetry (b) AC voltammetric total current data

2.3. FT-inverse FT protocol of data analysis

FT AC voltammetric data obtained experimentally or by simulation were then subjected to data analysis in which time domain data are converted to the frequency domain using Fourier transform (FT) algorithm to give the power spectrum. Frequencies in the region containing AC harmonics and aperiodic DC component in the power spectrum were then subjected to band filtering to provide DC or AC components as a function of time as shown in Figure 3.

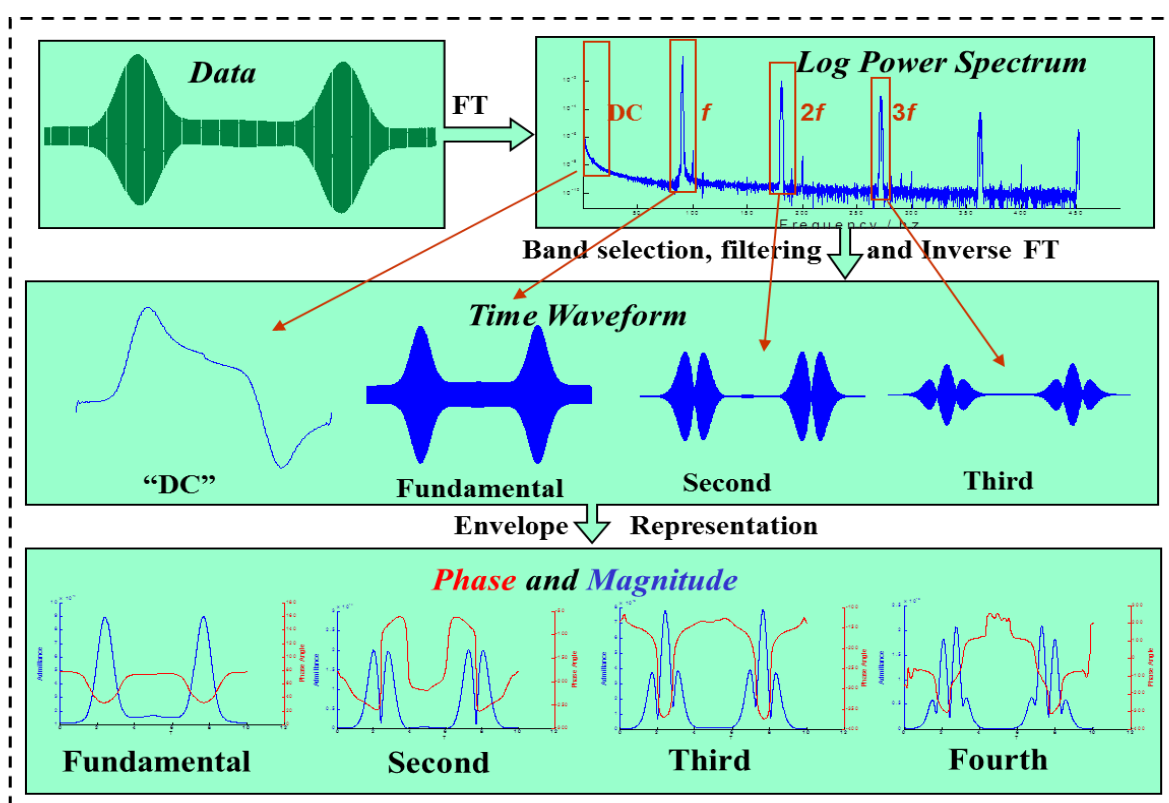


Figure 3: Schematic information of FT-Inverse FT data analysis protocol, reproduced from reference (6).

2.4. Simulations

If the electrode reaction is a one electron oxidation process, where a species R is oxidized to O by the loss of electrons to the electrode. Possible mass transport mechanisms are diffusion, convection, and migration. We concentrate only on the diffusion mechanism described by

Fick's second law of diffusion, for stationary electrode measurements. Migration may be neglected, due to the presence of a high concentration of supporting electrolyte solution. Convection is considered in case of rotating disk electrodes.

Under linear diffusion conditions, the mass transport for all diffusing species follows the relationship

$$\frac{\partial C}{\partial t} = D \frac{\partial^2 C}{\partial z^2} \quad (5)$$

where C and D are the concentration and diffusion coefficient of the species of interest, respectively, and z is the distance from electrode surface. The standard approach of modelling a macroelectrode using the one-dimensional diffusion equation was used in simulations.¹

Under rotating disk conditions mass transport is given as

$$\frac{\delta C}{\delta t} = D_c \frac{\delta^2 C}{\delta^2 z} + v_z \frac{\partial C}{\partial z} \quad (6)$$

Where z is the distance from the electrode surface, for a rotating Disk electrode, For rotating disk electrode simulations mass transport equation was solved by the Tokuda's method.²

At a microelectrode, radial diffusion of redox active specie can be given as

$$\frac{\delta C}{\delta t} = D_c \frac{\partial^2 C}{\partial r^2} + \frac{1}{r} \frac{\partial C}{\partial r} + \frac{\partial^2 C}{\partial z^2} \quad (7)$$

Where z is the distance from the electrode surface

For microelectrode, the mass transport equations can be solved numerically using a two dimensional FIRM algorithm (Fully Implicit Richtmeyer Modification), application of an expanding space grid and the initial and boundary conditions.³

Simulations were usually conducted using Monash Electrochemistry Simulator, a simulation software based on an expanding spatial grid originally introduced by Feldberg.^{4,5} Butler-Volmer Kinetics was applied for determination of electrode kinetics. Simulation requires information about several different parameters as given in Table 1

Table 1. Showing experimental and simulation parameters required in simulations

Range of DC applied potential	E_{start} and E_{rev} (V)
Formal potential	E^0 (V)
Amplitude of applied potential	ΔE (V)
Period of applied potential	P (s)
Frequency of applied potential	f (Hz)
Angular frequency of applied potential	ω (rad s ⁻¹)
DC Scan rate	v_{DC} (V s ⁻¹)
Bulk concentration of species	C (mol cm ⁻³)
Rate constant	k^0 (cm s ⁻¹)
Area of electrode	A (cm ²)
Diffusion coefficient	D (cm ² s ⁻¹)
Charge transfer coefficient	α
Uncompensated resistance	R_u (ohm)
Double layer capacitance	C_{dl} (μF cm ⁻²)
RDE rotation velocity	ω^* (rad s ⁻¹)

References:

- (1) Sher, A. A.; Bond, A. M.; Gavaghan, D. J.; Harriman, K.; Feldberg, S. W.; Duffy, N. W.; Guo, S. X.; Zhang, J. *Anal. Chem.* **2004**, 76, 6214.

- (2) Tokuda, K.; Bruckenstein, S. *J Electrochem Soc* **1979**, *126*, 431.
- (3) Lee, C. Y.; Elton, D.; Brajter-Toth, A.; Bond, A. M. *Electroanal.* **2013**, *25*, 931.
- (4) Feldberg, S. W. *J. Electroanal. Chem.* **1981**, *127*, 1.
- (5) Gavaghan, D. J.; Bond, A. M. *Electroanal.* **2006**, *18*, 333.
- (6) Bond, A. M.; Duffy, N. W.; Guo, S.-X.; Zhang, J.; Elton, D. *Anal. Chem.* **2005**, *77*, 186 A.

CHAPTER 3

ELECTRODE KINETICS STUDIES AT MACRODISK ELECTRODES: LOW FREQUENCY FT AC VOLTAMMETRY

Monash University

Declaration for Thesis Chapter [3]

Declaration by candidate

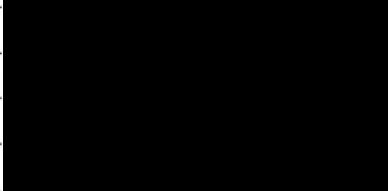
In the case of Chapter [3], the nature and extent of my contribution to the work was the following:

Nature of contribution	Extent of contribution (%)
Initiation, key ideas, experimental work, writing up	85 %

The following co-authors contributed to the work. If co-authors are students at Monash University, the extent of their contribution in percentage terms must be stated:

Name	Nature of contribution
Jie Zhang	Initiation, key ideas, writing up
Alan M. Bond	Initiation, key ideas, writing up
Ayman Nafady	Initiation, key ideas, experimental work
Inam-ul-Haque	Initiation, key ideas,

The undersigned hereby certify that the above declaration correctly reflects the nature and extent of the candidate's and co-authors' contributions to this work*.

Candidate's Signature		Date	28/11/2013
Jie Zhang			
Alan M. Bond			
Ayman Nafady			
Inam-ul-Haque			

Main Supervisor's Signature		Date	29/11/2013
-----------------------------	---	------	------------

*Note: Where the responsible author is not the candidate's main supervisor, the main supervisor should consult with the responsible author to agree on the respective contributions of the authors.

Electrode Kinetics Associated with Tetracyanoquinodimethane (TCNQ), $\text{TCNQ}^{\bullet-}$, and TCNQ^{2-} Redox Chemistry in Acetonitrile As Determined by Analysis of Higher Harmonic Components Derived from Fourier Transformed Large Amplitude ac Voltammetry

Kiran Bano, Ayman Nafady, Jie Zhang,* and Alan M. Bond*

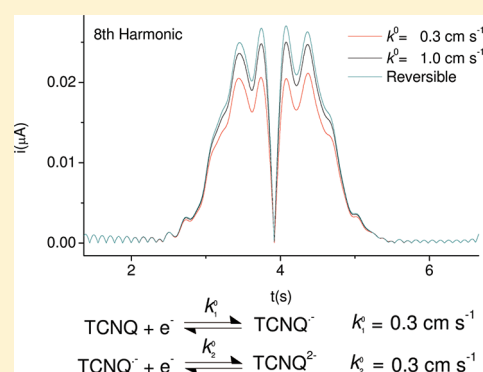
School of Chemistry, Monash University, Clayton, Victoria 3800, Australia

Inam-ul-Haque

Department of Chemistry, University of Engineering & Technology, G.T Road Lahore, 54890 Pakistan

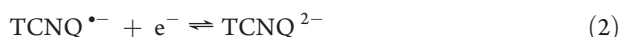
 Supporting Information

ABSTRACT: The dc and first to eighth harmonic components derived from Fourier transformed large amplitude ac voltammetry have been used to determine the heterogeneous electron transfer kinetics (k^0) of electron transfer processes involving reduction of 7,7,8,8-tetracyanoquinodimethane (TCNQ), oxidation and reduction of $\text{TCNQ}^{\bullet-}$, and oxidation of TCNQ^{2-} in acetonitrile. This protocol permits removal of a possible contribution from the cross redox reaction between TCNQ and TCNQ^{2-} . k^0 values were determined by comparison of the experimental data with simulations that take into account the effect of uncompensated resistance and double layer capacitance. Values of $0.30 \pm 0.05 \text{ cm s}^{-1}$ were obtained at platinum and glassy carbon electrodes for both $\text{TCNQ}^{0/\bullet-}$ and $\text{TCNQ}^{\bullet-/2-}$ processes when studies were undertaken over a range of concentrations using both reduction and oxidation perspectives. Difficulties associated with measurement of electrode kinetics near the reversible limit and comparisons with literature data are considered.



INTRODUCTION

7,7,8,8-Tetracyanoquinodimethane (TCNQ) under voltammetric conditions gives rise to two well-resolved one-electron-reduction processes (eqs 1 and 2) in organic solvents.¹



The heterogeneous electron transfer rate constant (k^0) for the $\text{TCNQ}^{0/\bullet-}$ process has been reported to range from 0.005 to 1.1 cm s^{-1} at Pt macro- or nanoelectrodes under transient or steady-state dc voltammetric conditions.^{1–4,5a} Sharp^{2b} determined the kinetics of the $\text{TCNQ}^{0/\bullet-}$ process in dimethylformamide, acetonitrile, and dimethyl sulfoxide solvents at Pt and Au microdisk electrodes using fast scan rate cyclic voltammetry with resistance compensation. The k^0 values in acetonitrile based on the scan rate dependence of the separation of reduction and oxidation peaks and the theory of Nicholson⁶ were reported to be 0.2 cm s^{-1} at Pt and 0.26 cm s^{-1} at Au. Sharp^{2a} also reported a much slower rate constant of about 0.0035 cm s^{-1} at a wax impregnated graphite electrode in acetonitrile. Khoo et al.³ found

that both reduction steps (eqs 1 and 2) in acetonitrile with different supporting electrolytes at Pt and glassy carbon (GC) macrodisk electrodes were essentially reversible in the time scale of their measurement (100 mV s^{-1}). Zhou and Evans, in a detailed study, suggested that $k^0 = 0.005 \text{ cm s}^{-1}$ for the $\text{TCNQ}^{2-/\bullet-}$ process and 0.006 cm s^{-1} for $\text{TCNQ}^{\bullet-/0}$ at a Pt electrode, based on comparison of experimental data with digital simulations of dc cyclic voltammetry.¹ However, the authors noted that the voltammograms were slightly affected by uncompensated resistance (R_u) that was not accommodated in digital simulations. Thus, these values probably represent lower limits. Russell et al.⁴ used a thin Au ring ultramicroelectrode to minimize the effect of R_u and to increase the rate of mass transport in a near-steady-state measurement of the one-electron reduction of TCNQ in acetonitrile. A k^0 value of $0.23 \pm 0.01 \text{ cm s}^{-1}$ was obtained. In order to further minimize the effect of R_u and to increase the mass transport, Mirkin used steady-state voltammetry with Pt nanoelectrodes and reported that k^0 for $\text{TCNQ}^{0/\bullet-}$ couple was 1.1 cm s^{-1} .^{5a} A survey

Received: May 28, 2011

Revised: October 17, 2011

Published: October 20, 2011

Table 1. Summary of Literature Kinetic Data (k^0 Value in cm s^{-1}) Available for $\text{TCNQ}^{0/+/-2-}$ Processes in Acetonitrile

process	ref 1.		ref 2.		ref 3.		ref 4.		ref 5a.	
	k^0	electrode	k^0	electrode	k^0	electrode	k^0	electrode	k^0	electrode
$\text{TCNQ}^{0/+}$			0.2	macro-Pt	reversible	macro-Pt and GC	0.23 ± 0.01	micro-ring Au	1.1	nano-Pt
			0.26	macro-Au						
			0.0035	macro-graphite						
$\text{TCNQ}^{+/-2-}$					reversible	macro-Pt and GC				
$\text{TCNQ}^{+/-0}$	0.006	macro-Pt								
$\text{TCNQ}^{2-/+}$	0.005	macro-Pt								

of electrode kinetic data available for both TCNQ processes is given in Table 1.

Conventional dc forms of voltammetry^{7,8} have been employed in most of the electrode kinetics studies. With this technique, electrode kinetic information has commonly been obtained from the difference in the reduction (E_p^{red}) and oxidation (E_p^{ox}) peak potentials as a function of scan rate in the case of transient cyclic voltammetry⁶ or the differences in the half wave potential $E_{1/2}$ and quarter potential $E_{1/4}$ (or $E_{3/4}$) from the reversible potential in the case of steady-state voltammetry.^{4,9} Since uncompensated resistance (iR_u effect) also affects differences in these potentials, in order to obtain accurate kinetic information, small electrodes or lower concentrations of analyte can be used so that effect of iR_u is minimized. Microelectrodes are commonly used to minimize iR_u drop under steady-state conditions.¹⁰ Alternatively, positive feedback iR_u compensation function built into the potentiostat can be employed.^{2b,11} In most studies highlighted above, the effect of uncompensated resistance was assumed to be negligible or was neglected. The effect of iR_u also can be taken into account in the development of theory.¹² However, as pointed out by Nicholson in his theoretical studies of transient dc voltammetry,¹³ there are limitations with this approach because uncompensated resistance and slow kinetics have similar effects on peak positions and other characteristics. Even if the problems that arise from the uncompensated resistance effect are overcome, an extensive series of experiments still need to be undertaken while maintaining the electrodes in a reproducible state. Moreover, the Faradaic to background capacitance current ratio becomes less favorable in the higher scan rate regime since capacitance current increases faster with scan rate than does the Faradaic current. These factors make dc transient cyclic voltammetry at a macrodisk electrode problematical for the measurement of fast electrode kinetics. Consequently, electrochemical techniques such as fast scan voltammetry,¹⁴ steady-state voltammetry,^{4,10,15} scanning electrochemical microscopy,⁵ and hydrodynamic voltammetry,¹⁶ which utilize microelectrodes or more advantageously nanoelectrodes as working electrodes have been advocated for this purpose. Nevertheless, limitations with nanoelectrodes arise from imperfections in disk geometry and the need to obtain data from a set of experiments with different electrode radii. In contrast, large amplitude Fourier transformed alternating current (FT ac) voltammetry advocated by Bond and co-workers represents a sophisticated method that can be applied at macrodisk electrodes.^{17,18} The higher order harmonic components generated by the large amplitude periodic perturbation have a very low background and are much more sensitive to evaluation of both the uncompensated resistance and electrode kinetics. Importantly, Zhang et al. have shown that the effect of slow electrode kinetics and uncompensated resistance

can be easily discriminated, when a series of higher harmonic components of Fourier transformed large amplitude ac voltammetry are analyzed.^{17c} Finally, and just as importantly, only one set of experiments is needed to estimate the capacitance, uncompensated resistance, and electrode kinetic parameters. In contrast, most other electrochemical methods require a series of experiments with either several electrodes of different diameters,^{4,10,15} a range of voltage ramps with variable scan rate, or variation in another time-dependent parameter.¹⁴

In this paper, $\text{TCNQ}^{+/-}$ and TCNQ^{2-} have been quantitatively generated by reductive bulk electrolysis of TCNQ. This protocol allows $\text{TCNQ}^{0/+}$, $\text{TCNQ}^{+/-2-}$, $\text{TCNQ}^{+/-0}$, and $\text{TCNQ}^{2-/+}$ processes to be investigated at GC and Pt macrodisk electrodes from three different initial redox levels. The electrode kinetics were probed by the large amplitude ac technique with perturbation by a sine wave onto the dc waveform. A low frequency sine wave was employed to minimize the effect of kinetic dispersion at the nonhomogeneous polycrystalline solid electrodes, and a range of concentrations were studied to ensure that the uncompensated resistance has been correctly accommodated in the simulations.

■ EXPERIMENTAL SECTION

Chemicals. 7,7,8,8-Tetracyanoquinodimethane (TCNQ; 98%), ferrocene (Fc; $\geq 98\%$); potassium ferricyanide ($\text{K}_3[\text{Fe}(\text{CN})_6]$), and potassium chloride (KCl) were used as supplied by Sigma-Aldrich. *n*-Tetrabutylammonium hexafluorophosphate (Bu_4NPF_6 ; 98% (Wako)) was recrystallized twice from ethanol to remove any iodide impurity. Unless otherwise stated, dried and distilled acetonitrile (MeCN; 99.9% (Sigma-Aldrich)) was used and experiments were undertaken under nitrogen in a drybox.

Apparatus. A conventional three-electrode cell was employed for voltammetric experiments undertaken with 1.0 mm GC or 1.5 mm Pt diameter macrodisk working electrodes. A Pt microdisk electrode (radius $r = 5 \mu\text{m}$) was used for some experiments under near-steady-state conditions with a scan rate of 20 mV s^{-1} . TCNQ reacts with silver to give AgTCNQ , so Pt wire immersed into the solution and separated from the bulk solution by a glass frit was used instead of silver as the quasi-reference electrode in order to maintain the reference potential constant during measurements. The counter electrode is also a Pt wire. Potentials derived from the Pt quasi reference electrode were calibrated against the Fc/Fc^+ internal reference potential by recording the cyclic voltammogram in a solution containing both TCNQ and Fc. Working electrodes were polished using a $0.3 \mu\text{m}$ alumina slurry on a polishing cloth (BAS), sonicated in deionized water, rinsed with water and acetone, and then dried with nitrogen. All voltammetric experiments were undertaken at room temperature of $20 \pm 2^\circ\text{C}$.

Areas of the macrodisk electrodes were calculated from peak currents for reduction of 1.00 mM $\text{K}_3\text{Fe}(\text{CN})_6$ in 0.1 M potassium chloride aqueous electrolyte solution as a function of scan rate and use of the Randles–Sevcik equation

$$I_p = 0.4463nFA \left(\frac{nFDv}{RT} \right)^{1/2} C \quad (3)$$

where I_p is the peak current, n (number of electrons transferred) = 1, C is the bulk concentration, D is the diffusion coefficient of ferricyanide which was taken to be $7.6 \times 10^{-6} \text{ cm}^2 \text{ s}^{-1}$, T is the absolute temperature, F is Faraday's constant, R is the universal gas constant, and A is the electrode area. The effective area of the GC electrode calculated from eq 3 was found to be 0.00875 cm^2 , and that of the Pt disk electrode was 0.022 cm^2 . The radius (r) of the Pt microdisk electrode was determined to be $5.0 \mu\text{m}$ based on the steady-state diffusion limiting current (I_l) for the reduction of ferricyanide using eq 4 and other parameters given above:

$$I_l = 4nFrDC \quad (4)$$

Instrumentation and Procedures. For some preliminary dc voltammetric studies under benchtop conditions, a Bioanalytical Systems (BAS) Model 100B electrochemical workstation was employed. For studies in the drybox, a BASi Epsilon electrochemical workstation was used. Fourier transformed large amplitude ac voltammetric experiments were undertaken with home-built instrumentation described elsewhere.¹⁸

Bulk electrolysis of a known concentration of TCNQ was carried out quantitatively (coulometric and steady-state voltammetric monitoring) in acetonitrile (0.1 M Bu_4NPF_6) solution in a three-compartment cell to provide the same concentration of $\text{TCNQ}^{\bullet-}$ and TCNQ^{2-} . A three-electrode configuration was employed using Pt mesh as the working and counter electrodes and Pt wire as a quasi reference electrode. The Pt quasi reference potential was then calibrated against that of the Fc/Fc^+ couple, and potentials employed are reported versus this reference system. Bulk electrolysis working and counter electrodes were first washed with acid piranha (3:1 hydrogen peroxide and sulfuric acid mixture) solution, thoroughly washed with water and acetone, air-dried, and then dried in an oven. Since $\text{TCNQ}^{\bullet-}$ and particularly TCNQ^{2-} are air sensitive, bulk electrolysis and subsequent electrochemical measurements at these redox levels were conducted in a drybox under a nitrogen atmosphere.

Diffusion coefficients of TCNQ, $\text{TCNQ}^{\bullet-}$, and TCNQ^{2-} were determined in separate experiments using a Pt micro disk electrode and GC or Pt macro disk electrodes.

Electrode kinetic data were derived from designated concentrations of TCNQ, $\text{TCNQ}^{\bullet-}$, and TCNQ^{2-} in acetonitrile (0.1 M Bu_4NPF_6). Uncompensated resistance was estimated in a potential region where no Faradaic current is present using the RC time constant method¹⁹ available with the BAS 100 instrument.

Simulation of Fourier Transformed Large Amplitude ac Voltammetric Data. All simulations were undertaken with Monash Electrochemistry Simulator (MECSIM) software. The details of the simulation of a process of the kind



based on use of the Butler–Volmer relationship are provided in refs 17c, 17f, and 17g, where E^0 is the reversible potential calculated as mean/average of the peak potentials for reduction and oxidation components of a cyclic voltammetric experiment, k^0 is the formal

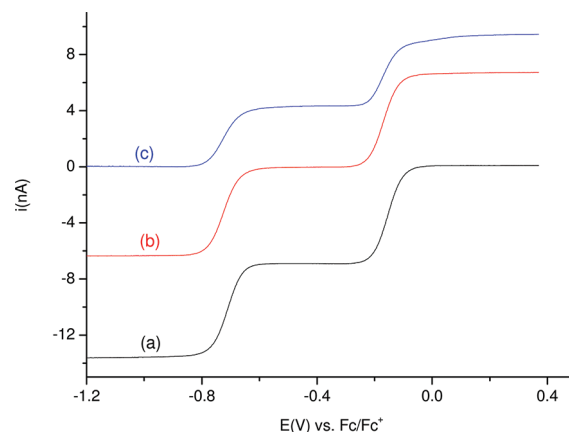


Figure 1. Linear sweep near-steady-state voltammograms at a Pt microdisk electrode ($r = 5 \mu\text{m}$, scan rate = 20 mV s^{-1}) in acetonitrile (0.1 M Bu_4NPF_6) containing 2.15 mM TCNQ (a) before electrolysis, (b) after reductive bulk electrolysis of TCNQ at -400 mV to generate $\text{TCNQ}^{\bullet-}$, and (c) after reductive bulk electrolysis of $\text{TCNQ}^{\bullet-}$ at -1000 mV to generate TCNQ^{2-} .

heterogeneous electron transfer rate constant, α is the electron transfer coefficient, and A and B represent TCNQ, $\text{TCNQ}^{\bullet-}$, or TCNQ^{2-} as appropriate.

RESULTS

Near-Steady-State Voltammetry at a Microdisk Electrode.

Since the $\text{TCNQ}^{0/\bullet-}$ and $\text{TCNQ}^{\bullet-/2-}$ reactions occur at an electrode–solution interface, both mass transport and heterogeneous electrode kinetics play a key role.¹⁹ In order to evaluate the electrode kinetics, it is therefore important to accurately quantify the diffusivity. The diffusion coefficients for TCNQ, $\text{TCNQ}^{\bullet-}$, and TCNQ^{2-} were determined from limiting current values derived from near-steady-state voltammograms using a $10 \mu\text{m}$ diameter Pt microdisk electrode and eq 4. Solutions of 2.15 mM $\text{TCNQ}^{\bullet-}$ and TCNQ^{2-} were obtained by quantitative reduction of 2.15 mM TCNQ using controlled potential bulk electrolysis at -400 and -1000 mV , respectively, vs Fc/Fc^+ combined with coulometric analysis. Steady-state voltammograms also were obtained before and after bulk electrolysis. Figure 1 contains those for TCNQ, $\text{TCNQ}^{\bullet-}$ (after bulk electrolysis of TCNQ to $\text{TCNQ}^{\bullet-}$), and TCNQ^{2-} (after electrolysis of $\text{TCNQ}^{\bullet-}$ to TCNQ^{2-}). The steady-state voltammogram obtained when TCNQ^{2-} was quantitatively oxidized back to TCNQ is indistinguishable from voltammogram a in Figure 1. This implies that each of TCNQ and its reduced forms are stable under drybox conditions, as is needed for the electrode kinetics studies.

Diffusion coefficients calculated from the near-steady-state diffusion controlled limiting current at Pt microdisk electrode and use of eq 4 were found to be 1.66×10^{-5} , 1.47×10^{-5} , and $1.05 \times 10^{-5} \text{ cm}^2 \text{ s}^{-1}$ for TCNQ, $\text{TCNQ}^{\bullet-}$, and TCNQ^{2-} , respectively, and in good agreement with values of $(1.44 \pm 0.03) \times 10^{-5}$, $(1.35 \pm 0.05) \times 10^{-5}$, and $(0.91 \pm 0.04) \times 10^{-5} \text{ cm}^2 \text{ s}^{-1}$ for TCNQ, $\text{TCNQ}^{\bullet-}$, and TCNQ^{2-} reported by Zhou and Evans for these three species.¹

Cyclic Voltammetry. Diffusion coefficients of $(1.65 \pm 0.04) \times 10^{-5} \text{ cm}^2 \text{ s}^{-1}$ (TCNQ), $(1.45 \pm 0.04) \times 10^{-5} \text{ cm}^2 \text{ s}^{-1}$ ($\text{TCNQ}^{\bullet-}$), and $(0.90 \pm 0.03) \times 10^{-5} \text{ cm}^2 \text{ s}^{-1}$ (TCNQ^{2-})

were calculated from the peak currents of dc voltammograms obtained from the GC macrodisk electrode (Figure 2) over the scan rate range of 100 mV s^{-1} to 1.0 V s^{-1} using eq 3. These values agree well with those obtained from the Pt microdisk electrode experiments.

Fourier Transformed Large Amplitude ac Voltammetry of TCNQ as a Function of Concentration. Fourier transformed large amplitude ac voltammetric experiments were carried out using a sine wave with an amplitude (ΔE) of 80 mV and frequency (f) of 9.0 Hz superimposed onto a dc waveform having a scan rate of 100 mV s^{-1} . Both the $\text{TCNQ}^{0/+}$ and $\text{TCNQ}^{•-/2-}$ processes are chemically and electrochemically reversible on the dc time scale. Comparison of experimental data and those predicted by digital simulations were used to assess the kinetics. It was assumed that the electrode area, concentration, uncompensated resistance, and diffusion coefficients of TCNQ , $\text{TCNQ}^{•-}$, and TCNQ^{2-} were accurately known, so that parameters varied in the simulations were the reversible potential (E^0), heterogeneous electron transfer kinetics (k^0), charge transfer coefficient (α), and double layer capacitance (C_{dl}). E^0 values were determined experimentally from dc cyclic voltammograms from the average of the reduction and oxidation peak potentials and from lower harmonic components (peak potential of fundamental and potential of minimal current between the two peaks in the second harmonic); all were found to be in excellent agreement. Capacitance was assessed from the fundamental harmonic in potential regions where no ac Faradaic current is present (either side of peak), while k^0 values were initially estimated from “best” fits of simulated and experimental data derived from the higher harmonic components which are more sensitive to variation in k^0 . Simulations are very insensitive to variation in α when a process is close to the reversible limit, which implies that α cannot be determined from the TCNQ electrochemistry. The charge transfer coefficient α was arbitrarily set as 0.50.

Since uncompensated resistance in the form of iR_u (Ohmic) drop has a significant effect on the characteristics of the nonlinear components of large amplitude ac voltammograms, voltammetric data were analyzed at three different TCNQ concentrations of 3.50, 1.93, and 0.36 mM in order to vary the effect of iR_u drop from significant (3.50 mM) to negligible (0.36 mM). Resulting data were compared with simulated ones up to the eighth harmonic. Parameters used for simulations of all FT ac data are summarized in Tables 2 and 3. The value of R_u is smaller when Pt was used as the working electrode, predominantly because its electrode area is larger than that of the GC electrode. The R_u value varied slightly from experiment to experiment even though the same working electrode was used. This occurs because the distances between working and reference electrodes varied slightly.

Initial experiments were conducted in acetonitrile (0.1 M Bu_4NPF_6) containing 1.93 mM TCNQ at both GC and Pt electrodes. Voltammograms for the $\text{TCNQ}^{0/+}$ reduction process at a GC electrode are displayed in Figure 3. Simulations using a k^0 value of 0.30 cm s^{-1} and other parameters in Table 2 provide excellent agreement with experiment for all eight harmonics (Figure 3). If both electron transfer $\text{TCNQ}^{0/+}$ and $\text{TCNQ}^{•-/2-}$ processes (involving $\text{TCNQ}^{0/+}$ and $\text{TCNQ}^{•-/2-}$) were recorded simultaneously at the GC electrode and experimentally determined diffusion coefficient values for TCNQ neutral, monoanion, and dianion and other parameters summarized in Table 3 were used in the simulations, then experimental data were in good agreement with simulations using k^0 values of 0.29 and 0.28 cm s^{-1} for the $\text{TCNQ}^{0/+}$ and $\text{TCNQ}^{•-/2-}$ processes, respectively (Figure S1 in the Supporting Information). In all

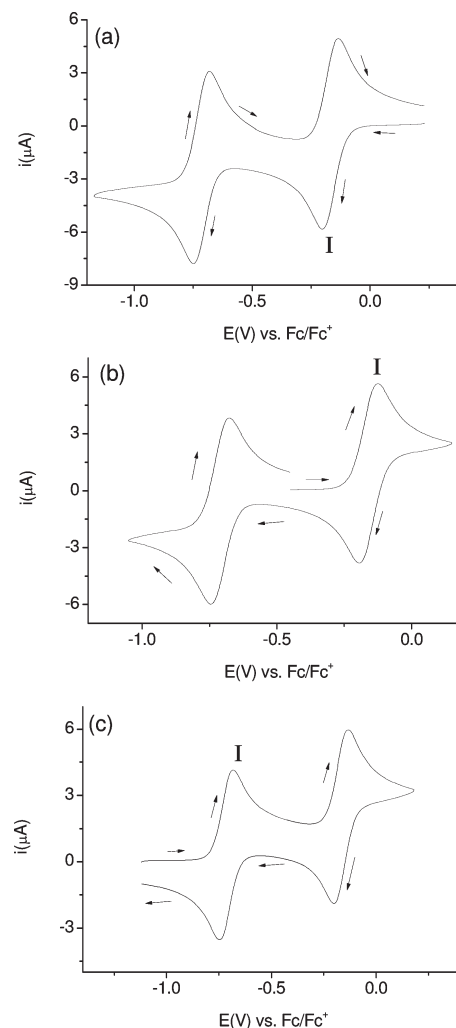


Figure 2. Cyclic voltammograms obtained at a GC electrode with a scan rate of 100 mV s^{-1} in acetonitrile (0.1 M Bu_4NPF_6) for 2.15 mM (a) TCNQ, (b) $\text{TCNQ}^{•-}$, and (c) TCNQ^{2-} . Note the initial potentials are set at 0.23, -0.45 , and -1.1 V , so the experiment commences in a potential region where no Faradaic current is present.

these simulations, the cross redox reaction, $\text{TCNQ} + \text{TCNQ}^{•-} \rightleftharpoons 2\text{TCNQ}^{•-}$, was neglected.

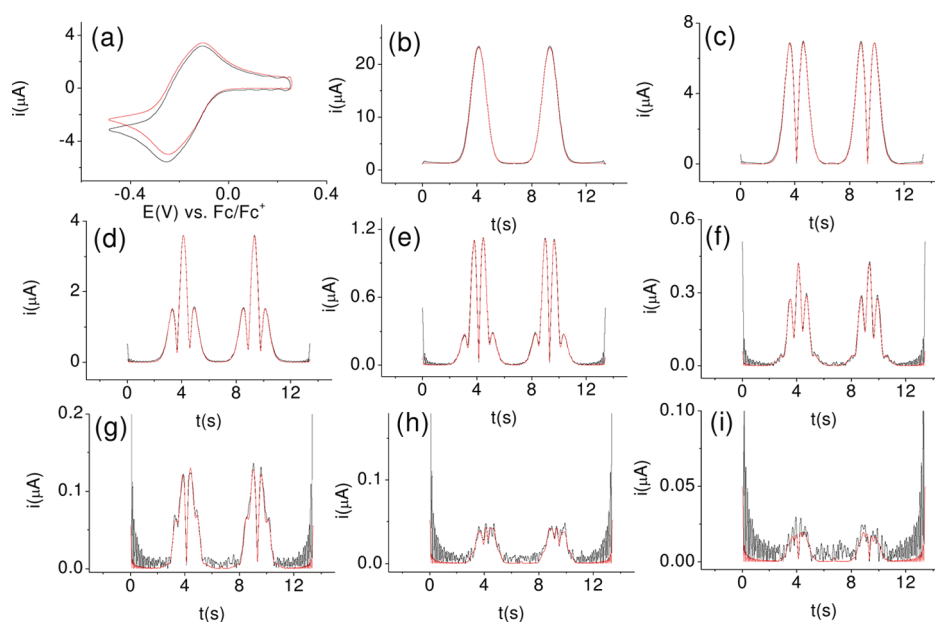
Voltammograms obtained at Pt electrode were also simulated and compared with ac harmonics obtained from the one-electron $\text{TCNQ}^{0/+}$ reduction alone and with both $\text{TCNQ}^{0/+}$ and $\text{TCNQ}^{•-/2-}$ reduction processes measured in the same experiment. In this case, simulations with k^0 values of 0.32 and 0.26 cm s^{-1} , respectively, for the $\text{TCNQ}^{0/+}$ and $\text{TCNQ}^{•-/2-}$ processes were in excellent agreement with experimental data (Figure 4 and Figure S2 in the Supporting Information). Experimental and simulated voltammograms for 0.36 and 3.50 mM TCNQ at GC and Pt are compared in the Supporting Information (Figures S3–S10). Electrode kinetics data in Tables 2 and 3 suggest that k^0 values are essentially independent of concentration. In the protocol used in this study, an initial guess of $k^0 = 0.03 \text{ cm s}^{-1}$ was made to comply with some literature estimates (Table 1), but experimental currents were much larger than predicted. Increasingly larger k^0 values were then introduced until shapes and current magnitudes for all harmonics agreed very well with the experimental results. A crucial assessment as to whether k^0 values collected in

Table 2. Parameters Used^a to Simulate the Reduction of TCNQ to TCNQ^{•−}

electrode	C (mM)	R _u (ohm)	C _{dl} (μF cm ^{−2})	A (cm ²)	k ⁰ (cm s ^{−1})	E ⁰ (V) vs Fc ^{0/+}	α
GC	3.50	420	25	0.00875	0.33	−0.170	0.50
	1.93	470	32	0.00875	0.30	−0.170	0.50
	0.36	450	28	0.00875	0.30	−0.170	0.50
Pt	3.50	300	17	0.022	0.29	−0.170	0.50
	1.93	240	15	0.022	0.33	−0.170	0.50
	0.36	220	20	0.022	0.33	−0.170	0.50

^a Other parameters are as defined in the text.**Table 3.** Parameters Used^a to Simulate the Consecutive Reduction of TCNQ to TCNQ^{•−} and TCNQ^{•−} to TCNQ^{2−}

electrode	C (mM)	R _u (ohm)	C _{dl} (μF cm ^{−2})	A (cm ²)	TCNQ ^{0/+−}		TCNQ ^{•−/2−}		α
					k ⁰ (cm s ^{−1})	E ⁰ (V) vs Fc ^{0/+}	k ⁰ (cm s ^{−1})	E ⁰ (V) vs Fc ^{0/+}	
GC	3.50	450	31	0.00875	0.32	−0.170	0.30	−0.715	0.50
	1.93	470	26	0.00875	0.29	−0.170	0.28	−0.715	0.50
	0.36	470	32	0.00875	0.32	−0.170	0.30	−0.715	0.50
Pt	3.50	315	15	0.022	0.32	−0.170	0.26	−0.715	0.50
	1.93	250	15	0.022	0.32	−0.170	0.26	−0.715	0.50
	0.36	250	23	0.022	0.32	−0.170	0.29	−0.715	0.50

^a Other parameters are as defined in the text.**Figure 3.** Comparison of simulated (red lines) and experimental (black lines) Fourier transformed large amplitude ac voltammograms for the one-electron TCNQ^{0/+−} reduction of 1.93 mM TCNQ in acetonitrile (0.1 M Bu₄NPF₆) at a GC electrode: (a) dc component; (b) first harmonic; (c) second harmonic; (d) third harmonic; (e) fourth harmonic; (f) fifth harmonic; (g) sixth harmonic; (h) seventh harmonic; (i) eighth harmonic. Other parameters are as defined in the text.

this manner represent absolute values or a lower limit will be provided later.

Fourier Transformed Large Amplitude ac Voltammetry of TCNQ^{•−}. In principle, the cross redox reaction, TCNQ + TCNQ^{2−} ⇌ 2TCNQ^{•−}, should be included in simulations of the TCNQ^{•−/2−} process derived from experimental data when TCNQ is present in the bulk solution. However, this would add to the complexity of the simulation and introduce unknown

parameters. As an alternative approach, we chose to analyze data obtained under conditions where this reaction is strictly absent; if the TCNQ^{•−/2−} reduction process and TCNQ^{•−/0} oxidation processes are investigated with TCNQ^{•−} rather than TCNQ or TCNQ^{2−} in the bulk solution, then by definition the cross redox reaction cannot occur.

A solution of 1.93 mM TCNQ^{•−} in acetonitrile (0.1 M Bu₄NPF₆) was obtained by bulk electrolysis of TCNQ at −400 mV vs Fc/Fc⁺.

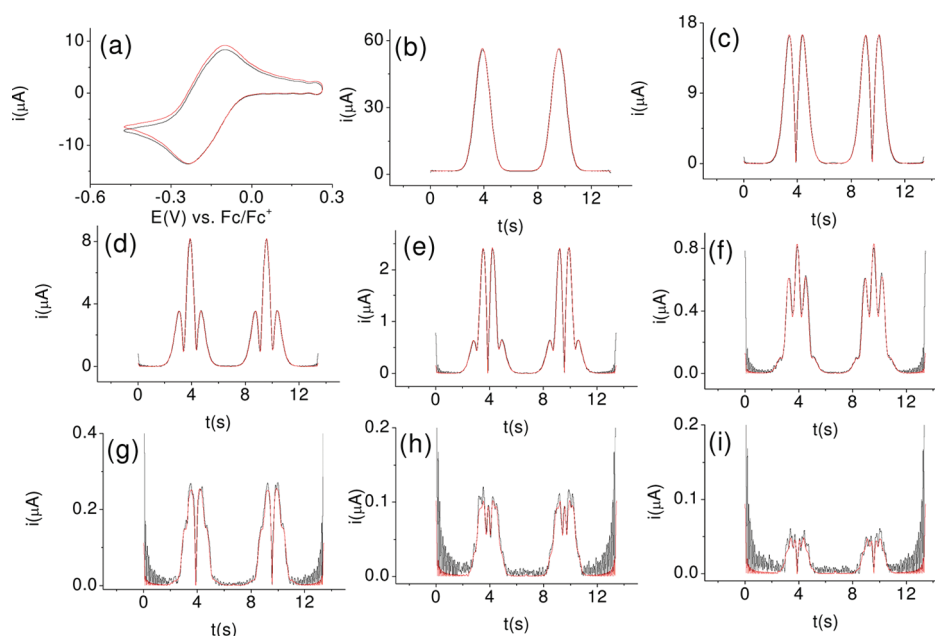


Figure 4. Comparison of simulated (red lines) and experimental (black lines) Fourier transformed large amplitude ac voltammograms for the one-electron $\text{TCNQ}^{0/+}$ reduction of 1.93 mM TCNQ in acetonitrile (0.1 M Bu_4NPF_6) at a Pt electrode: (a) dc component; (b) first harmonic; (c) second harmonic; (d) third harmonic; (e) fourth harmonic; (f) fifth harmonic; (g) sixth harmonic; (h) seventh harmonic; (i) eighth harmonic. Other parameters are as defined in the text.

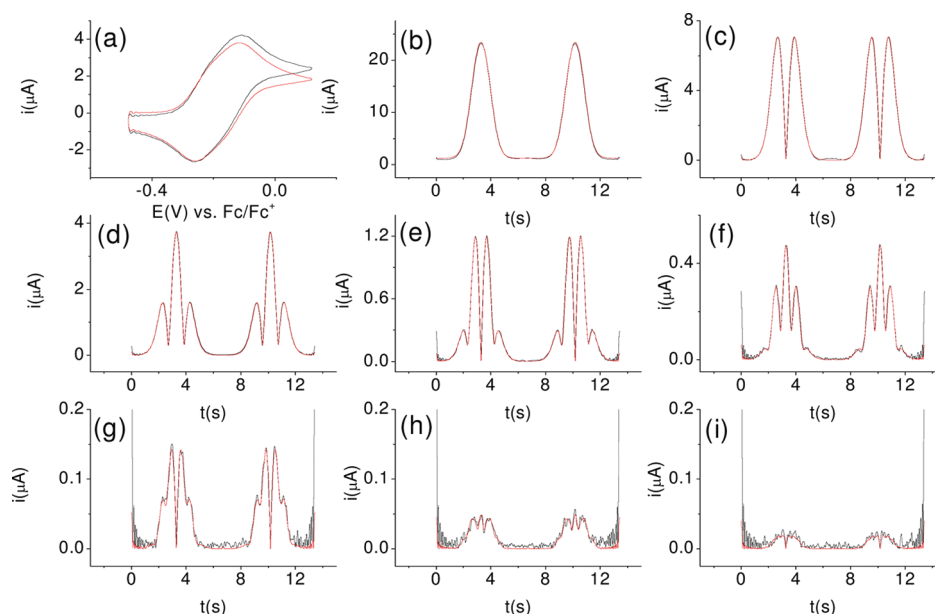


Figure 5. Comparison of simulated (red lines) and experimental (black lines) Fourier transformed large amplitude ac voltammograms obtained for the one-electron $\text{TCNQ}^{+/-}$ oxidation of 1.93 mM $\text{TCNQ}^{+/-}$ solution in acetonitrile (0.1 M Bu_4NPF_6) at a GC electrode: (a) dc component; (b) first harmonic; (c) second harmonic; (d) third harmonic; (e) fourth harmonic; (f) fifth harmonic; (g) sixth harmonic; (h) seventh harmonic; (i) eighth harmonic. Other parameters are as defined in the text.

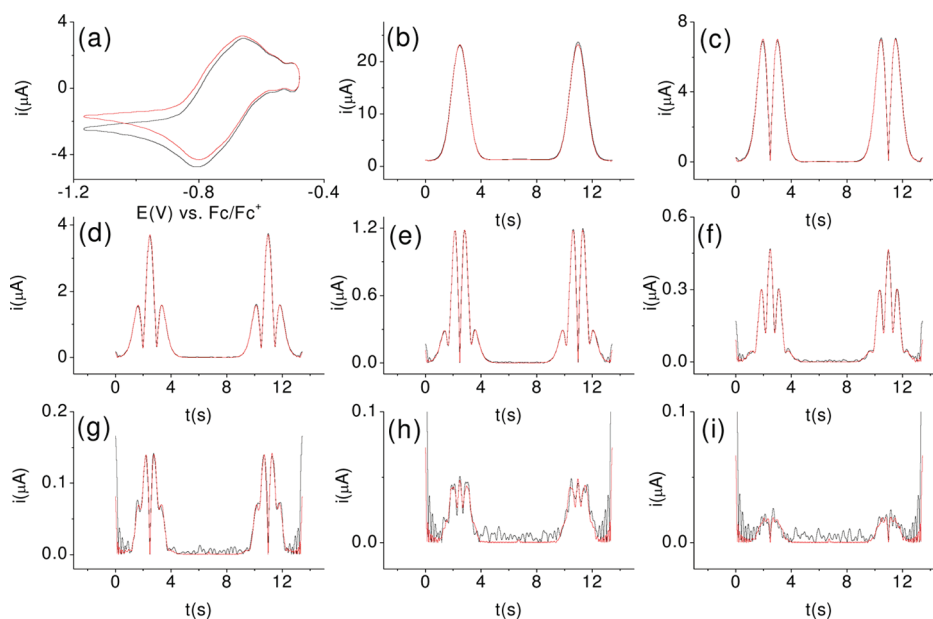
Figure 5 shows the experimental results compared with simulated ones for oxidation of 1.93 mM $\text{TCNQ}^{+/-}$ to TCNQ . Simulations using a k^0 value of 0.30 cm s^{-1} and other parameters given in Table 4 are in excellent agreement with the experimental results. The experimental and simulated comparisons for reduction of 1.93 mM $\text{TCNQ}^{+/-}$ to TCNQ^{2-} are presented in Figure 6. Simulations using k^0 values of 0.30 cm s^{-1} for

the reduction of $\text{TCNQ}^{+/-}$ to TCNQ^{2-} and other parameters in Table 5 also agree well with the experimental results.

The analogous experiments for oxidation and reduction of $\text{TCNQ}^{+/-}$ were also conducted at a Pt electrode. The results (Figures S11 and S12 in the Supporting Information) again lead to k^0 values of 0.30 cm s^{-1} for both reduction and oxidation of $\text{TCNQ}^{+/-}$.

Table 4. Parameters Used^a to Simulate the Oxidation of TCNQ^{•−} to TCNQ

electrode	C (mM)	R _u (ohm)	C _{dl} (μF cm ^{−2})	A (cm ²)	k ⁰ (cm s ^{−1})	E ⁰ (V) vs Fc ^{0/+}	α
GC	1.93	410	30	0.00875	0.30	−0.172	0.50
	0.31	310	24	0.00875	0.29	−0.172	0.50
Pt	1.93	310	22	0.022	0.30	−0.172	0.50
	0.31	300	15	0.022	0.30	−0.172	0.50

^a Other parameters are as defined in the text.**Figure 6.** Comparison of simulated (red lines) and experimental (black lines) Fourier transformed large amplitude ac voltammograms obtained for the one-electron TCNQ^{•−/2−} reduction of 1.93 mM TCNQ^{•−} solution in acetonitrile (0.1 M Bu₄NPF₆) at a GC electrode: (a) dc component; (b) first harmonic; (c) second harmonic; (d) third harmonic; (e) fourth harmonic; (f) fifth harmonic; (g) sixth harmonic; (h) seventh harmonic; (i) eighth harmonic. Other parameters are as defined in the text.**Table 5. Parameters Used^a to Simulate the Reduction of TCNQ^{•−} to TCNQ^{2−}**

electrode	C (mM)	R _u (ohm)	C _{dl} (μF cm ^{−2})	A (cm ²)	k ⁰ (cm s ^{−1})	E ⁰ (V) vs Fc ^{0/+}	α
GC	1.93	420	27	0.00875	0.30	−0.715	0.50
	0.31	400	23	0.00875	0.29	−0.715	0.50
Pt	1.93	350	20	0.022	0.30	−0.715	0.50
	0.31	386	27	0.022	0.30	−0.715	0.50

^a Other parameters are as defined in the text.

Voltammetric data were also acquired with a lower 0.31 mM concentration of TCNQ^{•−} to decrease the effect of uncompensated resistance. The results at GC and Pt electrodes are summarized in Tables 4 and 5 and Figures S13–S16 in the Supporting Information and again are consistent with a k^0 value of 0.3 cm s^{−1} for both processes.

In the case of TCNQ^{•−} oxidation to TCNQ, all data show that a k^0 value of 0.30 ± 0.05 cm s^{−1} is obtained at both Pt and GC electrodes. The ± 0.05 cm s^{−1} uncertainty associated with this k^0 value was estimated from six parallel experiments. However, this uncertainty of ± 0.05 cm s^{−1} in this and for all other k^0 determinations only reflects the reproducibility of the kinetic measurements under our experimental conditions. As discussed later, larger uncertainty could be introduced from systematic error associated with uncertainties in the diffusion

coefficient, electrode area, or other parameters employed in the simulations. The fact that the reduction TCNQ^{0/•−} and oxidation TCNQ^{•−/0} reactions share the same k^0 value (at the reversible potential E^0) within experimental uncertainty is totally expected on the basis of the Butler–Volmer relationship.

For the TCNQ^{•−/2−} reduction process (Tables 4 and 5) the same situation prevails with a k^0 value of 0.30 ± 0.05 cm s^{−1} being obtained at the two concentrations of TCNQ^{•−} and at both Pt and GC electrodes, and hence mimics the outcome found when TCNQ is in bulk solution. This implies that the contribution of the cross redox reaction to the voltammetric response when TCNQ is reduced consecutively to TCNQ^{•−} and then to TCNQ^{2−} is insignificant with respect to the determination of the electrode kinetics.

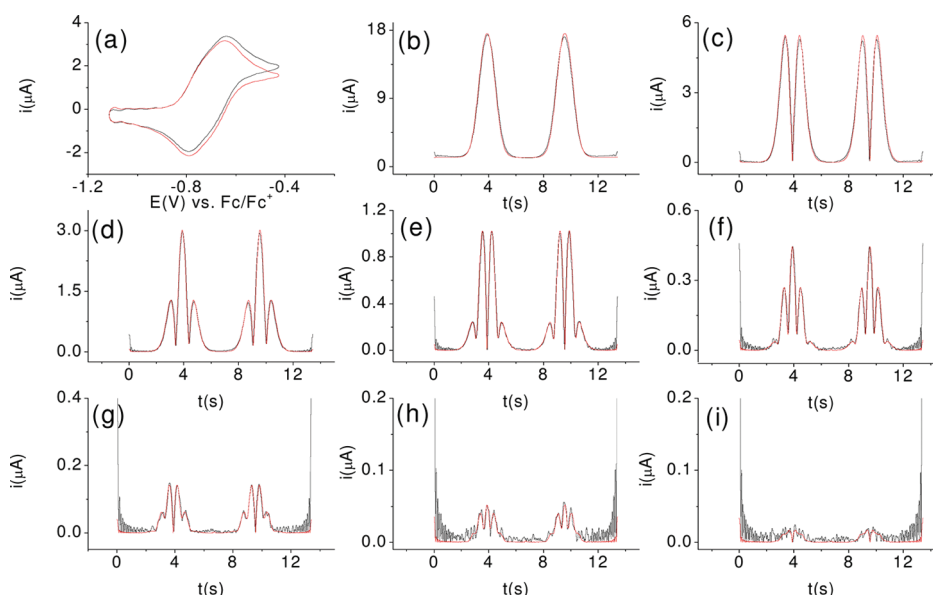


Figure 7. Comparison of simulated (red lines) and experimental (black lines) Fourier transformed large amplitude ac voltammograms obtained for the one-electron $\text{TCNQ}^{2-/\bullet-}$ oxidation of 1.70 mM TCNQ^{2-} in acetonitrile (0.1 M Bu_4NPF_6) at a GC electrode: (a) dc component; (b) first harmonic; (c) second harmonic; (d) third harmonic; (e) fourth harmonic; (f) fifth harmonic; (g) sixth harmonic; (h) seventh harmonic; (i) eighth harmonic. Other parameters are as defined in the text.

Table 6. Parameters Used^a to Simulate the Oxidation of TCNQ^{2-} to $\text{TCNQ}^{\bullet-}$

electrode	C (mM)	R_u (ohm)	C_{dl} ($\mu\text{F cm}^{-2}$)	A (cm^2)	k^0 (cm s^{-1})	E^0 (V) vs $\text{Fc}^{0/+}$	α
GC	1.70	420	31	0.00875	0.28	−0.710	0.50
	0.33	350	34	0.00875	0.28	−0.710	0.50
Pt	1.70	325	31	0.022	0.30	−0.710	0.50
	0.33	300	28	0.022	0.30	−0.710	0.50

^a Other parameters are as defined in the text.

Fourier Transformed Large Amplitude ac Voltammetry of TCNQ^{2-} . The initial set of experiments were conducted at the GC and Pt electrodes in acetonitrile (0.1 M Bu_4NPF_6) containing 1.70 and 0.33 mM TCNQ^{2-} generated by bulk reductive electrolysis of 1.70 mM TCNQ at −1100 mV. FT ac voltammograms for the $\text{TCNQ}^{2-/\bullet-}$ oxidation at a GC electrode are shown in Figure 7. Simulations using a k^0 value of 0.28 cm s^{-1} and other parameters in Table 6 provide excellent agreement with experiment for all eight harmonics (Figure 7). Simultaneous measurements of both the $\text{TCNQ}^{0/\bullet-}$ and $\text{TCNQ}^{\bullet-/2-}$ oxidation processes at a GC electrode could successfully be simulated (Figure S17 in the Supporting Information) with a k^0 value of 0.30 cm s^{-1} (Table 6). Again, the cross redox reaction, $\text{TCNQ} + \text{TCNQ}^{2-} \rightleftharpoons 2\text{TCNQ}^{\bullet-}$, was neglected in these simulations. Voltammetric experiments were also conducted for oxidation of 1.70 mM TCNQ^{2-} at a Pt electrode. Simulations with a k^0 value of 0.30 cm s^{-1} for both the $\text{TCNQ}^{2-/\bullet-}$ and $\text{TCNQ}^{\bullet-/0}$ processes concur with experimental data (Figures S18 and S19 in the Supporting Information).

Kinetic data obtained from voltammetric experiments conducted with the lower 0.33 mM concentration of TCNQ^{2-} are summarized in Tables 6 and 7. A k^0 value of $0.30 \pm 0.05 \text{ cm s}^{-1}$ is obtained with either 1.70 or 0.33 mM concentration of TCNQ^{2-} at both Pt and GC electrodes and agrees well with those obtained from reduction of $\text{TCNQ}^{\bullet-}$ to TCNQ^{2-} with either TCNQ (Table 3) or $\text{TCNQ}^{\bullet-}$ (Table 5) as the precursor present in bulk

solution. Comparison of experimental and simulated data for 0.33 mM TCNQ^{2-} is presented in Figures S20–S23 in the Supporting Information.

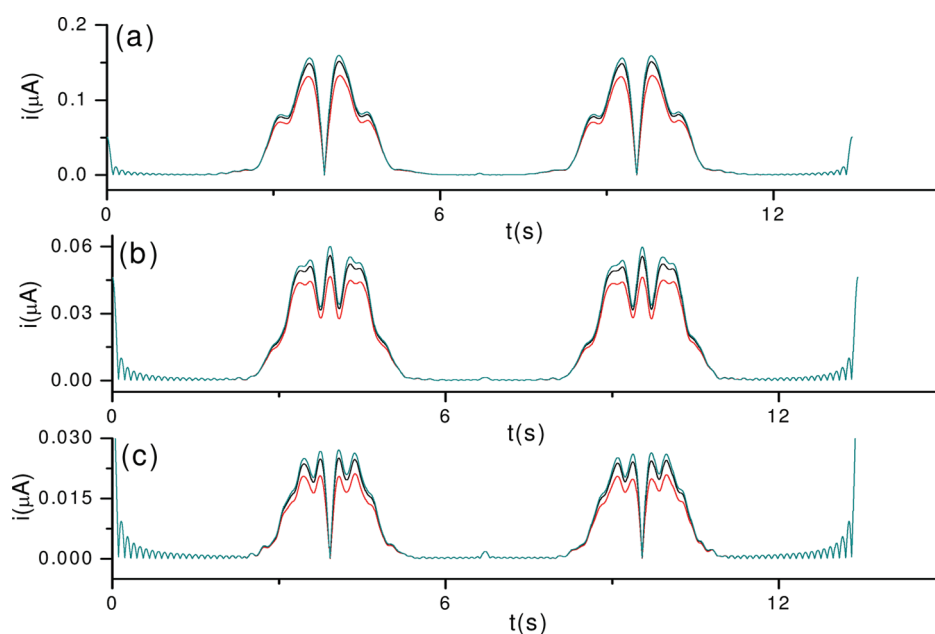
In the case of the oxidation of $\text{TCNQ}^{\bullet-}$ to TCNQ_0 with TCNQ^{2-} as the precursor, a k^0 value of $0.30 \pm 0.05 \text{ cm s}^{-1}$ is again obtained under all conditions and is essentially the same as that obtained for this process when $\text{TCNQ}^{\bullet-}$ is used as the precursor (Table 4) as well as that found for reduction of TCNQ to $\text{TCNQ}^{\bullet-}$ (Tables 2 and 3). The fact that the k^0 value that applies at E^0 is independent of the initial species present in solution is again totally consistent with predictions based on the Butler–Volmer relationship. Comparison of k^0 data from the different studies involving oxidation of TCNQ^{2-} to TCNQ again confirms that the impact of the cross reaction on the voltammetric response is insignificant with respect to electrode kinetic determinations for this process.

DISCUSSION

Comparison of k^0 Value for the $\text{TCNQ}^{0/\bullet-}$ Process with Literature Values. The k^0 value determined in this study for the $\text{TCNQ}^{0/\bullet-}$ process is $0.30 \pm 0.05 \text{ cm s}^{-1}$ at both Pt and GC electrodes and hence is very comparable to that of 0.2 cm s^{-1} reported by Sharp in the same electrolyte media at a Pt electrode using fast scan dc cyclic voltammetry with iR_u compensation.^{2b} According to Sharp,^{2b} the activation energy calculated using the

Table 7. Parameters Used^a to Simulate the Consecutive Oxidation of TCNQ²⁻ to TCNQ^{•-} and TCNQ^{•-} to TCNQ

electrode	C (mM)	R_u (ohms)	C_{dl} ($\mu\text{F cm}^{-2}$)	A (cm^2)	TCNQ ^{2-/•-}		TCNQ ^{•-/0}		α
					k^0 (cm s^{-1})	E^0 (V) vs $\text{Fc}^{0/+}$	k^0 (cm s^{-1})	E^0 (V) vs $\text{Fc}^{0/+}$	
GC	1.70	375	28	0.00875	0.3	0.710	0.30	-0.174	0.50
	0.33	350	32	0.00875	0.3	0.710	0.30	-0.174	0.50
Pt	1.70	325	28	0.022	0.3	0.710	0.30	-0.174	0.50
	0.33	300	32	0.022	0.28	0.710	0.30	-0.174	0.50

^a Other parameters are as defined in the text.**Figure 8.** Simulated Fourier transformed large amplitude ac voltammograms using parameters that apply to the reduction of 2.15 mM TCNQ in acetonitrile (0.1 M Bu_4NPF_6) at a GC electrode with k^0 values of 0.3 (red lines) and 1.0 cm s^{-1} (black lines) and a reversible process (light blue lines): (a) sixth harmonic; (b) seventh harmonic; (c) eighth harmonic. $R_u = 450 \text{ ohm}$, $D_{\text{TCNQ}} = 1.65 \times 10^{-5} \text{ cm}^2 \text{ s}^{-1}$, $D_{\text{TCNQ}^{\bullet-}} = 1.45 \times 10^{-5} \text{ cm}^2 \text{ s}^{-1}$, $C_{dl} = 20 \mu\text{F cm}^{-2}$, $A = 0.00875 \text{ cm}^2$.

k^0 values reported in his work agreed well with predictions based on Marcus theory.²⁰

The value of 0.30 cm s^{-1} obtained in this FT ac voltammetric study, at first glance, appears to be significantly lower than the value of 1.1 cm s^{-1} reported by Sun and Mirkin^{5a} from the steady-state voltammetry at a Pt nanoelectrode. However, detailed analysis of systematic error present in both data sets suggests that k^0 values are probably in agreement within experimental uncertainties. The finding that the calculated k^0 of $0.30 \pm 0.05 \text{ cm s}^{-1}$ is insensitive to the presence of the cross redox reaction is consistent with the electrode kinetics being very close to reversible limit or the upper level of detection. This scenario also has been recognized in dc voltammetry.²¹ Consequently, simulations were performed to find out how close the measured k^0 value approaches the upper limit measurable by large amplitude FT ac voltammetry with the D values and the impact of iR_u drop encountered in our measurements. Three cases were considered: (a) 0.3 cm s^{-1} (represents the k^0 value measured in this study), (b) 1.0 cm s^{-1} (represents close to the k^0 value for $\text{TCNQ}^{0/\bullet-}$ process reported by Mirkin),^{5a} and (c) a fully reversible case using the D value of $1.65 \times 10^{-5} \text{ cm}^2 \text{ s}^{-1}$ determined in this study for TCNQ. No distinction within experimental error is available in these simulations for $k^0 = 0.3$

and 1 cm s^{-1} as a reversible process with the aperiodic dc component, and measurable differences are also not available in the initial ac harmonics (first–fourth). However, in progressing to the fifth harmonic onward, significant distinctions in simulations based on k^0 values of 0.3 and 1 cm s^{-1} emerge (Figure 8). However, ultimately the distinction in outcome of simulations is confined to differences in current magnitude which requires that D , A , and R_u need to be accurately known, if k^0 is to be reliably estimated.

Differences in simulation with k^0 values of 0.30 and 1.0 cm s^{-1} were also observed in the higher harmonic components when a smaller diffusion coefficient of $0.9 \times 10^{-5} \text{ cm}^2 \text{ s}^{-1}$ was employed (representing the value found in the case of TCNQ^{2-}). However, the differences are now compressed; thus a k^0 value of 0.30 cm s^{-1} is even closer to the limit of detection when the D value is $0.9 \times 10^{-5} \text{ cm}^2 \text{ s}^{-1}$. Similarly, discrimination is enhanced when a larger diffusion coefficient value of $1.98 \times 10^{-5} \text{ cm}^2 \text{ s}^{-1}$ (value for TCNQ used by Mirkin) was used in the simulations.^{5a} This analysis raises the question as to whether the k^0 value of 0.3 cm s^{-1} obtained in this study and that of 1.1 cm s^{-1} by Mirkin actually differ within experimental uncertainties, particularly given the difference in the diffusion coefficient for TCNQ used in this ($1.65 \times 10^{-5} \text{ cm}^2 \text{ s}^{-1}$) and Mirkin's ($1.98 \times 10^{-5} \text{ cm}^2 \text{ s}^{-1}$) studies. Translation of combinations of parameters into a

dimensionless rate constant provides a clearer indication of the factors that affect the ability to reliably measure a k^0 value near the reversible limit. In our study, the dimensionless electron transfer rate constant can be written as $k^0/(fD)^{1/2}$, whereas in Mirkin's study the dimensionless form can be formulated as k^0r/D . Arguably, the apparently higher k^0 value reported by Mirkin can be attributed to the use of a higher diffusion coefficient in theory versus experiment comparisons. In our study D , R_w and A as well as k^0 determine the current magnitude used to estimate k^0 . In the Mirkin study, uncertainties in electrode radius and D contribute to systematic error. Thus, despite the apparently substantial numerical difference (factor of nearly 4), we conclude the k^0 values determined in the two studies probably agree within experimental uncertainties associated with systematic error.

In kinetics measurements employing the widely used dc voltammetric techniques, either the difference of quartile wave and half wave potentials (steady-state techniques) or peak to peak separations (transient techniques) are commonly employed to extract the dimensionless kinetics. This method of data analysis, although simple, is essentially a "two-point" analysis method. In contrast, our method is a global method of data analysis where essentially all data are utilized. In our case, we derive k^0 estimates by obtaining the "best fit" of our experimental results with the simulated data using all harmonics (peak heights, wave shapes, and other voltammetric features are taken into account). This minimizes uncertainties in the electrode area, diffusion coefficient, and concentration, noting that concentration and electrode area influence the voltammetric characteristics in a distinctly different way from the effect of diffusion coefficient, unless the electrochemical process is fully reversible.

Comparison of k^0 Value Obtained at GC and Pt Electrodes. Very similar k^0 values are obtained from both GC and Pt electrodes in this TCNQ study, even though the density of states for Pt is much higher than that of carbon, which might lead to the expectation of a lower rate at glassy carbon.^{2b,22} This observation of electrode independence concurs with a previous report by Sharp with respect to Pt and Au electrodes.^{2b} This failure to detect an electrode dependence suggests that the electrochemical reduction of TCNQ is an adiabatic process on the basis of Marcus theory.^{20,23} However, caution is needed as our values have not been corrected for double layer effects, which are expected to be different at Pt and GC electrodes. Furthermore, even if the TCNQ processes are not fully adiabatic so that k^0 at Pt would be expected to be greater than k^0 at GC on the basis of density of states arguments,²³ we may not be able to distinguish any difference since k^0 is being detected very near the limit of detection since uncertainty from systematic error in the absolute values is likely to be substantial in this kinetic regime.

CONCLUSIONS

The use of kinetically sensitive large amplitude FT ac cyclic voltammetry for the determination of electrode kinetics associated with $\text{TCNQ}^{0/+}$ and $\text{TCNQ}^{•-/-}$ processes in acetonitrile produces an estimate of k^0 values of about $0.30 \pm 0.05 \text{ cm s}^{-1}$ at both GC and Pt electrodes. This electrode independence is consistent with TCNQ electron transfer processes being fully adiabatic, although since the kinetic evaluation occurs very near the limit of the ability to distinguish from a reversible process, the absolute values contain significant uncertainty arising from systematic error. In principle, the application of higher frequency ac perturbations may be useful in improving the accuracy of the

measurement of fast kinetics. However, this approach will also lead to enhanced contributions from both R_u and capacitance, and hence is unlikely to increase the upper limit of measurement of k^0 significantly, if at all.

ASSOCIATED CONTENT

S Supporting Information. Section I shows the comparison of simulated and experimental files for reduction of 1.93, 3.50, and 0.36 mM TCNQ at Pt and GC in Figures S1–S10. Section II comprises experiment and theory comparisons for oxidation ($\text{TCNQ}^{•-/0}$) and reduction ($\text{TCNQ}^{•-/2-}$) for 1.93 and 0.31 mM TCNQ $^{•-}$ at GC and Pt electrodes in Figures S11–S16. A similar comparison is provided at both electrodes for oxidation of 1.70 and 0.33 mM TCNQ $^{2-/+}$ in Figures S17–S23 of section III. This material is available free of charge via the Internet at <http://pubs.acs.org>.

AUTHOR INFORMATION

Corresponding Author

*E-mail: jie.zhang@monash.edu (J.Z.); alan.bond@monash.edu (A.M.B.). Telephone: +61 3 9905 6289 (J.Z.); +61 3 9905 1338 (A.M.B.). Fax: +61 3 9905 4597 (J.Z.); +61 3 9905 4597 (A.M.B.).

ACKNOWLEDGMENT

J.Z. and A.M.B. would like to thank the Australian Research Council for financial support. K.B. acknowledges the awards of Monash University Science Faculty Dean's Postgraduate Research Scholarship and an International Research Support Initiative Program Scholarship from Higher Education Commission, Pakistan.

REFERENCES

- (1) Zhou, R.; Evans, D. H. *J. Electroanal. Chem.* **1995**, 385, 201.
- (2) (a) Sharp, M. *Electrochim. Acta* **1976**, 21, 973. (b) Sharp, M. *J. Electroanal. Chem.* **1978**, 88, 193.
- (3) Khoo, S. B.; Foley, J. K.; Pons, S. *J. Electroanal. Chem.* **1986**, 215, 273.
- (4) Russell, A.; Repka, K.; Dibble, T.; Ghoroghchian, J.; Smith, J. J.; Fleischmann, M.; Pitt, C. H.; Pons, S. *Anal. Chem.* **1986**, 58, 2961.
- (5) (a) Sun, P.; Mirkin, M. V. *Anal. Chem.* **2006**, 78, 6526. (b) Velmurugan, J.; Sun, P.; Mirkin, M. V. *J. Phys. Chem. C* **2009**, 113, 459. (c) Slevin, C. J.; Gray, N. J.; MacPherson, J. V.; Webb, M. A.; Unwin, P. R. *Electrochem. Commun.* **1999**, 1, 282. (d) Amemiya, S.; Nioradze, N.; Santhosh, P.; Deible, M. J. *Anal. Chem.* **2011**, 83, 5928. (e) Edwards, M. A.; Martin, S.; Whitworth, A. L.; Macpherson, J. V.; Unwin, P. R. *Physiol. Meas.* **2006**, 27, R63. (f) Dumitrescu, I.; Dudin, P. V.; Edgeworth, J. P.; Macpherson, J. V.; Unwin, P. R. *J. Phys. Chem. C* **2010**, 114, 2633. (g) Shao, Y. H.; Mirkin, M. V.; Fish, G.; Kokotov, S.; Palanker, D.; Lewis, A. *Anal. Chem.* **1997**, 69, 1627. (h) Mirkin, M. V.; Richards, T. C.; Bard, A. J. *J. Phys. Chem.* **1993**, 97, 7672.
- (6) Nicholson, R. S. *Anal. Chem.* **1965**, 37, 1351.
- (7) *Electrode Kinetics: Principles and methodology*; Bamford, C. H., Compton, R. G., Eds.; Elsevier: Amsterdam, Netherlands, 1986; Vol. 26, p 156.
- (8) Savéant, J. M. *Elements of Molecular and Biomolecular Electrochemistry*; Wiley: Hoboken, NJ, 2006.
- (9) Mirkin, M. V.; Bard, A. J. *Anal. Chem.* **1992**, 64, 2293.
- (10) (a) Bond, A. M.; Oldham, K. B.; Zoski, C. G. *Anal. Chim. Acta* **1989**, 216, 177. (b) Wightman, R. M. *Anal. Chem.* **1981**, 53, 1125.
- (11) Booman, G. L.; Holbrook, W. B. *Anal. Chem.* **1963**, 35, 1793.
- (12) Rudolph, M.; Reddy, D. P.; Feldberg, S. W. *Anal. Chem.* **1994**, 66, A589.

- (13) Nicholson, R. S. *Anal. Chem.* **1965**, 37, 667.
- (14) (a) Wipf, D. O.; Kristensen, E. W.; Deakin, M. R.; Wightman, R. M. *Anal. Chem.* **1988**, 60, 306. (b) Howell, J. O.; Wightman, R. M. *Anal. Chem.* **1984**, 56, 524. (c) Montenegro, M. I.; Pletcher, D. J. *Electroanal. Chem.* **1986**, 200, 371.
- (15) (a) Bond, A. M.; Henderson, T. L. E.; Mann, D. R.; Mann, T. F.; Thormann, W.; Zoski, C. G. *Anal. Chem.* **1988**, 60, 1878. (b) Watkins, J. J.; Chen, J. Y.; White, H. S.; Abruna, H. D.; Maisonneuve, E.; Amatore, C. *Anal. Chem.* **2003**, 75, 3962. (c) Penner, R. M.; Heben, M. J.; Longin, T. L.; Lewis, N. S. *Science* **1990**, 250, 1118.
- (16) (a) Rees, N. V.; Klymenko, O. V.; Coles, B. A.; Compton, R. G. *J. Electroanal. Chem.* **2002**, 534, 151. (b) Macpherson, J. V.; Beeston, M. A.; Unwin, P. R. *J. Chem. Soc., Faraday Trans.* **1995**, 91, 899. (c) Rees, N. V.; Compton, R. G. *Russ. J. Electrochem.* **2008**, 44, 368. (d) Rees, N. V.; Alden, J. A.; Dryfe, R. A. W.; Coles, B. A.; Compton, R. G. *J. Phys. Chem.* **1995**, 99, 14813.
- (17) (a) Lee, C. Y.; Bullock, J. P.; Kennedy, G. F.; Bond, A. M. *J. Phys. Chem. C* **2010**, 114, 10122. (b) O'Mullane, A. P.; Zhang, J.; Toth, A. B.; Bond, A. M. *Anal. Chem.* **2008**, 80, 4614. (c) Zhang, J.; Guo, S.-X.; Bond, A. M. *Anal. Chem.* **2007**, 79, 2276. (d) Zhang, J.; Bond, A. M. *J. Electroanal. Chem.* **2007**, 600, 23. (e) Fleming, B. D.; Zhang, J.; Bond, A. M.; Bell, S. G.; Wong, L.-L. *Anal. Chem.* **2005**, 77, 3502. (f) Sher, A. A.; Bond, A. M.; Gavaghan, D. J.; Harriman, K.; Feldberg, S. W.; Duffy, N. W.; Guo, S.-X.; Zhang, J. *Anal. Chem.* **2004**, 76, 6214. (g) Zhang, J.; Guo, S.-X.; Bond, A. M.; Marken, F. *Anal. Chem.* **2004**, 76, 3619. (h) Fleming, B. D.; Zhang, J.; Bond, A. M.; Bell, S. G.; Wong, L.-L. *Anal. Chem.* **2005**, 77, 3502.
- (18) Bond, A. M.; Duffy, N. W.; Guo, S.-X.; Zhang, J.; Elton, D. *Anal. Chem.* **2005**, 77, 186A.
- (19) Bard, A. J.; Faulkner, L. R. *Electrochemical Methods: Fundamentals and Applications*, 2nd ed.; Wiley: New York, 2001.
- (20) Marcus, R. A. *J. Chem. Phys.* **1956**, 24, 966. (b) Marcus, R. A. *J. Chem. Phys.* **1965**, 43, 679.
- (21) (a) Lehmann, M. W.; Evans, D. H. *Anal. Chem.* **1999**, 71, 1947. (b) Andrieux, C. P.; Savéant, J. M. *J. Electroanal. Chem.* **1970**, 28, 339.
- (22) McCreery, R. L. *Chem. Rev.* **2008**, 108, 2646.
- (23) Gosavi, S.; Marcus, R. A. *J. Phys. Chem. B* **2000**, 104, 2067.

Electrode Kinetics Associated with TCNQ, TCNQ⁻ and TCNQ²⁻ (TCNQ = 7,7,8,8-tetracyanoquinodimethane) Redox Chemistry in Acetonitrile as Determined by Analysis of Higher Harmonic Components Derived From Fourier Transformed Large Amplitude ac Voltammetry

Kiran Bano, Ayman Nafady, Jie Zhang* and Alan M. Bond*

School of Chemistry, Monash University,

Clayton, Victoria 3800, Australia

Inam-ul-Haque

Department of Chemistry, University of Engineering & Technology,

G.T Road Lahore, (54890) Pakistan

Email addresses:

[REDACTED]

Section I: FT ac voltammetric data of TCNQ

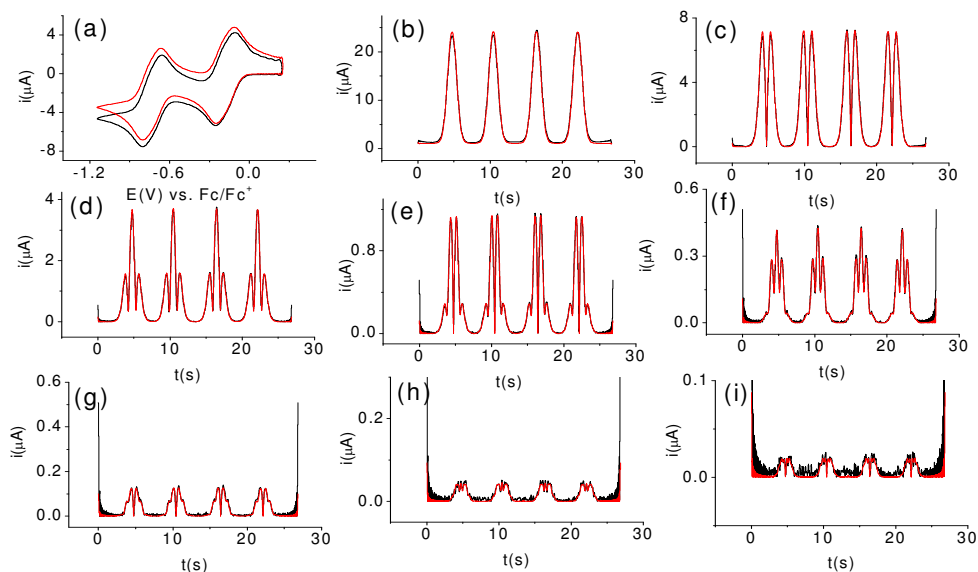


Figure S1. Comparison of experimental (—) and simulated (—) Fourier transformed large amplitude ac voltammograms for the consecutive one-electron $\text{TCNQ}^{0/-}$ and $\text{TCNQ}^{-/2-}$ reduction of 1.93 mM TCNQ in acetonitrile (0.1 M Bu_4NPF_6) at GC electrode (a)) dc component (b) 1st harmonic (c) 2nd harmonic (d) 3rd harmonic (e) 4th harmonic (f) 5th harmonic (g) 6th harmonic (h) 7th harmonic (i) 8th harmonic. Other parameters are described in the text.

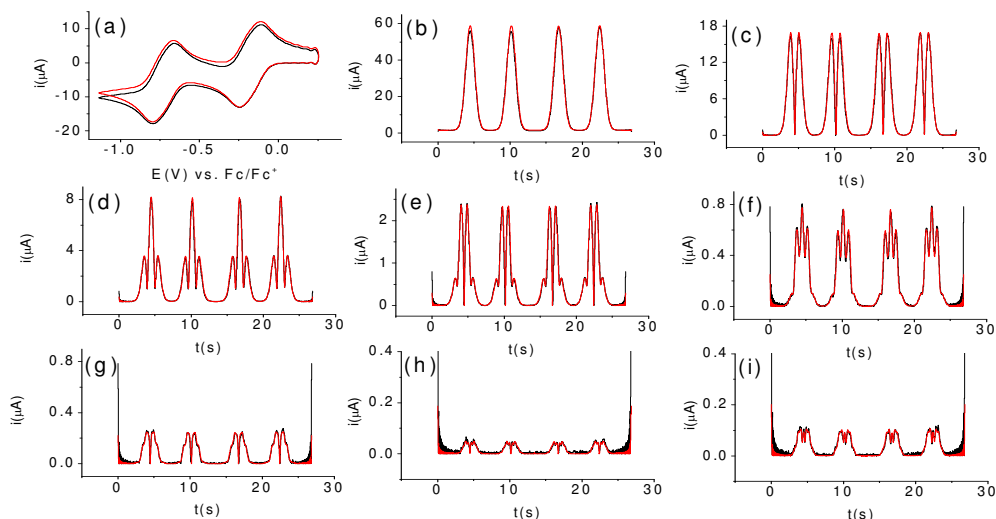


Figure S2. Comparison of experimental (—) and simulated (—) Fourier transformed large amplitude ac voltammograms for the consecutive one-electron $\text{TCNQ}^{0/-}$ and $\text{TCNQ}^{-/2-}$ reduction of 1.93 mM TCNQ in acetonitrile (0.1 M Bu_4NPF_6) at a Pt electrode (a)) dc component (b) 1st harmonic (c) 2nd harmonic (d) 3rd harmonic (e) 4th harmonic (f) 5th harmonic (g) 6th harmonic (h) 7th harmonic (i) 8th harmonic. Other parameters are described in the text.

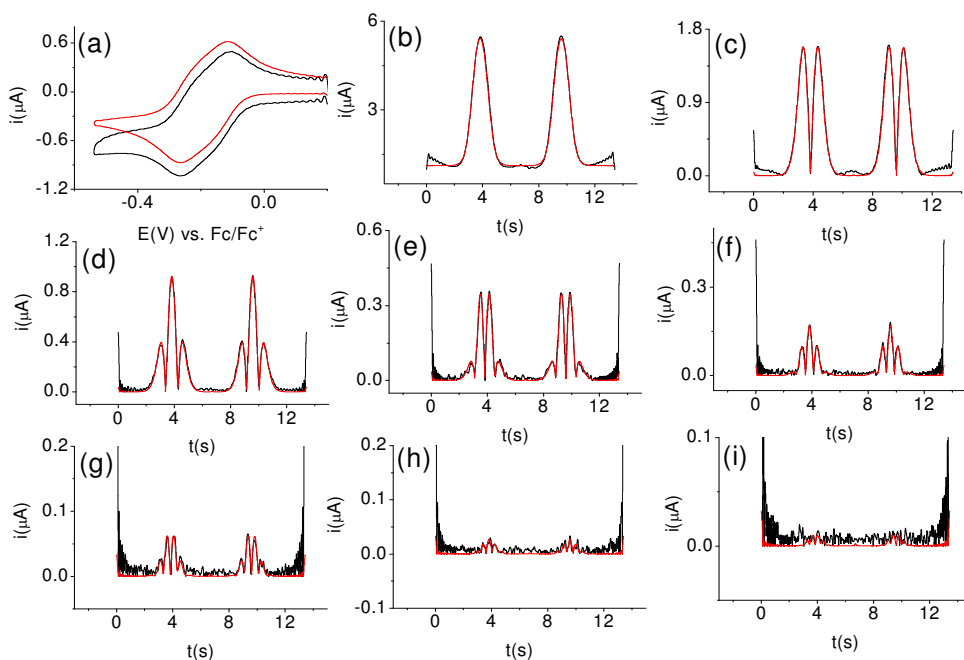


Figure S3. Comparison of experimental(—) and simulated(—) Fourier transformed large amplitude ac voltammograms for the one-electron $\text{TCNQ}^{0/-}$ reduction of 0.36 mM TCNQ in acetonitrile (0.1 M Bu_4NPF_6) at a GC electrode (a)) dc component (b) 1st harmonic (c) 2nd harmonic (d) 3rd harmonic (e) 4th harmonic (f) 5th harmonic (g) 6th harmonic (h) 7th harmonic (i) 8th harmonic. Other parameters are described in the text.

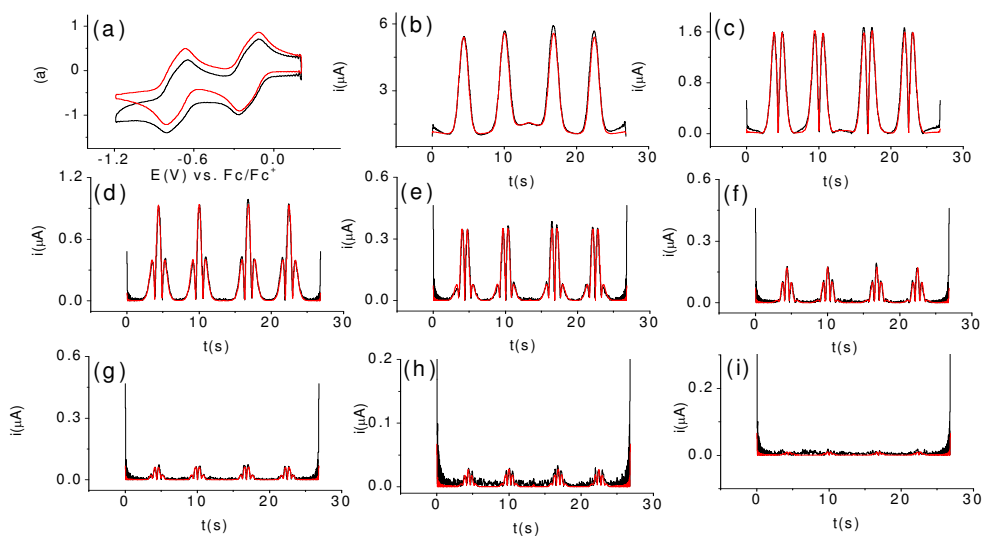


Figure S4. Comparison of experimental(—) and simulated(—) Fourier transformed large amplitude ac voltammograms for the consecutive one-electron $\text{TCNQ}^{0/-}$ and $\text{TCNQ}^{0.72-}$ reduction of 0.36 mM TCNQ in acetonitrile (0.1 M Bu_4NPF_6) at a GC electrode (a)) dc component (b) 1st harmonic (c) 2nd harmonic (d) 3rd harmonic (e) 4th harmonic (f) 5th harmonic (g) 6th harmonic (h) 7th harmonic (i) 8th harmonic. Other parameters are described in the text.

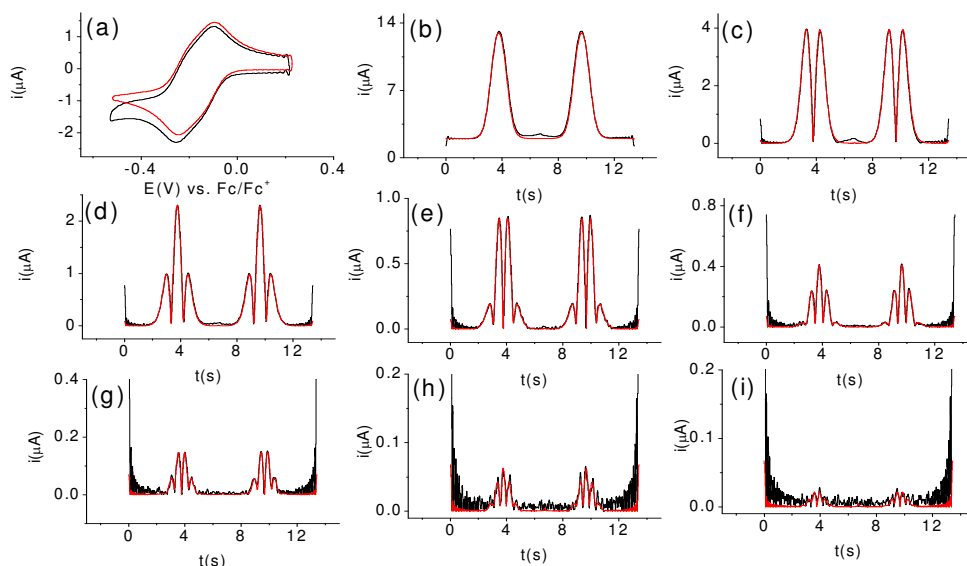


Figure S5. Comparison of experimental(—) and simulated(—) Fourier transformed large amplitude ac voltammograms for the one-electron $\text{TCNQ}^{0/-}$ reduction of 0.36 mM TCNQ in acetonitrile (0.1 M Bu_4NPF_6) at a Pt electrode (a)) dc component (b) 1st harmonic (c) 2nd harmonic (d) 3rd harmonic (e) 4th harmonic (f) 5th harmonic (g) 6th harmonic (h) 7th harmonic (i) 8th harmonic. Other parameters are described in the text.

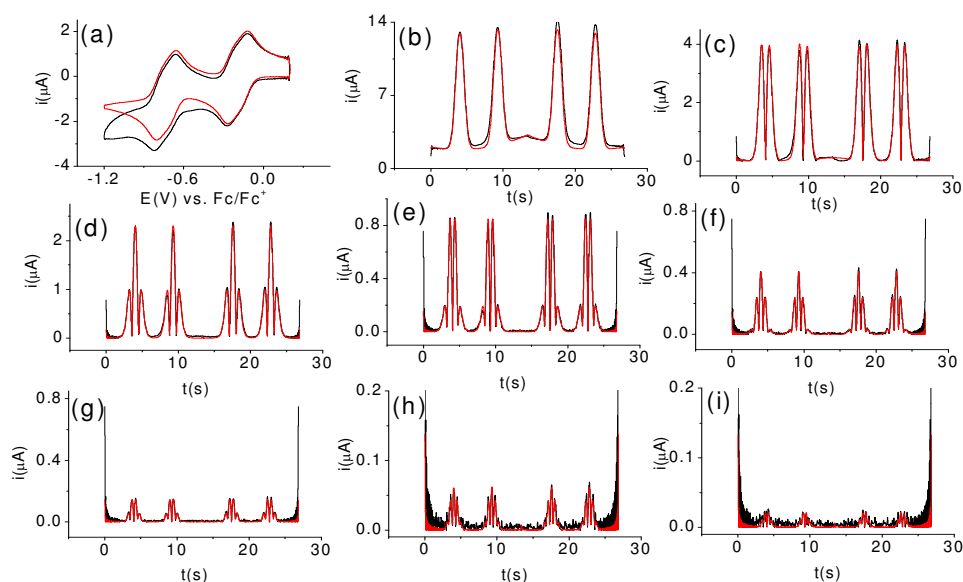


Figure S6. Comparison of experimental(—) and simulated(—) Fourier transformed large amplitude ac voltammograms for the consecutive one-electron $\text{TCNQ}^{0/-}$ and $\text{TCNQ}^{-1/2-}$ reduction of 0.36 mM TCNQ in acetonitrile (0.1 M Bu_4NPF_6) at a Pt electrode (a)) dc component (b) 1st harmonic (c) 2nd harmonic (d) 3rd harmonic (e) 4th harmonic (f) 5th harmonic (g) 6th harmonic (h) 7th harmonic (i) 8th harmonic. Other parameters are described in the text.

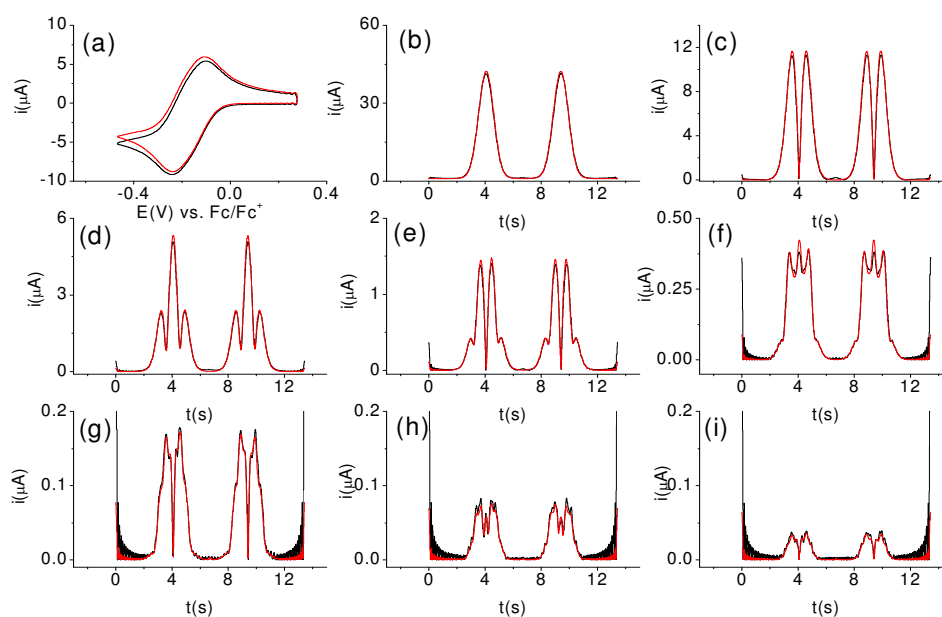


Figure S7. Comparison of experimental(—) and simulated(—) Fourier transformed large amplitude ac voltammograms for the one-electron $\text{TCNQ}^{0/-}$ reduction of 3.5 mM TCNQ in acetonitrile (0.1 M Bu_4NPF_6) at a glassy carbon electrode (a) dc component (b) 1st harmonic (c) 2nd harmonic (d) 3rd harmonic (e) 4th harmonic (f) 5th harmonic (g) 6th harmonic (h) 7th harmonic (i) 8th harmonic. Other parameters are described in the text.

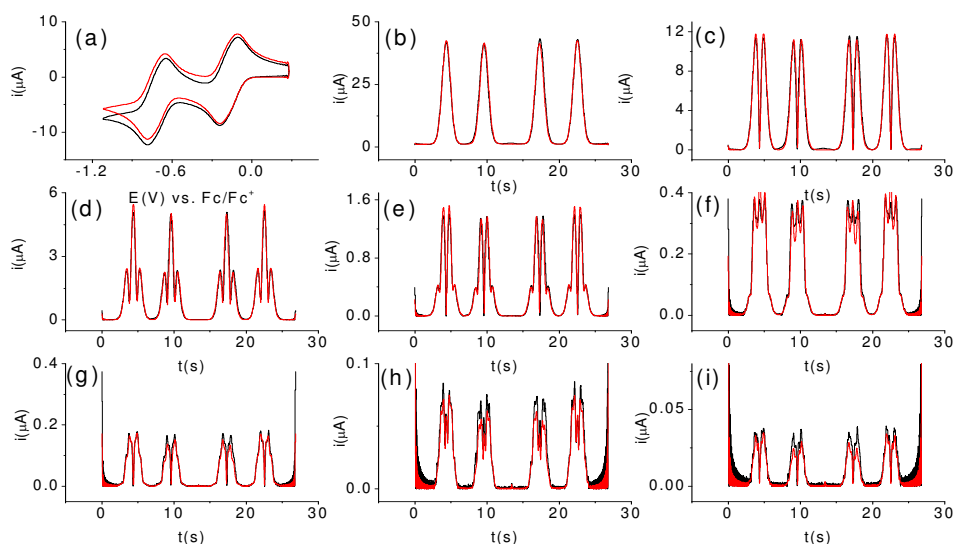


Figure S8. Comparison of experimental(—) and simulated(—) Fourier transformed large amplitude ac voltammograms for the consecutive one-electron $\text{TCNQ}^{0/-}$ and $\text{TCNQ}^{-1/2-}$ reduction of 3.5 mM TCNQ in acetonitrile (0.1 M Bu_4NPF_6) at a glassy carbon electrode (a) dc component (b) 1st harmonic (c) 2nd harmonic (d) 3rd harmonic (e) 4th harmonic (f) 5th harmonic (g) 6th harmonic (h) 7th harmonic (i) 8th harmonic. Other parameters are described in the text.

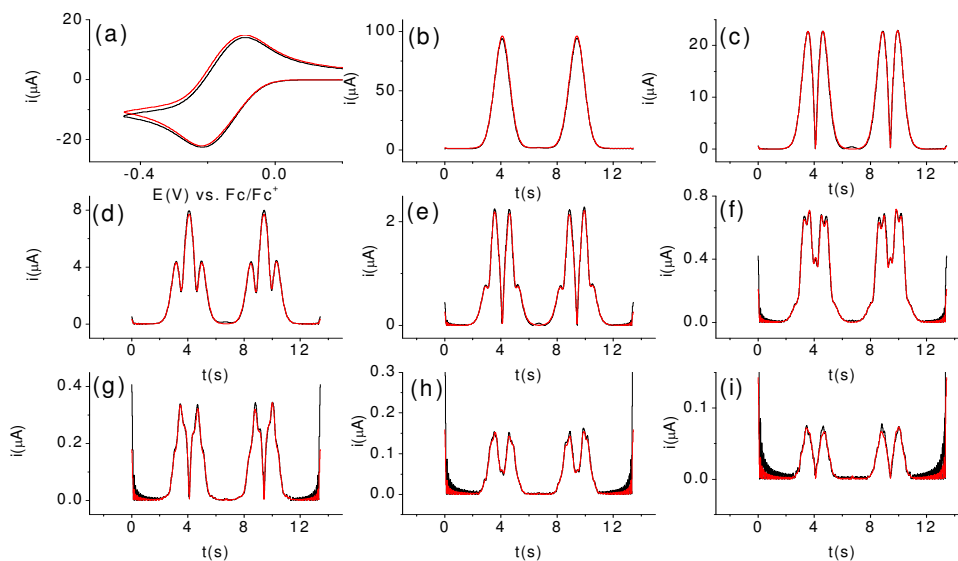


Figure S9. Comparison of experimental(—) and simulated(—) Fourier transformed large amplitude ac voltammograms for one-electron $\text{TCNQ}^{0/-}$ reduction of 3.5 mM TCNQ in acetonitrile (0.1 M Bu_4NPF_6) at a Pt electrode (a)) dc component (b) 1st harmonic (c) 2nd harmonic (d) 3rd harmonic (e) 4th harmonic (f) 5th harmonic (g) 6th harmonic (h) 7th harmonic (i) 8th harmonic. Other parameters are described in the text.

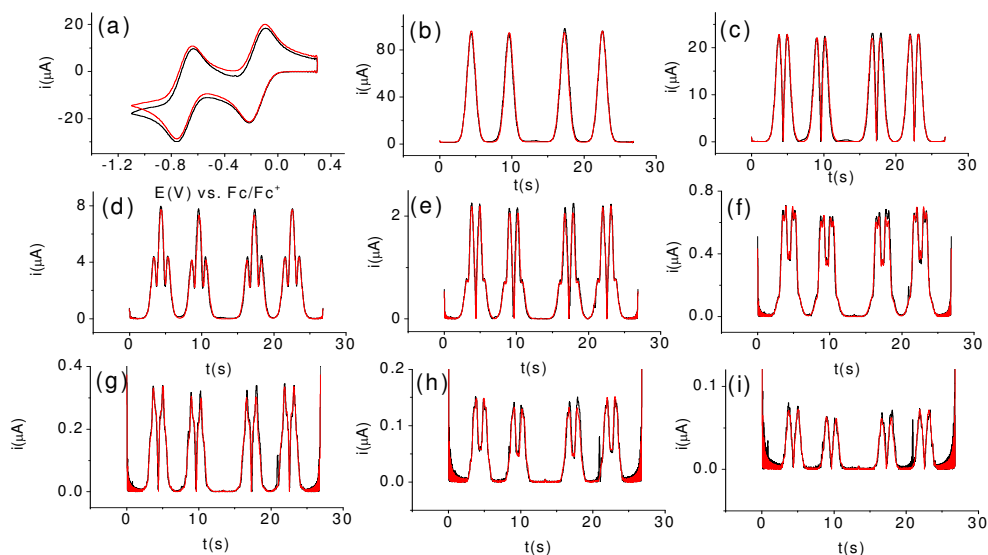


Figure S10. Comparison of experimental(—) and simulated(—) Fourier transformed large amplitude ac voltammograms for the consecutive one-electron $\text{TCNQ}^{0/-}$ and $\text{TCNQ}^{-/2-}$ reduction of 3.5 mM TCNQ in acetonitrile (0.1 M Bu_4NPF_6) at a Pt electrode (a)) dc component (b) 1st harmonic (c) 2nd harmonic (d) 3rd harmonic (e) 4th harmonic (f) 5th harmonic (g) 6th harmonic (h) 7th harmonic (i) 8th harmonic. Other parameters are described in the text.

Section II: FT ac voltammetric data of TCNQ⁻

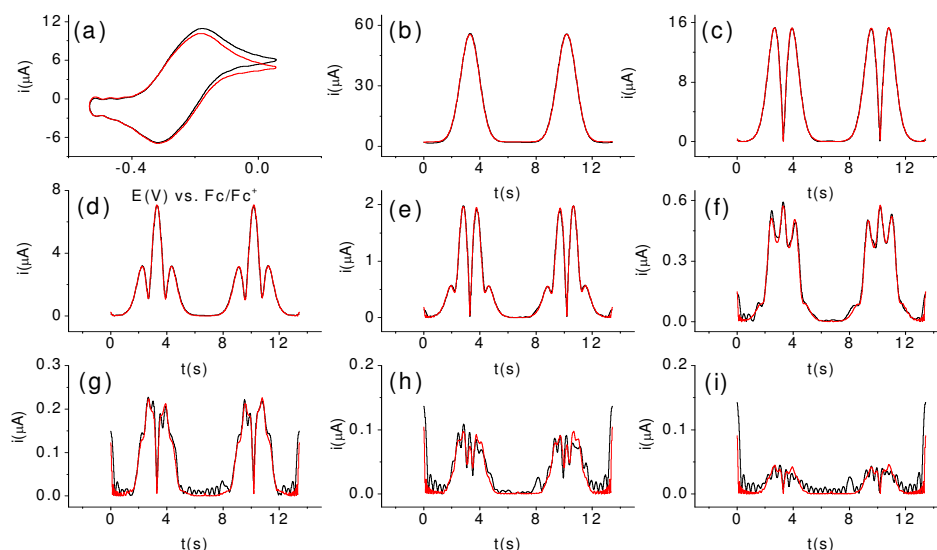


Figure S11. Comparison of experimental (—) and simulated (—) Fourier transformed large amplitude ac voltammograms for one-electron TCNQ⁻ oxidation of 1.93 mM TCNQ⁻ in acetonitrile (0.1 M Bu₄NPF₆) at a Pt electrode (a) 1st harmonic (b) 2nd harmonic (c) 3rd harmonic (d) 4th harmonic (e) 5th harmonic (f) 6th harmonic (g) 7th harmonic (h) 8th harmonic. Other parameters are described in the text.

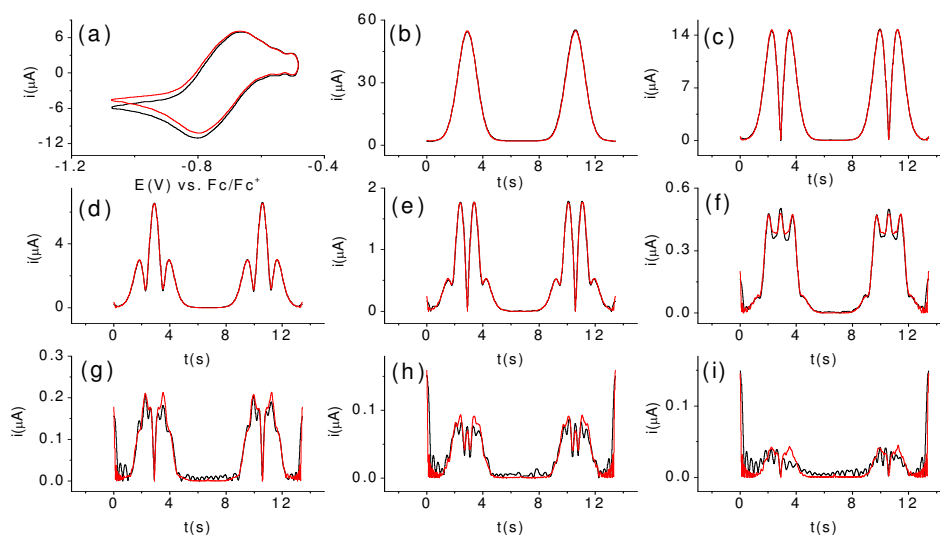


Figure S12. Comparison of experimental (—) and simulated (—) Fourier transformed large amplitude ac voltammograms for one-electron TCNQ⁻ reduction of 1.93 mM TCNQ⁻ in acetonitrile (0.1 M Bu₄NPF₆) at a Pt electrode (a) 1st harmonic (b) 2nd harmonic (c) 3rd harmonic (d) 4th harmonic (e) 5th harmonic (f) 6th harmonic (g) 7th harmonic (h) 8th harmonic. Other parameters are described in the text.

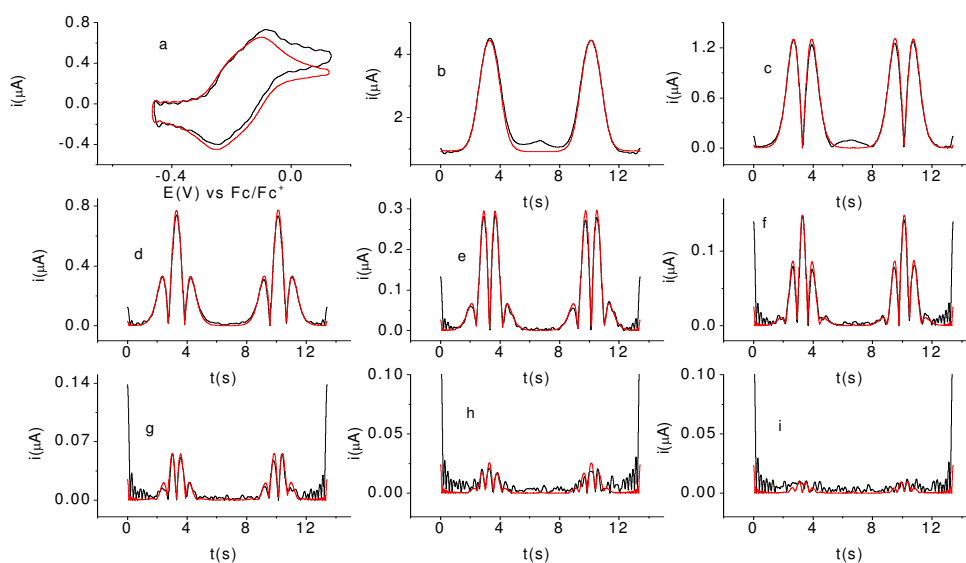


Figure S13. Comparison of experimental(—) and simulated(—) Fourier transformed large amplitude ac voltammograms for one-electron $\text{TCNQ}^{-/0}$ oxidation of 0.31 mM TCNQ^- in acetonitrile (0.1 M Bu_4NPF_6) at a glassy carbon electrode (a)) dc component (b) 1st harmonic (c) 2nd harmonic (d) 3rd harmonic (e) 4th harmonic (f) 5th harmonic (g) 6th harmonic (h) 7th harmonic (i) 8th harmonic. Other parameters are described in the text.

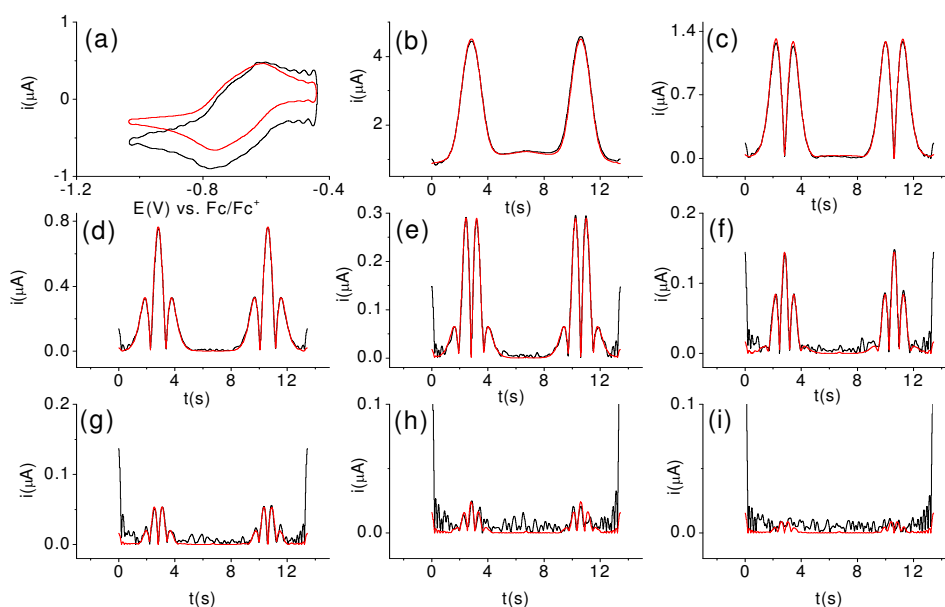


Figure S14. Comparison of experimental(—) and simulated(—) Fourier transformed large amplitude ac voltammograms for one-electron $\text{TCNQ}^{-/2-}$ reduction of 0.31 mM TCNQ^- in acetonitrile (0.1 M Bu_4NPF_6) at a glassy carbon electrode (a)) dc component (b) 1st harmonic (c) 2nd harmonic (d) 3rd harmonic (e) 4th harmonic (f) 5th harmonic (g) 6th harmonic (h) 7th harmonic (i) 8th harmonic. Other parameters are described in the text.

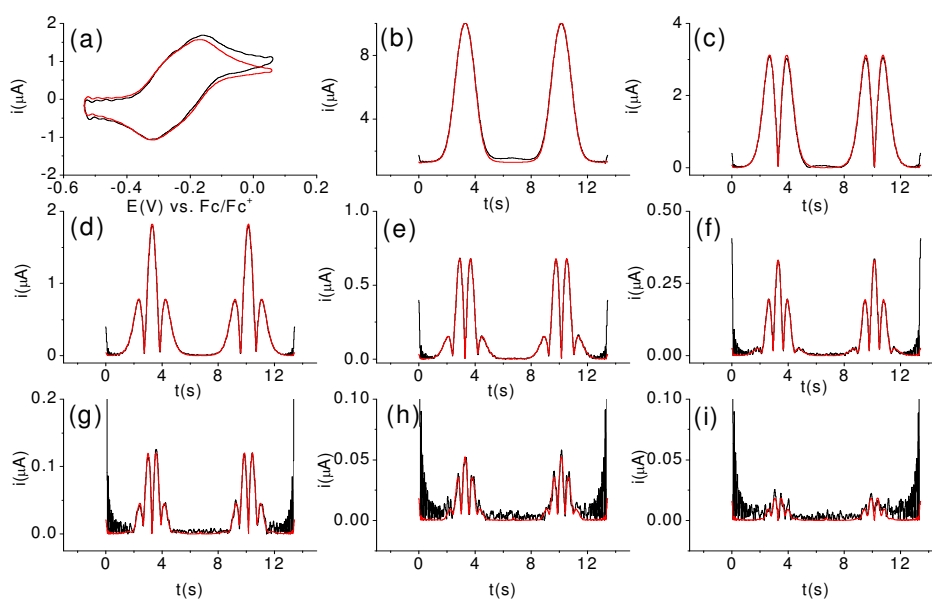


Figure S15. Comparison of experimental(—) and simulated(—) Fourier transformed large amplitude ac voltammograms for one-electron $\text{TCNQ}^{-/0}$ oxidation of 0.31 mM TCNQ^- in acetonitrile ($0.1 \text{ M Bu}_4\text{NPF}_6$) at a Pt electrode (a)) dc component (b) 1st harmonic (c) 2nd harmonic (d) 3rd harmonic (e) 4th harmonic (f) 5th harmonic (g) 6th harmonic (h) 7th harmonic (i) 8th harmonic. Other parameters are described in the text.

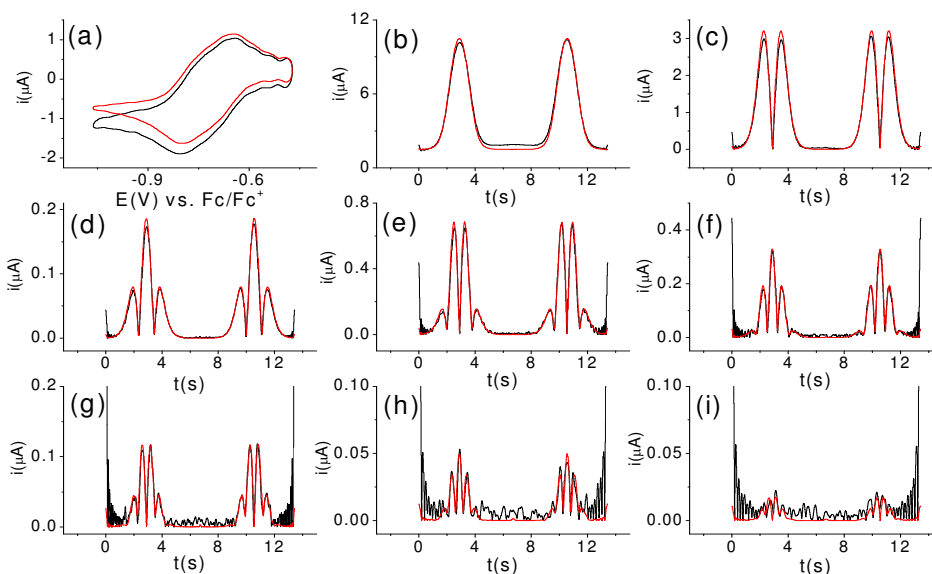


Figure S16. Comparison of experimental(—) and simulated(—) Fourier transformed large amplitude ac voltammograms for the one-electron reduction $\text{TCNQ}^{-/2-}$ of 0.31 mM TCNQ^- in acetonitrile ($0.1 \text{ M Bu}_4\text{NPF}_6$) at a Pt electrode (a)) dc component (b) 1st harmonic (c) 2nd harmonic (d) 3rd harmonic (e) 4th harmonic (f) 5th harmonic (g) 6th harmonic (h) 7th harmonic (i) 8th harmonic. Other parameters are described in the text.

Section III: FT ac voltammetric data of TCNQ²⁻

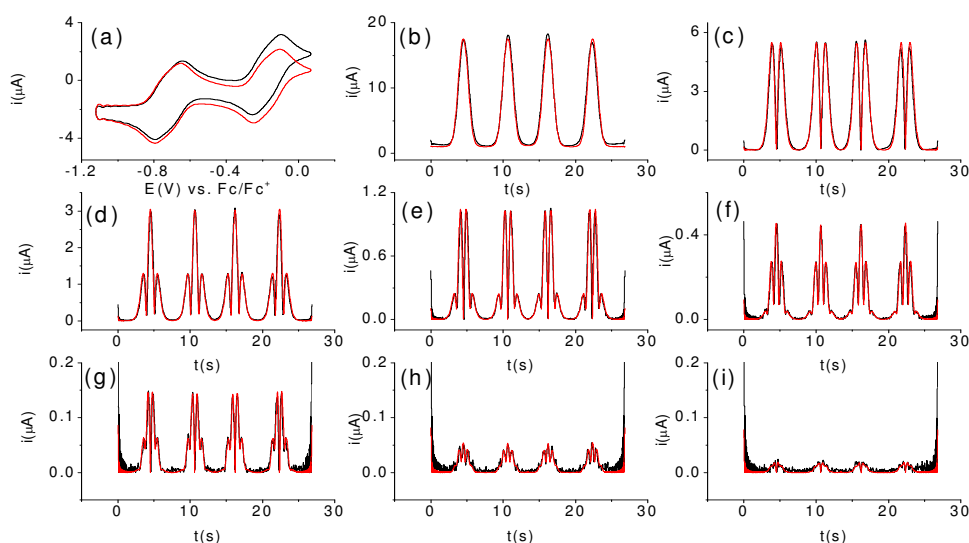


Figure S17. Comparison of experimental(—) and simulated(—) Fourier transformed large amplitude ac voltammograms for the consecutive one-electron TCNQ^{2-/·-} and TCNQ^{·-/0} oxidation of 1.7 mM TCNQ²⁻ in acetonitrile (0.1 M Bu₄NPF₆) at a GC electrode (a) 1st harmonic (b) 2nd harmonic (c) 3rd harmonic (d) 4th harmonic (e) 5th harmonic (f) 6th harmonic (g) 7th harmonic (h) 8th harmonic. Other parameters are described in the text.

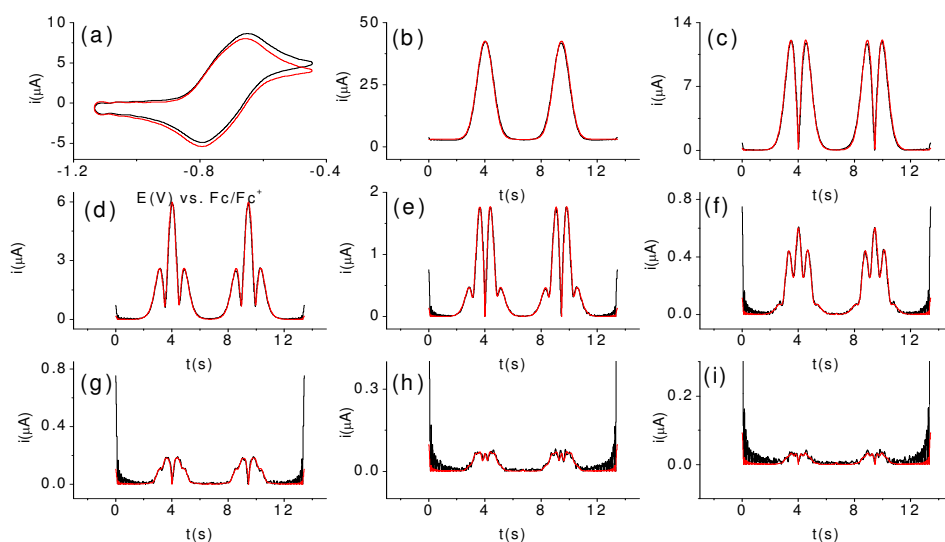


Figure S18. Comparison of experimental(—) and simulated(—) Fourier transformed large amplitude ac voltammograms for the one-electron TCNQ^{2-/·-} oxidation of 1.7 mM TCNQ²⁻ in acetonitrile (0.1 M Bu₄NPF₆) at a Pt electrode (a)) dc component (b) 1st harmonic (c) 2nd harmonic (d) 3rd harmonic (e) 4th harmonic (f) 5th harmonic (g) 6th harmonic (h) 7th harmonic (i) 8th harmonic. Other parameters are described in the text.

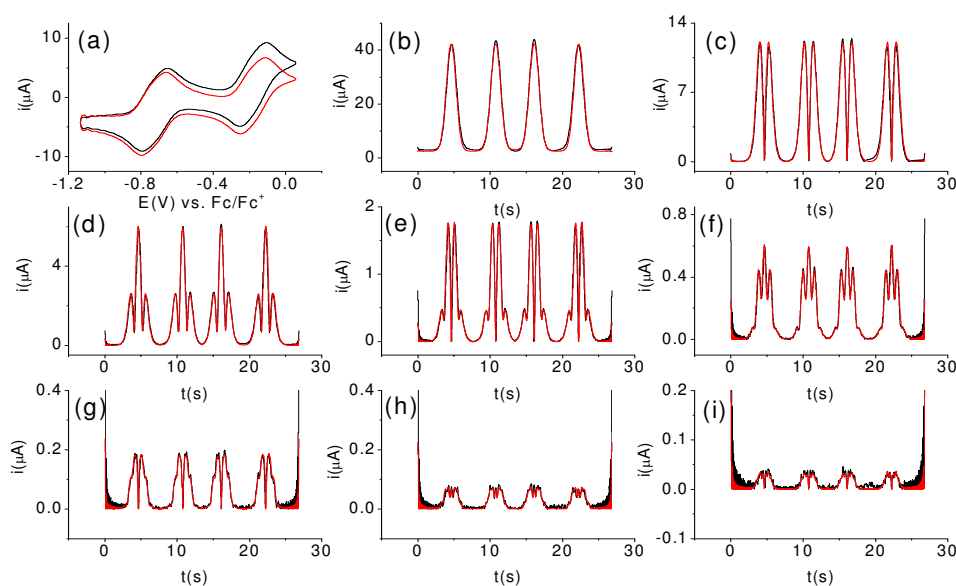


Figure S19. Comparison of experimental(—) and simulated(—) Fourier transformed large amplitude ac voltammograms for the consecutive one-electron $\text{TCNQ}^{2-/·-}$ and $\text{TCNQ}^{·-/0}$ oxidation of 1.7 mM TCNQ^{2-} in acetonitrile (0.1 M Bu_4NPF_6) at a Pt electrode (a) 1st harmonic (b) 2nd harmonic (c) 3rd harmonic (d) 4th harmonic (e) 5th harmonic (f) 6th harmonic (g) 7th harmonic (h) 8th harmonic. Other parameters are described in the text.

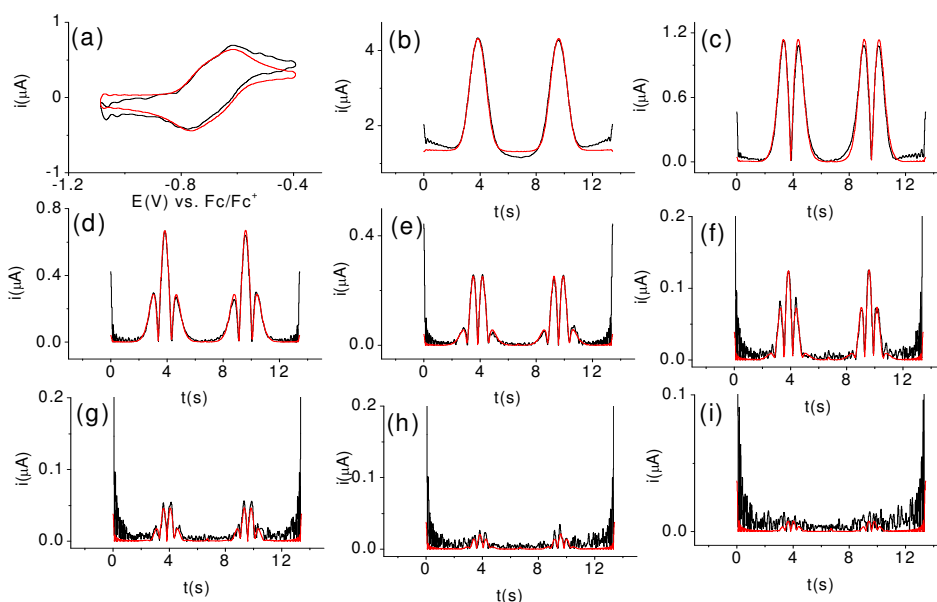


Figure S20. Comparison of experimental(—) and simulated(—) Fourier transformed large amplitude ac voltammograms for the one-electron $\text{TCNQ}^{2-/·-}$ oxidation of 0.33 mM TCNQ^{2-} in acetonitrile (0.1 M Bu_4NPF_6) at a glassy carbon electrode (a)) dc component (b) 1st harmonic (c) 2nd harmonic (d) 3rd harmonic (e) 4th harmonic (f) 5th harmonic (g) 6th harmonic (h) 7th harmonic (i) 8th harmonic. Other parameters are described in the text.

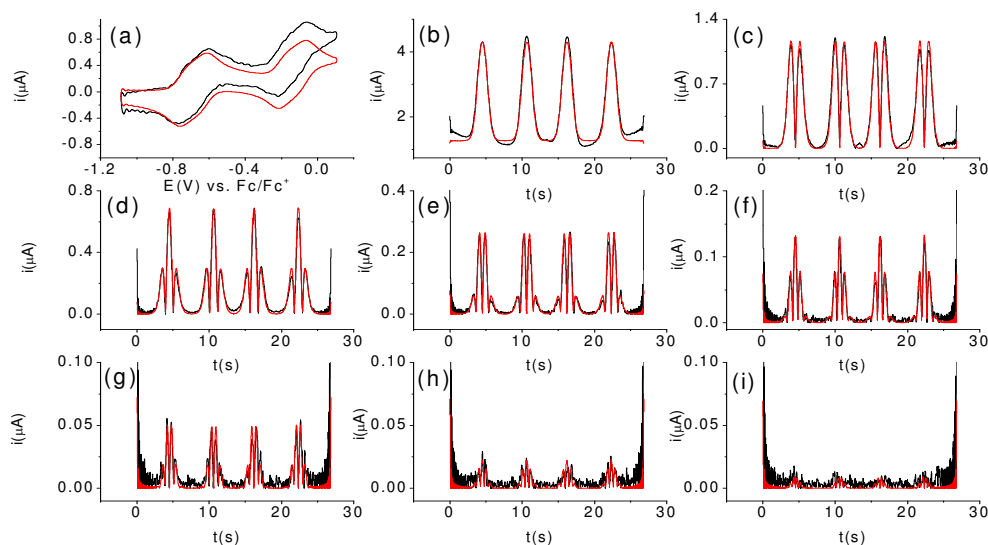


Figure S21. Comparison of experimental(—) and simulated(—) Fourier transformed large amplitude ac voltammograms for the consecutive one-electron $\text{TCNQ}^{2-/0}$ oxidation of 0.33 mM TCNQ^{2-} in acetonitrile (0.1 M Bu_4NPF_6) at a glassy carbon electrode (a)) dc component (b) 1st harmonic (c) 2nd harmonic (d) 3rd harmonic (e) 4th harmonic (f) 5th harmonic (g) 6th harmonic (h) 7th harmonic (i) 8th harmonic. Other parameters are described in the text.

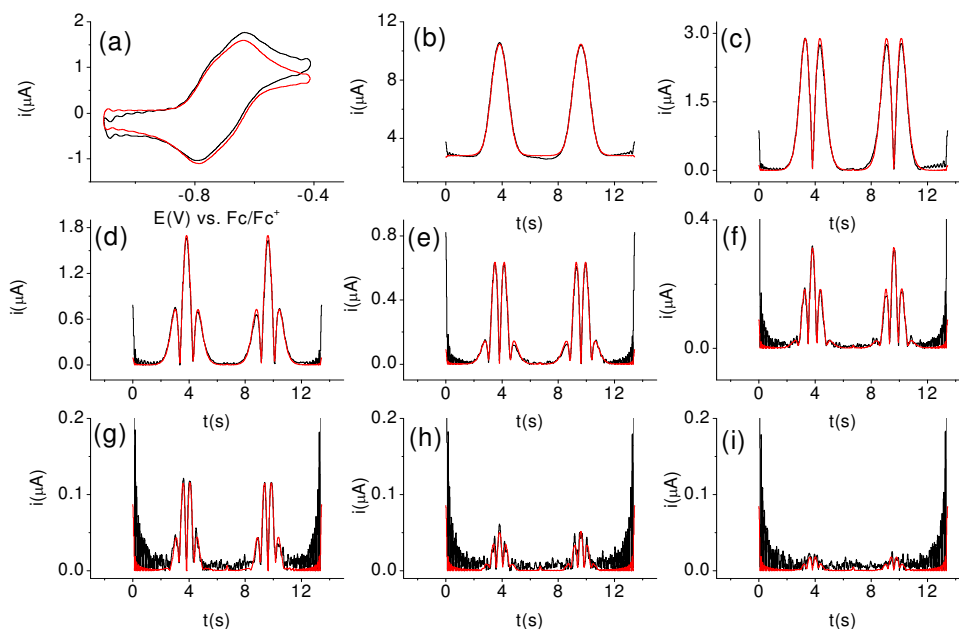


Figure S22. Comparison of experimental(—) and simulated(—) Fourier transformed large amplitude ac voltammograms for the one-electron $\text{TCNQ}^{2-/0}$ oxidation of 0.33 mM TCNQ^{2-} in acetonitrile (0.1 M Bu_4NPF_6) at a Pt electrode (a)) dc component (b) 1st harmonic (c) 2nd harmonic (d) 3rd harmonic (e) 4th harmonic (f) 5th harmonic (g) 6th harmonic (h) 7th harmonic (i) 8th harmonic. Other parameters are described in the text.

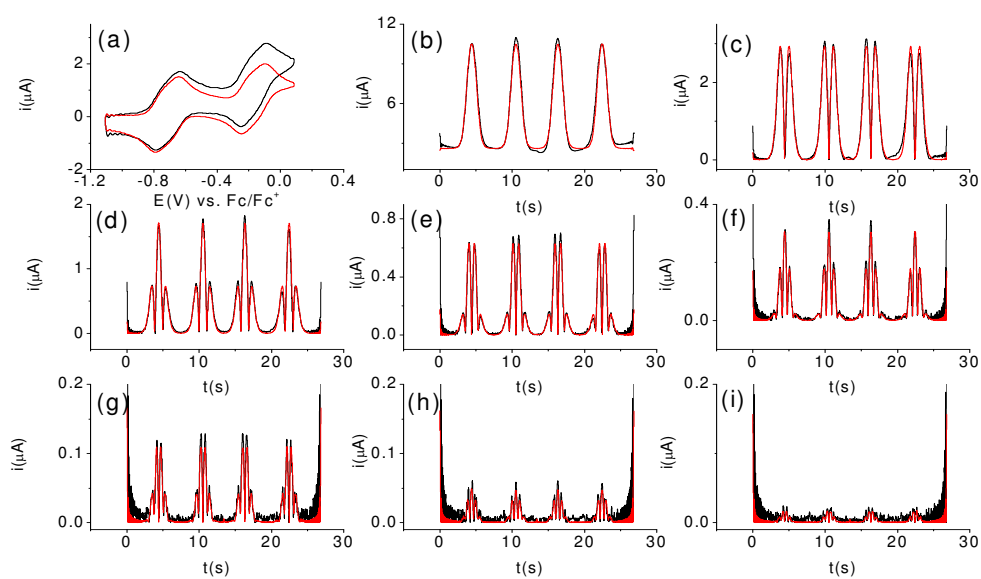


Figure S23. Comparison of experimental(—) and simulated(—) Fourier transformed large amplitude ac voltammograms for the consecutive one-electron $\text{TCNQ}^{2-/·-}$ and $\text{TCNQ}^{·-/0}$ oxidation of 0.33 mM TCNQ^{2-} in acetonitrile (0.1 M Bu_4NPF_6) at a Pt electrode (a)) dc component (b) 1st harmonic (c) 2nd harmonic (d) 3rd harmonic (e) 4th harmonic (f) 5th harmonic (g) 6th harmonic (h) 7th harmonic (i) 8th harmonic. Other parameters are described in the text.

CHAPTER 4

ELECTRODE KINETICS STUDIES AT ROTATING DISK ELECTRODES:

LOW FREQUENCY FT AC VOLTAMMETRY

Monash University

Declaration for Thesis Chapter [4]

Declaration by candidate

In the case of Chapter [4], the nature and extent of my contribution to the work was the following:

Nature of contribution	Extent of contribution (%)
Initiation, key ideas, experimental work, writing up	70 %

The following co-authors contributed to the work. If co-authors are students at Monash University, the extent of their contribution in percentage terms must be stated:

Name	Nature of contribution	
Jie Zhang	Initiation, key ideas, writing up	
Alan M. Bond	Initiation, key ideas, writing up	
Gareth F. Kennedy	Initiation, key ideas, experimental work, writing up	

The undersigned hereby certify that the above declaration correctly reflects the nature and extent of the candidate's and co-authors' contributions to this work*.

Candidate's Signature  Date 28/11/2013

Name	
Jie Zhang	
Alan M. Bond	
Gareth F. Kennedy	

Main Supervisor's Signature  Date 29/11/2013

*Note: Where the responsible author is not the candidate's main supervisor, the main supervisor should consult with the responsible author to agree on the respective contributions of the authors.

Cite this: DOI: 10.1039/c2cp23819e

www.rsc.org/pccp

PAPER

Large amplitude Fourier transformed ac voltammetry at a rotating disc electrode: a versatile technique for covering Levich and flow rate insensitive regimes in a single experiment†

Kiran Bano, Gareth F. Kennedy, Jie Zhang* and Alan M. Bond*

Received 1st December 2011, Accepted 7th February 2012

DOI: 10.1039/c2cp23819e

The theory for large amplitude Fourier transformed ac voltammetry at a rotating disc electrode is described. Resolution of time domain data into dc and ac harmonic components reveals that the mass transport for the dc component is controlled by convective-diffusion, while the background free higher order harmonic components are flow rate insensitive and mainly governed by linear diffusion. Thus, remarkable versatility is available; Levich behaviour of the dc component limiting current provides diffusion coefficient values and access to higher harmonics allows fast electrode kinetics to be probed. Two series of experiments (dc and ac voltammetry) have been required to extract these parameters; here large amplitude ac voltammetry with RDE methodology is used to demonstrate that kinetics and diffusion coefficient information can be extracted from a single experiment. To demonstrate the power of this approach, theoretical and experimental comparisons of data obtained for the reversible $[\text{Ru}(\text{NH}_3)_6]^{3+/2+}$ and quasi-reversible $[\text{Fe}(\text{CN})_6]^{3-/4-}$ electron transfer processes are presented over a wide range of electrode rotation rates and with different concentrations and electrode materials. Excellent agreement of experimental and simulated data is achieved, which allows parameters such as electron transfer rate, diffusion coefficient, uncompensated resistance and others to be determined using a strategically applied approach that takes into account the different levels of sensitivity of each parameter to the dc or the ac harmonic.

1 Introduction

dc voltammetric techniques are commonly classified as being based on stationary or hydrodynamic electrode configurations. The former are characterized by diffusion mass transport and the latter by convective-diffusion mass transport. Both methods are widely used in studies of electrode mechanisms^{1–6} and each has well established advantages and disadvantages.^{7–9} dc voltammetry at stationary macro disc electrodes has been extensively used to probe the kinetics and thermodynamics of heterogeneous electron transfer processes^{10,11} and coupled homogeneous chemical processes.⁶ Mass transport by linear diffusion coupled with the electrode process is well understood and the theory is well developed. In dc cyclic voltammetry a ramped waveform of known scan rate is applied to the working electrode and the resulting current is recorded as a function of applied potential with respect to the reference electrode.^{12,13} Data are collected over a range of scan rates and the experiments are relatively simple. For study of very fast electron transfer kinetics microelectrodes¹⁴ or even nano diameter electrodes¹⁵ may be used in order to

minimize the impact of uncompensated resistance.⁹ The use of these electrodes also provides an enhanced mass transport rate from radial diffusion under steady state conditions or provides access to shorter time domain when operated under transient conditions. However, nanoelectrodes have some limitations due to possible uncertainties in electrode geometries and obtaining data from a set of experiments under steady-state conditions with ideal nanoelectrodes of different dimensions is far from trivial.

Hydrodynamic voltammetry utilizes convective-diffusion mass transport and gives a steady state response even at macro electrodes.¹⁶ In this sense it has some of the features of voltammetry at stationary micro/nano electrodes. Provided the hydrodynamics are well defined, then this method is readily treated theoretically and analytical and mechanistic studies of simple redox, catalytic and biological processes have been widely undertaken at rotating disc electrodes (RDEs).^{8,16–19} For kinetic measurements, macro-sized rotating disc electrodes have several of the same advantages and limitations encountered when using macro-sized stationary electrodes. Thus, the steady state limiting current is unaffected by slow electron transfer kinetics and uncompensated resistance so the diffusion coefficients are easily determined from this parameter and use of the Levich equation. The RDE technique is particularly powerful for the investigation of catalytic processes associated with immobilized enzymes,

School of Chemistry, Monash University, Clayton, Victoria 3800, Australia. E-mail: kiran.bano@monash.edu

† Electronic supplementary information (ESI) available. See DOI: 10.1039/c2cp23819e

since the product of enzymatic reactions, which may inhibit the enzyme activity, is rapidly removed from the electrode surface after formation.²⁰ However, this method also suffers from some disadvantages. In particular, problems are encountered from the influence of uncompensated resistance when measurement of the half wave potential is needed to quantify the electrode kinetics.¹² Various micro-sized electrodes have been introduced to decrease the effect of uncompensated resistance.^{21–23} Channel and jet electrodes are potentially attractive for measurement of fast electron transfer kinetics but there are constraints when working with high viscosity solvents or under high pressure and experiments and electrodes designs are demanding.²¹

Another valuable method for quantitative evaluation of electrode kinetics is to use impedance spectroscopy in which a periodical ac waveform is superimposed onto the dc ramp.¹² In the case of Fourier Transformed (FT) large amplitude ac voltammetry it is now well known that dc and ac sets of harmonics can be obtained from a single experiment.^{24–26} At stationary macro electrodes, linear diffusion again governs the mass transport and the theory is generated in a manner analogous to that for dc voltammetry. Kinetic parameters can be extracted from higher harmonic ac components that have very low background current and enhanced sensitivity to both uncompensated resistance and electrode kinetics.²⁷

Theoretical studies with small amplitude ac perturbed voltammetry at a RDE for reversible and quasi-reversible processes have considered the effect of hydrodynamics and show that the ac response may not be affected by convective mass transport if the diffusion layer developed due to ac polarization is very thin.^{28,29} However, experimental studies using ac voltammetry at a RDE have been limited to the analytical determination of metals³⁰ and a few ac impedance studies.^{31–35} The use of higher order ac harmonics, that are now available, has yet to be explored.

By combining large amplitude FT ac voltammetry with the RDE method, the advantages of both techniques can be exploited in one experiment. This method allows the aperiodic dc and ac harmonics to be resolved, the dc term being dominated by convection rather than diffusion and *vice versa* for the higher order harmonics. The dc component in FT ac voltammetry should provide an optimal approach to determine the diffusion coefficient from the limiting current and ac harmonic components may then be used to extract information related to electrode mechanisms and kinetics. In this paper, the theory of FT ac voltammetry at a RDE has been developed and applied to the reversible $[\text{Ru}(\text{NH}_3)_6]^{3+/2+}$ and quasi reversible $[\text{Fe}(\text{CN})_6]^{3-/4-}$ processes in aqueous media. Theory and experiment comparisons confirm that convective-diffusion based Levich theory applies to the dc component and diffusion based theory to the higher order harmonics allowing flow rate dependent and flow rate insensitive regimes to be assessed from a single experiment.

2 Experimental

2.1 Materials and chemicals

Ruthenium hexamine trichloride, $[\text{Ru}(\text{NH}_3)_6]\text{Cl}_3$, (Aldrich), potassium chloride, KCl, (Merck) and potassium ferricyanide, $\text{K}_3[\text{Fe}(\text{CN})_6]$, (Sigma-Aldrich) were of analytical reagent grade

and used as supplied by the manufacturer. Double distilled water was used to prepare all solutions used in the voltammetric experiments.

2.2 Electrochemical procedures

All voltammetric experiments were carried out at $25 \pm 2^\circ\text{C}$ using a three electrode electrochemical cell configuration. Platinum and glassy carbon disc electrodes ($d = 3.0\text{ mm}$) used in stationary and rotating disc electrode modes were polished with $0.3\text{ }\mu\text{m}$ alumina (Buehler, Lake Bluff, IL) on a clean polishing cloth then rinsed with water, sonicated for 30 seconds and again rinsed with water and dried under nitrogen. A platinum wire was used as the auxiliary electrode and Ag/AgCl (3.0 M NaCl) as the reference electrode. Voltammetric studies were carried out on the reduction of $[\text{Ru}(\text{NH}_3)_6]^{3+}$ (1.1 mM and 0.14 mM) in aqueous 0.1 M KCl electrolyte medium and reduction of $[\text{Fe}(\text{CN})_6]^{3-}$ (0.98 and 0.14 mM) in aqueous 3.0 M KCl electrolyte medium. Previous studies^{27,36} have shown that the apparent kinetics (k^0 value) for the $\text{Fe}(\text{CN})_6^{3-/4-}$ process increases when the electrolyte concentration increases. Therefore, a relatively high electrolyte concentration was chosen in this process so that the advantage of using large amplitude Fourier transformed ac voltammetry at a rotating disc electrode for the evaluation of electrode kinetics could be fully demonstrated. Uncompensated resistance (R_u) was determined from the RC time constant at potentials where no Faradaic current was present. Conventional dc experiments were carried out with a CHI 400B dc potentiostat and all FT ac voltammetric experiments employed a sine wave of frequency 9.0 Hz and amplitude 80 mV superimposed on the dc ramp and were undertaken with a home built ac potentiostat.^{24,26} Rotating disc electrode experiments employed the RRDE-3A assembly from BAS Inc., Japan.

3 Theory

In this paper, a one-electron reduction reaction is considered



where O and R are the oxidized and reduced solution soluble species and k_f and k_b are the rates of the forward and backward reactions. The Faradaic current i_F derived from eqn (1) is given by

$$i_F = FA(k_b[\text{R}] - k_f[\text{O}]) \quad (2)$$

where [O] and [R] are the concentrations of O and R, respectively, A is the electrode area and F is Faraday's constant. If Butler–Volmer kinetics is obeyed, then the forward and backward heterogeneous charge-transfer rate constants k_f and k_b are given by eqn (3) and (4), respectively,

$$k_f = k^0 \exp \left[\frac{\alpha F}{RT} (E - E^0) \right] \quad (3)$$

$$k_b = k^0 \exp \left[\frac{-(1 - \alpha)F}{RT} (E - E^0) \right] \quad (4)$$

where E^0 is the formal reversible potential of the redox process, E is the potential (vs. the reference electrode), k^0 is the formal charge-transfer rate constant at potential E^0 (vs. the reference electrode),

α is the charge-transfer coefficient, R is the universal gas constant, F is Faraday's constant and T is the temperature (K).

The potential applied to the electrochemical cell is given by

$$E(t) = E_{\text{app}}(t) - (i_F + i_C)R_u \quad (5)$$

where R_u is the uncompensated resistance, i_C is the capacitive background current which in combination with i_F gives the total current (i) response ($i = i_F + i_C$). The applied potential, $E_{\text{app}}(t)$, is the sum of the dc ($E_{\text{dc}}(t)$) and ac ($E_{\text{ac}}(t)$) terms

$$E_{\text{app}}(t) = E_{\text{dc}}(t) + E_{\text{ac}}(t) \quad (6)$$

In this study $E_{\text{dc}}(t)$ is the ramped dc waveform used in dc cyclic voltammetry and for a reduction process the following relationships therefore apply

$$E_{\text{dc}}(t) = E_{\text{start}} - \nu t; 0 \leq t \leq t_s \quad (7)$$

$$E_{\text{dc}}(t) = E_{\text{start}} - 2\nu t_s + \nu t; t_s \leq t \leq 2t_s \quad (8)$$

$$E_{\text{ac}}(t) = \Delta E \sin(2\pi f t); 0 \leq t \leq 2t_s \quad (9)$$

where ν is the scan rate of the dc ramp, E_{start} is the starting or initial potential (V), t_s is the time required for a single sweep from E_{start} to E_{end} and f is the frequency (Hz) of the sinusoidal ac signal of amplitude ΔE (V) that is superimposed onto the dc ramped waveform.

If the background current contribution is modelled in terms of a non-linear capacitor as by Tokuda and Matsuda,²⁸ then

$$i_C = \left(E \frac{dC_{\text{dl}}}{dE} + C_{\text{dl}} \right) \frac{dE}{dt} \quad (10)$$

In this study the capacitor $C_{\text{dl}}(E)$ is described by the fourth order polynomial

$$C_{\text{dl}}(E) = \sum_{i=0}^4 a_i(E)^i \quad (11)$$

Values of i_C in the potential region where the Faradaic current is not present are calculated from eqn (11) and coefficients a_i are derived from a fit to the background current from the fundamental harmonic.

For a rotating disc electrode, mass transport for all species is given by,³⁷

$$\frac{\partial c}{\partial t} = D_c \frac{\partial^2 c}{\partial z^2} - \nu_z \frac{\partial c}{\partial z} \quad (12)$$

where D_c is the diffusion coefficient for either R or O and z is the distance from the electrode surface. Eqn (12) is subject to the initial condition

$$[\text{O}] = 0 \text{ and } [\text{R}] = [\text{R}]^* \text{ at } t = 0 \text{ for all } z \quad (13)$$

where $[\text{R}]^*$ is the bulk concentration of the R. This condition is also true for all values of t at the maximum distance from the electrode for all time.

Under steady-state conditions, the velocity of the laminar flow, resulting from a rotating plane, away from the electrode is given by

$$\nu_z = \sqrt{\omega^* \nu_k} H(\gamma) \quad \text{with} \quad \gamma = \left(\frac{\omega^*}{\nu_k} \right)^{1/2} z \quad (14)$$

where ν_k is the kinematic viscosity of the fluid, ω^* is the angular frequency of rotation,³⁰

$$H(\gamma) = - \frac{S(\gamma)}{1 + \frac{S(\gamma)}{0.88447}} \quad (15)$$

$$S(\gamma) = \sum_{j=2}^{10} b_j \gamma^j \quad (16)$$

In eqn (16), $b_2 = 0.51023$, $b_3 = -0.32381$, $b_4 = 0.34474$, $b_5 = -0.25972$, $b_6 = 0.16214$, $b_7 = -0.07143$, $b_8 = 0.019911$, $b_9 = -0.0030405$ and $b_{10} = 0.00019181$. Note that this formulation gives a very similar velocity profile to that obtained by Newman,³⁸ but with the advantage of not diverging for large Schmidt numbers ($Sc = \nu_k/D$).

In calculations based on these relationships, care must be taken to ensure that the minimum time-step and spatial step sizes are sufficiently small to accurately represent the system and that the maximum distance from the electrode is small enough to ensure stability of the solution. The maximum distance is determined using the method described in appendix C of the study by Feldberg *et al.*³⁹

The theory for the RDE technique with superimposed sinusoidal waveform was solved using the Monash Electro-Chemistry Simulator (MECSim) package which is written in Fortran 77. This software uses an expanding spatial grid⁴⁰ and is based on a fully implicit finite difference method with the Richtmeyer modification described in detail by Rudolph³⁷ with minor modifications introduced in other publications.^{25,27,41} The simulation package is available on request. The FT-inverse FT method used to resolve the total current derived from MECSim into dc and ac harmonic components is described below.

4 Results and discussion

In experimental studies on the $[\text{Ru}(\text{NH}_3)_6]^{3+/2+}$ and $[\text{Fe}(\text{CN})_6]^{3-/4-}$ processes large amplitude FT ac voltammetry at the RDE was carried out at a frequency (f) 9.0 Hz and an amplitude (ΔE) of 80 mV. This produces the total (dc and ac) current as a function of time as do simulations employed to mimic experimental data. Time domain data were converted to the frequency domain using the FT algorithm and represented as the power spectrum (Fig. 1). Desired ac harmonics and the aperiodic dc component were selected from the power spectrum; band filtering and application of inverse Fourier transforms gave the required dc or ac components. The aperiodic dc component was derived from data near 0 Hz. The ac harmonic components were obtained at multiples of the applied frequency ω . Thus, the current component obtained at ω is called the 1st or fundamental harmonic, while the second, third, fourth, fifth, *etc.* harmonics components are associated with the response at frequencies of 2ω , 3ω , 4ω , 5ω , respectively. The various components obtained from a simulated voltammogram are displayed as a log power spectrum of an FT ac voltammetric experiment in Fig. 1, while the dc and first to seventh harmonics derived from the inverse FT algorithm are displayed in Fig. 2. Fig. 2 also shows the strategy used to obtain the ac equivalent of half wave potentials, $E_{1/2}$, from forward and backward scans of both dc and ac components.

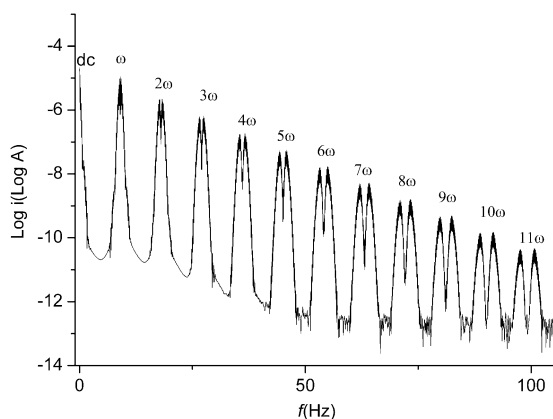


Fig. 1 Simulated RDE Log power spectrum obtained for a quasi-reversible one-electron reduction process using the following parameters: $C^* = 1 \text{ mM}$, $f = 9.0 \text{ Hz}$, $\Delta E = 80 \text{ mV}$, $v = 0.1 \text{ V s}^{-1}$, $\omega^* = 1000 \text{ rpm}$, $E^0 = 0 \text{ V}$, $k^0 = 0.015 \text{ cm s}^{-1}$, $\alpha = 0.5$, $D_O = D_R = 7.54 \times 10^{-6} \text{ cm}^2 \text{ s}^{-1}$, $v_k = 1.0 \times 10^{-2} \text{ cm}^2 \text{ s}^{-1}$, $A = 0.07 \text{ cm}^2$, $R_u = 0$ and $C_{dl} = 0$.

4.1 Theoretical predictions

In order to extract thermodynamic and kinetic information from large amplitude FT ac voltammetric data at a RDE, a number of parameters have to be estimated for even the simple electron transfer process $O + e^- \rightleftharpoons R$. In the first instance it will be assumed that the concentration (C), electrode area (A), uncompensated resistance (R_u), the angular frequency of rotation (ω^*), ac frequency (f), amplitude (ΔE), dc scan rate (v) and temperature (T) are known or can be determined from an independent experiment. The electrode area was calculated from the electrode diameter.

Parameters that need to be determined from the comparison of experimental data and simulation include reversible potential (E^0), heterogeneous electron transfer rate constant (k^0), charge transfer coefficient (α), diffusion coefficients (D)

and double layer capacitance (C_{dl}). Simulations were therefore undertaken to investigate how these parameters can be determined. Commonly, the prediction of the theory is presented in terms of dimensionless parameters. However, in the present case, with three time-dependent variables (scan rate, rotation rate and frequency), this approach is complex. Thus, in order to simplify understanding of the outcome, real terms rather than dimensionless ones are used in the discussion of the theory below. Values of some parameters, such as D , v_k , C_{dl} , A , bulk concentration of the analyte (C^*), T (20°C) and R , chosen for simulations are typical for experimental conditions of this study.

4.1.1 Determination of double layer capacitance. As described in the literature,⁴² the double layer capacitance and its dependence on potential can be modelled by fitting a polynomial to a fundamental harmonic component in potential regions where no ac Faradaic current is present. As is the case with stationary electrodes, at the RDE it was found that a small contribution from the background current is present in 2nd and 3rd harmonic components but 4th and higher harmonics are devoid of background capacitive current. It is essential that the background current is accurately modelled so that the iR_u drop is correctly computed.

4.1.2 Determination of $(E_{1/2})_m$. In the case of RDE voltammetry, the half wave potential, $E_{1/2}$, is an important parameter as it is related to E^0 but it is affected by the magnitude of R_u and for a non-reversible process depends on k^0 and rotation rate as well as E^0 . If a cycle scan of the dc component is used then $(E_{1/2})_m$ may be obtained as the average of $E_{1/2}$ found in the forward scan direction, $(E_{1/2})_f$ and in the backward scan direction, $(E_{1/2})_b$. In the case of FT ac voltammetry at an RDE, the amplitude and frequency of the sinusoidal perturbation also may be significant. Simulations were therefore undertaken to ascertain the influence of

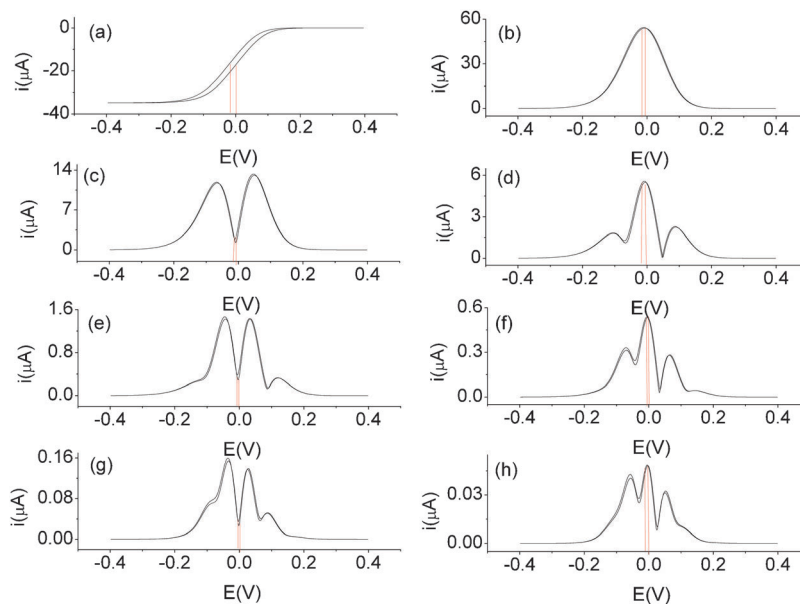


Fig. 2 Simulated Fourier transformed large amplitude ac voltammograms: (a) dc, (b–f) 1st–5th harmonics (parameters for simulation are defined in the caption to Fig. 1); and the representation of a method used to determine $E_{1/2}$ from forward and backward scans of both dc component and ac harmonics.

Table 1 $(E_{1/2})_m$ values and their ac analogues for a reversible one-electron reduction process estimated as a function of RDE rotation rate when simulations are based on parameters $C^* = 1$ mM, $R_u = 100$ ohm, $f = 9.0$ Hz, $\Delta E = 80$ mV, $D_O = D_R = 7.54 \times 10^{-6}$ cm² s⁻¹, $A = 0.07$ cm², $v = 0.1$ V s⁻¹, $v_k = 1.0 \times 10^{-2}$ cm² s⁻¹ and $E^0 = 0$ V

ω^*/rpm	$(E_{1/2})_m/V$	$(E_{1/2})_m$ analogues (V) for designated ac component							
	dc	1st	2nd	3rd	4th	5th	6th	7th	8th
0	0.000	0.000	0.000	0.000	0.000	0.000	0.000	0.000	0.000
500	-0.001	-0.001	-0.001	-0.001	-0.001	-0.001	-0.001	-0.001	-0.001
2500	-0.002	-0.002	-0.002	-0.002	-0.002	-0.002	-0.002	-0.002	-0.002
5000	-0.003	-0.003	-0.003	-0.003	-0.003	-0.003	-0.003	-0.003	-0.003
1000	-0.005	-0.005	-0.005	-0.005	-0.005	-0.005	-0.005	-0.005	-0.005

the ac perturbation and rotation rate on reversible and quasi-reversible systems. $(E_{1/2})_m$ was calculated from the dc component as $(E_{1/2})_m = [(E_{1/2})_f + (E_{1/2})_b]/2$. Analogous potentials derived from cyclic ac RDE voltammograms from each harmonic were calculated from peak currents of (odd harmonics) and current minima (even harmonics) as shown in Fig. 2.

For a fully reversible system (simulated by use of $k^0 = 1 \times 10^4$ cm s⁻¹, $\alpha = 0.5$ and $R_u = 100$ ohm), $(E_{1/2})_m$ was calculated from the dc component and the analogous parameters (see above) from ac harmonics at rotation rates of 500, 1000, 1500, 2000, 2500, 3000, 3500, 4000, 4500, 5000 and 10000 rpm, assuming D_O and D_R to be equal. In these simulations, $(E_{1/2})_m$ was always found to be well approximated to E^0 within an uncertainty of ± 5 mV which is encountered practically. This outcome implies that $(E_{1/2})_m$ and the ac analogues of this parameter are insensitive to the rotation rate. Consequently, for a reversible system, a good approximation of the E^0 value needed for inclusion in the simulation can be obtained directly from $(E_{1/2})_m$ for the dc component or from ac data provided the value of R_u is small. The results of various calculations using a range of rotation rates are summarized in Table 1; $(E_{1/2})_m$ obtained under stationary electrode conditions is also included, where it is known that $(E_{1/2})_m = E^0$.

Simulations were also undertaken with a higher uncompensated resistance for a reversible process (simulated by use of $k^0 = 1 \times 10^4$ cm s⁻¹, $\alpha = 0.5$ and $R_u = 500$ ohm). Variation in $(E_{1/2})_m$ for a reversible electrochemical process with higher resistance of 500 ohm was also studied at various rotation rates as above and values are given in Table 2. $(E_{1/2})_m$ and the ac analogues become more negative with increase in the rotation rate so in this case $(E_{1/2})_m$ only provides a reasonably good estimate of (E^0) at the low rotation rate of 500 rpm. This potential shift arises because when higher resistance is present, then enhanced and now a significant iR drop at higher rotation rates (i becomes larger) causes $(E_{1/2})_m$ to shift more negative potential.¹³

For a quasi-reversible process (simulated by use of $k^0 = 0.008$ cm s⁻¹, $\alpha = 0.5$ and $R_u = 0$ ohm), $(E_{1/2})_m$ and their ac analogues also were determined from simulations undertaken as a function of rotation rate. Data in Table 3 show how increased convective mass transport influences the $(E_{1/2})_m$ type of parameters for the dc component and ac harmonics. These results demonstrate that all values shift negatively under convective mass transport conditions, but the shift is less significant for the higher harmonics and for the lower rotation rate data. Therefore, the best estimation of E^0 is obtained from $(E_{1/2})_m$ analogues derived from the higher harmonics, especially those obtained under low rotation rate conditions.

4.1.3 Estimation of diffusion coefficient from the limiting current in the dc component. When using dc voltammetry at RDE, the diffusion coefficient of species (O) can be determined from the limiting current and use of the Levich equation.¹³

$$I_{\text{lim}} = -0.62nFAD_O^{2/3}\nu_k^{-1/6}[O]^*\omega^{1/2} \quad (17)$$

where $[O]^*$ is bulk solution concentration of O.

Fourier transformed large amplitude ac voltammetry allows the dc component to be resolved from the ac components. If the ac sinusoidal perturbation does not affect the limiting current of the dc component, then the Levich equation should be applicable to the dc component of ac voltammetry at a rotating disc electrode and hence can be used to determine the diffusion coefficient. In order to validate this assumption, simulations were carried out in the absence of a sine wave perturbation (*i.e.* dc voltammetry) and with a sine wave perturbation with an amplitude of 80 mV, a frequency of 9.0 Hz and RDE rotation rates of 500 to 10000 rpm. In the case of quasi-reversible system ($k^0 = 0.008$ cm s⁻¹, $\alpha = 0.5$), analysis of the dc component showed that although the shape is altered by the ac perturbation, the limiting current is unaltered as shown in Fig. 3. Furthermore, as expected,

Table 2 $(E_{1/2})_m$ values and their ac analogues for a reversible one-electron reduction process estimated as a function of RDE rotation rate: when simulations are based on parameters $C^* = 1$ mM, $R_u = 500$ ohm, $f = 9.0$ Hz, $\Delta E = 80$ mV, $D_O = D_R = 7.54 \times 10^{-6}$ cm² s⁻¹, $A = 0.07$ cm², $v = 0.1$ V s⁻¹, $v_k = 1.0 \times 10^{-2}$ cm² s⁻¹ and $E^0 = 0$ V

ω^*/rpm	$(E_{1/2})_m/V$	$(E_{1/2})_m$ analogues (V) for designated ac component							
	dc	1st	2nd	3rd	4th	5th	6th	7th	8th
0	0.000	-0.001	-0.001	-0.001	-0.001	-0.001	-0.001	-0.001	-0.001
500	-0.008	-0.006	-0.006	-0.006	-0.006	-0.006	-0.006	-0.006	-0.006
2500	-0.013	-0.013	-0.013	-0.013	-0.013	-0.013	-0.013	-0.013	-0.013
5000	-0.019	-0.019	-0.019	-0.019	-0.019	-0.019	-0.019	-0.019	-0.019
10000	-0.028	-0.027	-0.027	-0.027	-0.027	-0.027	-0.027	-0.027	-0.027

Table 3 $(E_{1/2})_m$ values and their ac analogues for a quasi-reversible one-electron reduction process estimated as a function of RDE rotation rate when simulations are based on parameters $C^* = 1 \text{ mM}$, $k^0 = 0.008 \text{ cm s}^{-1}$, $\alpha = 0.5$, $R_u = 0.0 \text{ ohm}$, $f = 9.0 \text{ Hz}$, $\Delta E = 80 \text{ mV}$, $D_O = D_R = 7.54 \times 10^{-6} \text{ cm}^2 \text{ s}^{-1}$, $A = 0.07 \text{ cm}^2$, $v = 0.1 \text{ V s}^{-1}$, $v_k = 1.0 \times 10^{-2} \text{ cm}^2 \text{ s}^{-1}$ and $E^0 = 0 \text{ V}$

ω^*/rpm	$(E_{1/2})_m/\text{V}$	$(E_{1/2})_m$ analogues (V) for designated ac component							
	dc	1st	2nd	3rd	4th	5th	6th	7th	8th
0	0.000	0.000	0.000	0.000	0.000	0.000	0.000	0.000	0.000
500	-0.006	-0.007	-0.008	-0.006	-0.002	-0.003	-0.001	-0.001	-0.001
2500	-0.015	-0.017	-0.017	-0.014	-0.006	-0.008	-0.003	-0.007	-0.003
5000	-0.030	-0.025	-0.025	-0.021	-0.009	-0.013	-0.003	-0.009	-0.003
10 000	-0.046	-0.037	-0.035	-0.033	-0.021	-0.021	-0.006	-0.015	-0.005

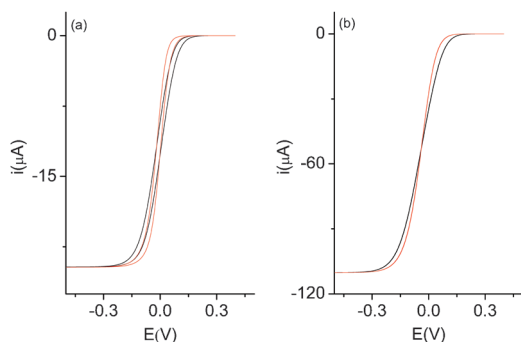


Fig. 3 Comparison of simulated dc components (—) without and (—) with an ac perturbation of $f = 9.0 \text{ Hz}$, $\Delta E = 80 \text{ mV}$, at rotation rates of (a) 500 rpm and (b) 10 000 rpm. Other simulation parameters include $C^* = 1 \text{ mM}$, $k^0 = 0.008 \text{ cm s}^{-1}$, $\alpha = 0.5$, $R_u = 0$, $D_O = D_R = 7.54 \times 10^{-6} \text{ cm}^2 \text{ s}^{-1}$, $A = 0.07 \text{ cm}^2$, $v = 0.1 \text{ V s}^{-1}$, $v_k = 1.0 \times 10^{-2} \text{ cm}^2 \text{ s}^{-1}$ and $E^0 = 0 \text{ V}$.

hysteresis is observed in the dc component in the lower rotation rate cases in Fig. 3(a) when the scan rate v is high (0.1 V s^{-1}); with increase in the rotation rate hysteresis becomes less obvious (Fig. 3(b)). It is concluded that the diffusion coefficient can be determined from the dc component of FT ac voltammetry at a RDE and hysteresis at the low rotation rate is an effect of the scan rate and not of the ac perturbation. Similar conclusions with respect to the limiting current were reached for the reversible case where data presented in Fig. 4 show that although the shape of the dc component voltammogram is altered, the limiting current

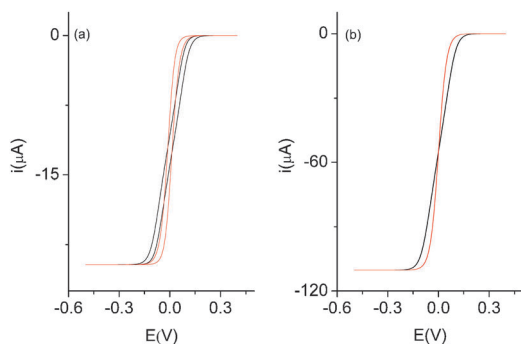


Fig. 4 Comparison of simulated dc components (—) without and (—) with ac perturbation of $f = 9.0 \text{ Hz}$, $\Delta E = 80 \text{ mV}$, at rotation rates of (a) 500 rpm and (b) 10 000 rpm for a reversible electron transfer process, other simulation parameters include $C^* = 1 \text{ mM}$, $R_u = 0$, $D_O = D_R = 7.54 \times 10^{-6} \text{ cm}^2 \text{ s}^{-1}$, $A = 0.07 \text{ cm}^2$, $v = 0.1 \text{ V s}^{-1}$, $v_k = 1.0 \times 10^{-2} \text{ cm}^2 \text{ s}^{-1}$ and $E^0 = 0 \text{ V}$.

is not affected by the rotation rate. It is also obvious from Fig. 4 that $(E_{1/2})_m$ remains unaltered even at 10 000 rpm when $R_u = 0$.

4.1.4 Effect of convection on the ac harmonics. It has been demonstrated in the earlier studies by Tokuda and Matsuda^{28,29} that the ac current obtained from small amplitude ac perturbation is relatively insensitive to convective mass transport compared to dc voltammetry. Numerical simulations were undertaken in this study to investigate how convective mass transport affects the ac components under large amplitude conditions.

For a fully reversible electron transfer reaction in the absence of uncompensated resistance, ac voltammograms (frequency of 9 Hz and amplitude of 80 mV) were simulated under both stationary and rotated (500 and 10 000 rpm) conditions. The fundamental and second harmonic components are shown in Fig. 5. Under the low rotation rate (500 rpm) conditions, convective mass transport has negligible effects on the ac harmonics. With the high rotation rate (10 000 rpm) conditions, small effects of convective mass transport are observed in the 1st–3rd harmonics. However, the effect becomes negligible in the 4th and higher harmonics (results not shown). In the presence of uncompensated resistance (Fig. S1, ESI[†]), ac harmonics remain essentially unaltered with a rotation rate of 500 rpm. In contrast, a small effect from convective mass transport is now observed even in the 5th harmonic with a rotation rate of 10 000 rpm. In the case of a higher frequency (90.0 Hz), no significant difference was observed in

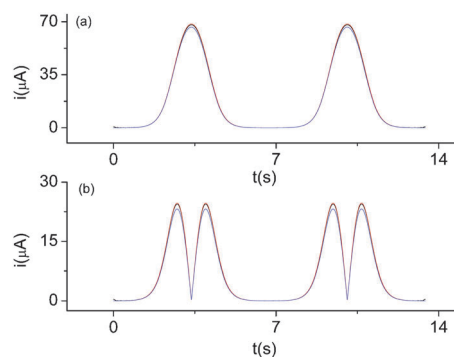


Fig. 5 Simulated Fourier transformed large amplitude ac voltammograms for a reversible process. (a) 1st harmonic, (b) 2nd harmonic with ω^* of 0 (—), 500 (—) and 10 000 (—) rpm, $C^* = 1 \text{ mM}$, $f = 9.0 \text{ Hz}$, $\Delta E = 80 \text{ mV}$, $R_u = 0 \text{ ohm}$, $D = 6.8 \times 10^{-6} \text{ cm}^2 \text{ s}^{-1}$, $C = 0 \text{ } \mu\text{F cm}^{-2}$, $A = 0.07 \text{ cm}^2$, and $v_k = 1.0 \times 10^{-2} \text{ cm}^2 \text{ s}^{-1}$. Note that 0 and 500 rpm data are essentially indistinguishable.

ac currents for any harmonic using rotation rates over the range of 0 to 10000 rpm in either the presence (100 ohm) or absence of resistance. All these results are fully predictable since the depletion layer due to the ac perturbation is much thinner than the convective diffusion layer thickness; thus the ac response is essentially unperturbed by convection, for either higher harmonic or higher frequency conditions.

For a quasi reversible system ($k^0 = 0.02 \text{ cm s}^{-1}$), the effect of convective mass transport on the ac harmonics is enhanced, as shown in large amplitude ac voltammograms obtained at a frequency of 9 Hz and an amplitude of 80 mV both in the presence and absence of uncompensated resistance (Fig. S2 and S3, ESI†). This increased sensitivity is due to the fact that the apparent reversibility is now a function of mass transport rate. However, the extent of influence of convective mass transport still remains small, especially when compared to that on the dc voltammograms or dc components of ac voltammograms. A small effect of convective mass transport on ac harmonics was still observed for a quasi-reversible process with a higher frequency (90.0 Hz) ac perturbation.

The effects of convective mass transport on ac harmonics were also investigated under reversible and quasi-reversible conditions where the amplitude of ac perturbation is 40 or 160 mV instead of 80 mV. The relative influence of convective mass transport on the ac harmonics remains similar to that observed at 80 mV.

4.1.5 Determination of heterogeneous electron transfer constant from ac harmonics and the upper limit of determination of k^0 . One of the major advantages of large amplitude ac voltammetry at the stationary electrode is that the higher harmonics are highly sensitive to electrode kinetics.²⁵ Investigation highlighted in Section 4.1.4 implies that this advantage of large amplitude ac voltammetry is retained under hydrodynamic conditions. Therefore, various simulations were undertaken with different k^0 values to ascertain the upper limit of kinetic determination using ac harmonics. Simulations (Fig. 6) with k^0 values of 0.5, 1 and 10 cm s^{-1} demonstrate that the current magnitude increases gradually when k^0 is varied from 0.5 to 1 cm s^{-1} but for values $\geq 2 \text{ cm s}^{-1}$ becomes constant and hence represents a reversible process in the case of 7th harmonic. Variations of the current magnitude

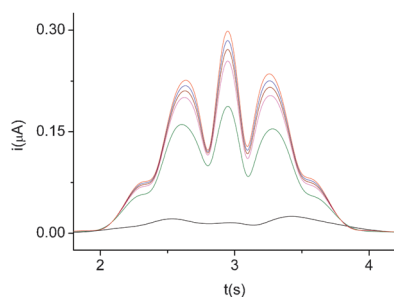


Fig. 6 Simulated Fourier transformed large amplitude ac voltammograms (7th harmonic) with k^0 values of (—) 0.01 cm s^{-1} , (—) 0.1 cm s^{-1} , (—) 0.3 cm s^{-1} , (—) 0.5 cm s^{-1} , (—) 1.0 cm s^{-1} , (—) reversible, $C^* = 1 \text{ mM}$, $f = 9.0 \text{ Hz}$, $\Delta E = 80 \text{ mV}$, $R_u = 120 \text{ ohm}$, $D = 6.8 \times 10^{-6} \text{ cm}^2 \text{ s}^{-1}$, $C = 12 \text{ } \mu\text{F cm}^{-2}$, $A = 0.07 \text{ cm}^2$, $\omega^* = 3000 \text{ rpm}$ and $v_k = 1.0 \times 10^{-2} \text{ cm}^2 \text{ s}^{-1}$.

with k^0 in the higher harmonics, where data are flow rate insensitive, are similar to those found with a stationary electrode. Thus determination of k^0 values $\geq 2.0 \text{ cm s}^{-1}$ is not readily accomplished unless high frequencies are employed, but an enhanced iR_u drop and capacitance problems are expected to complicate data analysis under these higher frequency conditions.

4.2 Experimental results

Once all the parameters including R , C_{dl} , $(E_{1/2})_m$ (see Section 4.1.2 and Fig. 2 for definition of this term), D , C , T and A are known or evaluated independently, simulations can be performed to estimate k^0 and α . FT ac voltammetric data at a rotating disc electrode for the reversible $[\text{Ru}(\text{NH}_3)_6]^{3+/2+}$ and quasi-reversible $[\text{Fe}(\text{CN})_6]^{3-/4-}$ systems were collected and analysed according to the theory and procedures described above.

4.2.1 Effect of hydrodynamic mass transport on the dc and ac current

(a) *dc limiting current and diffusion coefficient estimation.* The $[\text{Ru}(\text{NH}_3)_6]^{3+/2+}$ process at a glassy carbon electrode and the $[\text{Fe}(\text{CN})_6]^{3-/4-}$ one at both glassy carbon and platinum rotating disc electrodes were examined under dc and ac voltammetric conditions. As concluded from analysis of simulations, diffusion coefficient values should be readily estimated from the limiting current of dc voltammetry, or the dc component derived from FT ac voltammetry. The average D value derived from limiting current data obtained for the reduction of 1.1 mM and 0.14 mM $[\text{Ru}(\text{NH}_3)_6]^{3+}$ in aqueous 0.1 M KCl electrolyte under a wide range of conditions and by the use of the Levich equation was found to be $(6.83 \pm 0.06) \times 10^{-6} \text{ cm}^2 \text{ s}^{-1}$ using either ac or dc voltammetry and in close agreement with the literature value of $6.7 \times 10^{-6} \text{ cm}^2 \text{ s}^{-1}$.¹⁵ Individual values of diffusion coefficients for $[\text{Ru}(\text{NH}_3)_6]^{3+}$ at given concentrations and rotation rates are summarized in Table 4.

Reduction of $[\text{Fe}(\text{CN})_6]^{3-}$ is an inner sphere electron transfer process and hence electrode surface dependent so RDE studies on this process were carried out at two different electrodes surfaces (platinum and glassy carbon) at 0.98 mM and 0.14 mM ferricyanide concentration. Diffusion coefficient values were again calculated using the Levich equation from limiting currents from dc RDE voltammograms and the dc component from

Table 4 Diffusion coefficients obtained for $[\text{Ru}(\text{NH}_3)_6]^{3+}$ in aqueous 0.1 M KCl electrolyte using a glassy carbon rotating disc electrode. Values were calculated from i_L values obtained from dc and ac voltammetry (dc component) and use of the Levich equation with $A = 0.07 \text{ cm}^2$, $v = 0.1 \text{ V s}^{-1}$ and $v_k = 1.0 \times 10^{-2} \text{ cm}^2 \text{ s}^{-1}$

C	1.1 mM		0.15 mM	
	ω^*/rpm	$D (\text{ac voltammetry})/\text{cm}^2 \text{ s}^{-1}$	$D (\text{dc voltammetry})/\text{cm}^2 \text{ s}^{-1}$	$D (\text{ac voltammetry})/\text{cm}^2 \text{ s}^{-1}$
500		6.88×10^{-6}	6.82×10^{-6}	6.80×10^{-6}
1000		6.86×10^{-6}	6.81×10^{-6}	6.84×10^{-6}
1500		6.84×10^{-6}	6.80×10^{-6}	6.82×10^{-6}
2000		6.80×10^{-6}	6.81×10^{-6}	6.84×10^{-6}
2500		6.82×10^{-6}	6.84×10^{-6}	6.89×10^{-6}
3000		6.82×10^{-6}	6.87×10^{-6}	6.88×10^{-6}

Table 5 Diffusion coefficients obtained for $[\text{Fe}(\text{CN})_6]^{3-}$ in aqueous 3.0 M KCl electrolyte using a glassy carbon rotating disc electrode. Values were calculated from i_L values obtained from dc and ac voltammetry (dc component) and use of the Levich equation with $A = 0.07 \text{ cm}^2$, $\nu = 0.1 \text{ V s}^{-1}$ and $\nu_k = 1.0 \times 10^{-2} \text{ cm}^2 \text{ s}^{-1}$

C	0.98 mM		0.14 mM	
ω^*/rpm	D (ac voltammetry)/ $\text{cm}^2 \text{ s}^{-1}$	D (dc voltammetry)/ $\text{cm}^2 \text{ s}^{-1}$	D (ac voltammetry)/ $\text{cm}^2 \text{ s}^{-1}$	D (dc voltammetry)/ $\text{cm}^2 \text{ s}^{-1}$
500	7.54×10^{-6}	7.54×10^{-6}	7.54×10^{-6}	7.52×10^{-6}
1000	7.55×10^{-6}	7.54×10^{-6}	7.54×10^{-6}	7.53×10^{-6}
1500	7.54×10^{-6}	7.55×10^{-6}	7.55×10^{-6}	7.50×10^{-6}
2000	7.54×10^{-6}	7.54×10^{-6}	7.54×10^{-6}	7.52×10^{-6}
2500	7.52×10^{-6}	7.54×10^{-6}	7.54×10^{-6}	7.52×10^{-6}
3000	7.52×10^{-6}	7.52×10^{-6}	7.52×10^{-6}	7.51×10^{-6}

Table 6 Diffusion coefficients obtained for $[\text{Fe}(\text{CN})_6]^{3-}$ in aqueous 3.0 M KCl electrolyte using a platinum rotating disc electrode. Values were calculated from i_L values obtained from dc and ac voltammetry (dc component) and use of the Levich equation with $A = 0.07 \text{ cm}^2$, $\nu = 0.1 \text{ V s}^{-1}$ and $\nu_k = 1.0 \times 10^{-2} \text{ cm}^2 \text{ s}^{-1}$

C	0.98 mM		0.14 mM	
ω^*/rpm	D (ac voltammetry)/ $\text{cm}^2 \text{ s}^{-1}$	D (dc voltammetry)/ $\text{cm}^2 \text{ s}^{-1}$	D (ac voltammetry)/ $\text{cm}^2 \text{ s}^{-1}$	D (dc voltammetry)/ $\text{cm}^2 \text{ s}^{-1}$
500	7.54×10^{-6}	7.54×10^{-6}	7.56×10^{-6}	7.54×10^{-6}
1000	7.55×10^{-6}	7.54×10^{-6}	7.55×10^{-6}	7.54×10^{-6}
1500	7.54×10^{-6}	7.55×10^{-6}	7.55×10^{-6}	7.55×10^{-6}
2000	7.54×10^{-6}	7.52×10^{-6}	7.55×10^{-6}	7.55×10^{-6}
2500	7.52×10^{-6}	7.54×10^{-6}	7.55×10^{-6}	7.52×10^{-6}
3000	7.52×10^{-6}	7.52×10^{-6}	7.55×10^{-6}	7.55×10^{-6}

FT ac RDE voltammograms. Average D values derived from either dc and ac voltammetry at the GC electrodes were again found to be identical and $(7.53 \pm 0.03) \times 10^{-6} \text{ cm}^2 \text{ s}^{-1}$ which is in good agreement with the literature value of $7.4 \times 10^{-6} \text{ cm}^2 \text{ s}^{-1}$ in 1.0 M KCl.⁴³ The average D value obtained at platinum was also $(7.54 \pm 0.02) \times 10^{-6} \text{ cm}^2 \text{ s}^{-1}$. Individual D values obtained as a function of rotation rate, concentration and electrode surface are provided in Tables 5 and 6. Levich behaviour was observed when the limiting current derived from the dc component was plotted *versus* square root of the rotation rate as shown in Fig. S4, ESI.†

(b) *Effect of the rotation rate on ac harmonics and determination of k^0 values.* In the FT ac voltammetric experiment, the dc component is governed by convective-diffusion and the limiting current obeys the Levich equation as shown in Fig. 7(a). In sharp contrast, the ac harmonics for the reduction of 0.98 mM $[\text{Fe}(\text{CN})_6]^{3-}$ are almost independent of rotation rate (500 rpm and 3000 rpm cases are given in Fig. 7b–f). Small differences associated with rotation rate variation are observed in the 1st, 2nd and 3rd harmonics, but in the kinetically sensitive higher harmonics, no difference was observed in the ac current at these two rotation rates. The conclusion of this outcome is that detailed electrode kinetic information can be extracted from the ac component using FT ac voltammetry using stationary electrode theory, even under rotating disc electrode conditions. Since D values can be calculated from the dc component, this technique actually allows mass transport and kinetic data to be evaluated from a single experiment.

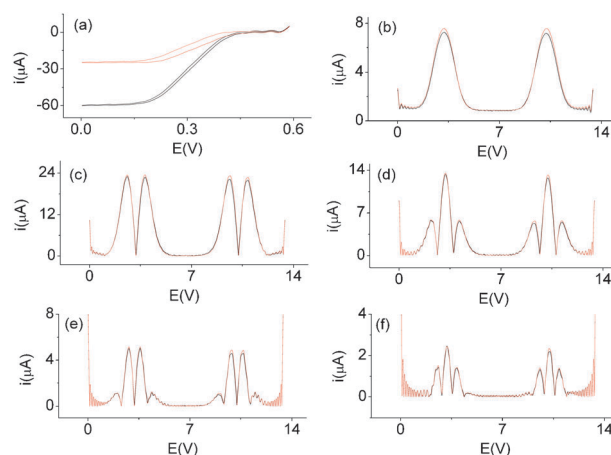


Fig. 7 Comparison of dc and ac components for 0.98 mM $[\text{Fe}(\text{CN})_6]^{3-}$ reduction in 3.0 M KCl at a glassy carbon electrode with rotation rates of (—) 500 rpm and (—) 3000 rpm, dc component (a) 1st harmonic, (b) 2nd harmonic, (c) 3rd harmonic, (d) 4th harmonic, (e) 5th harmonic, (f) 6th harmonic, $f = 9.0 \text{ Hz}$, $\Delta E = 80 \text{ mV}$, $A = 0.07 \text{ cm}^2$, $\nu = 0.1 \text{ V s}^{-1}$.

4.2.2 Comparison of simulated and experimental data for the $[\text{Ru}(\text{NH}_3)_6]^{3+/2+}$ process. The FT-ac voltammetric reduction of 1.1 mM and 0.14 mM $[\text{Ru}(\text{NH}_3)_6]^{3+}$ at a glassy carbon electrode allowed parameters described above to be determined from the comparison of experimental and simulated data. $(E_{1/2})_m$, taken as E^0 , was determined to be $0.143 \pm 0.002 \text{ V vs. Ag/AgCl}$ and almost independent of rotation rate in both experimental dc or ac component data. The D value used for simulations was $6.83 \times 10^{-6} \text{ cm}^2 \text{ s}^{-1}$ as deduced from the limiting current of the dc component and use of the Levich equation. Uncompensated resistance was measured from the RC time constant to be 122 ohm and the capacitance as deduced from the fundamental harmonic component was $20 \mu\text{F cm}^{-2}$. Simulations were then conducted at variable rotation rates. It emerged by varying k^0 and α that all simulations with $k^0 \geq 2 \text{ cm s}^{-1}$ agreed very well with experimental data. The $[\text{Ru}(\text{NH}_3)_6]^{3+/2+}$ process is therefore reversible under the FT ac conditions at a RDE which agrees with the literature value of 17 cm s^{-1} obtained at platinum.¹⁵ As found experimentally, theoretically predicted limiting currents values from the dc component were strongly dependent on the rotation rate and in convective mass transport control. A comparison of experimental and simulated dc components for a reversible electron transfer process as a function of rotation rate is presented in Fig. 8 using the following simulation parameters $D = 6.83 \times 10^{-6} \text{ cm}^2 \text{ s}^{-1}$, $R_u = 122 \text{ ohm}$ and $C_{dl} = 20 \mu\text{F cm}^{-2}$ (assumed to be potential independent).

The ac components obtained at different rotation rates revealed that the 1st harmonic component slightly decreases with increase in the rotation rate of the RDE while all other harmonics are almost independent of the rotation rate. The lack of sensitivity to convection can be attributed to the fact that the ac depletion layer is thinner than the hydrodynamic mass transport layer as pointed out by Tokuda and Matsuda in their studies of the 1st harmonic under small amplitude conditions.^{28,29} However, we now show that 2nd and higher order harmonics are even less sensitive to the rotation rate

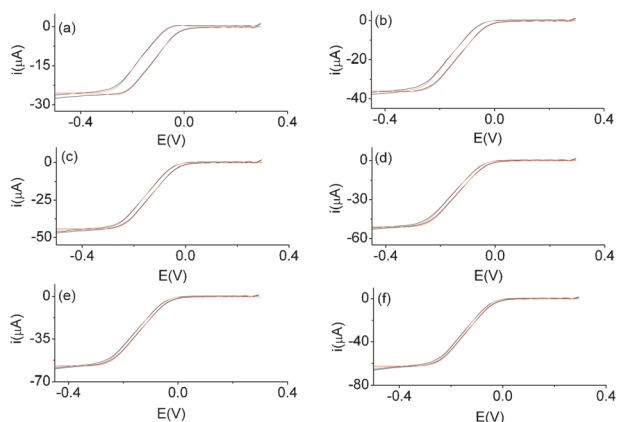


Fig. 8 Comparison of experimental (—) dc components of FT ac voltammograms for reduction of 1.1 mM $[\text{Ru}(\text{NH}_3)_6]^{3+}$ in aqueous 0.1 M KCl electrolyte at a glassy carbon electrode with rotation rates of (a) 500 rpm, (b) 1000 rpm, (c) 1500 rpm, (d) 2000 rpm, (e) 2500 rpm, (f) 3000 rpm, and simulated ones (—) for a reversible electron transfer process obtained with $D = 6.83 \times 10^{-6} \text{ cm}^2 \text{ s}^{-1}$, $R_u = 122 \text{ ohm}$, $C_{dl} = 20 \mu\text{F cm}^{-2}$, $A = 0.07 \text{ cm}^2$, $\nu = 0.1 \text{ V s}^{-1}$, $\nu_k = 1.0 \times 10^{-2} \text{ cm}^2 \text{ s}^{-1}$ and $E^0 = 0.143 \text{ V}$.

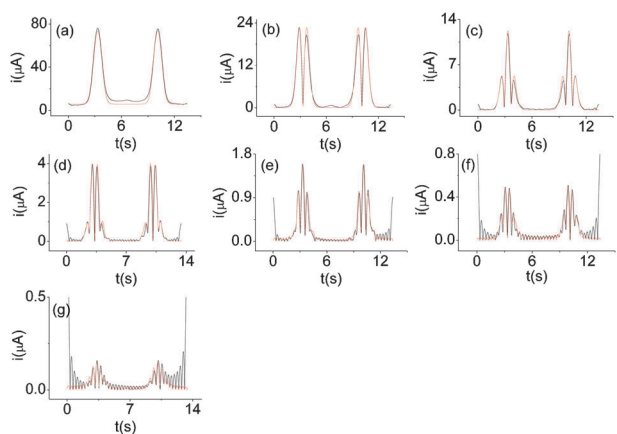


Fig. 9 Comparison of experimental (—) FT ac voltammograms obtained for reduction of 1.1 mM $[\text{Ru}(\text{NH}_3)_6]^{3+}$ in 0.1 M aqueous KCl electrolyte at a glassy carbon electrode with a rotation rate 3000 rpm (a) 1st harmonic, (b) 2nd harmonic, (c) 3rd harmonic, (d) 4th harmonic, (e) 5th harmonic, (f) 6th harmonic, (g) 7th harmonic, and simulated ones (—) for a reversible electron transfer process obtained with $D = 6.83 \times 10^{-6} \text{ cm}^2 \text{ s}^{-1}$, $R_u = 122 \text{ ohm}$, $C_{dl} = 20 \mu\text{F cm}^{-2}$, $A = 0.07 \text{ cm}^2$, $\nu = 0.1 \text{ V s}^{-1}$, $\nu_k = 1.0 \times 10^{-2} \text{ cm}^2 \text{ s}^{-1}$ and $E^0 = 0.143 \text{ V}$.

than the fundamental harmonic. However, our simulation can accommodate the contribution of convection to ac data.

Simulation of ac voltammetric data for a reversible process is compared with experimental data in Fig. 9 for the reduction of 1.1 mM $[\text{Ru}(\text{NH}_3)_6]^{3+}$ at a rotation rate of 500 rpm. Reversibility was also found for the reduction of 0.14 mM $[\text{Ru}(\text{NH}_3)_6]^{3+}$ in 0.1 M KCl using parameters described in Table 7.

4.2.3 Comparison of simulations and experimental data for the $[\text{Fe}(\text{CN})_6]^{3-/4-}$ process. For the quasi-reversible $[\text{Fe}(\text{CN})_6]^{3-/4-}$ system in aqueous 3.0 M KCl electrolyte, FT ac RDE voltammetric studies at $[\text{Fe}(\text{CN})_6]^{3-}$ concentrations

Table 7 Parameters extracted from simulation of the ac components of FT ac voltammetry of $[\text{Ru}(\text{NH}_3)_6]^{3+}$ in 0.1 M aqueous KCl electrolyte at a glassy carbon RDE with a rotation rate of 500–3000 rpm, $D = 6.82 \times 10^{-6} \text{ cm}^2 \text{ s}^{-1}$

Conc./mM:	1.1	0.14
$C_{dl}/\mu\text{F cm}^{-2}$	20	15
$k^0/\text{cm s}^{-1}$	≥ 2	≥ 2
R_u/ohm	122	120
$(E_{1/2})_m/\text{V}$	0.143	0.143

of 0.98 and 0.14 mM were undertaken at rotating glassy carbon and platinum electrodes. The first to sixth harmonics along with the dc component were compared with simulated data. Voltammograms were simulated using experimentally determined uncompensated resistance of 30 ohm, $(E_{1/2})_m = E^0 = 0.315 \text{ V vs. Ag/AgCl}$, $D = 7.54 \times 10^{-6} \text{ cm}^2 \text{ s}^{-1}$ and α was assumed to be 0.5. Simulations of the dc component for reduction of 0.98 mM $[\text{Fe}(\text{CN})_6]^{3-}$ at a rotating glassy carbon electrode are in excellent agreement with the experimental data at all rotation rates with $k^0 = 0.07 \text{ cm s}^{-1}$ (Fig. 10). Experimental and simulated data for ac harmonic components 1 to 5 were also found to be in excellent agreement using parameters given in Table 8 and Fig. 11, with a wide range of rotation rates.

FT ac voltammetric data recorded at a platinum RDE could be modelled using simulations with the same R_u , D and α values used for the GC studies. However, a k^0 value of 0.2 cm s^{-1} is now needed to model experimental data using other parameters summarized in Table 8. A comparison of experimental and simulated dc components at various rotation rates is provided in Fig. 12. Likewise, ac harmonic components are compared in Fig. 13. Excellent agreement was observed between all experimental and simulated data.

k^0 values for the $[\text{Fe}(\text{CN})_6]^{3-/4-}$ process obtained at platinum and glassy carbon electrodes in this study are in close agreement with literature values of 0.24 cm s^{-1} and 0.04 cm s^{-1} , respectively.^{44,45} The $[\text{Fe}(\text{CN})_6]^{3-/4-}$ process is a

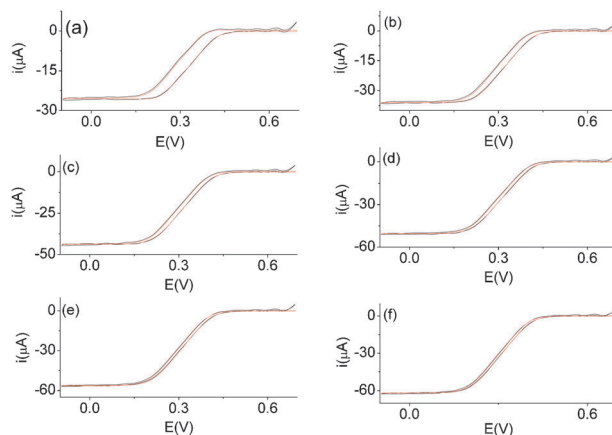


Fig. 10 Comparison of experimental (—) dc components of FT ac voltammograms for reduction of 0.98 mM $[\text{Fe}(\text{CN})_6]^{3-}$ in aqueous 3.0 M KCl electrolyte at a glassy carbon electrode rotated at (a) 500 rpm, (b) 1000 rpm, (c) 1500 rpm, (d) 2000 rpm, (e) 2500 rpm, (f) 3000 rpm, and simulated ones (—) obtained with $D = 7.54 \times 10^{-6} \text{ cm}^2 \text{ s}^{-1}$, $R_u = 30 \text{ ohm}$, $C_{dl} = 30 \mu\text{F cm}^{-2}$, $k^0 = 0.07 \text{ cm s}^{-1}$ and $\alpha = 0.5$, $A = 0.07 \text{ cm}^2$, $\nu = 0.1 \text{ V s}^{-1}$, $\nu_k = 1.0 \times 10^{-2} \text{ cm}^2 \text{ s}^{-1}$ and $E^0 = 0.315 \text{ V}$.

Table 8 Parameters extracted from ac harmonic components of FT ac voltammograms for reduction of $[\text{Fe}(\text{CN})_6]^{3-}$ in 3.0 M aqueous KCl electrolyte at RDEs, with a rotation rate of 500–3000 rpm, $D = 7.54 \times 10^{-6} \text{ cm}^2 \text{ s}^{-1}$

Conc./mM	0.98		0.14	
Electrode	Glassy carbon	Platinum	Glassy carbon	Platinum
$C_{\text{dl}}/\mu\text{F cm}^{-2}$	30	150	27	150
$k^0/\text{cm s}^{-1}$	0.07	0.2	0.07	0.2
α	0.5	0.5	0.5	0.5
R_u/ohm	30	30	30	30
$(E_{1/2})_{\text{m}}/\text{V}$	0.315	0.315	0.315	0.315

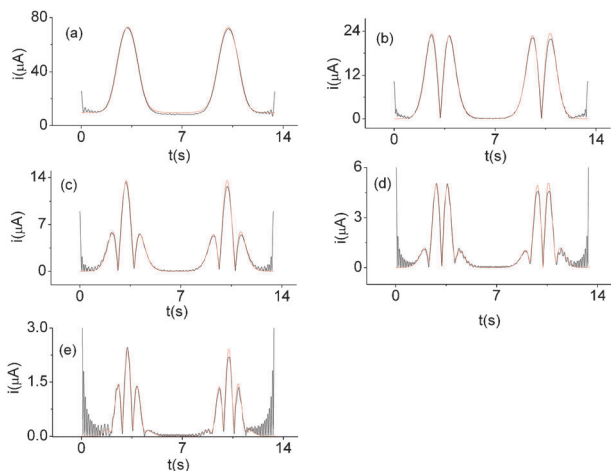


Fig. 11 Comparison of experimental (—) FT ac voltammograms for reduction of 0.98 mM $[\text{Fe}(\text{CN})_6]^{3-}$ in aqueous 3.0 M KCl electrolyte at a glassy carbon electrode rotated at 3000 rpm, (a) 1st harmonic, (b) 2nd harmonic, (c) 3rd harmonic, (d) 4th harmonic, (e) 5th harmonic, and simulated ones (—) obtained with $D = 7.54 \times 10^{-6} \text{ cm}^2 \text{ s}^{-1}$, $R_u = 30 \text{ ohm}$, $C_{\text{dl}} = 30 \mu\text{F cm}^{-2}$, $k^0 = 0.07 \text{ cm s}^{-1}$, $\alpha = 0.5$, $A = 0.07 \text{ cm}^2$, $v = 0.1 \text{ V s}^{-1}$, $v_k = 1.0 \times 10^{-2} \text{ cm}^2 \text{ s}^{-1}$ and $E^0 = 0.315 \text{ V}$.

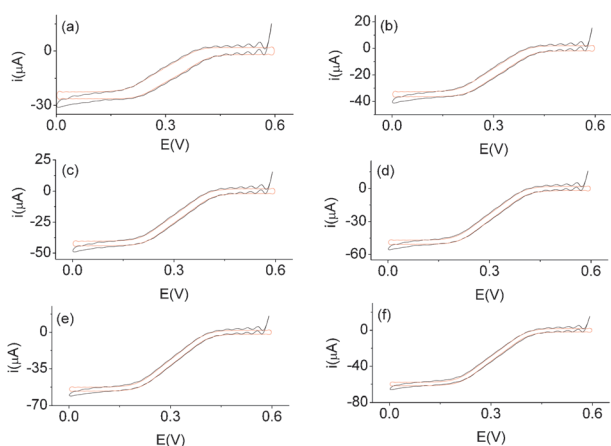


Fig. 12 Comparison of experimental (—) dc components of FT ac voltammograms for reduction of 0.98 mM $[\text{Fe}(\text{CN})_6]^{3-}$ in aqueous 3.0 M KCl electrolyte at a platinum electrode rotated at (a) 500 rpm, (b) 1000 rpm, (c) 1500 rpm, (d) 2000 rpm, (e) 2500 rpm, (f) 3000 rpm, and simulated ones (—) obtained with $D = 7.5 \times 10^{-6} \text{ cm}^2 \text{ s}^{-1}$, $R_u = 30 \text{ ohm}$, $C_{\text{dl}} = 150 \mu\text{F cm}^{-2}$, $k^0 = 0.2 \text{ cm s}^{-1}$, $\alpha = 0.5$, $A = 0.07 \text{ cm}^2$, $v = 0.1 \text{ V s}^{-1}$, $v_k = 1.0 \times 10^{-2} \text{ cm}^2 \text{ s}^{-1}$ and $E^0 = 0.315 \text{ V}$.

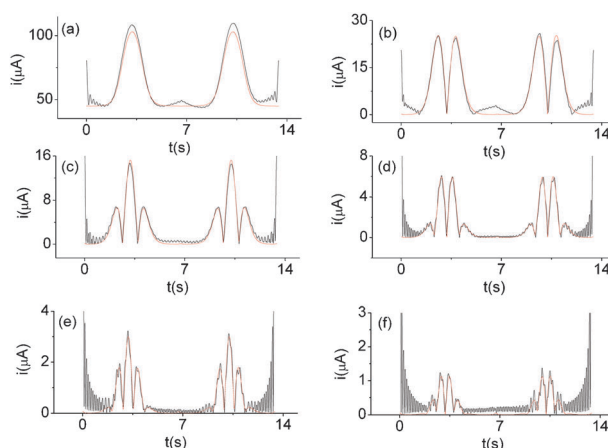


Fig. 13 Comparison of experimental (—) FT ac voltammograms for reduction of 0.98 mM $[\text{Fe}(\text{CN})_6]^{3-}$ in aqueous 3.0 M KCl electrolyte at a platinum electrode rotated at 3000 rpm (a) 1st harmonic, (b) 2nd harmonic, (c) 3rd harmonic, (d) 4th harmonic, (e) 5th harmonic, (f) 6th harmonic, and simulated ones (—) obtained with $D = 7.5 \times 10^{-6} \text{ cm}^2 \text{ s}^{-1}$, $R_u = 30 \text{ ohm}$, $C_{\text{dl}} = 150 \mu\text{F cm}^{-2}$, $k^0 = 0.2 \text{ cm s}^{-1}$, $\alpha = 0.5$, $A = 0.07 \text{ cm}^2$, $v = 0.1 \text{ V s}^{-1}$, $v_k = 1.0 \times 10^{-2} \text{ cm}^2 \text{ s}^{-1}$ and $E^0 = 0.315 \text{ V}$.

nonadiabatic process,⁴⁶ therefore, the higher k^0 value at a platinum electrode, which has a higher density of state than carbon,^{47,48} is consistent with the density of state argument.⁴⁹

5 Conclusion

Resolution of large amplitude FT ac voltammetric data obtained at a rotating disc electrode into dc and ac harmonic components allows the hydrodynamics to be analysed from the dc component and flow rate insensitive data to be obtained from the higher harmonics. Thus, all parameters related to mass transport and electrode kinetics are available from a single experiment. The theory for the technique has been described and applied to analysis of the reversible $[\text{Ru}(\text{NH}_3)_6]^{3+/2+}$ and quasi-reversible $[\text{Fe}(\text{CN})_6]^{3-/4-}$ processes. Excellent agreement between theoretical and experimental data is obtained over a wide range of electrode rotation rates.

Acknowledgements

KB acknowledges the award of Monash University, Science Dean's Postgraduate Research Scholarship. Financial support from the Australian Research Council also is gratefully acknowledged.

References

- 1 A. Tegou, S. Papadimitriou, I. Mintsouli, S. Armanyanov, E. Valova, G. Kokkinidis and S. Sotiropoulos, *Catal. Today*, 2011, **170**, 126.
- 2 T. R. Ralph, M. L. Hitchman, J. P. Millington and F. C. Walsh, *Electrochim. Acta*, 2005, **51**, 133.
- 3 E. R. Vago and E. J. Calvo, *J. Chem. Soc., Faraday Trans.*, 1995, **91**, 2323.
- 4 R. J. Klingler and J. K. Kochi, *J. Phys. Chem.*, 1981, **85**, 1731.
- 5 C. Amatore, J. M. Saveant and D. Tessier, *J. Electroanal. Chem.*, 1983, **146**, 37.
- 6 A. Molina, J. Gonzalez, E. Laborda, M. C. Henstridge and R. G. Compton, *Electrochim. Acta*, 2011, **56**, 7404.

- 7 A. M. Bond, T. L. E. Henderson, D. R. Mann, T. F. Mann, W. Thormann and C. G. Zoski, *Anal. Chem.*, 1988, **60**, 1878.
- 8 A. M. Janiszewska and M. Grzeszczuk, *Electroanalysis*, 2004, **16**, 1673.
- 9 D. O. Wipf, E. W. Kristensen, M. R. Deakin and R. M. Wightman, *Anal. Chem.*, 1988, **60**, 306.
- 10 D. Y. Kim, J. Wang, J. Yang, H. W. Kim and G. M. Swain, *J. Phys. Chem. C*, 2011, **115**, 10026.
- 11 A. W. Taylor, F. L. Qiu, J. P. Hu, P. Licence and D. A. Walsh, *J. Phys. Chem. B*, 2008, **112**, 13292.
- 12 A. M. Bond, *Broadening Electrochemical Horizons*, Oxford University Press, 2002.
- 13 A. J. Bard and L. R. Faulkner, *Electrochemical Methods: Fundamentals and Applications*, John Wiley & Sons, New York, 2nd edn, 2001.
- 14 (a) A. M. Bond, K. B. Oldham and C. G. Zoski, *Anal. Chim. Acta*, 1989, **216**, 177; (b) R. M. Wightman, *Anal. Chem.*, 1981, **53**, 1125.
- 15 (a) P. Sun and M. V. Mirkin, *Anal. Chem.*, 2006, **78**, 6526; (b) C. J. Slevin, N. J. Gray, J. V. MacPherson, M. A. Webb and P. R. Unwin, *Electrochem. Commun.*, 1999, **1**, 282.
- 16 C. Earles and J. O. Schenk, *Anal. Biochem.*, 1998, **264**, 191.
- 17 W. B. Burnette, M. D. Bailey, S. Kukoyi, R. D. Blakely, C. G. Trowbridge and J. B. J. Justice, *Anal. Chem.*, 1996, **69**, 2932.
- 18 N. P. C. Stevens and A. M. Bond, *J. Electroanal. Chem.*, 2002, **538–539**, 25.
- 19 R. D. Martin, M. A. Beeston, P. R. Unwin and M. E. Laing, *J. Chem. Soc., Faraday Trans.*, 1994, **90**, 3109.
- 20 G. Goldet, A. F. Wait, J. A. Cracknell, K. A. Vincent, M. Ludwig, O. Lenz, B. Friedrich and F. A. Armstrong, *J. Am. Chem. Soc.*, 2008, **130**, 11106.
- 21 N. V. Rees, J. A. Alden, R. A. W. Dryfe, B. A. Coles and R. G. Compton, *J. Phys. Chem.*, 1995, **99**, 14813.
- 22 N. V. Rees and R. G. Compton, *Russ. J. Electrochem.*, 2008, **44**, 368.
- 23 N. V. Rees, O. V. Klymenko, B. A. Coles and R. G. Compton, *J. Electroanal. Chem.*, 2002, **534**, 151.
- 24 S.-X. Guo, J. Zhang, D. M. Elton and A. M. Bond, *Anal. Chem.*, 2003, **76**, 166.
- 25 J. Zhang, S.-X. Guo, A. M. Bond and F. Marken, *Anal. Chem.*, 2004, **76**, 3619.
- 26 A. M. Bond, N. W. Duffy, S.-X. Guo, J. Zhang and D. Elton, *Anal. Chem.*, 2005, **77**, 186A.
- 27 J. Zhang, S.-X. Guo and A. M. Bond, *Anal. Chem.*, 2007, **79**, 2276.
- 28 K. Tokuda and H. Matsuda, *J. Electroanal. Chem.*, 1977, **82**, 157.
- 29 K. Tokuda and H. Matsuda, *J. Electroanal. Chem.*, 1978, **90**, 149.
- 30 N. Kanzaki, Y. Kanzaki and S. Bruckenstein, *Anal. Chem.*, 1977, **49**, 1789.
- 31 I. V. Aokia, M. Bernard, S. I. C. de Torresib, C. Deslouis, H. G. de Melo, S. Joiret and S. Tribollet, *Electrochim. Acta*, 2001, **46**, 1871.
- 32 N. Le Poul, S. J. Green and Y. Le Mest, *J. Electroanal. Chem.*, 2006, **596**, 47.
- 33 S. B. Emery, J. L. Hubble and D. Roy, *Electrochim. Acta*, 2005, **50**, 5659.
- 34 G. Schone, W. Wiesbeck and W. J. Lorenz, *J. Electroanal. Chem.*, 1987, **229**, 407.
- 35 S. N. Shkerin and M. V. Perfilov, *Soviet Electrochem.*, 1990, **26**, 1303.
- 36 C. Beriet and D. Pletcher, *J. Electroanal. Chem.*, 1993, **361**, 93.
- 37 M. Rudolph, in *Physical Electrochemistry: Principles, Methods, and Applications*, ed. I. Rubinstein, Marcel Dekker, New York, 1995, p. 81.
- 38 J. Newman, *J. Phys. Chem.*, 1966, **70**, 1327.
- 39 S. W. Feldberg, C. I. Goldstein and M. J. Rudolph, *J. Electroanal. Chem.*, 1996, **413**, 25.
- 40 S. W. Feldberg, *J. Electroanal. Chem.*, 1981, **127**, 1.
- 41 C. Y. Lee, J. P. Bullock, G. F. Kennedy and A. M. Bond, *J. Phys. Chem. A*, 2010, **114**, 10122.
- 42 A. M. Bond, N. W. Duffy, D. M. Elton and B. D. Fleming, *Anal. Chem.*, 2009, **81**, 8801.
- 43 S. J. Konopka and B. McDuffie, *Anal. Chem.*, 1970, **42**, 1741.
- 44 P. H. Daum and C. G. Enke, *Anal. Chem.*, 1969, **41**, 653.
- 45 W. J. Blaedel and R. C. Engstrom, *Anal. Chem.*, 1978, **50**, 476.
- 46 D. E. Khoshtariya, T. D. Dolidze, L. D. Zusman and D. H. Waldeck, *J. Phys. Chem. A*, 2001, **105**, 1818.
- 47 R. J. Forster, P. Loughman and T. E. Keyes, *J. Am. Chem. Soc.*, 2000, **122**, 11948.
- 48 R. L. McCreery, *Chem. Rev.*, 2008, **108**, 2646.
- 49 S. Gosavi and R. A. Marcus, *J. Phys. Chem. B*, 2000, **104**, 2067.

Large Amplitude Fourier Transformed ac Voltammetry at a Rotating Disc Electrode: A Versatile Technique for Covering Levich and Flow Rate Insensitive Regimes in a Single Experiment

Kiran Bano, Gareth F. Kennedy, Jie Zhang* and Alan M. Bond*

School of Chemistry, Monash University

Clayton, Victoria 3800, Australia

Email addresses: 

Supporting Information

The Electronic Supplementary Information contains:

1. Simulation results obtained at various rotation rates for
 - (i) Reversible system with resistance
 - (ii) Quasi-reversible system without resistance
 - (iii) Quasi-reversible system with resistance
2. Levich plot for the $[\text{Fe}(\text{CN})_6]^{3-/4-}$ process

1. Simulation results obtained at various rotation rates for

(i) Reversible system with resistance

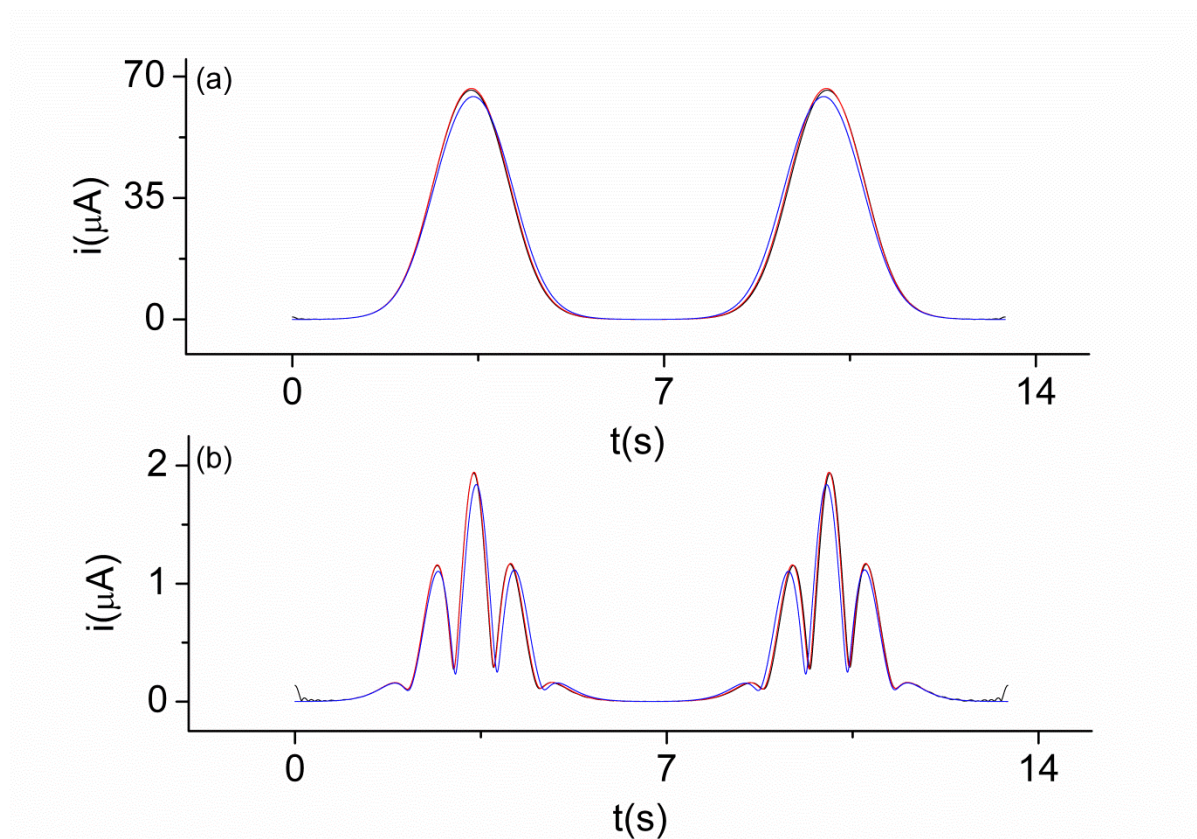


Fig. S1. Simulated Fourier transformed large amplitude ac voltammograms (a) 1st harmonic (b) 5th harmonic with ω^* of 0 (—), 500 (—) and 10000 (—) rpm, $C^* = 1$ mM, $f = 9.0$ Hz, $\Delta E = 80$ mV, $R_u = 100$ ohm, $k^0 = \text{reversible}$, $D = 6.8 \times 10^{-5} \text{ cm}^2 \text{ s}^{-1}$, $C = 0 \mu\text{F cm}^{-2}$, $A = 0.07 \text{ cm}^2$, and $v_k = 1.0 \times 10^{-2} \text{ cm}^2 \text{ s}^{-1}$. Note that 0 and 500 rpm data are essentially indistinguishable.

(ii) Quasi-reversible system without resistance

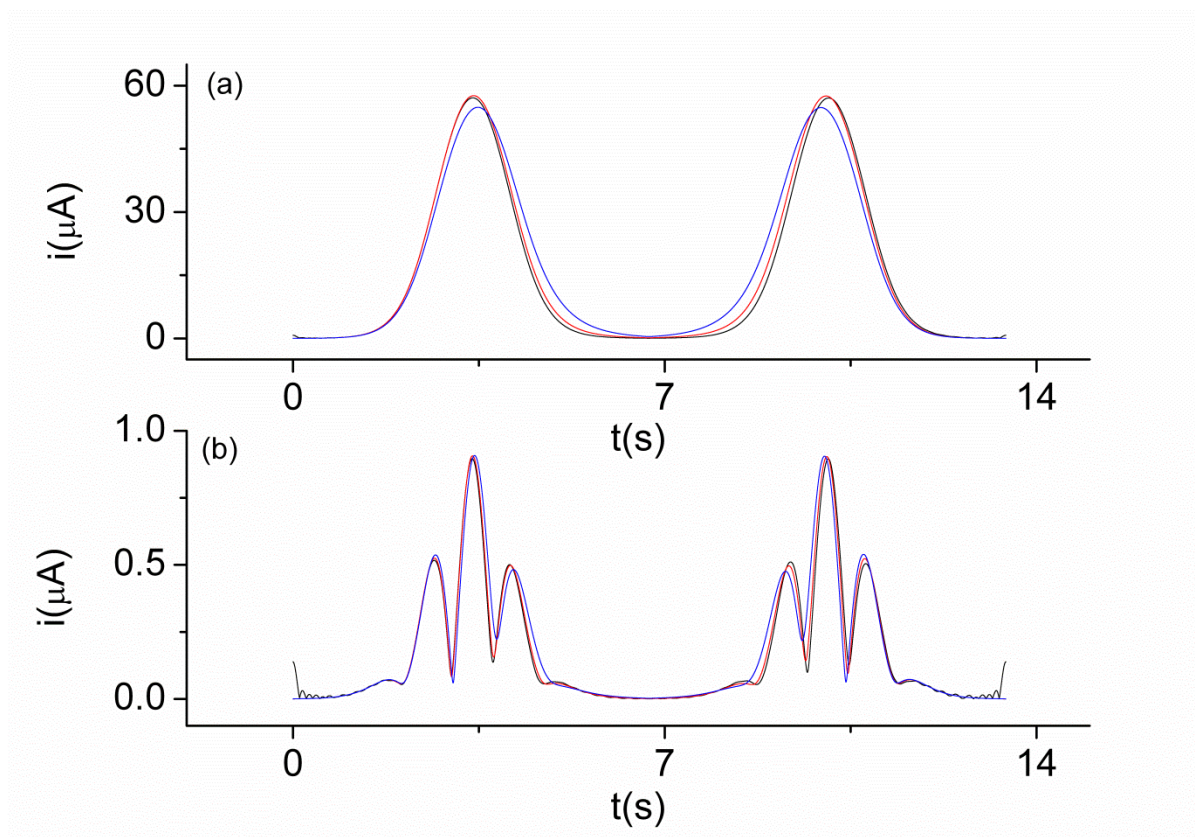


Fig. S2. Simulated Fourier transformed large amplitude ac voltammograms (a) 1st harmonic (b) 5th harmonic with ω^* of 0 (—), 500 (—) and 10000 (—) rpm, $C^* = 1$ mM, $f = 9.0$ Hz, $\Delta E = 80$ mV, $R_u = 0$ ohm, $k^0 = 0.02$ cm s⁻¹, $D = 6.8 \times 10^{-5}$ cm² s⁻¹, $C = 0$ μF cm⁻², $A = 0.07$ cm², and $v_k = 1.0 \times 10^{-2}$ cm² s⁻¹. Note that 0 and 500 rpm data are largely overlapped.

(iii) Quasi-reversible system with resistance

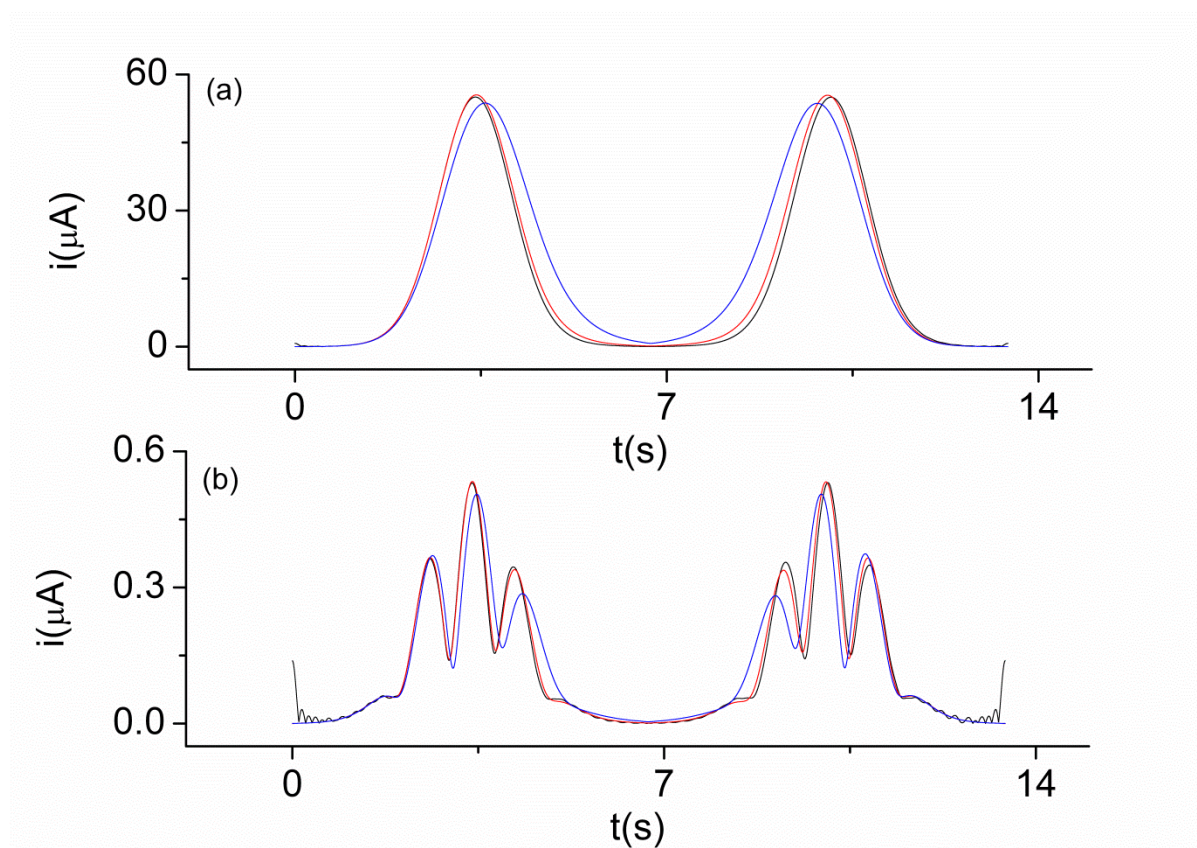


Fig. S3. Simulated Fourier transformed large amplitude ac voltammograms (a) 1st harmonic (b) 5th harmonic with ω^* of 0 (—), 500 (—) and 10000 (—) rpm, $C^* = 1$ mM, $f = 9.0$ Hz, $\Delta E = 80$ mV, $R_u = 100$ ohm, $k^0 = 0.02$ cm s⁻¹, $D = 6.8 \times 10^{-5}$ cm² s⁻¹, $C = 0$ μF cm⁻², $A = 0.07$ cm², and $v_k = 1.0 \times 10^{-2}$ cm² s⁻¹. Note that 0 and 500 rpm data are essentially indistinguishable at 5th harmonic.

2. Levich plot for the $[\text{Fe}(\text{CN})_6]^{3-/4-}$ process

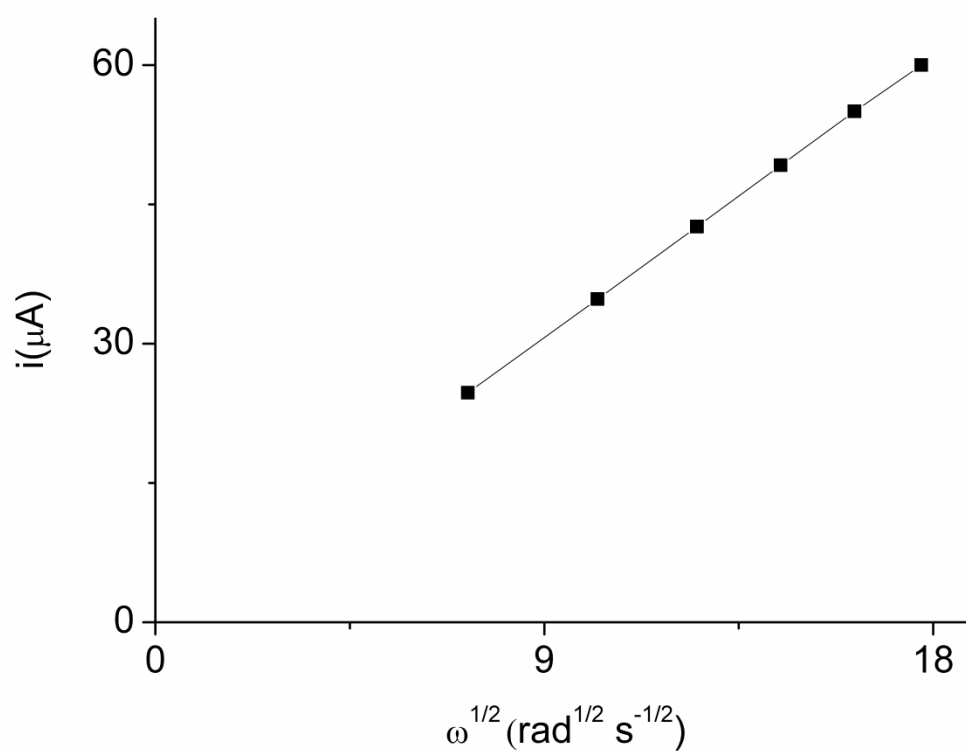


Fig. S4. Levich plot for the reduction of 0.98 mM $[\text{Fe}(\text{CN})_6]^{3-}$ in aqueous 3.0 M KCl electrolyte at a platinum RDE, based on the limiting current derived from dc component of FT ac voltammograms versus square root of rotation rate, $\nu = 0.1 \text{ V s}^{-1}$.

CHAPTER 5

ELECTRODE KINETICS STUDIES AT MACRODISK ELECTRODES: HIGH FREQUENCY FT AC VOLTAMMETRY

Declaration for Thesis Chapter [5]

Declaration by candidate

In the case of Chapter [5], the nature and extent of my contribution to the work was the following:

Nature of contribution	Extent of contribution (%)
Initiation, key ideas, experimental work, writing up	40 %

The following co-authors contributed to the work. If co-authors are students at Monash University, the extent of their contribution in percentage terms must be stated:

Name	Nature of contribution	
Jie Zhang	Initiation, key ideas, writing up	
Alan M. Bond	Initiation, key ideas, writing up	
Shaimaa Ahmad	Initiation, key ideas, experimental work, writing up	
Lisandra L. Martin	Initiation, key ideas, writing up	

The undersigned hereby certify that the above declaration correctly reflects the nature and extent of the candidate's and co-authors' contributions to this work*.

Candidate's
Signature

Date

Name	Signatures
Jie Zhang	
Alan M. Bond	
Shaimaa Ahmad	
Lisandra L. Martin	

Supervisor's signature	
------------------------	--

Fourier-Transformed Large-Amplitude AC Voltammetric Study of Tetrathiafulvalene (TTF): Electrode Kinetics of the $\text{TTF}^0/\text{TTF}^{\bullet+}$ and $\text{TTF}^{\bullet+}/\text{TTF}^{2+}$ Processes

Alan M. Bond,* Kiran Bano, Shaimaa Adeel, Lisandra L. Martin, and Jie Zhang*[a]

Large-amplitude Fourier-transformed (FT) AC voltammetry was used at high frequency to study the electrode kinetics of tetrathiafulvalene (TTF), its radical cation $\text{TTF}^{\bullet+}$ and that of the dication TTF^{2+} in acetonitrile (0.1 M Bu_4NPF_6). The two oxidized forms were prepared by quantitative bulk electrolysis of TTF under dry-box conditions. A high frequency of 233 Hz was used at glassy carbon (GC) and platinum (Pt) macro disk electrodes to enhance the kinetic sensitivity and hence upper limit of the measurable heterogeneous charge transfer rate constant (k^0). Difficulties associated with the use of high frequencies at

macro disk electrodes are discussed. Comparison of experimental data with simulations is used to extract k^0 and other parameters for each of the $\text{TTF}^{0/+}$ and $\text{TTF}^{\bullet+/2+}$ processes from both reduction and oxidation perspectives. k^0 values for $\text{TTF}^{0/+}$ and $\text{TTF}^{\bullet+/0}$ processes are $\geq 1.0 \text{ cm s}^{-1}$ and consequently regarded as reversible under the AC conditions used. However, the significantly slower quasi-reversible behaviour observed for the $\text{TTF}^{\bullet+/2+}$ redox couple, with k^0 being $0.3 \pm 0.05 \text{ cm s}^{-1}$, can be precisely estimated.

1. Introduction

Large-amplitude Fourier-transformed (FT) AC voltammetry provides significant advantages over DC methods in quantitative studies of kinetics of electrode processes.^[1] Theoretical models of all aspects of the electrode process, as probed by the FT AC method, have been developed using numerical simulations.^[2] If large amplitudes of the AC signal are employed, a major advantage is that the higher-order AC harmonic components are virtually free of background capacitance current and are also highly sensitive to electrode kinetics.^[3] In particular, comparison of experimental data with the numerical simulations provides good estimates of the electrode kinetics (k^0), reversible potential (E^0), charge transfer coefficient (α), uncompensated resistance (R_u) and double-layer capacitance (C_{dl}). k^0 values up to about 1.0 cm s^{-1} have been determined by this method. However, studies of electrode kinetics at close to the reversible limit at macro disk electrodes in conventional organic solvents are problematic.^[4] In the FT AC method, the current magnitude for quasi-reversible process is a function of k^0 up to the limit where the process is so fast that reversible behaviour is encountered.


Recently, FT AC voltammetry was used for the determination of the electrode kinetics of the TCNQ (7,7,8,8-tetracyanoquinodimethane) processes ($\text{TCNQ}^{0/+}$ and $\text{TCNQ}^{\bullet-/2-}$) in acetonitrile. For these processes k^0 values of about $0.30 \pm 0.05 \text{ cm s}^{-1}$ were

reported at both GC and Pt electrodes.^[4] In this paper, oxidation of TTF is now studied in acetonitrile (0.1 M Bu_4NPF_6) to probe the fast electrode kinetics that applies in this case. In organic solvents, TTF undergoes two well-separated one-electron oxidation processes at polycrystalline electrodes.^[5] The $\text{TTF}^{0/+}$ process leads to the formation of monocation radical ($\text{TTF}^{\bullet+}$), while subsequent formation of dication (TTF^{2+}) occurs in the second oxidation $\text{TTF}^{\bullet+/2+}$ step.

To date, relatively little attention has been given to electrode kinetic studies on the TTF processes. However, in one detailed study, the $k_{\text{TTF}^{0/+}}^0$ value of the $\text{TTF}^{0/+}$ couple was reported to be in the range of 0.03 cm s^{-1} to 2.2 cm s^{-1} at a Pt macro disk electrode in organic solvents of different polarities containing 0.1 M NaClO_4 as the supporting electrolyte.^[6] For the first $\text{TTF}^{0/+}$ oxidation process, the diffusion coefficient (D), E^0 and k^0 values have been evaluated over a range of temperature using cyclic voltammetry. α was assumed to be 0.50 in this study and k^0 was deduced from the separation of oxidation and reduction peak potentials. This work showed that the dynamics of solvent reorientation affects the value of k^0 for the $\text{TTF}^{0/+}$ couple, although the process lies close to the reversible limit under conditions of DC cyclic voltammetry.^[6] The process also is expected to lie close to the reversible limit in acetonitrile when probed by FT AC method or any other technique applied under stationary solution conditions at a macro disk electrode. No reports appear to be available on the electron transfer kinetics of the $\text{TTF}^{\bullet+/2+}$ redox process.

In this study, solutions of known concentration of $\text{TTF}^{\bullet+}$ and TTF^{2+} were quantitatively generated in acetonitrile (0.1 M Bu_4NPF_6) using oxidative bulk electrolysis of TTF. In the initial oxidation step, a persistent solution of red-coloured $\text{TTF}^{\bullet+}$ was produced where the second oxidation step generated the

[a] Prof. A. M. Bond, K. Bano, S. Adeel, Prof. L. L. Martin, Dr. J. Zhang
School of Chemistry
Monash University
Clayton, Victoria 3800 (Australia)
E-mail: [redacted]

 Supporting information for this article is available on the WWW under <http://dx.doi.org/10.1002/celc.201300129>.

yellow-coloured TTF^{2+} . The use of three redox levels, TTF, TTF^{+} and TTF^{2+} , allowed processes to be studied from the oxidation and reduction perspectives and also to confirm that the cross redox reaction $\text{TTF}^{2+} + \text{TTF} \rightleftharpoons 2\text{TTF}^{+}$ does not affect the interpretation of results. The electrode kinetics was probed by the large-amplitude FT AC technique using a sine wave perturbation of amplitude (ΔE) = 80 mV with a high-frequency (f) = 233 Hz superimposed onto the DC waveform; conditions that are conducive to the measurement of fast electron transfer kinetics. Two concentrations were studied at each redox level to ensure that the uncompensated resistance has been correctly accommodated in the simulations. Studies were also undertaken at both GC and Pt electrodes to ascertain if k^0 depends on the electrode material. Via this protocol, it was found that for the $\text{TTF}^{0/+}$ process can be regarded as reversible under all conditions employed. In contrast, the $\text{TTF}^{+/2+}$ process was measurably slower and in a regime where the electrode kinetics could be reliably quantified.

2. Results

2.1. DC Voltammetry and Diffusion Coefficients of TTF, TTF^{+} and TTF^{2+} in Acetonitrile

Cyclic voltammograms at a macroelectrode and near-steady-state voltammograms obtained with a microelectrode for 1.0 mM TTF, 1.0 mM TTF^{+} and 1.0 mM TTF^{2+} are shown in Figure 1. The diffusion coefficients for TTF, TTF^{+} and TTF^{2+} were determined from peak current values derived from transient cyclic voltammograms (Figure 1a) and limiting currents from near-steady-state voltammograms (Figure 1b). 1.0 mM TTF^{+} and 1.0 mM TTF^{2+} solutions were quantitatively produced by oxidative bulk electrolysis of neutral 1.0 mM TTF in acetonitrile (0.1 M Bu_4NPF_6) using an applied potential (E_{appl}) of 0.120 V and 0.620 V (vs. $\text{Fc}^{0/+}$) respectively. This outcome is established by noting the change in the relative positions of the zero current in near-steady-state Pt micro disk electrode voltammograms before and after stepwise bulk electrolysis to generate a persistent solution of red-coloured TTF^{+} or yellow-coloured TTF^{2+} .

Each of TTF and its cations give rise to the expected two chemically reversible one-electron processes. The midpoint potentials (E_m) calculated from the average of the oxidation and reduction peak potentials recorded under transient conditions for $\text{TTF}/\text{TTF}^{+}$ and $\text{TTF}^{+}/\text{TTF}^{2+}$ redox couples are essentially identical, irrespective of initial redox level. Assuming E_m is equivalent to E^0 , then $E^0(1) = -0.074$ V and $E^0(2) = 0.311$ V vs.

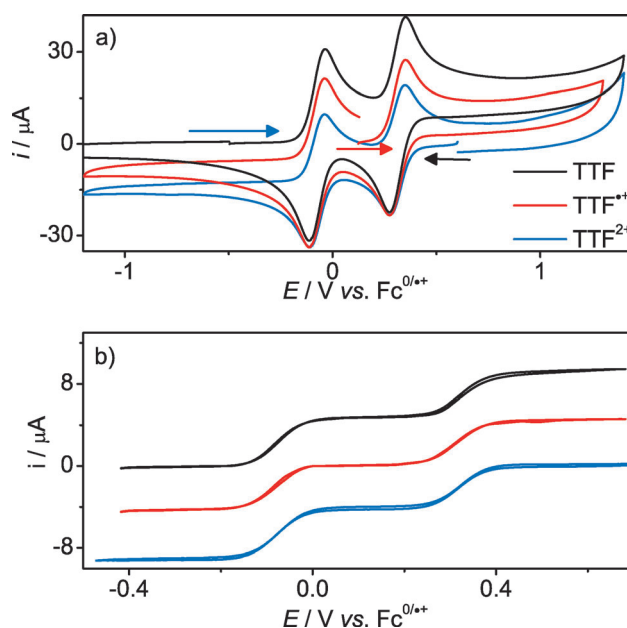


Figure 1. DC Voltammograms obtained from 1.0 mM TTF, TTF^{+} and TTF^{2+} in acetonitrile (0.1 M Bu_4NPF_6): a) transient DC cyclic voltammograms at a 3.0 mm diameter macro disk GC electrode ($\nu = 100 \text{ mVs}^{-1}$) and b) near-steady-state voltammograms at a 12.0 μm diameter Pt microdisk electrode ($\nu = 20 \text{ mVs}^{-1}$).

$\text{Fc}^{0/+}$. From Figure 1, it is also apparent on the basis of the magnitudes of the relevant limiting current values, that the diffusion coefficient (D) for TTF is larger than that of TTF^{+} and TTF^{2+} . D_{TTF} , $D_{\text{TTF}^{+}}$ and $D_{\text{TTF}^{2+}}$ values calculated from the near-steady-state voltammograms using Pt micro disk electrode and transient cyclic voltammograms are provided in Table 1 and agree well.

2.2. Simulation of Large-Amplitude FT AC Voltammetry and Comparison with Experimental Data

All simulations were undertaken with Monash Electrochemistry Simulator (MECSim) software written in Fortran. This software is based on expanding spatial grid formulation^[7] and uses the numerical method given by Rudolph^[8] with minor modifications.^[9] The simulation of an electrode process in Equation (1) is based on use of the Butler–Volmer relationship:^[10]



Table 1. Diffusion coefficients derived from voltammetry of 1.0 mM TTF, TTF^{+} and TTF^{2+} in MeCN (0.1 M Bu_4NPF_6).

Technique	Voltammetric Equation ^[a]	$D_{\text{TTF}} \times 10^5$ [cm ² s ⁻¹]	$D_{\text{TTF}^{+}} \times 10^5$ [cm ² s ⁻¹]	$D_{\text{TTF}^{2+}} \times 10^5$ [cm ² s ⁻¹]
Cyclic voltammetry	$I_p = (2.69 \times 10^5) n^{3/2} A D^{1/2} C \nu^{1/2}$	2.20	1.95	1.65
Near-steady-state voltammetry using microelectrode	$I_{\text{lim}} = 4 n F r D C$	2.10	1.90	1.60

[a] I_p = peak current (A), I_{lim} = limiting current (A), n = number of electrons transferred in the redox event, A = electrode area (cm²), F = Faraday's constant (C mol⁻¹), D = diffusion coefficient (cm² s⁻¹), C = concentration (mol cm⁻³) and ν = scan rate (V s⁻¹).

where E^0 is the reversible potential calculated as the average of the peak potentials for reduction and oxidation components of a cyclic voltammetric experiment, k^0 is the formal heterogeneous electron transfer rate constant, α is the charge transfer coefficient and A and B represent TTF, TTF^{+} or TTF^{2+} as appropriate.

Simulations were undertaken using a sine wave with $\Delta E = 80$ mV and $f = 233.0$ Hz superimposed onto the DC ramp along with other known experimentally based parameters. It was assumed that the electrode area, concentration, temperature, uncompensated resistance and diffusion coefficients of TTF, TTF^{+} or TTF^{2+} were accurately known from other measurements. Parameters computed in the simulation were k^0 , α , E^0 and C_{dl} . E^0 values were also estimated experimentally from lower harmonic components (peak potential of fundamental and potential of minimum current between the two peaks in the second harmonic) and from DC cyclic voltammograms as the average of the reduction and oxidation peak potentials. Capacitance was calculated from the fundamental harmonic in potential regions where no AC Faradaic current is present (either side of peak). The potential-dependent C_{dl} was modelled by using the second-order polynomial function, $C_{\text{dl}} = c_0 + c_1(E - E_c) + c_2(E - E_c)^2$ where E is the applied potential and E_c , c_0 , c_1 and c_2 are constants with appropriate units. k^0 values were initially estimated from best fits of simulated and experimental data derived from the higher harmonic components, which are more sensitive to variation in k^0 . Estimates of R_u values were obtained using the BAS electrochemical work station and analysis of the RC time constant^[10] derived from application of a small potential step in a potential region where no faradaic reaction occurs.

In earlier TCNQ studies,^[4] a frequency of 9.0 Hz was used for the study of this close to reversible system and up to eight harmonics were obtained. In the case of TTF, use of a higher frequency of 233 Hz was explored to probe the fast electron transfer kinetics at macro disk electrodes. At 233 Hz the data analysis was restricted to 6–7 harmonics because the higher frequency gives a much higher capacitive current as well as larger Faradaic current, which leads to increase in the ohmic (iR_u) drop. However, from the data analysis point of view, although the number of harmonics available with excellent signal to noise ratio is reduced at 233 Hz, peak splitting arising from iR_u drop helps to discriminate between the contribution of slow kinetics and uncompensated resistance.

2.3. AC Voltammetric Oxidation of TTF in Acetonitrile (0.1 M Bu_4NPF_6) as a Function of Concentration and Electrode Material: An Initial Estimation of the Electrode Kinetics

The $\text{TTF}^{0/+}$ oxidation process was found to be essentially reversible on the time scale of FT AC voltammetry. In initial attempts to extract the electrode kinetic parameters for the $\text{TTF}^{0/+}$ process, studies were undertaken on a 0.12 mM TTF solution in acetonitrile (0.1 M Bu_4NPF_6). Use of a low TTF concentration minimizes complications from iR_u drop which otherwise can be substantial when working at the high frequency of 233 Hz. Two sets of AC data were obtained: the first confined

to the potential region where only the first $\text{TTF}^{0/+}$ process is present and second covering the potential region encompassing both the $\text{TTF}^{0/+}$ and $\text{TTF}^{+/2+}$ processes. The initial approach represents a heuristic form of data analysis where parameters were varied until the experimentalist decides that a good fit between experiment and theory has been achieved. More detailed analysis of the significance of the electrode kinetics analysis is provided later in this paper.

FT AC voltammetric data derived from oxidation of 0.12 mM TTF were modelled as described above. Diffusion coefficient values estimated from near-steady-state voltammetry were confirmed by fitting of the AC 1st and 2nd harmonic components where reversibility of the process could be assured. C_{dl} values estimated from the non-faradaic component of the fundamental harmonic given in Table 2 represents values cal-

Table 2. Parameters used^[a] in simulations to obtain initial estimates of the electrode kinetics for the $\text{TTF}^{0/+}$ process in MeCN (0.1 M Bu_4NPF_6).

Electrode	C [mM]	R_u [ohm]	C_0, C_2 [$\mu\text{F cm}^{-2}$]	$k_{\text{TTF}^{0/+}}^0$ [cm s^{-1}]	E^0 vs. $\text{Fc}^{0/+}$ [V]	α
Pt	0.12	510	12.50, 1.40	1.00	−0.074	0.50
	1.00	510	11.00, 2.00	1.00	−0.074	0.50
GC	0.12	250	13.60, 2.40	1.00	−0.074	0.50
	1.00	260	12.00, 15.00	1.00	−0.074	0.50

[a] $A_{\text{GC}} = 0.019 \text{ cm}^2$, $A_{\text{Pt}} = 0.00785 \text{ cm}^2$, $f = 233 \text{ Hz}$, $\Delta E = 80 \text{ mV}$, $D_{\text{TTF}} = 2.1 \times 10^{-5} \text{ cm}^2 \text{ s}^{-1}$, $D_{\text{TTF}^{+}} = 2.0 \times 10^{-5} \text{ cm}^2 \text{ s}^{-1}$, $D_{\text{TTF}^{2+}} = 1.6 \times 10^{-5} \text{ cm}^2 \text{ s}^{-1}$, $c_1 = 0 \mu\text{F cm}^{-2}$ and $T = 298 \text{ K}$.

culated from only the first term $c_0 = 16 \mu\text{F cm}^{-2}$ in the polynomial series. This term provides a dominant contribution with $c_1 = 0$ and $c_2 = 2.4 \mu\text{F cm}^{-2}$. Importantly, the kinetically more sensitive fourth to seventh AC harmonic components are devoid of background current so they were used to extract initial estimate of kinetics parameters based on a comparison of experimental and simulated data.

A comparison of experimental and simulated results for the oxidation of 0.12 mM TTF at a Pt electrode is presented in Figure 2 when simulations were carried out using the parameters given in Table 2. Excellent agreement between experiment at a Pt electrode and theory was obtained for all AC harmonic components with $k_{\text{TTF}^{0/+}}^0 = 1.0 \text{ cm s}^{-1}$, $R_u = 510 \text{ ohm}$ and $\alpha = 0.50$. When data were collected over a wider potential range, the peak current magnitudes for the $\text{TTF}^{0/+}$ and $\text{TTF}^{+/2+}$ processes are indistinguishable in the first three harmonics. Initial simulations of the experimental data commenced with both the $k_{\text{TTF}^{0/+}}^0$ and $k_{\text{TTF}^{+/2+}}^0$ values set at 1.0 cm s^{-1} , which provides an excellent fit for the first $\text{TTF}^{0/+}$ process in all harmonics and also for the first three harmonics of the $\text{TTF}^{+/2+}$ one. However, the peak current magnitudes for 4th to 6th harmonics are slightly smaller than predicted on this basis, which suggests that k^0 in the $\text{TTF}^{+/2+}$ process is $< 1.0 \text{ cm s}^{-1}$ and hence quasi-reversible. The value of $k_{\text{TTF}^{+/2+}}^0$ was then refined by matching the peak magnitudes and shapes in the 5th–6th harmonic until satisfactory agreement with experiment was found at $k_{\text{TTF}^{0/+}}^0 = 0.8 \text{ cm s}^{-1}$ and $k_{\text{TTF}^{+/2+}}^0 = 0.4 \text{ cm s}^{-1}$. The plateau-like shape observed in the DC component was most probably due

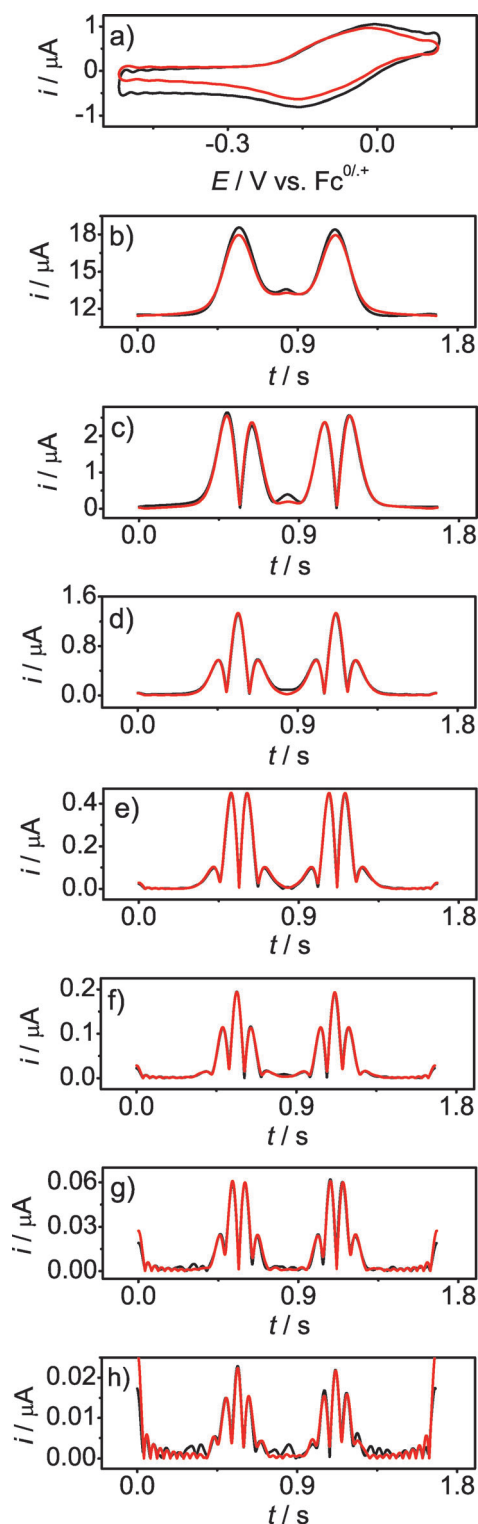


Figure 2. Comparison of simulated (—) and experimental (—) large-amplitude FT AC voltammograms for the $\text{TTF}^{0/+}$ oxidation process obtained for the oxidation process from 0.12 mM TTF in acetonitrile (0.1 M Bu_4NPF_6) at a Pt electrode: a) aperiodic DC component, b)–h) 1st–7th harmonics; $\nu = 0.774 \text{ V s}^{-1}$; simulation and other experimental parameters are as described in Table 2.

to imperfect modelling of DC capacitance current which is significant at lower concentrations. This conclusion is supported by the observation that at the higher 1.0 mM concentration

(see the Supporting Information) agreement of simulated and experimental DC data is excellent. Polynomial fitting of non-linear capacitance estimated from fundamental harmonic and other parameters extracted from analysis of the 1st–6th harmonics were too noisy to be used in the data analysis.

According to theory, electrode materials with a higher density of states, such as metals, should give rise to larger k^0 values than those with a lower density of state such as carbon.^[11] FT AC voltammetric oxidation of 0.12 mM TTF was therefore

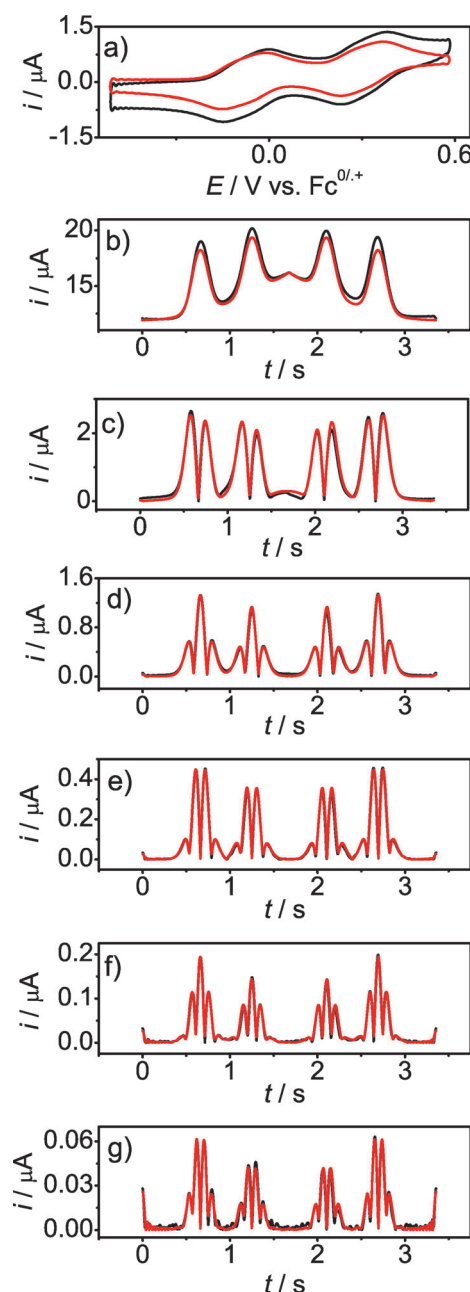


Figure 3. Comparison of simulated (—) and experimental (—) large-amplitude FT AC voltammograms for the $\text{TTF}^{0/+2+}$ oxidation processes obtained for the oxidation process from 0.12 mM TTF in acetonitrile (0.1 M Bu_4NPF_6) at a Pt electrode: a) aperiodic DC component, b)–g) 1st–6th harmonics; $\nu = 0.655 \text{ V s}^{-1}$; simulation and other experimental parameters are as described in Table 3.

Table 3. Parameters used^[a] in simulations of the consecutive oxidation of TTF to TTF^{0/+} and TTF^{0/+} to TTF²⁺ in MeCN (0.1 M Bu₄NPF₆) in order to obtain estimates of the electrode kinetic parameters.

Electrode	C [mm]	R _u [ohm]	c ₀ , c ₂ [μF cm ⁻²]	TTF ^{0/+}			TTF ^{+/2+}		
				k _{TTF^{0/+}} ⁰ [cm s ⁻¹]	E ⁰ vs. Fc ^{0/+} [V]	α	k _{TTF^{+/2+}} ⁰ [cm s ⁻¹]	E ⁰ vs. Fc ^{0/+} [V]	α
Pt	0.12	440	13.00, 1.30	1.00	-0.074	0.50	0.40	0.311	0.50
	1.00	510	11.00, 1.50	1.00	-0.074	0.50	0.32	0.311	0.50
GC	0.12	310	8.00, 5.00	0.70	-0.074	0.50	0.39	0.311	0.50
	1.00	310	11.00, 6.70	0.70	-0.074	0.50	0.30	0.311	0.50

[a] A_{GC} = 0.019 cm², A_{Pt} = 0.00785 cm², f = 233 Hz, ΔE = 80 mV, D_{TTF} = 2.1 × 10⁻⁵ cm² s⁻¹, D_{TTF^{+/2+}} = 2.0 × 10⁻⁵ cm² s⁻¹, D_{TTF²⁺} = 1.6 × 10⁻⁵ cm² s⁻¹, c₁ = 0 μF cm⁻² and T = 298 K.

2.4. Studies on the Oxidation and Reduction of TTF⁺ in MeCN (0.1 M Bu₄NPF₆)

If TTF⁺ rather than TTF or TTF²⁺ are present in the bulk solution, voltammetric data for the TTF^{+/2+} process can be studied in the absence of the cross redox reaction, TTF + TTF²⁺ ⇌ 2TTF⁺. Thus, oxidation and reduction of 1.0 mM TTF⁺ generated by bulk electrolysis was also studied by large-amplitude

FT AC voltammetry (f = 233 Hz, ΔE = 80 mV).

Experimental results for the oxidation of 0.1 mM TTF⁺ to TTF²⁺ at the Pt electrode agree well with simulated data in Figure 4. For each of the DC and AC harmonics components examined with k_{TTF^{+/2+}}⁰ = 0.35 cm s⁻¹ and α = 0.50 along with other parameters given in Table 4. At a GC electrode, use of k_{TTF^{+/2+}}⁰ = 0.36 provided a good fit of simulated and experimen-

Table 4. Parameters used^[a] in simulations undertaken to extract the electrode kinetic parameters for the TTF^{+/2+} oxidation process in MeCN (0.1 M Bu₄NPF₆).

Electrode	C [mm]	R _u [ohm]	c ₀ , c ₂ [μF cm ⁻²]	TTF ^{+/2+}		
				k _{TTF^{+/2+}} ⁰ [cm s ⁻¹]	E ⁰ vs. Fc ^{0/+} [V]	α
Pt	0.10	500	11.00, 0.00	0.35	0.311	0.50
	1.00	510	16.00, 0.80	0.35	0.311	0.50
GC	0.10	190	15.00, 5.00	0.36	0.311	0.50
	1.00	250	13.70, 7.00	0.36	0.311	0.50

[a] A_{GC} = 0.019 cm², A_{Pt} = 0.00785 cm², f = 233 Hz, ΔE = 80 mV, D_{TTF^{+/2+}} = 2.0 × 10⁻⁵ cm² s⁻¹, D_{TTF²⁺} = 1.6 × 10⁻⁵ cm² s⁻¹ and T = 298 K.

also studied at a GC electrode to ascertain if the electrode material plays a role in the electrode kinetics. AC voltammetric data were obtained at this electrode material in exactly the same way as at the platinum electrode; comparisons of simulation with the experimental data based solely on measurement of the TTF^{0/+} process at GC electrode were excellent (Figure S1) with k_{TTF^{0/+}}⁰ = 1.0 cm s⁻¹ and use of other parameters as summarized in Table 1. The smaller uncompensated resistance value at GC (~300 ohm) as compared to that at Pt (~500 ohm) is attributed predominantly to the larger diameter (d_{GC} = 1.5 mm versus d_{Pt} = 1.0 mm). In experiments over a larger potential range where both TTF^{0/+} and TTF^{+/2+} processes are present, the provisional values of k_{TTF^{0/+}}⁰ and k_{TTF^{+/2+}}⁰ at GC electrode were again determined by comparison of experimental and theoretical data (Figure S2) using the above mentioned strategy. k_{TTF^{0/+}}⁰ = 0.70 cm s⁻¹ and k_{TTF^{+/2+}}⁰ = 0.39 cm s⁻¹ were deduced via this approach, and are similar to values determined at the Pt electrode.

Since iR_u drop also has a considerable impact on the characteristics of the non-linear components of large-amplitude AC voltammograms, k_{TTF^{0/+}}⁰ and k_{TTF^{+/2+}}⁰ values were also determined from 1.0 mM TTF concentration. Estimates of k_{TTF^{0/+}}⁰ and k_{TTF^{+/2+}}⁰ again were derived as above when the TTF^{0/+} and TTF^{+/2+} processes were studied from oxidation of 1.0 mM TTF solution. A comparison of experimental and simulated data at GC and Pt electrodes is given for this condition in Figures S3–S6 using parameters summarized in Tables 1 and 2. Using k_{TTF^{0/+}}⁰ and k_{TTF^{+/2+}}⁰ values of about 1.0 cm s⁻¹ and 0.35 cm s⁻¹ fitted the experimental data at Pt and GC electrodes. The R_u value varied slightly from experiment to experiment, even when the same working electrode was used. This is attributed to the slight variations in the distance between working and reference electrode. The possible effect of the cross redox reaction TTF²⁺ + TTF ⇌ 2TTF⁺ that can occur when TTF²⁺ was generated in the presence of TTF in the bulk solution was not considered and in all of these cases α was assumed to be 0.50.

From these initial observations k_{TTF^{+/2+}}⁰ is significantly less than the k_{TTF^{0/+}}⁰ and readily measurable by large-amplitude FT AC voltammetry. Furthermore, k_{TTF^{0/+}}⁰ and k_{TTF^{+/2+}}⁰ appear to be the same at Pt and GC electrodes. However, k_{TTF^{0/+}}⁰ which is provisionally given a value of about 1.0 cm s⁻¹, produces close to reversible behaviour, so careful consideration needs to be given to decide if this is an absolute value or a lower limit.

tal data, as shown in Figure S7. At a higher concentration of 1.0 mM TTF⁺, simulations with k_{TTF^{+/2+}}⁰ values of 0.36 and 0.35 cm s⁻¹ at Pt and GC electrodes, respectively, also agreed well with the experimental data (Figures S8 and S9).

The electrode kinetics for the reduction of 0.1 mM and 1.0 mM TTF⁺ to TTF were also probed by simulation versus experiment comparisons at Pt and GC electrodes. Use of a k_{TTF^{+/0}}⁰ value of 1.0 cm s⁻¹ and α = 0.50 to simulate the reduction of 0.1 mM TTF⁺ at a Pt electrode provided excellent agreement with experimental data as shown in Figure 5. Table 5 summarizes the simulation parameters used to obtain values derived from the reduction of 1.0 mM and 0.1 mM TTF⁺. Use of k_{TTF^{+/0}}⁰ = 1.0 cm s⁻¹ and α = 0.50 for the reduction of TTF⁺ at GC agrees well with experimental data as shown in Figures S10–S12. Thus, the same k⁰ and α values may use to simulate the TTF^{0/+} process via oxidation of TTF or reduction of TTF⁺, which is as expected on the basis of Butler–Volmer theory. Capacitance in all of the simulations was described by c₀, c₁ and c₂ terms in Table 4 and Table 5.

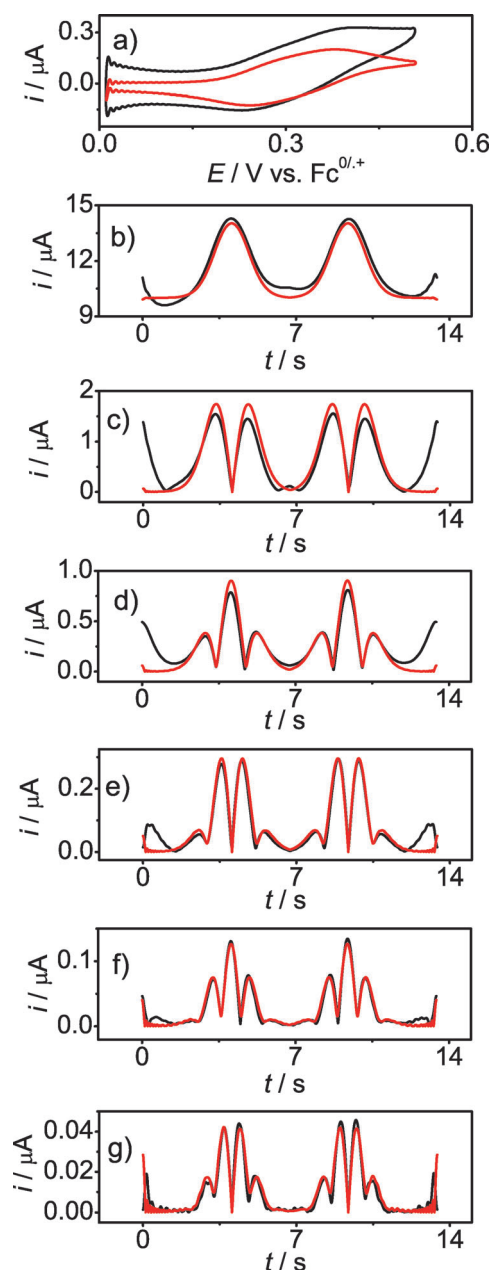


Figure 4. Comparison of simulated (—) and experimental (—) large-amplitude FT AC voltammograms obtained for the one-electron $\text{TTF}^{2+}/^{2+}$ oxidation process from 0.1 mM TTF^{2+} in acetonitrile (0.1 M Bu_4NPF_6) at a Pt electrode: a) aperiodic DC component, b)–g) 1st–6th harmonics; $\nu = 0.074 \text{ V s}^{-1}$; simulation and other experimental parameters are as described in Table 4.

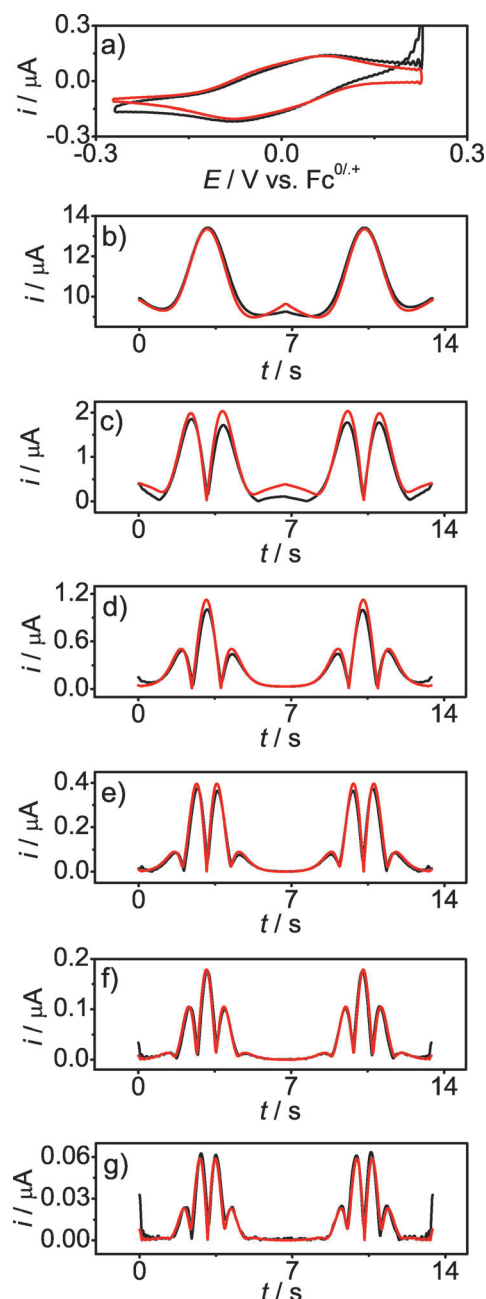


Figure 5. Comparison of simulated (—) and experimental (—) large-amplitude FT AC voltammograms obtained for the one-electron $\text{TTF}^{2+}/^{+0}$ reduction process from 0.1 mM TTF^{2+} in acetonitrile (0.1 M Bu_4NPF_6) at a Pt electrode: a) aperiodic DC component, b)–g) 1st–6th harmonics; $\nu = 0.074 \text{ V s}^{-1}$; simulation and other experimental parameters are as described in Table 5.

Table 5. Parameters used^[a] in simulations undertaken to estimate the electrode kinetics for the reduction of $\text{TTF}^{2+}/^{+0}$ in MeCN (0.1 M Bu_4NPF_6).

Electrode	C [mm]	R_{e} [ohm]	C_0, C_1, C_2 [$\mu\text{F cm}^{-2}$]	$k_{\text{TTF}^{2+}/^{+0}}^0$ [cm s^{-1}]	E^0 vs. $\text{Fc}^{0/+}$ [V]	α
Pt	0.10	450	13.50, 0.20, 7.50	1.00	−0.074	0.50
	1.00	500	14.00, 5.00, 0.00	1.00	−0.074	0.50
GC	0.10	250	10.00, 3.00, 17.00	1.00	−0.074	0.50
	1.00	300	13.00, 5.00, 0.00	1.00	−0.074	0.50

[a] $A_{\text{GC}} = 0.019 \text{ cm}^2$, $A_{\text{Pt}} = 0.00785 \text{ cm}^2$, $f = 233 \text{ Hz}$, $\Delta E = 80 \text{ mV}$, $D_{\text{TTF}} = 2.1 \times 10^{-5} \text{ cm}^2 \text{ s}^{-1}$, $D_{\text{TTF}^{+0}} = 2.0 \times 10^{-5} \text{ cm}^2 \text{ s}^{-1}$ and $T = 298 \text{ K}$.

2.5. Studies on the Reduction of TTF^{2+} in MeCN (0.1 M Bu_4NPF_6)

The assumption that the $\text{TTF}^{2+}/^{+0}$ redox process is quasi-reversible under FT AC voltammetric condition used in this study, was further confirmed by measuring $k_{\text{TTF}^{2+}/^{+0}}^0$ and α from reduction of TTF^{2+} . In this case, a set of experiments was conducted using 0.8 mM TTF^{2+} in the bulk acetonitrile (0.1 M Bu_4NPF_6) solution where the dication was generated from oxidative bulk electrolysis of TTF. As in other cases, electrochemical measure-

ments were carried out for the individual $\text{TTF}^{2+/+}$ and two-step $\text{TTF}^{2+/+}/0$ reductions. The same heuristic approach of comparing experiment with theory as described above was used to extract the kinetic parameters. Again, the cross redox reaction, $\text{TTF} + \text{TTF}^{2+} \rightleftharpoons 2\text{TTF}^{+}$, was neglected in these simulations.

FT AC voltammograms for the reduction of TTF^{2+} to TTF^{+} at Pt are shown in Figure 6. Simulations with $k_{\text{TTF}^{2+/+}}^0 = 0.32 \text{ cm s}^{-1}$ and other parameters given in Table 6 provide excellent agreement. Similarly, $k_{\text{TTF}^{2+/+}}^0$ and $k_{\text{TTF}^{+}/0}^0$ values were estimated at the Pt electrode from simulation of the $\text{TTF}^{2+/+}/0$ processes using parameters given in Table 7. The correspond-

Table 6. Parameters used^[a] in simulations undertaken to estimate the electrode kinetics for the reduction of $\text{TTF}^{2+/+}$ in MeCN (0.1 M Bu_4NPF_6).

Electrode	C [mM]	R_u [ohm]	C_0, C_1, C_2 [$\mu\text{F cm}^{-2}$]	$k_{\text{TTF}^{2+/+}}^0$ [cm s^{-1}]	E^0 vs. $\text{Fc}^{0/+}$ [V]	α
Pt	0.80	350	14.80, 0.10, 0.80	0.32	0.311	0.50
GC	0.80	320	26.00, 12.00, 8.00	0.39	0.311	0.50

[a] $A_{\text{GC}} = 0.019 \text{ cm}^2$, $A_{\text{Pt}} = 0.00785 \text{ cm}^2$, $f = 233 \text{ Hz}$, $\Delta E = 80 \text{ mV}$, $D_{\text{TTF}^{+}} = 2.0 \times 10^{-5} \text{ cm}^2 \text{ s}^{-1}$, $D_{\text{TTF}^{2+}} = 1.6 \times 10^{-5} \text{ cm}^2 \text{ s}^{-1}$ and $T = 293 \text{ K}$.

ing voltammograms are shown in Figure 7. The electrode kinetic values obtained agreed well with those derived from oxi-

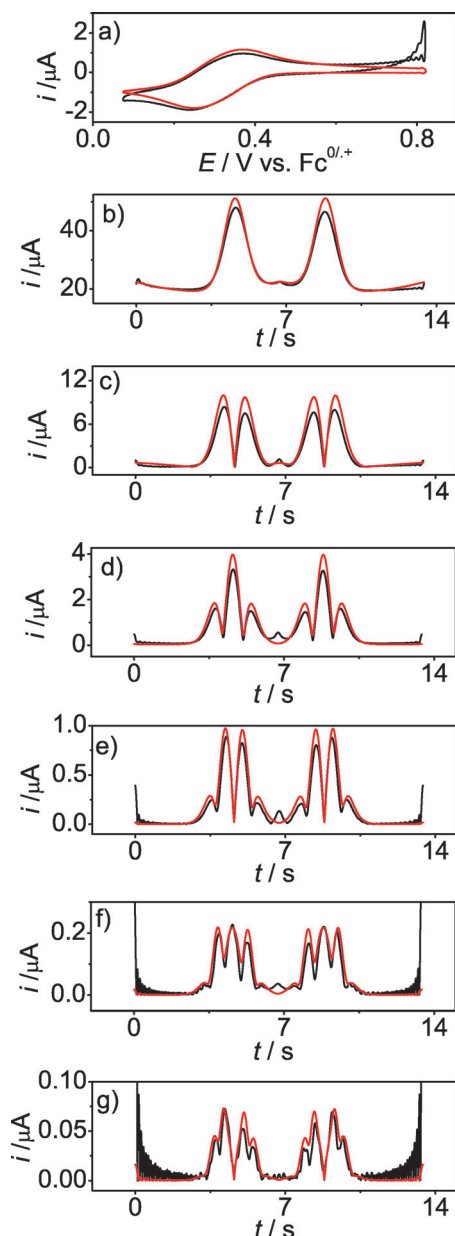


Figure 6. Comparison of simulated (—) and experimental (—) large-amplitude FT AC voltammograms obtained for the one-electron $\text{TTF}^{2+/+}$ reduction process from 0.8 mM TTF^{2+} in acetonitrile (0.1 M Bu_4NPF_6) at a Pt electrode: a) aperiodic DC component, b)–g) 1st–6th harmonics; $\nu = 0.1114 \text{ V s}^{-1}$; simulation and other experimental parameters are as described in Table 6.

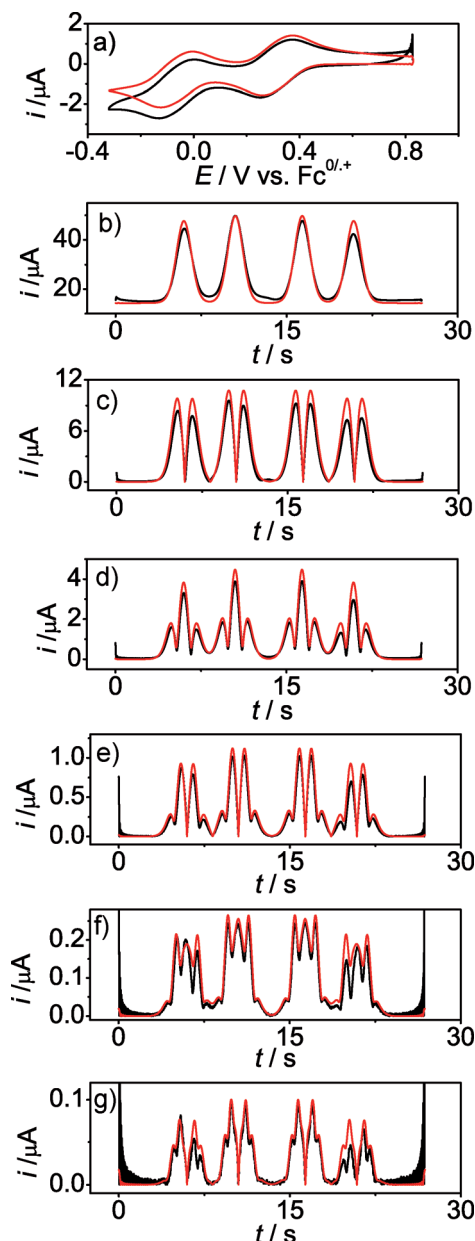


Figure 7. Comparison of simulated (—) and experimental (—) large-amplitude FT AC voltammograms obtained for the one-electron $\text{TTF}^{2+/+}$ reduction processes from 0.8 mM TTF^{2+} in acetonitrile (0.1 M Bu_4NPF_6) at a Pt electrode: a) aperiodic DC component, b)–g) 1st–6th harmonics; $\nu = 0.0856 \text{ V s}^{-1}$; simulation and other experimental parameters are as described in Table 7.

Table 7. Parameters used^[a] in simulations undertaken to estimate the electrode kinetics for the consecutive $\text{TTF}^{2+/1+}$ and $\text{TTF}^{1+/0}$ reduction processes in MeCN (0.1 M Bu_4NPF_6).

Electrode	C [mm]	R_u [ohm]	C_0, C_1, C_2 [$\mu\text{F cm}^{-2}$]	$\text{TTF}^{2+/1+}$			$\text{TTF}^{1+/0}$		
				$k_{\text{TTF}^{2+/1+}}^0$ [cm s^{-1}]	E^0 vs. $\text{Fc}^{0/+}$ [V]	α	$k_{\text{TTF}^{1+/0}}^0$ [cm s^{-1}]	E^0 vs. $\text{Fc}^{0/+}$ [V]	α
Pt	0.80	415	15.70, 1.00, 0.00	0.40	0.311	0.50	0.90	−0.074	0.50
GC	0.80	305	39.00, 13.00, 1.50	0.39	0.311	0.50	1.00	−0.074	0.50

[a] $A_{\text{GC}} = 0.019 \text{ cm}^2$, $A_{\text{Pt}} = 0.00785 \text{ cm}^2$, $f = 233 \text{ Hz}$, $\Delta E = 80 \text{ mV}$, $D_{\text{TTF}} = 2.1 \times 10^{-5} \text{ cm}^2 \text{ s}^{-1}$, $D_{\text{TTF}^{1+}} = 2.0 \times 10^{-5} \text{ cm}^2 \text{ s}^{-1}$, $D_{\text{TTF}^{2+}} = 1.6 \times 10^{-5} \text{ cm}^2 \text{ s}^{-1}$ and $T = 298 \text{ K}$.

dation of TTF^{1+} to TTF^{2+} , commencing either with TTF (Table 2 and Table 3) or TTF^{1+} (Table 4 and Table 5) present in bulk solution. Comparison of experimental and simulated data at a GC electrode is presented in Figures S13 and S14 and simulation parameters are summarized in Table 6 and Table 7.

3. Discussion

In the above heuristic approach of data analysis, extraction of kinetic parameters was carried out by matching the experimental and simulated current magnitudes and peak shapes of the AC harmonics. However it needs to be recognized that in the presence of a significant contribution from R_u the estimated $k_{\text{TTF}^{1+/0}}^0 \sim 1.0 \text{ cm s}^{-1}$ value is close to the reversible limit. To illustrate the difficulty of quantifying the electrode kinetics of very fast processes in this study, simulations were undertaken on a one-electron transfer process to establish the effect of uncompensated resistance. Peak currents for the 5th harmonic obtained from simulations with k^0 values 0.3 cm s^{-1} , 1.0 cm s^{-1} and fully reversible are plotted versus $\ln R_u$ in Figure 8. It is evident from these data that a k^0 value 0.3 cm s^{-1} can in fact be estimated precisely using a frequency of 233 Hz using the 5th harmonic. In contrast, a k^0 value of 1.0 cm s^{-1} has considerable uncertainty as small uncertainty in R_u can be important. Thus

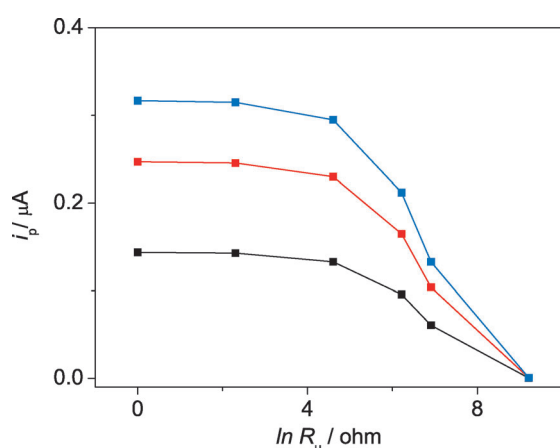


Figure 8. Plots of peak currents of the 5th harmonic obtained from simulated large-amplitude FT AC voltammograms vs. $\ln R_u$ for k^0 values of 0.3 cm s^{-1} (■), 1.0 cm s^{-1} (■) and for the fully reversible case (■). Other parameters include $f = 233 \text{ Hz}$, $\Delta E = 80 \text{ mV}$, $C = 0.1 \text{ mM}$, $D = 2.10 \times 10^{-5} \text{ cm}^2 \text{ s}^{-1}$, $C_{\text{dl}} = 11 \mu\text{F cm}^{-2}$, $E^0 = 0.00 \text{ V}$, $\nu = 0.10 \text{ V s}^{-1}$, $\alpha = 0.50$, and $A = 0.00785 \text{ cm}^2$.

a k^0 value $\geq 1.0 \text{ cm s}^{-1}$ rather than an absolute value is probably the preferred format for presenting the results from this study. The conclusion that $\text{TTF}^{0/+}$ process is reversible ($k^0 \geq 1.0 \text{ cm s}^{-1}$) is in agreement with a k^0 value of 2.2 cm s^{-1} derived from fast-scan cyclic voltammetry and data analysis by Nicolson's method.^[6,12] In contrast, the $\text{TTF}^{1+/2+}$ process clearly is

quasi-reversible rather than reversible with $k^0 = 0.35 \pm 0.05 \text{ cm s}^{-1}$ and significantly slower than the $\text{TTF}^{0/+}$ one. Part of the origin of this difference may be related to a stronger ion-pairing influence on the $\text{TTF}^{1+/2+}$ process. The charge difference (0 to +1 versus +1 to +2) also may play a role in terms of Marcus theory.^[13] The Frumkin double-layer effect,^[10,14] being different for both processes, also may lead to differences in kinetics for the $\text{TTF}^{0/+}$ $\text{TTF}^{1+/2+}$ processes.

Traditional theory^[15] predicts that electron transfer rates should be directly proportional to the density of states of the electrode. The concept has been validated by measurement of electrode kinetics of a variety of electron transfer processes.^[16] However in this case, differences in the density of states of GC and Pt do not lead to differences in electron transfer kinetics of the $\text{TTF}^{1+/2+}$ redox process. Although, it is known in case of ferricyanide^[17] that the electrode kinetics are highly dependent of the surface quality, cleanliness and the nature of the carbon, we believe that the TTF processes are adiabatic and less prone to changes in carbon surface. According to the predictions of Marcus and Gosavi's, the coupling strength between the redox centre and the electrode makes the electron-transfer rate less sensitive to density of states.^[18] Similar electrode kinetics observed on GC and Pt electrode infers that TTF redox processes are adiabatic according to Marcus.^[13] However, the contribution of Frumkin correction^[14a,19] was ignored in this study and work terms also need to be considered.

4. Conclusions

The use of the kinetically sensitive higher harmonics available from large-amplitude FT AC voltammetry with a frequency of 233 Hz allows the electrode kinetics associated with $\text{TTF}^{0/+}$ and $\text{TTF}^{1+/2+}$ processes in acetonitrile to be estimated at Pt and GC electrodes. Via heuristic forms of data analysis, the electrode kinetics for the $\text{TTF}^{0/+}$ process is concluded to be very fast ($k_{\text{TTF}^{0/+}}^0 \geq 1.0 \text{ cm s}^{-1}$), implying that the process is either at or close to the reversible limit. In contrast $k_{\text{TTF}^{1+/2+}}^0 \sim 0.35 \text{ cm s}^{-1}$ could be reliably estimated for the quasi-reversible $\text{TTF}^{1+/2+}$ process. The fact that kinetic parameters for the $\text{TTF}^{1+/2+}$ were found to be similar on GC and Pt electrodes suggests that this electron transfer process is adiabatic.

Experimental Section

Chemicals

Tetrathiafulvalene (TTF) 99% (Aldrich) and ferrocene (Fc) $\geq 98\%$ (Aldrich) were used as received from the manufacturer. *n*-tetrabutylammonium hexafluorophosphate (Bu_4NPF_6) 98%, (Wako) was recrystallized twice from ethanol. This supporting electrolyte and distilled acetonitrile (MeCN) 99.9%, (Sigma-Aldrich) were dried and stored under nitrogen in a dry box.

Instrumentation and Apparatus

For DC voltammetric studies, Bioanalytical Systems (BAS) model 100B or BASi Epsilon electrochemical workstations were used. Fourier transformed large amplitude AC voltammetric experiments were undertaken with home built instrumentation described elsewhere.^[20]

A conventional three-electrode cell configuration was used for voltammetric experiments. The working electrodes were GC ($d = 1.5$ mm and 3.0 mm) Pt ($d = 1.0$ mm) diameter platinum (Pt) macro disks. A Pt micro disk electrode (radius, $d = 12$ μm) was used for some experiments under near-steady-state conditions with a scan rate of 20 mV s^{-1} . A Pt wire in a glass capillary was used as a quasi-reference electrode and a Pt wire was used as the auxiliary electrode. Potentials derived from the Pt quasi-reference electrode were calibrated against the $\text{Fc}^{0/+}$ external reference potential scale. Working electrodes were polished with $0.3 \mu\text{m}$ and then $0.05 \mu\text{m}$ alumina slurries on a polishing cloth (BAS), sonicated in deionised water, rinsed with water and acetone and then dried with nitrogen. All voltammetric experiments were undertaken in a dry box under nitrogen at room temperature of $25 \pm 2^\circ\text{C}$.

Generation of TTF^{+} and TTF^{2+} Solutions

Bulk electrolysis of a known concentration of TTF was carried out quantitatively (coulometric and near-steady-state voltammetric monitoring) in acetonitrile ($0.1 \text{ M } \text{Bu}_4\text{NPF}_6$) solution in a three compartment cell to provide known concentrations of TTF^{+} and TTF^{2+} . Each compartment was separated by a fine glass frit to minimize solution mixing in these experiments. Large-area GC felt cloth (2×2 cm) or a GC basket net was employed as the working electrode, Pt mesh was used as the counter electrode and a Pt wire as the quasi-reference electrode. The Pt quasi-reference potential was then calibrated against that of the Fc/Fc^{+} couple and potentials employed are reported versus this reference system. Bulk electrolysis working and counter electrodes were first washed with acidic piranha (3:1 hydrogen peroxide and sulphuric acid mixture) solution, thoroughly washed with water and acetone, air dried and then finally dried in an oven. Since TTF^{2+} is moisture sensitive, bulk electrolysis and subsequent electrochemical measurements were conducted in a dry box under a nitrogen atmosphere.

Acknowledgements

The authors greatly acknowledge the Australian Research Council for financial support. K.B. and S.A. both acknowledge their awards of Monash University Science Faculty Dean's Postgraduate Research Scholarships.

Keywords: electrode kinetics • electron transfer kinetics • Fourier-transformed AC voltammetry • radical cations • tetrathiafulvalene

- [1] a) C. Y. Lee, A. M. Bond, *Langmuir* **2010**, *26*, 5243; b) C. Y. Lee, S. X. Guo, A. F. Murphy, T. McCormac, J. Zhang, A. M. Bond, G. Zhu, C. L. Hill, Y. V. Geletii, *Inorg. Chem.* **2012**, *51*, 11521; c) C. Y. Lee, G. P. Stevenson, A. Parkin, M. M. Roessler, R. E. Baker, K. Gillow, D. J. Gavaghan, F. A. Armstrong, A. M. Bond, *J. Electroanal. Chem.* **2011**, *656*, 293; d) B. Lertanantawong, A. P. O'Mullane, J. Zhang, W. Surareungchai, M. Somasundrum, A. M. Bond, *Anal. Chem.* **2008**, *80*, 6515; e) M. J. A. Shiddiky, A. P. O'Mullane, J. Zhang, L. D. Burke, A. M. Bond, *Langmuir* **2011**, *27*, 10302; f) J. Zhang, S. X. Guo, A. M. Bond, F. Marken, *Anal. Chem.* **2004**, *76*, 3619; g) K. Bano, G. F. Kennedy, J. Zhang, A. M. Bond, *Phys. Chem. Phys.* **2012**, *14*, 4742.
- [2] D. J. Gavaghan, A. M. Bond, *Electroanalysis* **2006**, *18*, 333.
- [3] J. Zhang, S. X. Guo, A. M. Bond, *Anal. Chem.* **2007**, *79*, 2276.
- [4] K. Bano, A. Nafady, J. Zhang, A. M. Bond, I. U. Haque, *J. Phys. Chem. C* **2011**, *115*, 24153.
- [5] M. Bendikov, F. Wudl, D. F. Perepichka, *Chem. Rev.* **2004**, *104*, 4891.
- [6] G. Grampp, A. Kapturkiewicz, W. Jaenicke, *Ber. Bunsenges. Phys. Chem.* **1990**, *94*, 439.
- [7] S. W. Feldberg, *J. Electroanal. Chem.* **1981**, *127*, 1.
- [8] M. Rudolph, D. P. Reddy, S. W. Feldberg, *Anal. Chem.* **1994**, *66*, A589.
- [9] S. W. Feldberg, C. I. Goldstein, M. Rudolph, *J. Electroanal. Chem.* **1996**, *413*, 25–36.
- [10] A. J. Bard, L. R. Faulkner, *Electrochemical Methods: Fundamentals and Applications*, Wiley, New York, **2001**.
- [11] R. L. McCreery, *Chem. Rev.* **2008**, *108*, 2646.
- [12] R. S. Nicholson, *Anal. Chem.* **1965**, *37*, 1351.
- [13] R. A. Marcus, *J. Chem. Phys.* **1956**, *24*, 966.
- [14] a) W. R. Fawcett, *Langmuir* **1989**, *5*, 661; b) A. Frumkin, *Adv. Electrochem. Electrochem. Eng.* **1961**, *1*, 65.
- [15] R. Parsons, *Surf. Sci.* **1964**, *2*, 418.
- [16] a) K. K. Cline, M. T. McDermott, R. L. McCreery, *J. Phys. Chem.* **1994**, *98*, 5314; b) P. M. Hallam, C. E. Banks, *Electrochem. Commun.* **2011**, *13*, 8.
- [17] S. C. S. Lai, A. N. Patel, K. McKelvey, P. R. Unwin, *Angew. Chem.* **2012**, *124*, 5501; *Angew. Chem. Int. Ed.* **2012**, *51*, 5405.
- [18] S. Gosavi, R. A. Marcus, *J. Phys. Chem. B* **2000**, *104*, 2067.
- [19] A. Frumkin, *Z. Phys. Chem.* **1933**, *A164*, 321.
- [20] A. M. Bond, N. W. Duffy, D. M. Elton, B. D. Fleming, *Anal. Chem.* **2009**, *81*, 8801.

Received: August 14, 2013

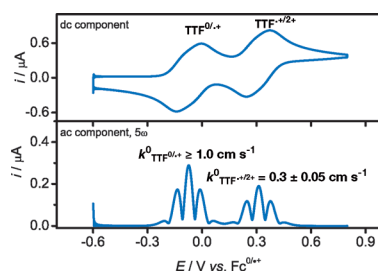
Published online on ■■■ ■■, 2013

FULL PAPERS

A. M. Bond,* K. Bano, S. Adeel,
L. L. Martin, J. Zhang*



Fourier-Transformed Large-Amplitude AC Voltammetric Study of Tetrathiafulvalene (TTF): Electrode Kinetics of the $\text{TTF}^0/\text{TTF}^{+\cdot}$ and $\text{TTF}^{+\cdot}/\text{TTF}^{2+}$ Processes



At the limit: Fourier-transformed large-amplitude AC voltammetry at a macro disk electrode is used to determine the electrode kinetics of the tetrathiafulvalene (TTF), $\text{TTF}^{+\cdot}$ and TTF^{2+} processes.

Fourier Transformed Large Amplitude AC Voltammetric study of
Tetrathiafulvalene (TTF): Electrode kinetics of the $\text{TTF}^0/\text{TTF}^{\bullet+}$ and
 $\text{TTF}^{\bullet+}/\text{TTF}^{2+}$ processes

Authors

Kiran Bano, Shaimaa Adeel, Lisa Martin, Jie Zhang* and Alan M. Bond*

School of Chemistry, Monash University,

Clayton, Victoria 3800, Australia

Email addresses: 

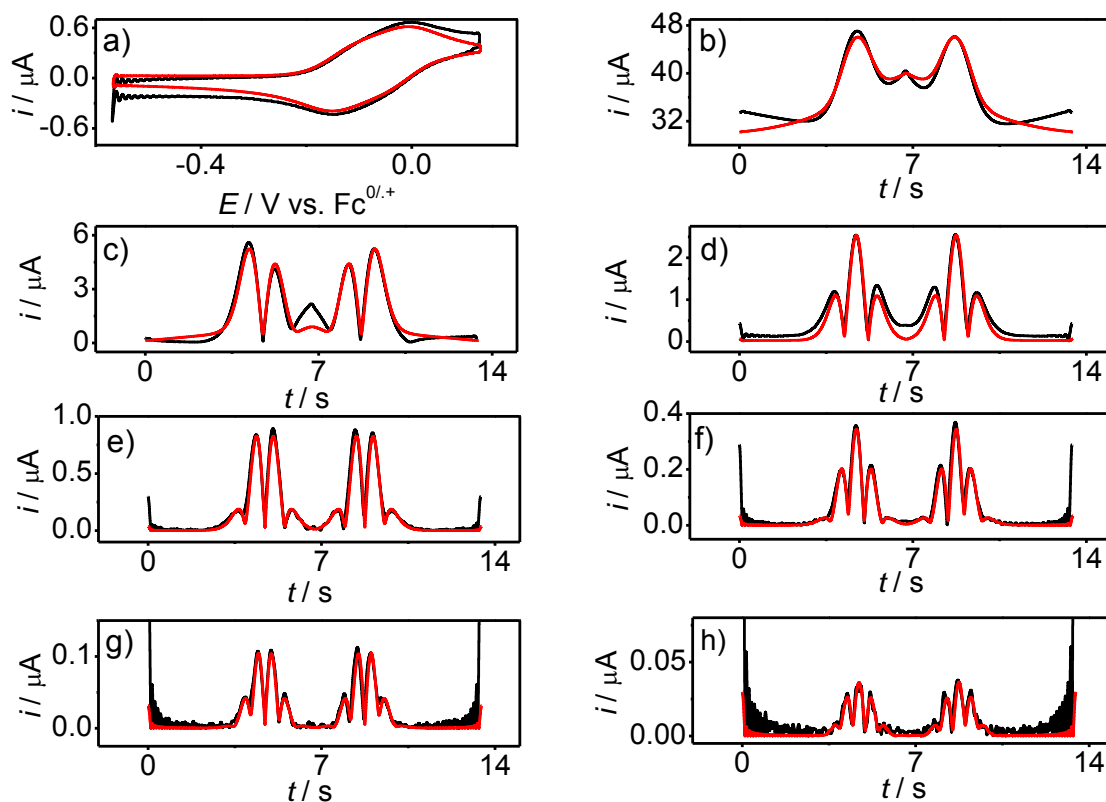


Figure S1. Comparison of simulated (—) and experimental (—) large amplitude FT AC voltammograms for $\text{TTF}^{0/+}$ process obtained for the oxidation of 0.12 mM TTF in acetonitrile (0.1 M Bu_4NPF_6) at a GC electrode (a) aperiodic dc component (b-h) 1st - 7th harmonics; $v = 0.104 \text{ V s}^{-1}$, Simulation and other experimental parameters as described in Table 2

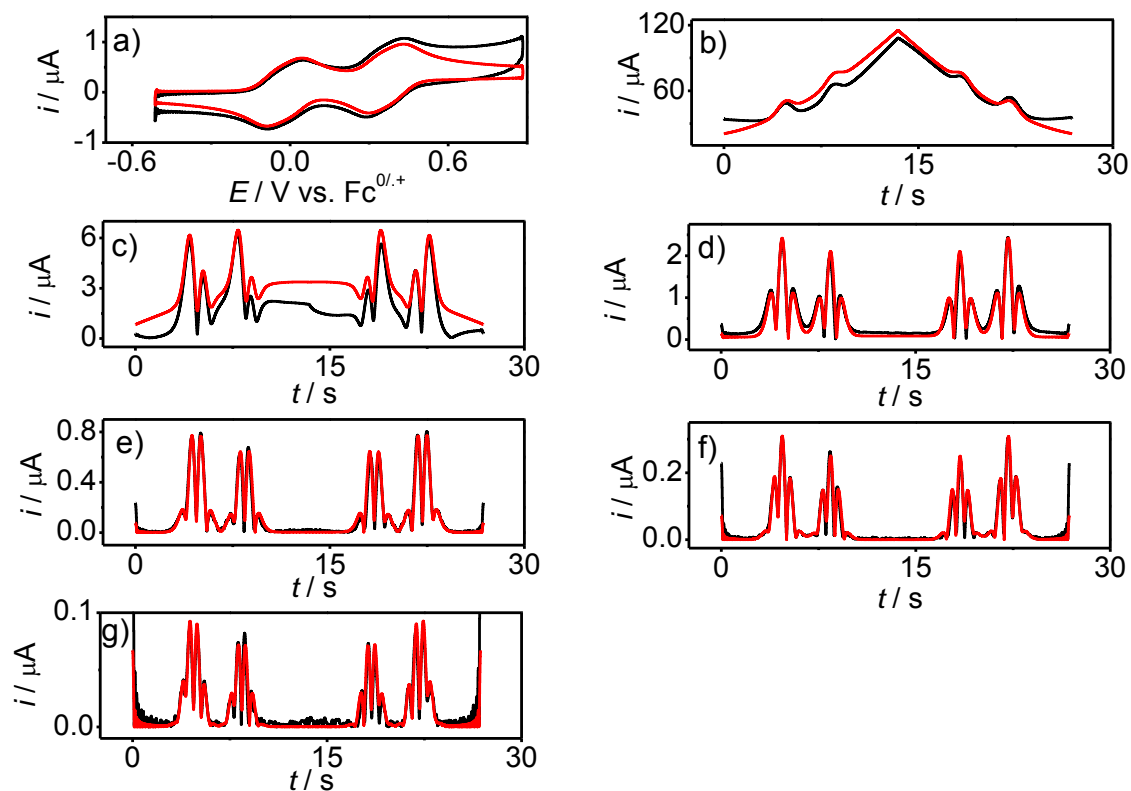


Figure S2. Comparison of simulated (—) and experimental (—) large amplitude FT AC voltammograms for the $\text{TTF}^{0/+ / 2+}$ process obtained for the oxidation of 0.12 mM TTF in acetonitrile (0.1 M Bu_4NPF_6) at a GC electrode (a) aperiodic dc component (b-g) 1st - 6th harmonics; $v = 0.0894 \text{ V s}^{-1}$, Simulation and other experimental parameters as described in Table 3

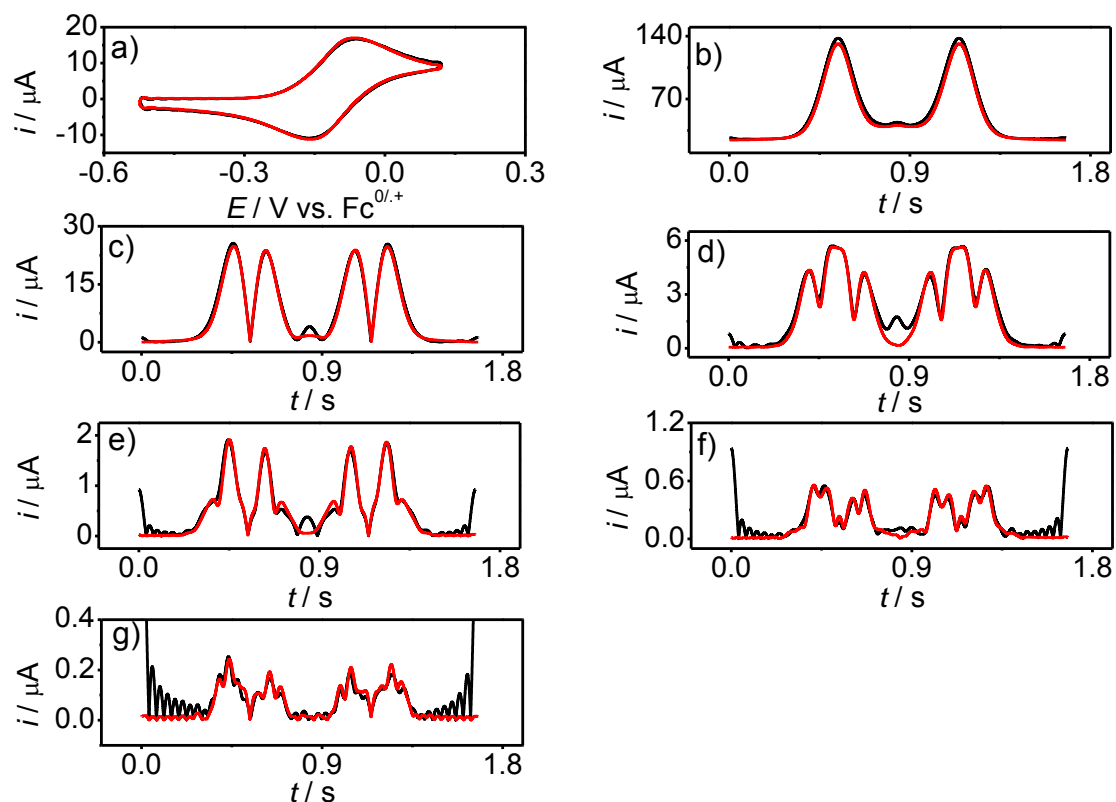


Figure S3. Comparison of simulated (—) and experimental (—) large amplitude FT AC voltammograms for the $\text{TTF}^{0/+}$ process obtained for the oxidation of 1.0 mM TTF^{*+} in acetonitrile (0.1 M Bu_4NPF_6) at a GC electrode (a) aperiodic dc component (b-g) 1st - 6th harmonics; $v = 0.774 \text{ V s}^{-1}$, Simulation and other experimental parameters as described in Table 2

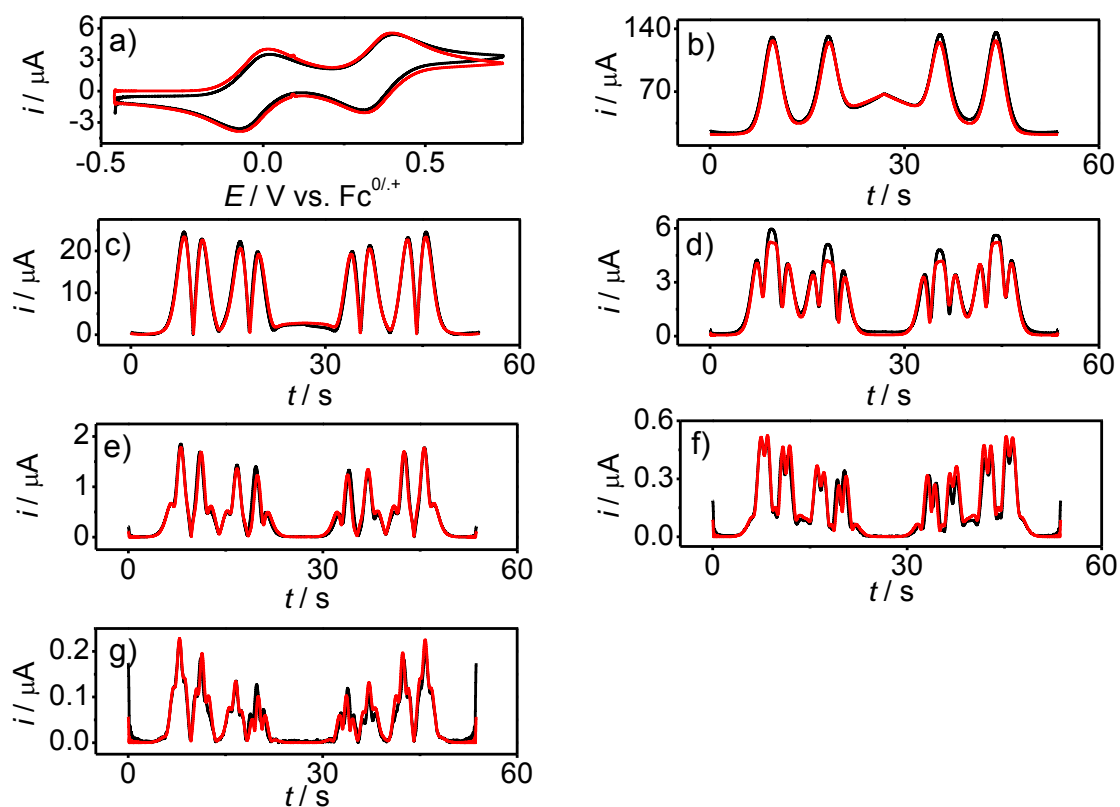


Figure S4. Comparison of simulated (—) and experimental (—) large amplitude FT AC voltammograms for the $\text{TTF}^{0/+2}$ process obtained for the oxidation of 1.0 mM TTF in acetonitrile (0.1 M Bu_4NPF_6) at a GC electrode (a) aperiodic dc component (b-g) 1st - 6th harmonics; $v = 0.0447 \text{ V s}^{-1}$, Simulation and other experimental parameters as described in Table 3

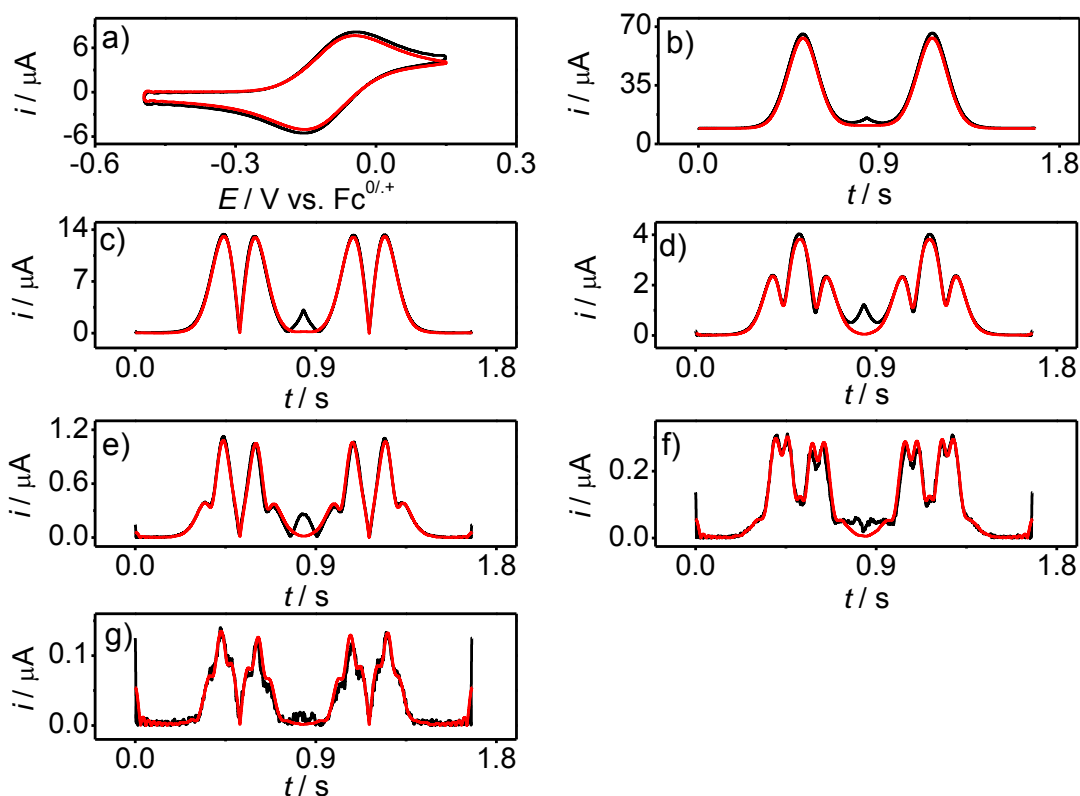


Figure S5. Comparison of simulated (—) and experimental (—) large amplitude FT AC voltammograms for the $\text{TTF}^{0/+}$ process obtained for the oxidation of 1.0 mM TTF in acetonitrile (0.1 M Bu_4NPF_6) at a Pt electrode (a) aperiodic dc component (b-g) 1st - 6th harmonics; $v = 0.774 \text{ V s}^{-1}$, Simulation and other experimental parameters as described in Table 2.

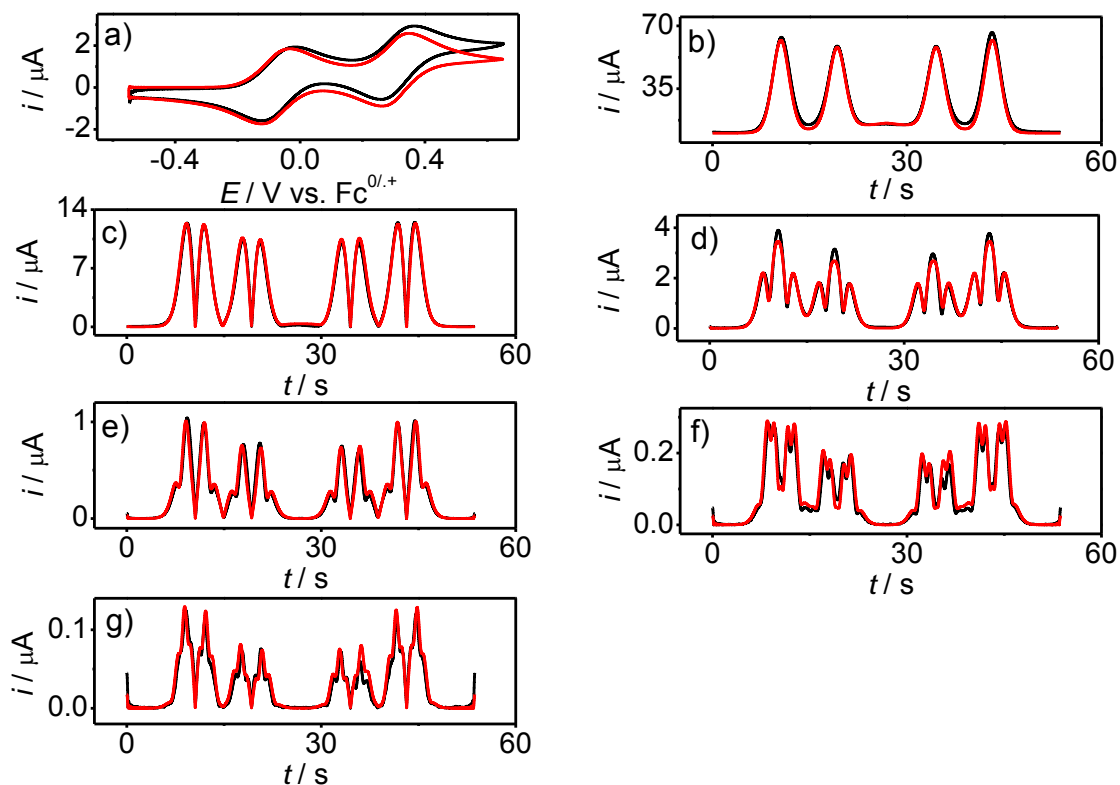


Figure S6. Comparison of simulated (—) and experimental (—) large amplitude FT AC voltammograms for the $\text{TTF}^{0/+2+}$ process obtained for the oxidation of 1.0 mM TTF in acetonitrile (0.1 M Bu_4NPF_6) at a Pt electrode (a) aperiodic dc component (b-g) 1st - 6th harmonics; $v = 0.0447 \text{ V s}^{-1}$, Simulation and other experimental parameters as described in Table 3.

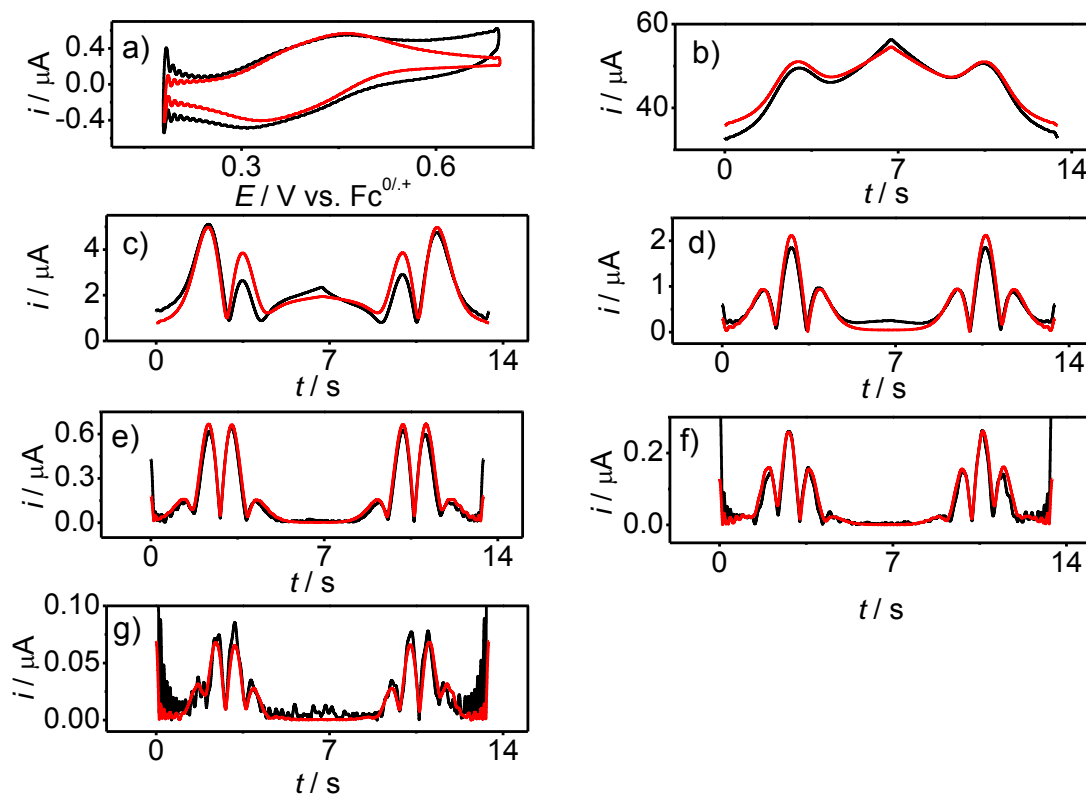


Figure S7. Comparison of simulated (—) and experimental (—) large amplitude FT AC voltammograms for the $\text{TTF}^{\bullet+}/2+$ process obtained for the oxidation of 0.1 mM $\text{TTF}^{\bullet+}$ in acetonitrile (0.1 M Bu_4NPF_6) at a GC electrode (a) aperiodic dc component (b-g) 1st - 6th harmonics; $v = 0.0774 \text{ V s}^{-1}$, Simulation and other experimental parameters as described in Table 4

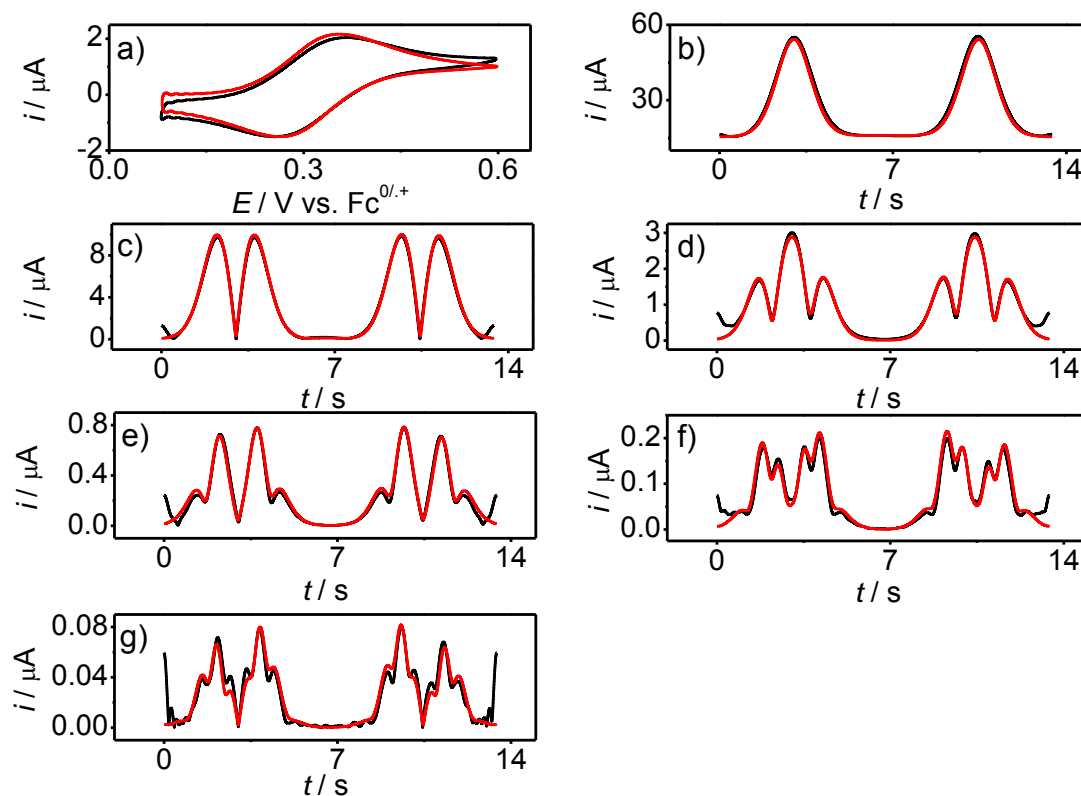


Figure S8. Comparison of simulated (—) and experimental (—) large amplitude FT AC voltammograms for the $\text{TTF}^{*/+2+}$ process obtained for the oxidation of 1.0 mM TTF^{*+} in acetonitrile (0.1 M Bu_4NPF_6) at a Pt electrode (a) aperiodic dc component (b-g) 1st - 6th harmonics; $v = 0.07749 \text{ V s}^{-1}$, Simulation and other experimental parameters as described in Table 4

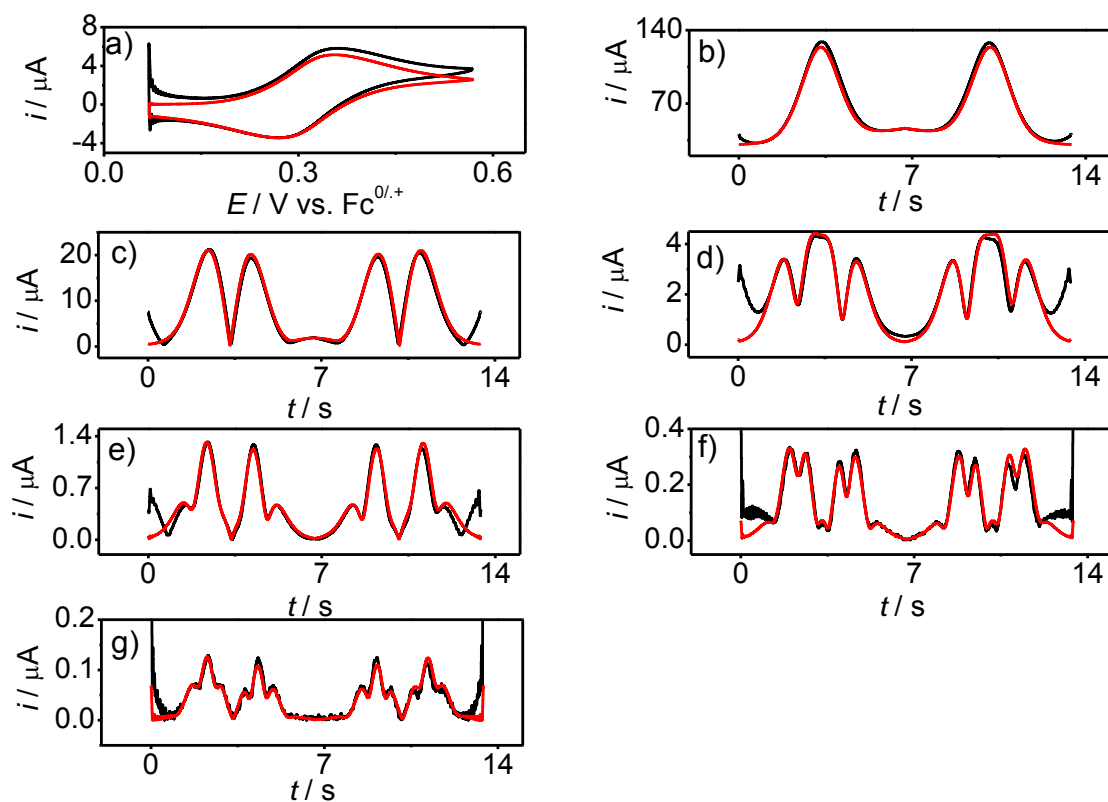


Figure S9. Comparison of simulated (—) and experimental (—) large amplitude FT AC voltammograms for the $\text{TTF}^{\bullet+}/2+$ process obtained for the oxidation of 1.0 mM $\text{TTF}^{\bullet+}$ in acetonitrile (0.1 M Bu_4NPF_6) at a GC electrode (a) aperiodic dc component (b-g) 1st - 6th harmonics; $v = 0.104 \text{ V s}^{-1}$, Simulation and other experimental parameters as described in Table 4

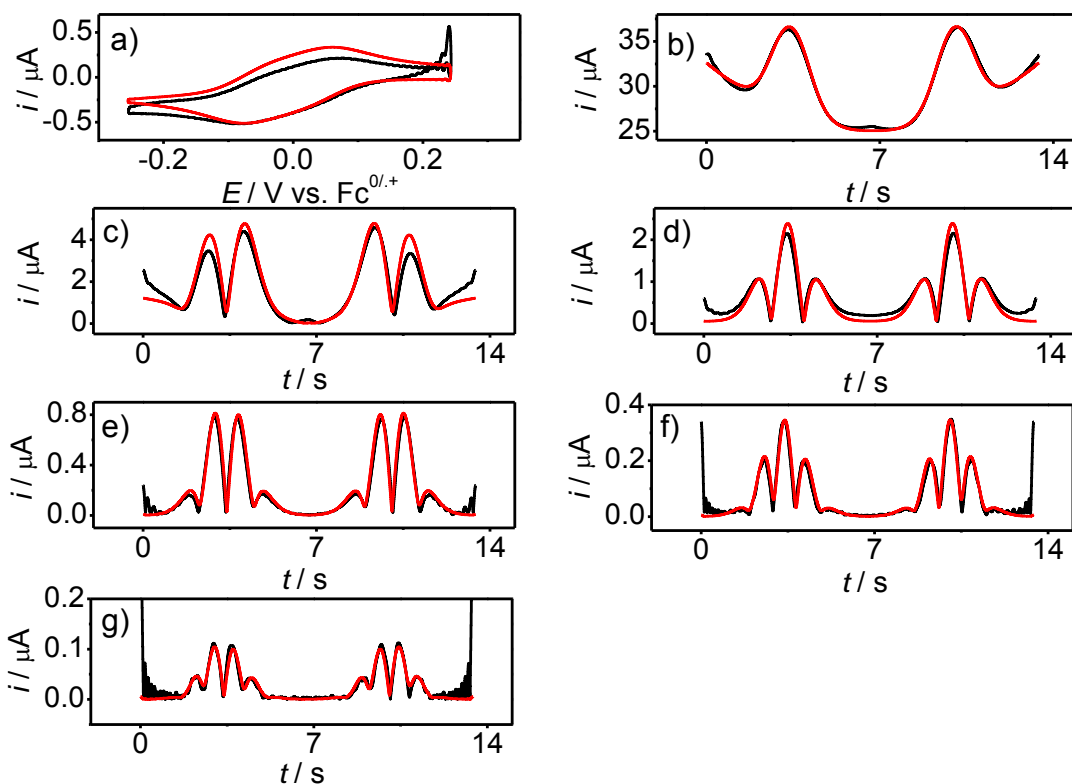


Figure S10. Comparison of simulated (—) and experimental (—) large amplitude FT AC voltammograms for the $\text{TTF}^{\bullet+/0}$ process obtained for the reduction of 0.1 mM $\text{TTF}^{\bullet+}$ in acetonitrile (0.1 M Bu_4NPF_6) at a GC electrode (a) aperiodic dc component (b-g) 1st - 6th harmonics; $v = 0.0745 \text{ V s}^{-1}$, Simulation and other experimental parameters as described in Table 5

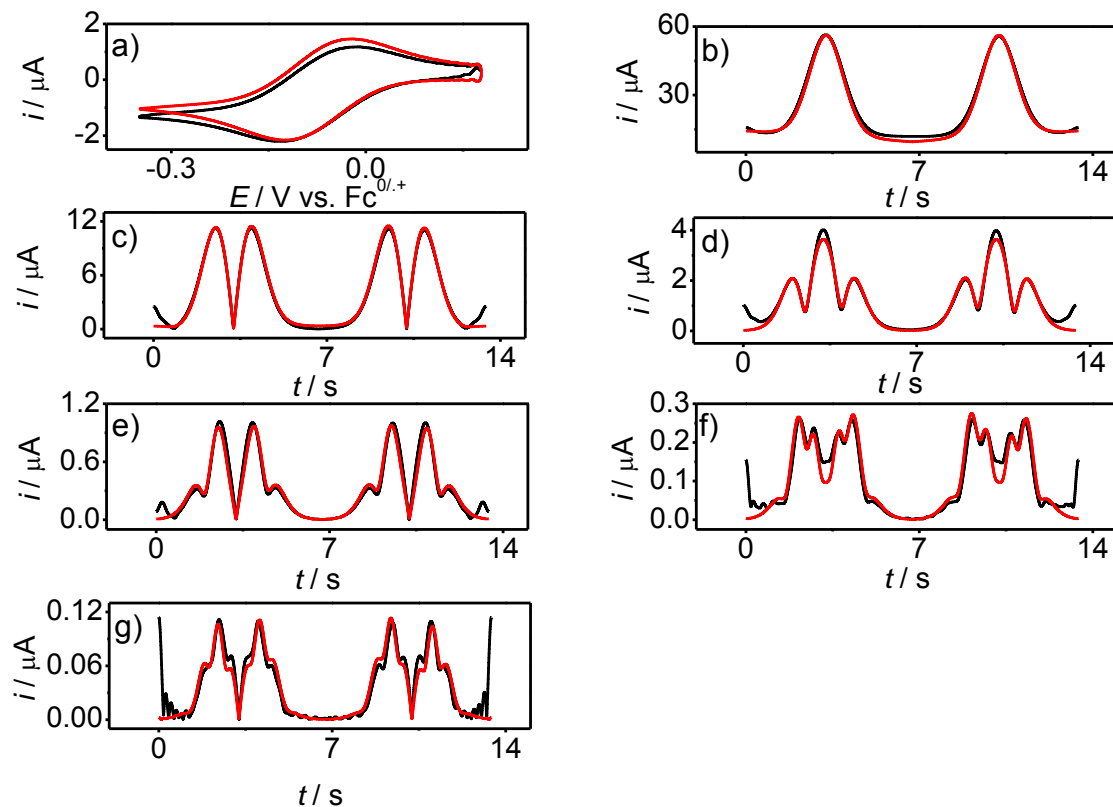


Figure S11. Comparison of simulated (—) and experimental (—) large amplitude FT AC voltammograms for the $\text{TTF}^{\bullet+}/0$ process obtained for the reduction of 1.0 mM $\text{TTF}^{\bullet+}$ in acetonitrile (0.1 M Bu_4NPF_6) at a Pt electrode (a) aperiodic dc component (b-g) 1st - 6th harmonics; $v = 0.0789 \text{ V s}^{-1}$, Simulation and other experimental parameters as described in Table 5

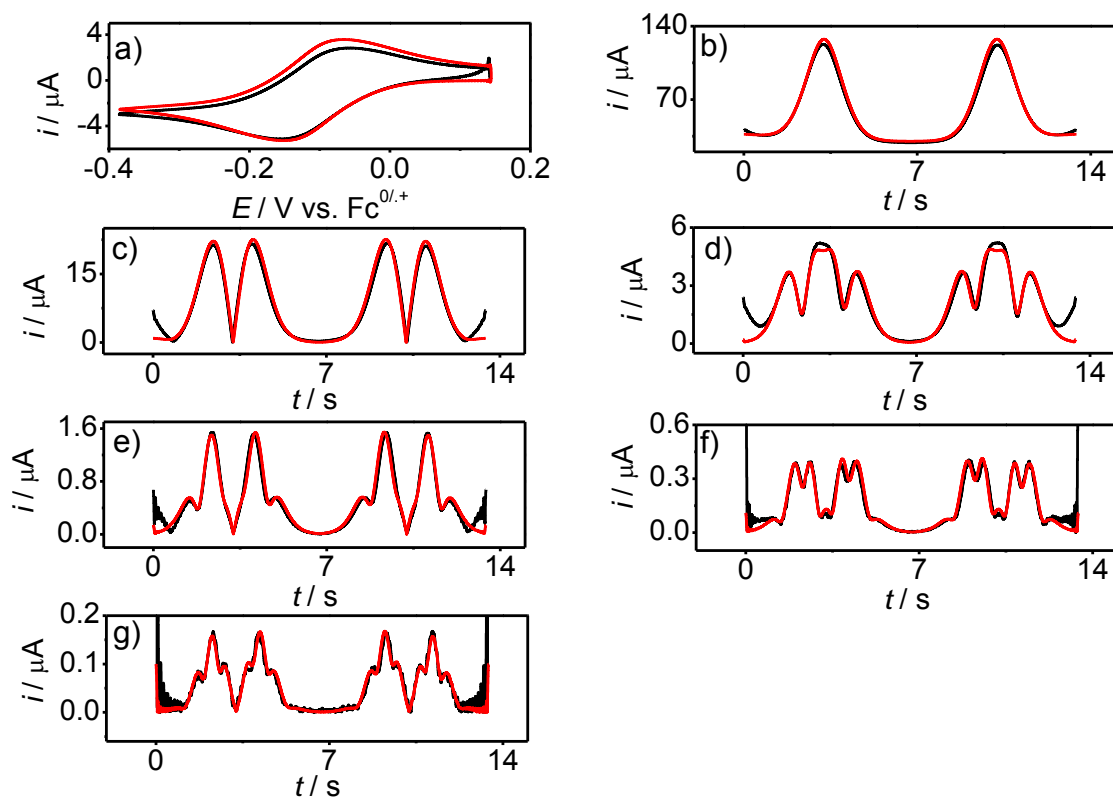


Figure S12. Comparison of simulated (—) and experimental (—) large amplitude FT AC voltammograms for the $\text{TTF}^{+/0}$ process obtained for the reduction of 1.0 mM TTF^{+} in acetonitrile (0.1 M Bu_4NPF_6) at a GC electrode (a aperiodic dc component (b-g) 1st - 6th harmonics; $v = 0.0789 \text{ V s}^{-1}$, Simulation and other experimental parameters as described in Table 5

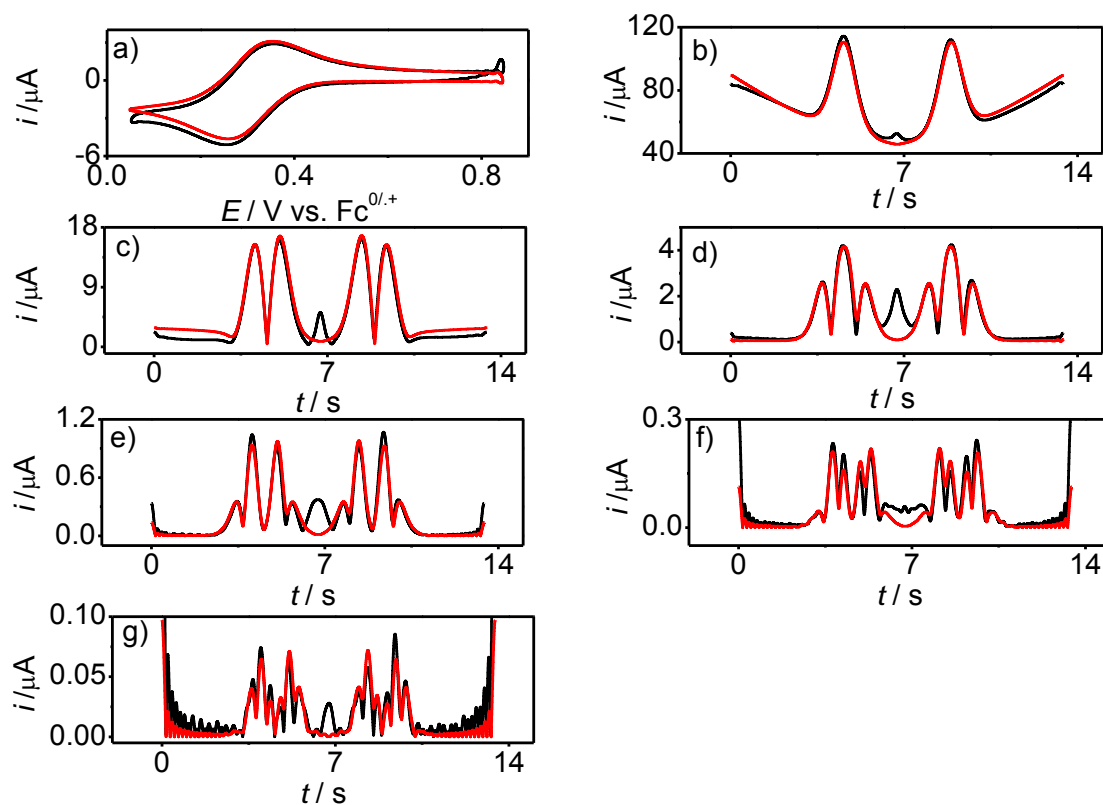


Figure S13. Comparison of simulated (—) and experimental (—) large amplitude FT AC voltammograms for the $\text{TTF}^{2+/\bullet+}$ process obtained for the reduction of 0.8 mM TTF^{2+} in acetonitrile (0.1 M Bu_4NPF_6) at a GC electrode (a) aperiodic dc component (b-g) 1st - 6th harmonics; $v = 0.119 \text{ V s}^{-1}$, Simulation and other experimental parameters as described in Table 6

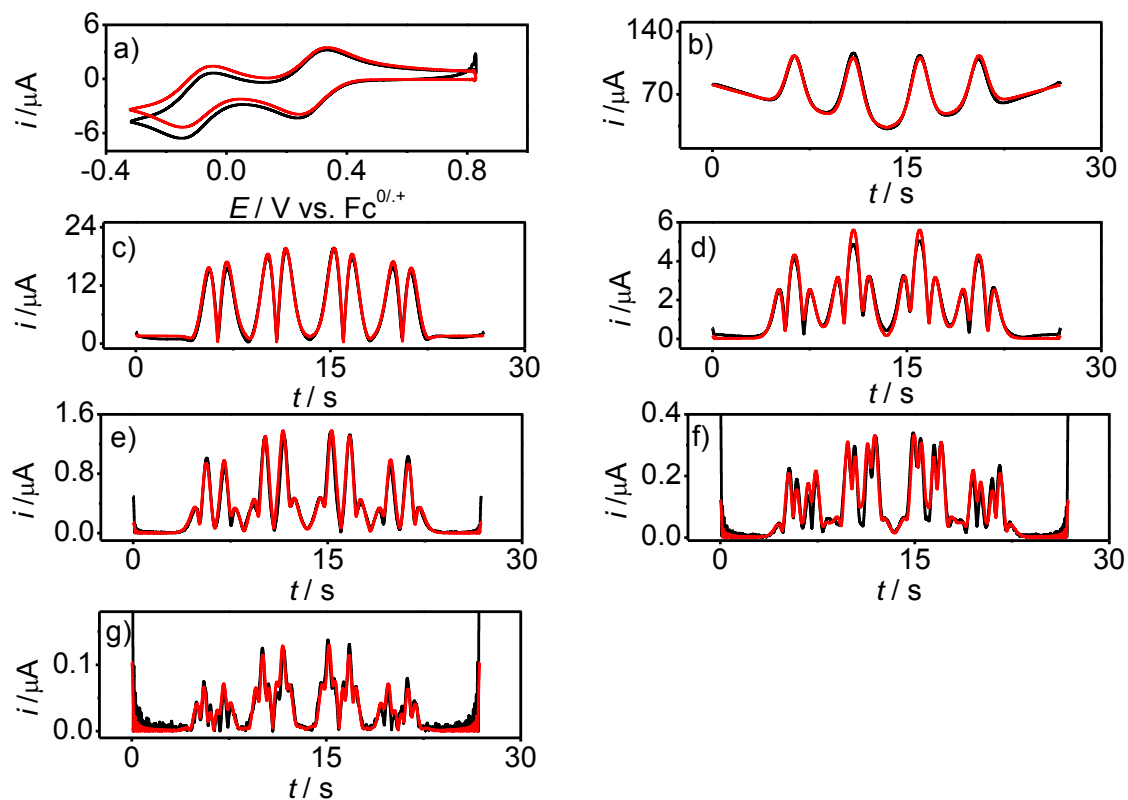


Figure S14. Comparison of simulated (—) and experimental (—) large amplitude FT AC voltammograms for the $\text{TTF}^{2+/\bullet+/0}$ process obtained for the reduction of 0.8 mM TTF^{2+} in acetonitrile (0.1 M Bu_4NPF_6) at GC electrode (a) aperiodic dc component (b-g) 1st - 6th harmonics; $v = 0.0856 \text{ V s}^{-1}$, Simulation and other experimental parameters as described in Table 7

CHAPTER 6

**ELECTRODE KINETICS STUDIES MICRODISK ELECTRODES: HIGH
FREQUENCY FT AC VOLTAMMETRY TO STUDY THE EFFECT OF
SOLVENTS VISCOSITY**

Monash University

Declaration for Thesis Chapter [6]

Declaration by candidate

In the case of Chapter [6], the nature and extent of my contribution to the work was the following:

Nature of contribution	Extent of contribution (%)
Initiation, key ideas, experimental work, writing up	80 %

The following co-authors contributed to the work. If co-authors are students at Monash University, the extent of their contribution in percentage terms must be stated:

Name		
Jie Zhang	Initiation, key ideas, writing up	
Alan M. Bond	Initiation, key ideas, writing up	

The undersigned hereby certify that the above declaration correctly reflects the nature and extent of the candidate's and co-authors' contributions to this work*.

Candidate's Signature  Date 28/11/2013

Name		
Jie Zhang		
Alan M. Bond		

Main Supervisor's Signature  Date 29/11/2013


*Note: Where the responsible author is not the candidate's main supervisor, the main supervisor should consult with the responsible author to agree on the respective contributions of the authors.

CHAPTER 6

INVESTIGATIONS OF FAST ELECTRODE KINETICS IN CONVENTIONAL SOLVENTS AND IONIC LIQUIDS USING LARGE AMPLITUDE FT AC VOLTAMMETRY UNDER HIGH FREQUENCY

Kiran Bano, Jie Zhang* and Alan M. Bond*

School of Chemistry, Monash University, Clayton, Victoria 3800, Australia

Corresponding authors: 

Abstract

High frequency (1.23 kHz) large amplitude (80 mV) FT AC voltammetry has been used at carbon fiber and Pt microdisk electrodes to probe the fast electron transfer kinetics associated with the reduction of 2,3,5,6-tetrafluoro-7,7,8,8-tetracyanoquinodimethane (F_4TCNQ) in the ionic liquids (ILs). The limitations encountered at macroelectrodes in the ILs under experimental conditions of this chapter are discussed and data are compared with kinetic studies at macrodisk electrodes in the conventional molecular solvent MeCN at high frequency. In the case of the $F_4TCNQ^{0/\bullet-}$ process the effect of solvent viscosity ranging from low viscosity molecular solvent MeCN ($\eta = 0.3$ cP) to high viscosity ionic liquid BMIMPF₆ ($\eta = 371$ cP) on mass transport is significant as being the electrode materials and structure of the cation of an ionic liquid.

6.1. Introduction

A quantitative study of the fundamental properties of an electrode process requires a detailed knowledge of electrode kinetics, thermodynamics and mass transport mechanisms.¹⁻¹¹ Many techniques, including voltammetry (transient and steady state) and impedance spectroscopy have been used¹²⁻¹⁸ in this active area of research. In transient DC cyclic voltammetry, Nicholson's method^{7,13} that uses separation of peak potentials (ΔE_p) as a function of scan rate is commonly used to determine the electron transfer kinetics. However, these values are strongly affected by errors arising from the uncompensated resistance (ohmic drop) that increases the peak separation.¹² It requires many experiments and only a very limited information is obtained from data analysis.

In order to obtain reliable fast scan rate voltammetric data to quantify fast electrode kinetics, the ohmic drop should be minimized. The experimental time scales should be 5-10 times the cell time constant (RC time constant). These criteria are most easily met by decreasing the electrode size to the micro level. Microelectrodes, possess adequate properties like faster double layer charging and higher mass transport rate with reduced iR_u drop at short time scale (high scan rate); these characteristics reduce the cell time constant in transient voltammetry and allow their applications to the study of fast electrode kinetics ($k^0 > 0.1 \text{ cm s}^{-1}$).²²⁻²⁶ Microelectrodes have been widely used for fast electrode kinetic measurements under transient conditions at fast scan rate and steady-state conditions at slow scan rates.²⁷ Under steady-state conditions, the difference of two quartile potentials²⁸ ($E_{1/4}-E_{3/4}$) may be used as a function of electrode radius in a similar manner to the Nicholson's method derived for cyclic voltammetry. Alternatively, steady-state may be achieved by using hydrodynamic voltammetry²⁹⁻³⁴ in flowing solutions. This increases the mass transport and allows to measure k^0 values in the $1-10 \text{ cm s}^{-1}$ range.

Another method of avoiding some of the limitations associated with transient DC voltammetry is to use AC techniques. In AC voltammetry, a sinusoidal perturbation of a certain frequency and amplitude is superimposed onto the DC potential. Impedance spectroscopy is a special case of this approach, when small amplitude is used to obtain the impedance spectra and equivalent circuits are used to prove a theoretical relevance. As the time scale is different for DC and AC measurements, the DC component can be separated from AC component. If the amplitude of the signal is sufficiently large, higher order harmonic components that are devoid of capacitive current, provide kinetically sensitive information. This technique has been employed at macroelectrodes for kinetics studies,^{19,20} where the parameters of interest can be quantified, along with capacitance by comparing simulated and experimental AC voltammograms. This AC method with large amplitude also may be used on rotating disc electrode or a stationary macroelectrode;¹⁹⁻²¹ but has not been applied at microelectrodes.

To date, large amplitude AC voltammetry has been used at low frequencies in studies of fast electron transfer kinetics e.g. about 10-200 Hz. Although, use of higher frequencies provides greater kinetic sensitivity but the large currents lead to a large total (faradaic plus background) current and hence larger iR_u drop which reduces the number of kinetically sensitive harmonics that are accessible. Indeed, the use of microelectrode and AC voltammetry can provide a useful approach to minimize the iR_u drop. For high frequency measurements, the electrodes shall retain the transient conditions and use of planar diffusion which is simple to model.

In this study, reduction of F₄TCNQ (2,3,5,6-tetrafluoro-7,7,8,8-tetracyanoquinodimethane) has been studied as an example of a fast electron transfer process using high frequency large amplitude AC voltammetry at the microdisk electrodes in the conventional molecular solvent

acetonitrile, *N, N*, dimethyl sulfoxide and ionic liquids having a range of viscosities and other properties that could monitor the rate of electron transfer.

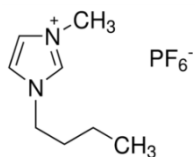
Electrode kinetics data for reduction of F₄TCNQ were obtained in the conventional solvents at macrodisk electrodes ($d = 1.0$ mm), however, in ionic liquids, microelectrodes were used ($d = 125$ μm and $d = 33$ μm). In highly viscous ILs small diffusion coefficient (slow diffusion rates) results in longer time being required to reach steady state.³⁵ The relative contribution of the linear and radial diffusion at a disk electrode depends on (D/r^2) where D is the diffusion coefficient, and r is the electrode radius.³⁶ Since D is small in ionic liquids, it follows that if the microelectrode radius is small, then so is D/r^2 term and a transient response at microelectrode is more readily achieved in an ionic liquid. AC voltammetric data obtained in ILs can then still be modelled using theory for linear diffusion. The uses of microelectrodes in ILs at high AC frequency are therefore considered in this chapter.

6.2. Chemicals and experimental procedure

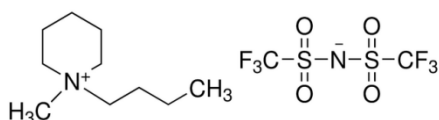
6.2.1. Reagents

2,3,5,6-Tetrafluoro-7,7,8,8-tetracyanoquinodimethane (F₄TCNQ, Beijing Health), acetonitrile (MeCN, Sigma-Aldrich), *N, N*, dimethyl sulfoxide (DMSO, Sigma-Aldrich), *n*-tetrabutylammonium hexafluorophosphate (Bu₄NPF₆) 98%, (Wako) was recrystallised twice from ethanol. 1-butyl-1-methylpyrrolidinium bis(trifluoromethyl-sulfonyl)imide (BMPYTFSI, iolitec), 1-butyl-1-methylpiperidinium bis(trifluoromethylsulfonyl)imide (BMPIPTFSI, iolitec), 1-butyl-3-methylimidazolium hexafluorophosphate (BMIMPF₆, Merck)

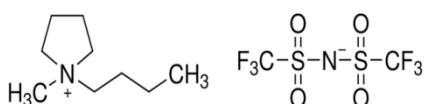
6.2.2. Structures of ionic liquids



1-butyl-3-methylimidazolium hexafluorophosphate, (BMIMPF₆)



1-butyl-1-methylpiperidinium bis(trifluoromethylsulfonyl)imide, (BMPIPTFSI)



1-butyl-1-methylpyrrolidinium bis(trifluoromethylsulfonyl)imide, (BMPYTFSI)

6.2.3. Instrumentation and procedure

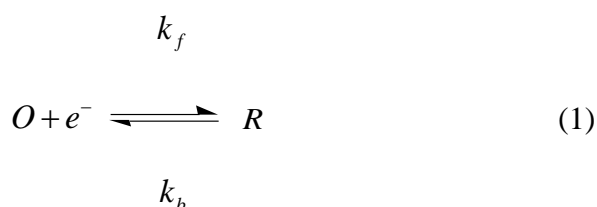
All electrochemical experiments were carried out in a glove box under a nitrogen atmosphere at room temperature ($T = 20 \pm 2$ °C). A standard electrochemical cell with a three electrode configuration was used. Working electrodes were either macrodisk (platinum (Pt), $d = 1.0$ mm, gold (Au), $d = 2.0$ mm, glassy carbon (GC), $d = 1.0$ mm and boron doped diamond (BDD), $d = 1.0$ mm) or microdisk (Pt ($d = 125$ μm) and carbon fiber ($d = 33$ μm)). The effective electrode areas of working electrodes were calculated from the slope of Q vs. $t^{1/2}$ derived from chronocoulometric reduction of 1.0 mM potassium ferricyanide in aqueous (0.1 M KCl) using $D = 7.6 \times 10^{-6}$ $\text{cm}^2 \text{s}^{-1}$. In this case, the electrode area of the Pt 1.0 mm diameter electrode was calculated to be 0.007847 cm^2 while A values of 1.22×10^{-4} cm^2 and 8.54×10^{-6} cm^2 were found for Pt and carbon fiber microelectrodes respectively.

Uncompensated resistance was measured using the *RC* time constant method available with the BAS 100 instrument in a potential region where no faradaic current is present.

Working electrodes were polished with aqueous 0.05 μm alumina slurry on a clean polishing cloth, then consecutively washed and rinsed with water, 0.05 M nitric acid, water and acetone. Platinum wire was used for auxiliary electrode and another platinum wire was used as quasi-reference electrodes. Potentials were then calibrated against the $\text{Fc}^{0/+}$ process (Fc = ferrocene) by addition of ferrocene into F_4TCNQ solutions in ionic liquids. DC cyclic voltammetric experiments were undertaken with CHI 400B electrochemical workstation and large amplitude FT AC voltammetric ones with home built instrumentation.³⁷ FT AC voltammetric experiments employed a sine wave having amplitude of 80 mV and frequencies of 9.0 Hz, 528 Hz or 1.23 kHz.

6.2.4. Simulations and AC data analysis

Simulations of FT AC voltammograms with an in-house software called MECSim (Monash Electrochemistry Simulator) is written in Fortran. This software uses the comparatively efficient expanding spatial grid formulation³⁸ and is based on the mathematical approach described by Rudolph³⁹ with minor alterations. Simulations assumed the Butler-Volmer theory¹² applied for electron transfer reaction given in eq. (1)



where k_f and k_b are the potential dependent rate constants for forward and backward electron transfer reactions, E^0 is the formal reversible potential. In this k_f and k_b may be written in the

form of k^0 , α is a charge transfer coefficient and k^0 value is the formal charge-transfer rate constant at potential E^0 (vs. the reference electrode).

FT AC voltammetric data obtained experimentally or by simulation were then subjected to data analysis in which time domain data are converted to the frequency domain using FT algorithm to give the power spectrum. Frequencies in the region containing AC harmonics and aperiodic DC component in the power spectrum were then subjected to band filtering to provide DC or AC components as a function of time. Out of five unknown parameters needed to determine the electrode kinetics, viz. R_u , E^0 , k^0 , α and C_{dl} (double layer capacitance), R_u was determined experimentally from the RC time constant where no faradaic current was present, E^0 was estimated from current minima of 2nd harmonic, C_{dl} was quantified from the background current in the fundamental harmonic and k^0 was extracted from higher harmonic components. In order to define C_{dl} , a non-linear capacitor model was used where necessary, using the procedure defined elsewhere.³⁷

6.3. Results

6.3.1. Theoretical analysis of kinetic sensitivity

A comprehensive analysis is carried out to determine the upper limit of detection of k^0 available at a macroelectrode ($d = 1.0$ mm) and a microelectrode ($d = 125$ μm). The resistance of 1.0 mm diameter electrode is assumed as 127 ohm and resistance of 125 μm diameter electrode is considered as 8000 ohm in theoretical studies.

For the microelectrode ($d = 125$ μm) and $D = 2.0 \times 10^{-5}$ $\text{cm}^2 \text{s}^{-1}$; simulated peak currents of the sixth harmonic are confirmed as a function of $\log_{10} k^0$ using the parameters given in Figure 1. The upper limit of k^0 quantification is determined both at low (9.0 Hz) and high (1.23 kHz) frequency from I_p versus $\log_{10} k^0$ graphs given in Figure 1. Kinetic sensitivity at a microelectrode is decided from Figure 1 on the basis of distance from the straight line region

where peak currents of 6th harmonic become independent of k^0 and electron transfer processes are considered reversible. From these results it is concluded that use of microelectrode at 9.0 Hz allows to measure the k^0 value of about 0.5 cm s⁻¹ as shown in Figure 1a. Whereas at the higher frequency (1.23 kHz) on the basis of data shown in Figure 1b the upper limit available for the determination of k^0 is about 10.0 cm s⁻¹. However, the size of microelectrode ($d = 125 \mu\text{m}$) in this case is not small enough to achieve steady-state.

The above simulations indicate that the use of a microelectrode at higher frequency provides advantages in the study of fast electrode kinetics with large amplitude AC voltammetry. Though, other factors also affect the kinetic sensitivity, one major one is the value of diffusion coefficients, with $D = 1.0 \times 10^{-8} \text{ cm}^2 \text{ s}^{-1}$ as in an IL case very little information (up to three harmonics at 1.23 kHz) is accessible at the macroelectrode since only three harmonics can be obtained. Whereas, at microelectrode, eight harmonics can be found as shown in Figure 2.

Kinetic sensitivity analysis is also carried under the conditions where the diffusion coefficient is reduced to $10^{-8} \text{ cm}^2 \text{ s}^{-1}$ as is relevant to ionic liquid media. Figure 3 shows that at 9.0 Hz and under this low D value, k^0 value can be measured up to 0.01 cm s⁻¹. Whereas, with a higher frequency of 1.23 kHz, the upper limit of kinetics measurement increases to 0.1 cm s⁻¹. Therefore, a high frequency of 1.23 kHz requires the use of microelectrode in highly viscous ILs.

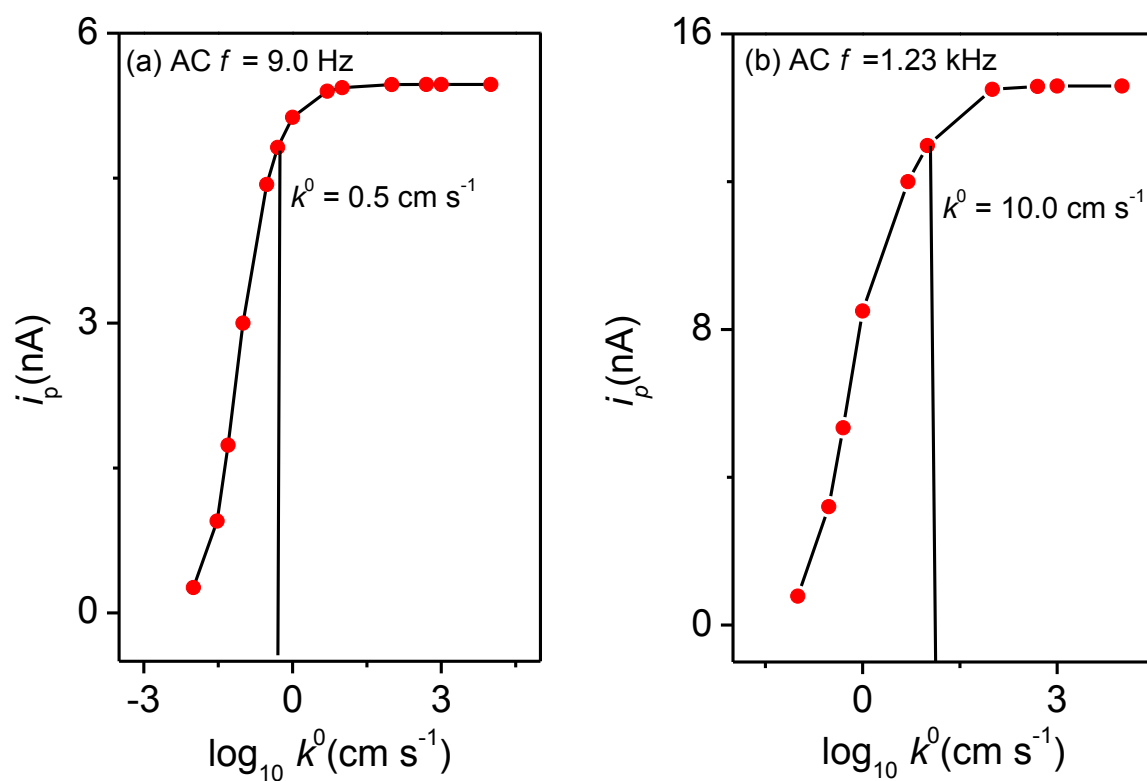


Figure 1: Peak currents of 6th harmonic versus $\log_{10} k^0$ obtained at frequencies (a) 9.0 Hz and (b) 1.23 kHz, $\Delta E = 80$ mV, $C = 2.0$ mM, $R_u = 8000$ ohm, $D = 2.0 \times 10^{-5}$ cm² s⁻¹, $C_{dl} = 10$ μ F cm⁻² and $A = 1.22 \times 10^{-4}$ cm².

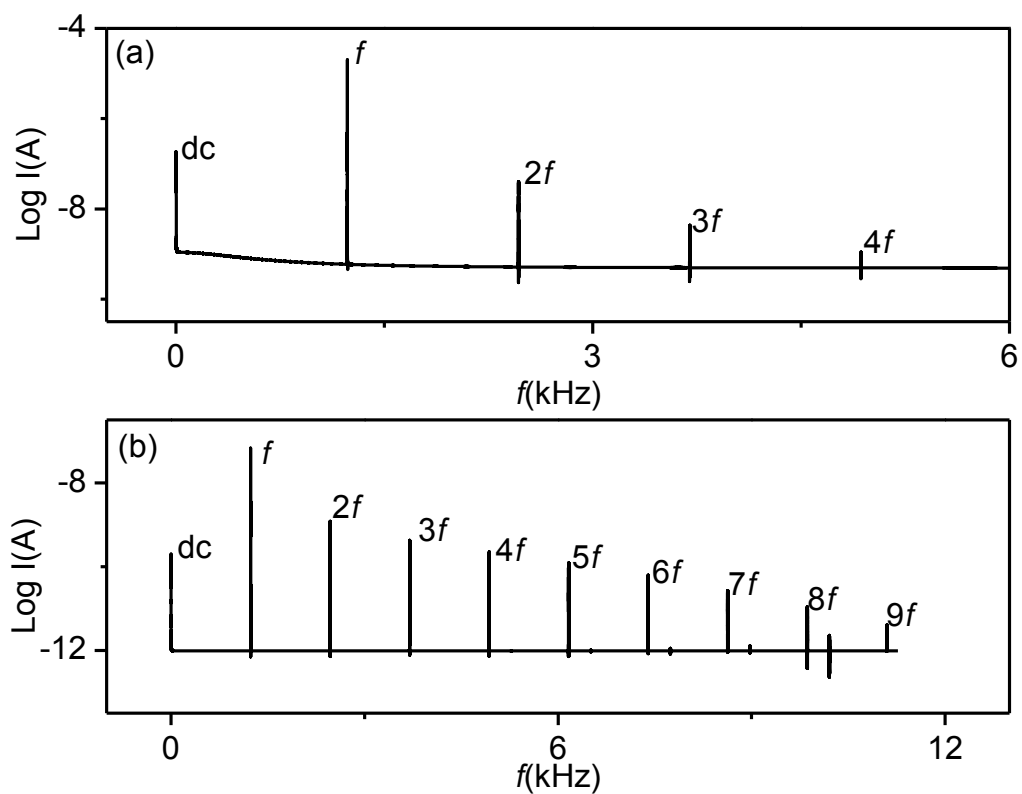


Figure 2: Log power spectrum obtained theoretically (a) at macroelectrode ($d = 1.0$ mm) and (b) at microelectrode ($d = 125$ μm) where $C = 5.0$ mM, $f = 1.23$ kHz, $\Delta E = 80$ mV, $R_u = 5000$ ohm, $D = 1.0 \times 10^{-8}$ cm² s⁻¹, $k^0 = 1.0$ cm s⁻¹ and $C_{dl} = 10.0$ μF cm⁻².

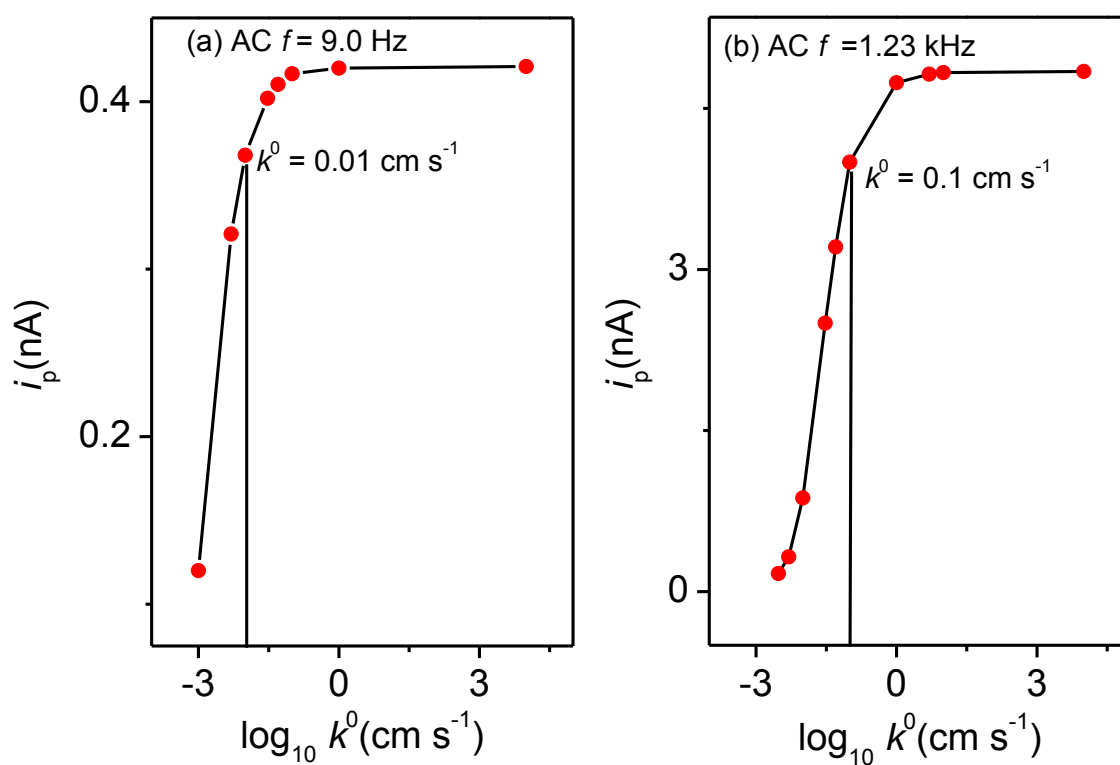
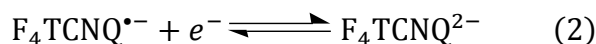


Figure 3: Peak currents of 6th harmonic versus $\log_{10} k^0$ obtained at frequencies (a) 9.0 Hz and (b) 1.23 kHz, $\Delta E = 80$ mV, $C = 2.0$ mM, $R_u = 8000$ ohm, $D = 1.0 \times 10^{-8}$ cm² s⁻¹, $C_{dl} = 10.0$ μ F cm⁻² and $A = 1.22 \times 10^{-4}$ cm².

6.3.2. Voltammetric reduction of F₄TCNQ

F₄TCNQ undergoes two consecutive one electron reduction processes, the F₄TCNQ^{0/•-} (neutral to radical anion) and the F₄TCNQ^{•-/2-} from radical anion to dianion as given in



In this chapter, only initial F₄TCNQ^{0/•-} reduction process has been studied in various solvents. Initially, voltammetric studies were conducted in the molecular solvents acetonitrile, and dimethylsulfoxide (DMSO) at a Pt macrodisk electrodes (d = 1.0 mm). DC cyclic voltammograms of F₄TCNQ in different solvents are shown in Figure 4. The diffusion coefficient of F₄TCNQ has been calculated from the peak current for the reduction of F₄TCNQ in MeCN and DMSO (Figures 4a and 4b) and the ILs BMPYTFSI, BMIMPF₆ and BMPIPTFSI (Figures 4c-4e) using the Randles-Sevcik relationship,

$$i_p = -0.4463nFA \left(\frac{nFDv}{RT} \right)^{1/2} C \quad (3)$$

where I_p is the reduction peak current, n is the number of electrons transferred ($n = 1$), C is the bulk solution concentration, D is the diffusion coefficient of F₄TCNQ, T is the absolute temperature, R is the universal gas constant, F is Faraday's constant and A is the electrode area. The diffusion coefficients of ferrocene are also included in Table 1. The smaller D value of F₄TCNQ is attributed to the large size.

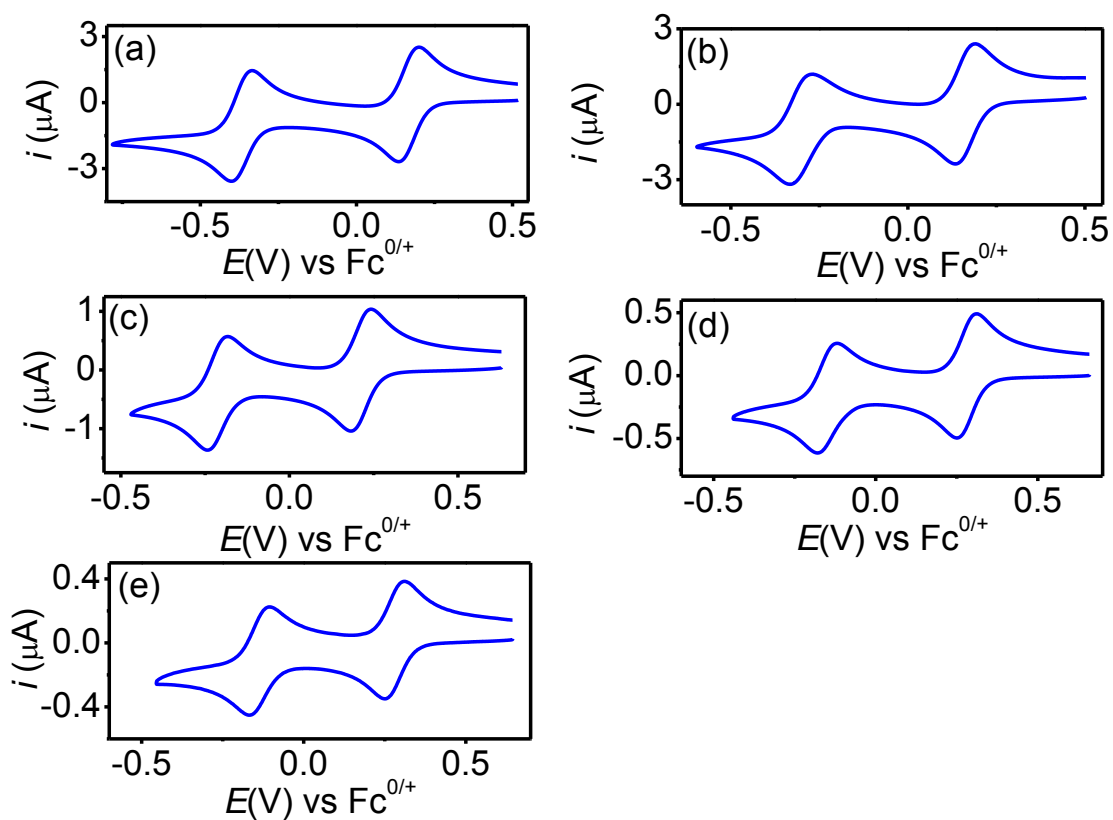


Figure 4: DC voltammograms at Pt electrode ($d = 1.0$ mm) (a) 0.9 mM F_4TCNQ in 0.1 M Bu_4NPF_6 in acetonitrile (b) 2.2 mM F_4TCNQ in 0.1 M Bu_4NPF_6 in DMSO (c) 7.24 mM F_4TCNQ in BMPYTFSI (d) 7.0 mM F_4TCNQ in BMIMPF₆ (e) 4.9 mM F_4TCNQ in BMPIP TFSI, $v_{DC} = 0.1$ V s⁻¹.

Table 1: Diffusion coefficients of F₄TCNQ and Ferrocene in molecular solvents and ionic liquids

Solvent	Viscosity at 20 °C (cp)	F ₄ TCNQ Diffusion Coefficient (cm ² s ⁻¹)	Fc Diffusion Coefficient (cm ² s ⁻¹)
BMIMPF₆	371	8.0×10^{-9}	7.63×10^{-9} (Literature) ⁴⁰
BMPIPTFSI	183	1.04×10^{-8}	3.68×10^{-8}
BMPYTFSI	71	3.9×10^{-8}	7.32×10^{-8}
DMSO	1.98	2.64×10^{-6}	4.4×10^{-6} (Literature) ⁴¹
MeCN	0.35	1.98×10^{-5}	2.4×10^{-5} (Literature) ⁴¹

6.3.3. FT AC voltammetry in MeCN at a macroelectrode

The heterogeneous electron transfer kinetics for the F₄TCNQ^{0/+•} process in MeCN (0.1 M Bu₄NPF₆) at four electrodes (GC, Pt, Au and BDD) was initially studied by FT AC voltammetry over frequencies ranging from 9.0 Hz to 234 Hz. Thus, the high kinetic sensitivity of high frequencies is offered to some degree by the need to take into account the higher iR_u drop and larger C_{dl} values. In an experiment $f = 234$ Hz and amplitude 80 mV were used for comparison of experimental and simulated data. Simulations initially employed experimentally derived values of C , A , R_u and D , k^0 values were then estimated by comparison of theory versus experiment, while α , the charge transfer coefficient was assumed to be 0.50 for outer-sphere electron transfer reaction.

Excellent agreement between simulated and experimental data is obtained (Figure 5) with $k^0 = 1.0 \text{ cm s}^{-1}$ at Pt electrode along with other parameters $A = 0.00785 \text{ cm}^2$, C_{dl} ($c_0 = 11.0$, $c_1 = 1.0$) $\mu\text{F cm}^{-2}$, $R_u = 525 \text{ ohm}$ and $\alpha = 0.50$. Whereas at the gold electrode $k^0 = 1.0 \text{ cm s}^{-1}$ along with $A = 0.019 \text{ cm}^2$, $C_{dl} = 20.5 \mu\text{F cm}^{-2}$ and $R_u = 370$ are found to provide good agreement

with the theory (Figure 6). At a macrodisk GC electrode using $A = 0.00785 \text{ cm}^2$, C_{dl} ($c_0 = 28.0$, $c_1 = 14.0$, $c_2 = 1.50$) $\mu\text{F cm}^{-2}$ and $R_u = 590 \text{ ohm}$, k^0 is estimated to be 0.9 cm s^{-1} (Figure 7). At a BDD electrode, simulations with $k^0 = 1.0 \text{ cm s}^{-1}$, $R_u = 546 \text{ ohm}$ and $C_{\text{dl}} = 6.0 \mu\text{F cm}^{-2}$ are used to get excellent agreement with experiment (Figure 8).

All of these k^0 values are very close to the upper limit of measurement and appear to be the upper limit on the 234 Hz frequency. Assuming no systematic errors arising from C , D , A and R_u to the k^0 estimates, it can be concluded that differences in the density of state of metal and carbon electrodes do not appear to contribute to k^0 . In all cases, α is considered 0.50 and differences in the density of states of metals and carbon electrodes cannot be observed. Lack of electrode dependence suggests that the $\text{F}_4\text{TCNQ}^{0/\bullet-}$ process in acetonitrile is adiabatic.⁴²

Table 2. Parameters used^a in simulations undertaken to estimate the electrode kinetics for the reduction of 1.9 mM F_4TCNQ in MeCN (0.1 M Bu_4NPF_6).

Electrode	R_u	$C_{\text{dl}}(c_0, c_1, c_2)$	k^0	E^0 vs. $\text{Fc}^{0/+}$	α
	(ohm)	($\mu\text{F cm}^{-2}$)	(cm s^{-1})	(V)	
Pt	525	11.00, 1.00, 0.00	1.00	0.289	0.50
Au	370	20.50, 3.00, 1.50	1.00	0.289	0.50
GC	580	28.00, 14.00, 1.50	0.90	0.289	0.50
BDD	546	6.00, 0.00, 0.00	1.00	0.289	0.50

^a $A_{\text{Au}} = 0.019 \text{ cm}^2$, $A_{\text{GC}} = A_{\text{BDD}} = A_{\text{Pt}} = 0.00785 \text{ cm}^2$, $f = 234 \text{ Hz}$, $\Delta E = 80 \text{ mV}$, $D = 1.98 \times 10^{-5} \text{ cm}^2 \text{ s}^{-1}$ and $T = 293 \text{ K}$

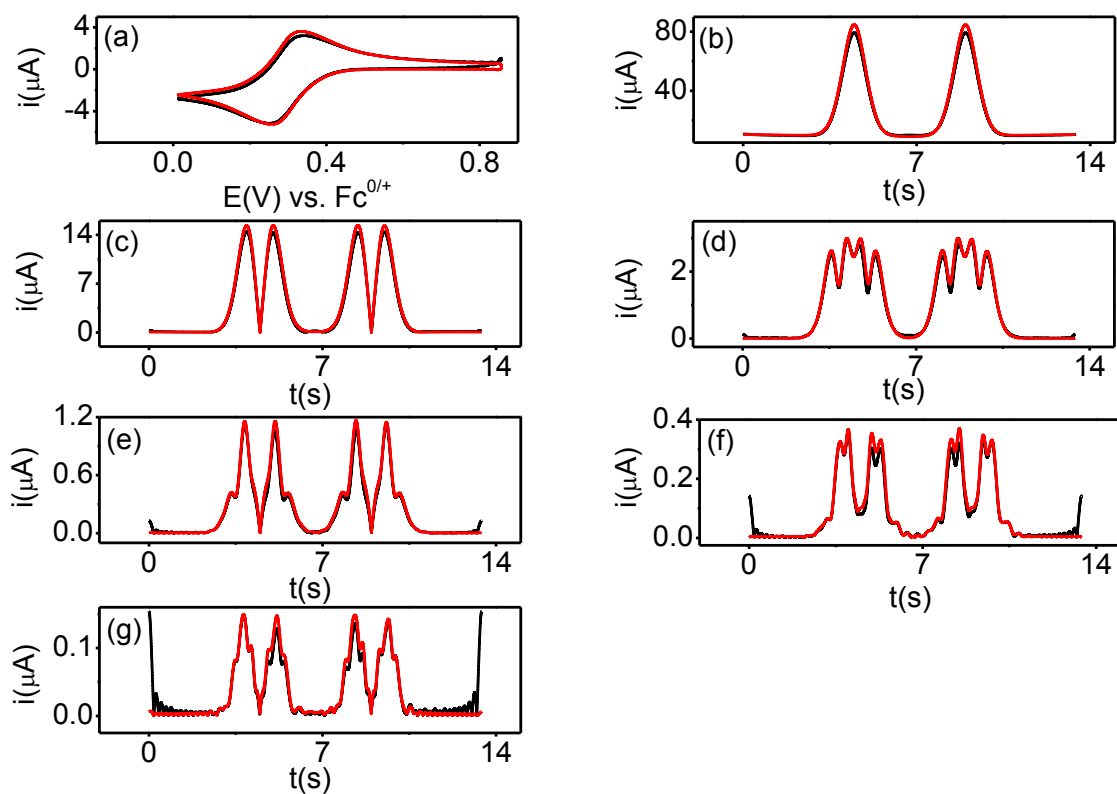


Figure 5: Comparison of experimental (—) and simulated (—) FT AC voltammograms for the reduction of 1.9 mM F_4TCNQ in acetonitrile(0.1 M Bu_4NPF_6) at a Pt macrodisk electrode (a) DC component (b-g) 1st to 6th harmonic; $v_{DC} = 0.126 \text{ V s}^{-1}$ and other simulation parameters are described in Table 2.

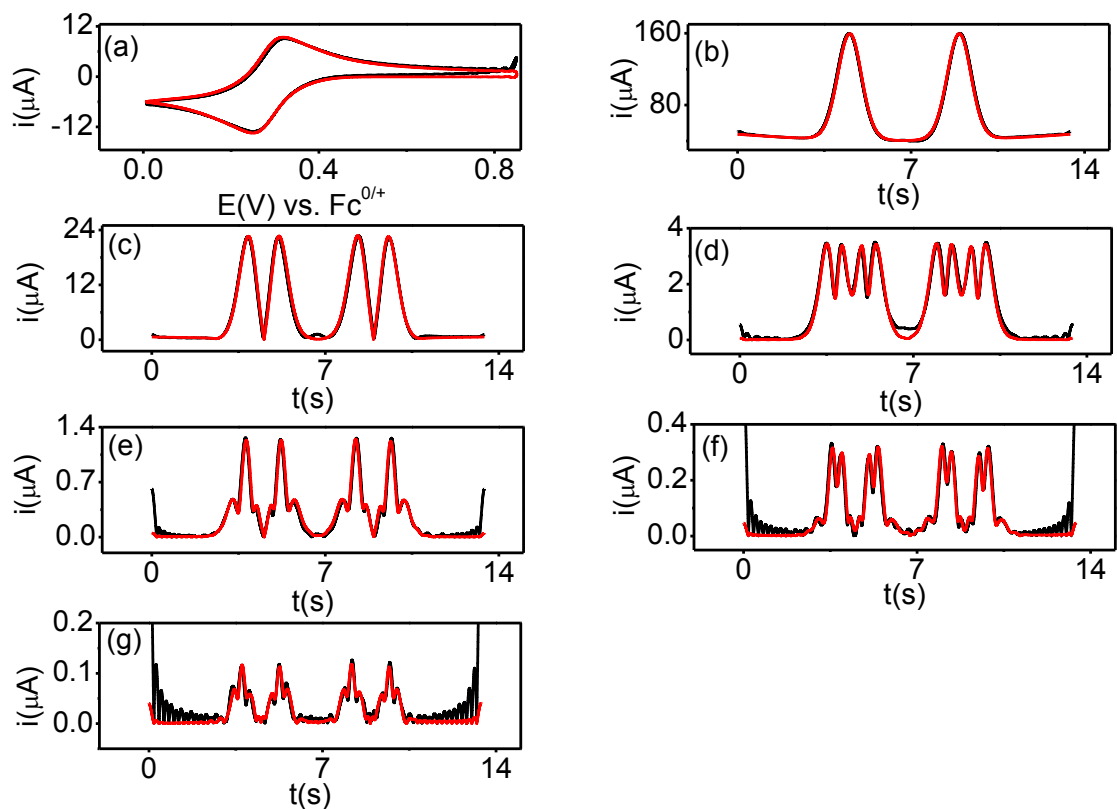


Figure 6: Comparison of experimental (—) and simulated (—) FT AC voltammograms for the reduction of 1.9 mM F_4TCNQ in acetonitrile(0.1 M Bu_4NPF_6) at Au macrodisk electrode (a) DC component (b-g) 1st to 6th harmonic; $v_{DC} = 0.126 \text{ V s}^{-1}$ and other simulation parameters are described in Table 2

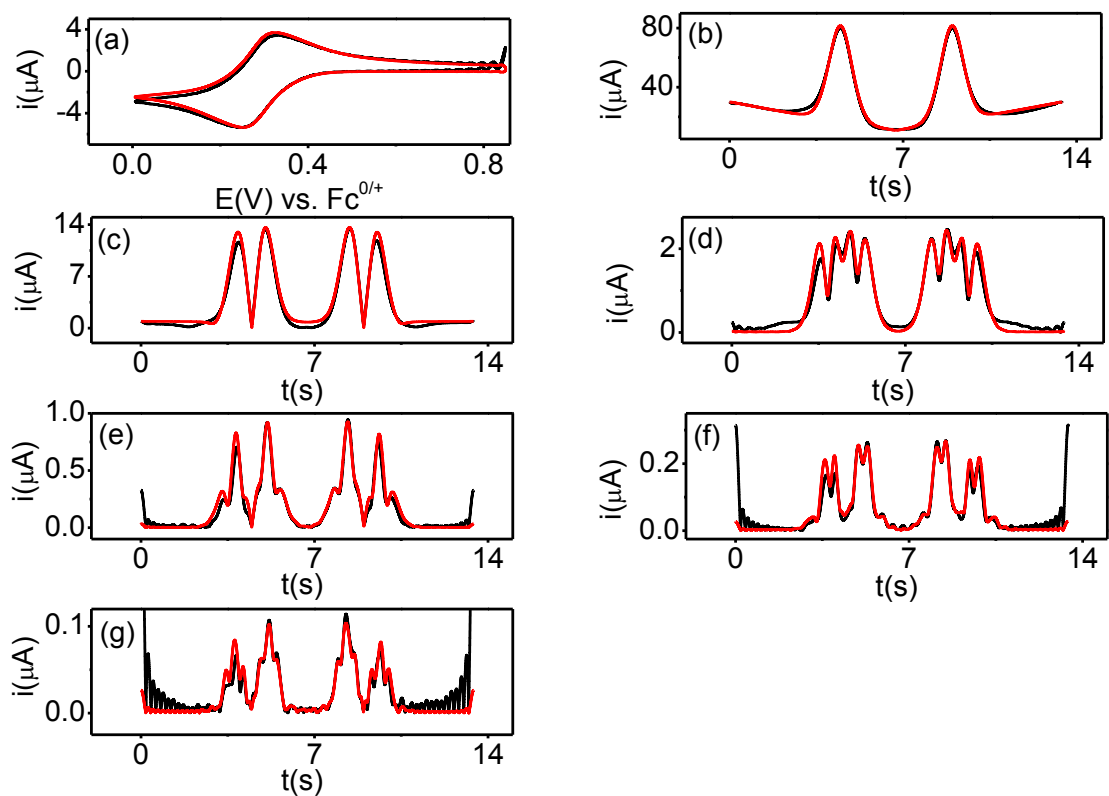


Figure 7: Comparison of experimental (—) and simulated (—) FT AC voltammograms for the reduction of 1.9 mM F_4TCNQ in acetonitrile(0.1 M Bu_4NPF_6) at a GC macrodisk electrode (a) DC component (b-g) 1st to 6th harmonic; $v_{DC} = 0.126 \text{ V s}^{-1}$ and other simulation parameters are described in Table 2

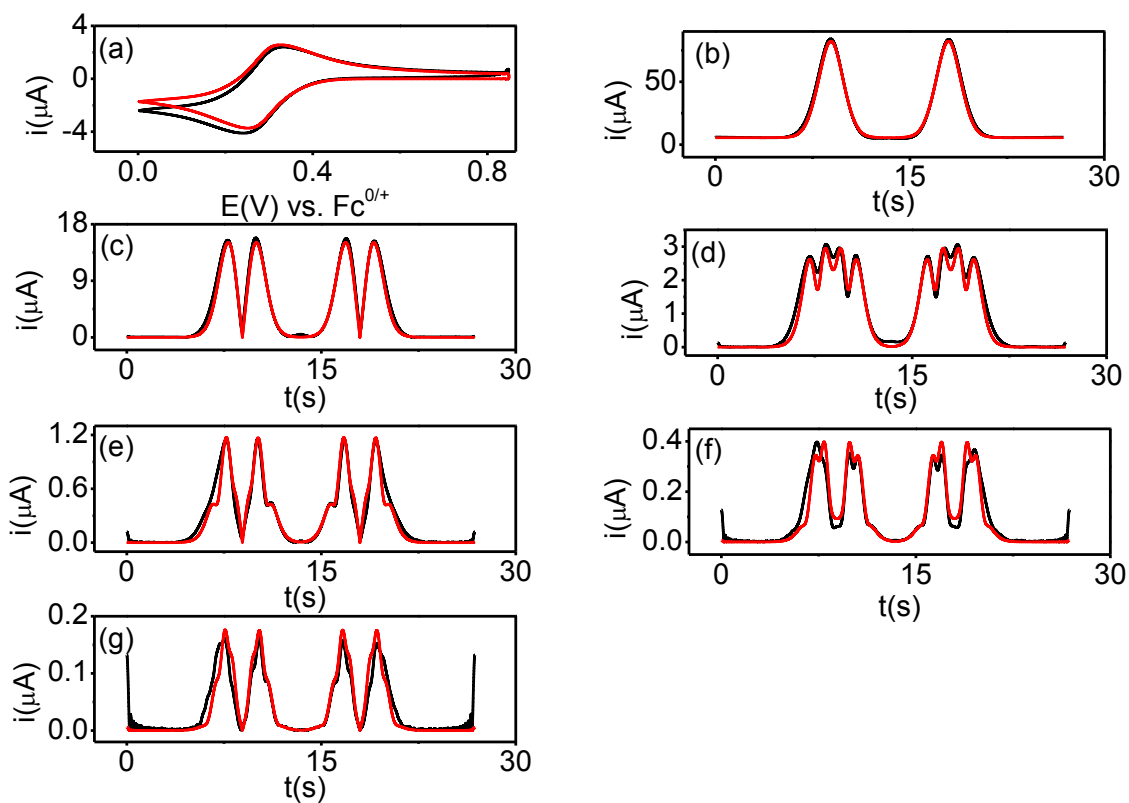


Figure 8: Comparison of experimental (—) and simulated (—) FT AC voltammograms for the reduction of 1.9 mM F_4TCNQ in acetonitrile(0.1 M Bu_4NPF_6) at a BDD macrodisk electrode (a) DC component (b-g) 1st to 6th harmonic; $v_{DC} = 0.126 \text{ V s}^{-1}$ and other simulation parameters are described in Table 2

6.3.4. Large amplitude FT AC voltammetry in DMSO with macrodisk electrodes

FT AC voltammetric studies were also undertaken in DMSO (0.1 M Bu₄NPF₆) with 1.55 mM F₄TCNQ. DMSO has a higher viscosity than acetonitrile and R_u values are also higher, thus, limiting the frequency that can be used to study the electrode kinetics. At lower frequencies (9-36 Hz) eight to nine harmonics can be obtained with excellent signal to noise ratio, while at higher frequencies ($f > 36$ Hz), not only the number of accessible harmonics decreases down but the larger iR_u drop and high capacitance introduces more complications in the measurement of electron transfer kinetics. Therefore, the low frequency of 9.0 Hz is used in this case while amplitude is retained at 80 mV.

Under these conditions k^0 value at the Pt macrodisk electrode is estimated to be 0.10 cm s⁻¹ by the comparison of experiment and theory (Figure 9) using $A = 0.00785$ cm², C_{dl} ($c_0 = 22.55$, $c_1 = 40.5$, $c_2 = 41.0$) $\mu\text{F cm}^{-2}$ and $R_u = 2850$ ohm. At Au electrode (Figure 10), $k^0 = 0.15$ cm s⁻¹ is found using C_{dl} ($c_0 = 39.50$, $c_1 = 40.5$, $c_2 = 36.0$) $\mu\text{F cm}^{-2}$ and $R_u = 1600$ ohm.

At the GC electrode $k^0 = 0.07$ cm s⁻¹ is deduced using $A = 0.00785$ cm², C_{dl} ($c_0 = 39.5$, $c_1 = 40.5$, $c_2 = 36.0$) $\mu\text{F cm}^{-2}$ and $R_u = 2650$ ohm in simulations to match the peak heights and peak splitting of AC harmonic components as shown in Figure 11. Whereas at BDD, $k^0 = 0.06$ cm s⁻¹ is found with $A = 0.00785$ cm², $k^0 = 0.06$ cm s⁻¹, C_{dl} ($c_0 = 7.0$, $c_1 = 8.5$, $c_2 = 8.0$) $\mu\text{F cm}^{-2}$ and $R_u = 2200$ ohm and comparison of theory and experiment is shown in Figure 12.

On the basis of the above data, k^0 values in DMSO as summarized in Table 3 are an order of magnitude lower than in MeCN. Electrode dependence is not seen, however, values measured are near the limit of detection. Use of high frequency is trivial to have any solid conclusion about the difference in electrode kinetics at metal electrodes as compared with carbon. But

high frequency can't be employed for macroelectrode studies in DMSO due to the problems discussed above.

Table 3. Parameters used^a in simulations undertaken to estimate the electrode kinetics for the reduction of 1.55 mM F₄TCNQ in DMSO (0.1 M Bu₄NPF₆).

Electrode	R_u	$C_{dl}(c_0, c_1, c_2)$	k^0	E^0 vs. Fc ^{0/+}	α
	(ohm)	($\mu\text{F cm}^{-2}$)	(cm s^{-1})	(V)	
Pt	2850	22.00, 40.00, 41.00	0.10	0.228	0.50
Au	1600	39.50, 40.50, 36.50	0.15	0.228	0.50
GC	2650	39.50, 40.50, 36.00	0.11	0.228	0.50
BDD	2200	6.00, 0.00, 0.00	0.06	0.228	0.50

^a $A_{\text{Au}} = 0.019 \text{ cm}^2$, $A_{\text{GC}} = A_{\text{BDD}} = A_{\text{Pt}} = 0.00785 \text{ cm}^2$, $f = 9.0 \text{ Hz}$, $\Delta E = 80 \text{ mV}$, $D = 2.64 \times 10^{-6} \text{ cm}^2 \text{ s}^{-1}$ and $T = 293 \text{ K}$

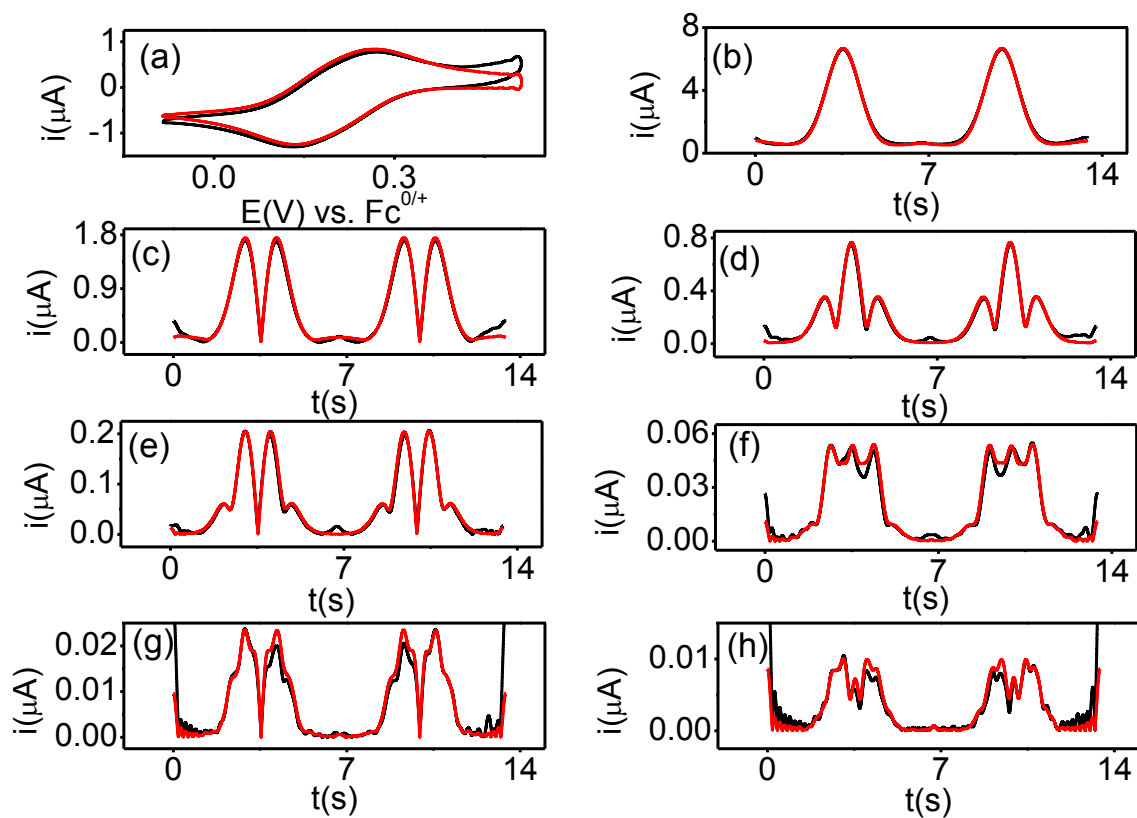


Figure 9: Comparison of experimental (—) and simulated (—) FT AC voltammograms for the reduction of 1.55 mM F_4TCNQ in DMSO (0.1 M Bu_4NPF_6) at a Pt macrodisk electrode (a) DC component (b-h) 1st to 7th harmonic; $v_{DC} = 0.0894 \text{ V s}^{-1}$ and other simulation parameters are described in Table 3

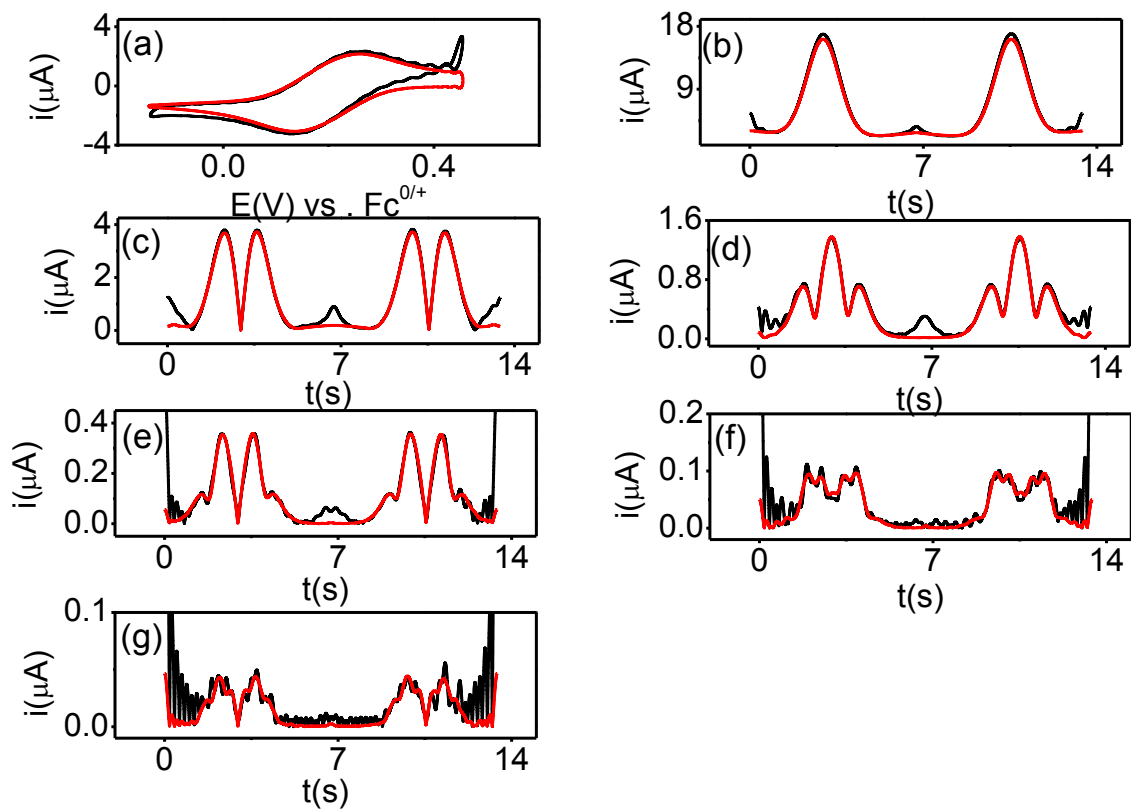


Figure 10: Comparison of experimental (—) and simulated (—) FT AC voltammograms for the reduction of 1.55 mM F_4TCNQ in DMSO (0.1 M Bu_4NPF_6) at Au macrodisk electrode (a) DC component (b-g) 1st to 6th harmonic; $\nu_{\text{DC}} = 0.0894 \text{ V s}^{-1}$ and other simulation parameters are described in Table 3

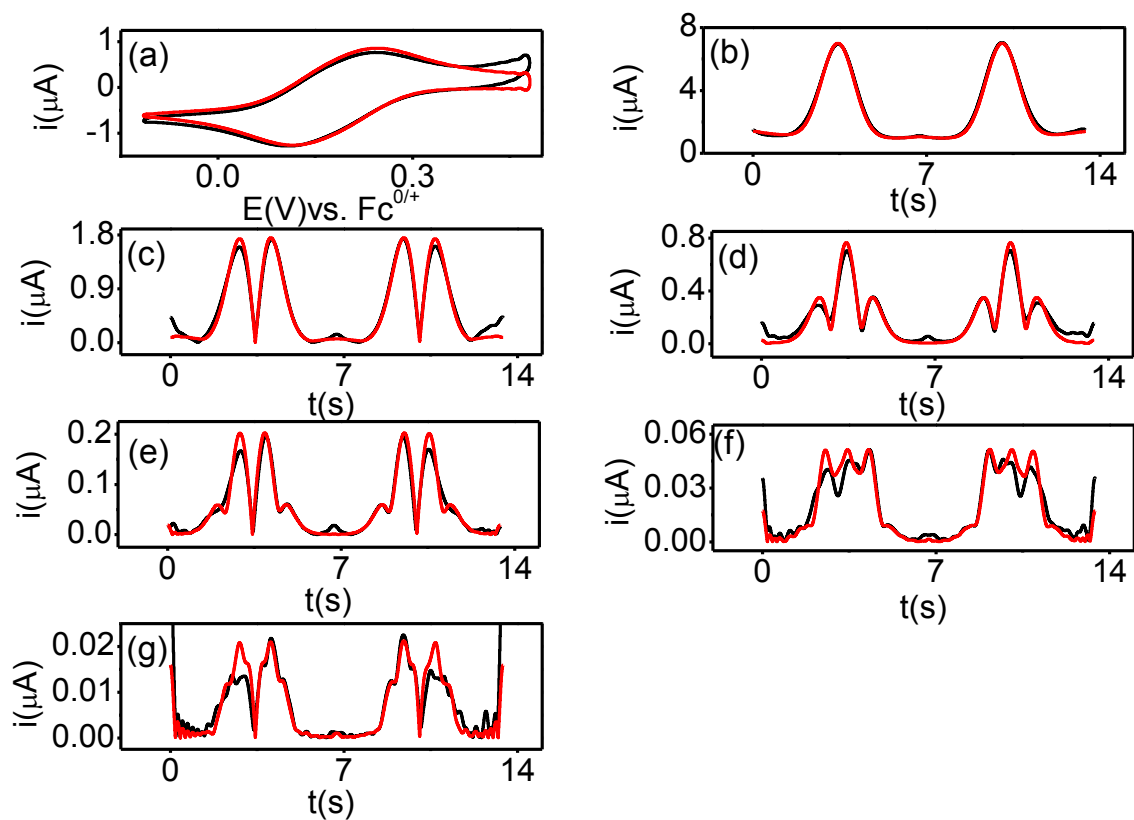


Figure 11: Comparison of experimental (—) and simulated (—) FT AC voltammograms for the reduction of 1.55 mM F_4TCNQ in DMSO (0.1 M Bu_4NPF_6) at a GC macrodisk electrode (a) DC component (b-g) 1st to 6th harmonic; $\nu_{\text{DC}} = 0.0894 \text{ V s}^{-1}$ and other simulation parameters are described in Table 3

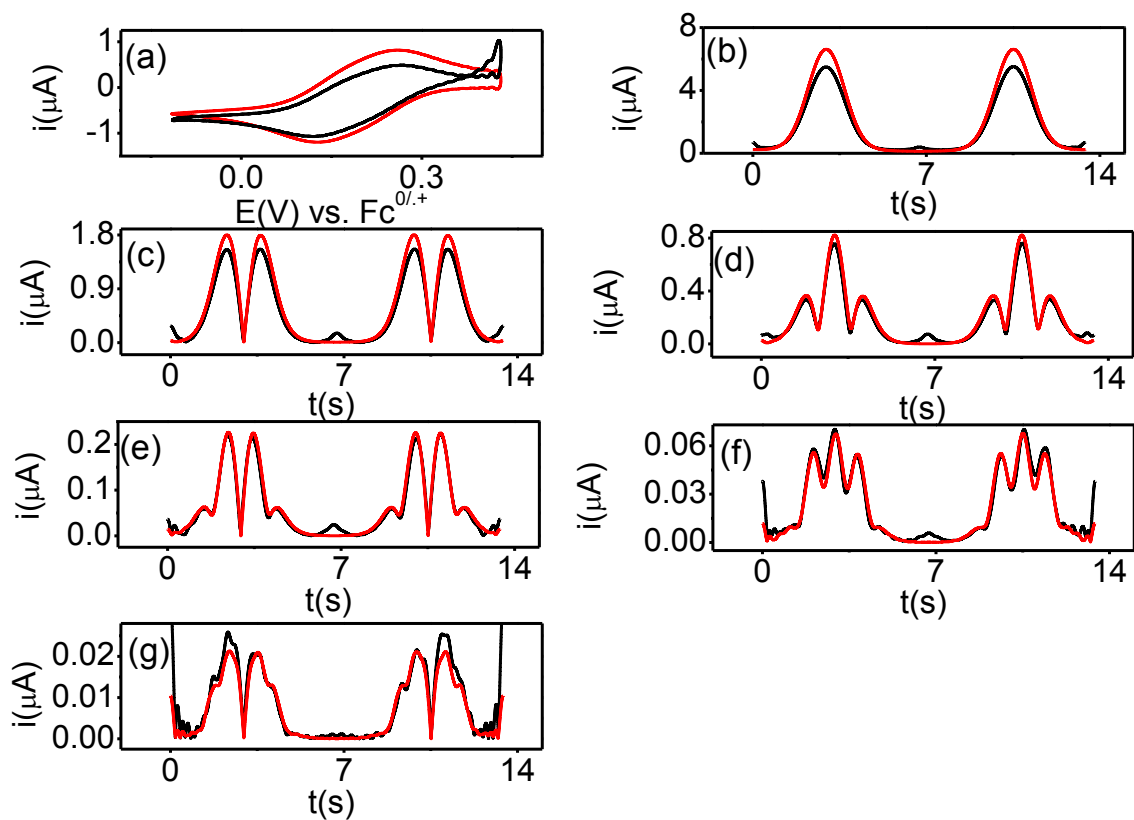


Figure 12: Comparison of experimental (—) and simulated (—) FT AC voltammograms for the reduction of 1.55 mM F_4TCNQ in DMSO (0.1 M Bu_4NPF_6) at a BDD macrodisk electrode (a) DC component (b-g) 1st to 6th harmonic; $\nu_{DC} = 0.08196 \text{ V s}^{-1}$ and other simulation parameters are described in Table 3

6.3.5. FTAC voltammetry of F₄TCNQ in ionic liquids: Qualitative comparison of macro and microelectrode FT AC voltammetric data

In preliminary investigations, large amplitude FT AC voltammetry was applied to the reduction of 7.2 mM F₄TCNQ solution in BMPYTFSI at a Pt macro (d = 1.0 mm) and microdisk (d = 125 μm) electrodes. The results obtained at macrodisk electrode with $f = 1.23$ kHz and $\Delta E = 80$ mV are given in Figure 13. Under these conditions, the DC component is well defined, but first harmonic contains a large contribution from capacitance current. The second to fourth AC harmonics also can be extracted, but still contain a contribution from the background, current and the k^0 value cannot be determined

At both the platinum (d = 125 μm) and carbon fiber microdisk (d = 33 μm) electrodes, iR_u is much smaller. Now seven harmonics can be obtained with a frequency of 1.83 kHz. At the smaller electrode (d = 33 μm), DC component is very small and difficult to measure, but the signal to noise ratio for the AC harmonic components is excellent. In order to quantify kinetics, frequencies of up to 1.23 kHz are used in this chapter with microelectrodes in ionic liquids. Transient voltammetric responses where planar diffusion is dominating mass transport are readily achieved in ionic liquids at moderate DC scan rate ($v_{DC} = 0.1$ V s⁻¹).

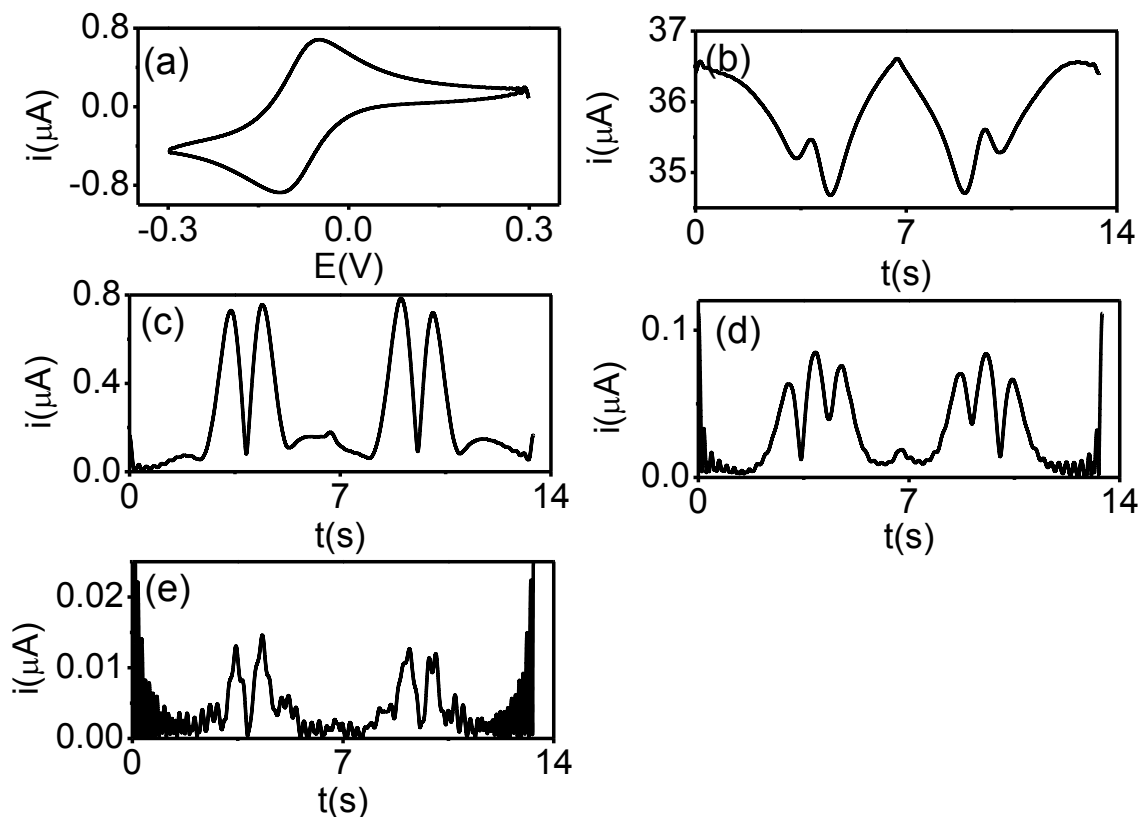


Figure 13: FT AC voltammetric data for the reduction of 7.24 mM F_4TCNQ in BMPYTFSI at Pt ($d = 1.0$ mm), (a) DC component (b-e) 1st – 4th harmonic, $f = 1.23$ kHz and $\Delta E = 80$ mV.

6.3.6. Quantitative voltammetric studies at microdisk electrodes in BMIMPF₆

AC voltammetric data obtained for the reduction of 7.0 mM F₄TCNQ in BMIM PF₆ at the platinum microdisk electrode was first examined qualitatively at 9.0 Hz, 1.23 kHz and 1.833 kHz. Eight harmonics can be obtained at 9.0 Hz and six at 1.23 kHz which is adequate for k^0 estimation but the number of harmonics available is further reduced when $f = 1.83$ kHz, so 1.23 kHz data is selected as being suitable to extract electrode kinetic parameters for reduction of F₄TCNQ in BMIMPF₆ ionic liquid at Pt electrode. $D = 0.7 \times 10^{-8} \text{ cm}^2 \text{ s}^{-1}$ estimated by DC voltammetry (section 6.3.1) and $C_{dl} = 8.0 \text{ } \mu\text{F cm}^{-2}$ obtained from fundamental harmonic were used in simulations with other parameters $A = 1.22 \times 10^{-4} \text{ cm}^2$, $R_u = 4300 \text{ ohm}$, $f = 1.23 \text{ kHz}$ and $\Delta E = 80 \text{ mV}$ and again α is assumed to be 0.50. In this case, simulation and experimental data (Figure 14) are in good agreement for $k^0 = 0.003 \text{ cm s}^{-1}$. Thus, a large decrease in the heterogeneous electron transfer rate constant is found for reduction of F₄TCNQ in BMIMPF₆ as compared to the data obtained in molecular solvents.

At the carbon fiber microelectrode, the electrochemical reduction of 7.0 mM F₄TCNQ in BMIMPF₆ is studied at $f = 9.0 \text{ Hz}$. Under these conditions only five harmonics are obtained which indicates that the electron transfer kinetics is slower at carbon electrode than at platinum and it is confirmed from experiments performed at 1.23 kHz and 1.83 kHz. Thus higher frequency is not required and as shown in section 6.3.1. k^0 values in iLs case can be determined up to 0.01 cm s^{-1} using 9.0 Hz frequency. To mimic the F₄TCNQ reduction at the carbon fiber electrode, simulations with $D = 0.7 \times 10^{-8} \text{ cm}^2 \text{ s}^{-1}$, $R_u = 35000 \text{ ohm}$ and $C_{dl} = 21 \mu\text{F cm}^{-2}$ are considered with $k^0 = 0.0016 \text{ cm s}^{-1}$. A comparison of experiment and theory is presented in Figure 15. Thus k^0 for the F₄TCNQ^{0/+•} process is a factor of 2 lower than found at Pt. Electron transfer coefficient α is considered 0.50 in each case indicating that F₄TCNQ^{0/+•} process is an outer-sphere electron transfer reaction.

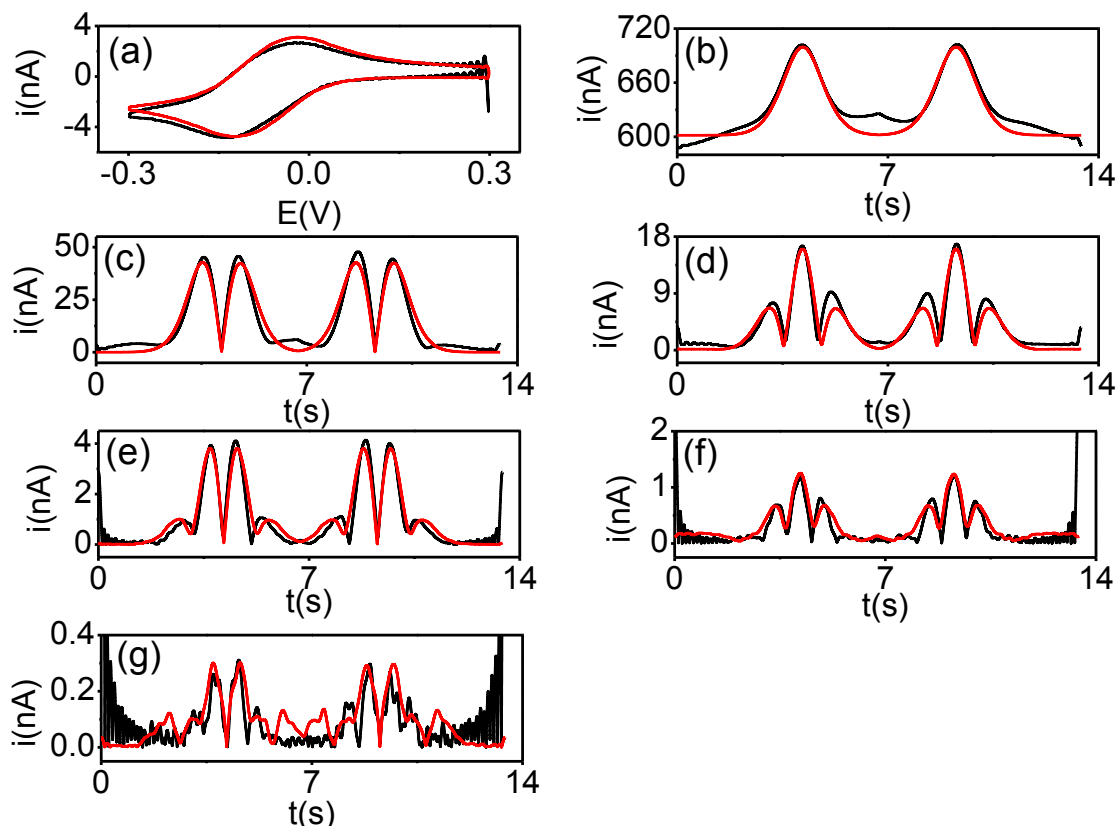


Figure 14: Comparison of experimental (—) and simulated (—) FT AC voltammograms for the reduction of 7.0 mM F_4TCNQ in $BMIMPF_6$ at a platinum microdisk electrode (a) DC component (b-g) 1st to 6th harmonics, simulation and experimental parameters include $A = 1.22 \times 10^{-4} \text{ cm}^2$, $f = 1.23 \text{ kHz}$, $\Delta E = 80 \text{ mV}$, $C_{dl} = 8.0 \text{ } \mu\text{F cm}^{-2}$, $D = 0.7 \times 10^{-8} \text{ cm}^2 \text{ s}^{-1}$, $v_{DC} = 0.0894 \text{ V s}^{-1}$, $E^0 = 0.258 \text{ V vs. Fc}^{0/+}$, $R_u = 4300 \text{ ohm}$, $k^0 = 0.003 \text{ cm s}^{-1}$, $\alpha = 0.50$ and $T = 293 \text{ K}$

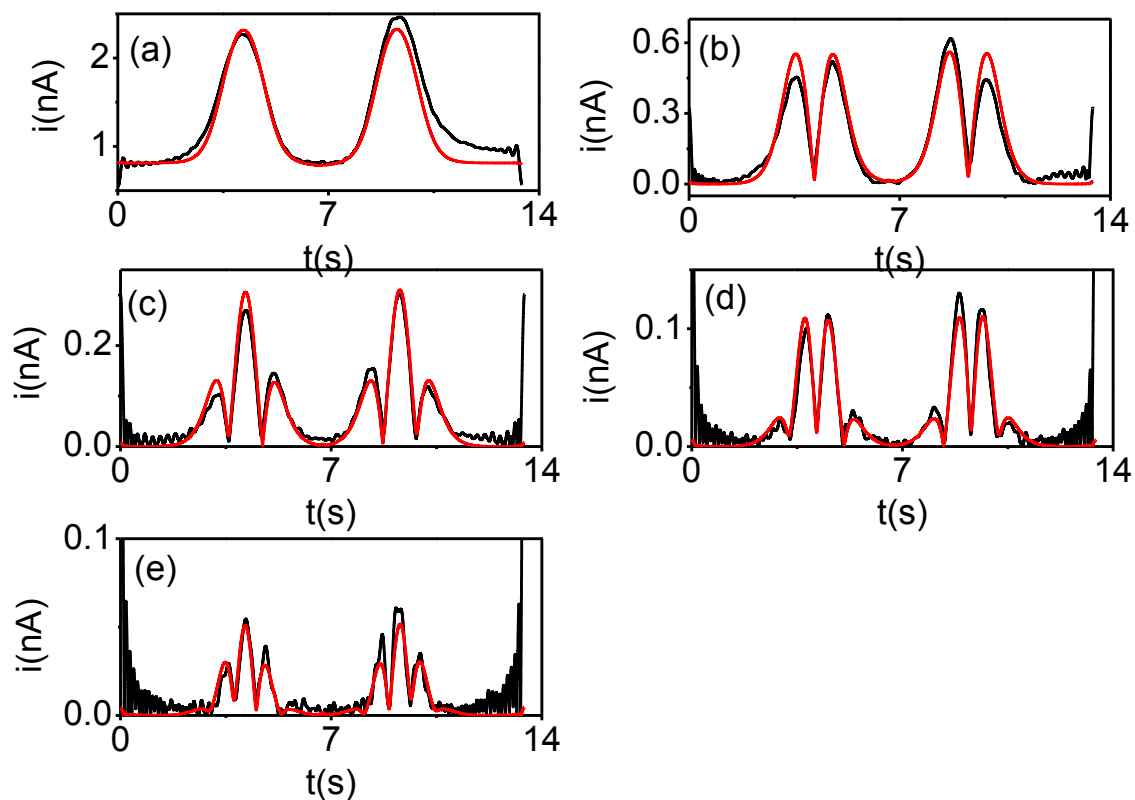


Figure 15: Comparison of experimental (—) and simulated (—) FT AC voltammograms for the reduction of 7.0 mM F_4TCNQ in $BMIMPF_6$ at a carbon fiber microdisk electrode (a-e) 1st to 5th harmonics, simulation and experimental parameters include $A = 8.54 \times 10^{-6} \text{ cm}^2$, $f = 1.23 \text{ kHz}$, $\Delta E = 80 \text{ mV}$, $C_{dl} = 22.0 \text{ } \mu\text{F cm}^{-2}$, $D = 0.7 \times 10^{-8} \text{ cm}^2 \text{ s}^{-1}$, $v_{DC} = 0.0894 \text{ V s}^{-1}$, $E^0 = 0.249 \text{ V vs. Fc}^{0/+}$, $R_u = 35000 \text{ ohm}$, $k^0 = 0.0017 \text{ cm s}^{-1}$, $\alpha = 0.50$ and $T = 293 \text{ K}$

6.3.7. Quantitative FT AC voltammetric studies in BMPIPTFSI

In ionic liquid BMPIPTFSI ($\eta = 183$ cP), FT AC voltammetric data are again obtained at the platinum and carbon fiber microdisk electrodes. At platinum, AC frequency up to 1.23 kHz is used, while in case of the carbon electrode, the AC frequency is restricted to 9.0 Hz where five harmonics can be obtained.

In the case of platinum microdisk electrode, five harmonics are obtained at 1.23 kHz for the reduction of 4.9 mM F_4TCNQ in BMPIPTFSI. Experimental data are then simulated by applying the theory of linear diffusion as described above. Use of the following parameter C_{dl} ($c_0 = 8.0$, $c_1 = 1.0$, $c_2 = 1.0$) $\mu F\ cm^{-2}$, $A = 1.22 \times 10^{-4}\ cm^2$, $k^0 = 0.0037\ cm\ s^{-1}$, $\alpha = 0.50$, $D = 1.04 \times 10^{-8}\ cm^2\ s^{-1}$, $f = 1.23\ kHz$, $\Delta E = 80\ mV$ and $R_u = 5000\ ohm$ provides a good agreement with experiment (Figure 16). The k^0 value of $0.0037\ cm\ s^{-1}$ is close to that of $0.003\ cm\ s^{-1}$ obtained for $F_4TCNQ^{0/+}$ process in BMIMPF₆.

In case of carbon fiber microdisk electrode, FT AC voltammetric data obtained at 9.0 Hz agrees well with simulations undertaken with $A = 8.54 \times 10^{-6}\ cm^2$, $C_{dl} = 19.0\ \mu F\ cm^{-2}$, $R = 45000\ ohm$, $D = 1.04 \times 10^{-8}\ cm^2\ s^{-1}$, $f = 9.0\ Hz$ and $\Delta E = 80\ mV$ along with $k^0 = 0.00072\ cm\ s^{-1}$ and $\alpha = 0.50$, which is slower than that of $0.0016\ cm\ s^{-1}$ obtained in BMIMPF₆ when using this electrode. Comparison of theory and experiment for the FT AC voltammetric data at carbon fiber is given in Figure 17.

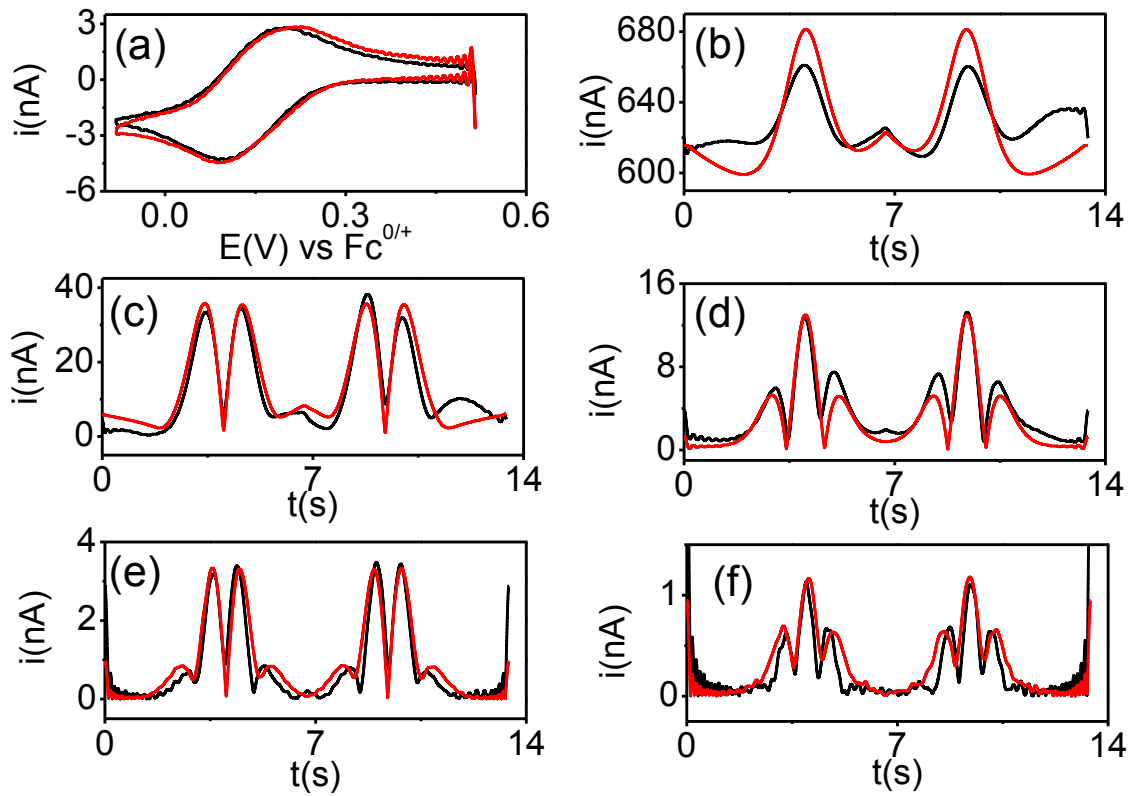


Figure 16: Comparison of experimental (—) and simulated (—) FT AC voltammograms for the reduction of 7.0 mM F_4TCNQ in BMPIPTFSI at a platinum microdisk electrode (a) DC component (b-f) 1st to 5th harmonics,, simulation and experimental parameters include $A = 1.22 \times 10^{-4} \text{ cm}^2$, $f = 1.23 \text{ kHz}$, $\Delta E = 80 \text{ mV}$, $C_{dl} (c_0 = 8.0, c_1 = 1.0, c_2 = 1.0) \mu\text{F cm}^{-2}$, $D = 1.04 \times 10^{-8} \text{ cm}^2 \text{ s}^{-1}$, $v_{DC} = 0.0894 \text{ V s}^{-1}$, $E^0 = 0.2035 \text{ V vs. Fc}^{0/+}$, $R_u = 5000 \text{ ohm}$ $k^0 = 0.0037 \text{ cm s}^{-1}$, $\alpha = 0.50$ and $T = 293 \text{ K}$

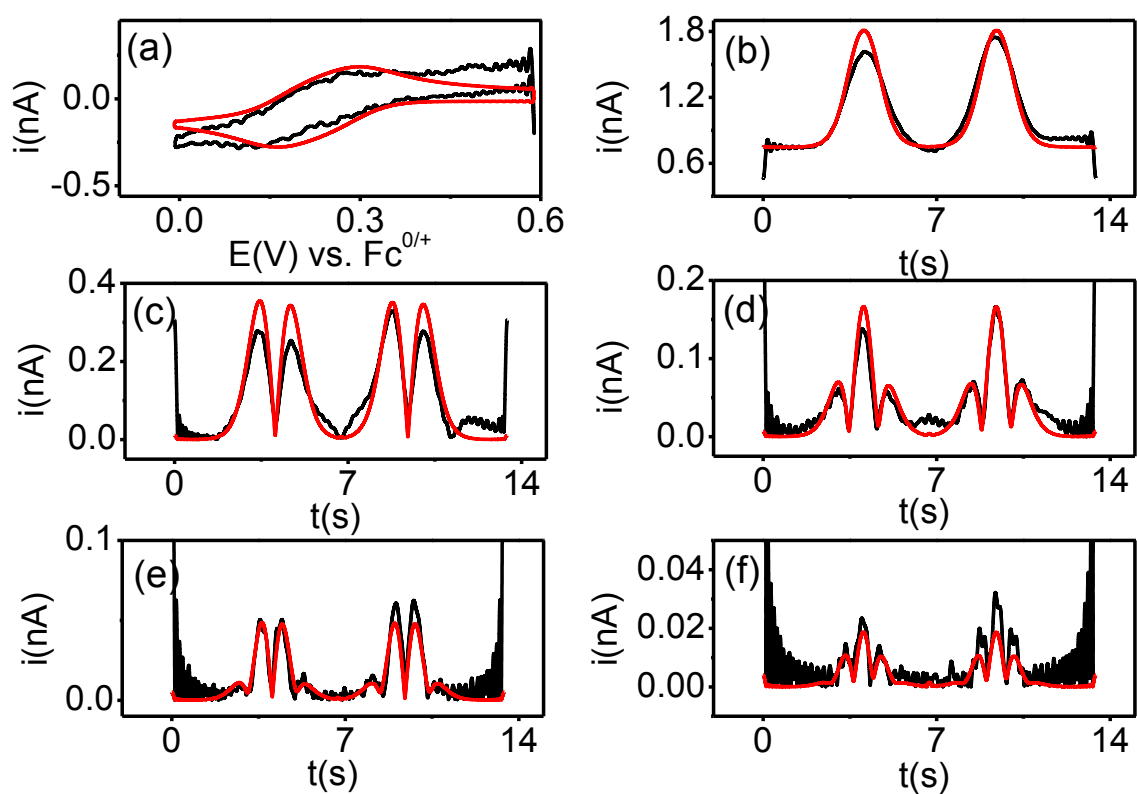


Figure 17: Comparison of experimental (—) and simulated (—) FT AC voltammograms for the reduction of 7.0 mM F_4TCNQ in BMPIPTFSI at a carbon fiber microdisk electrode (a) DC component (b-g) 1st to 5th harmonics, simulation and experimental parameters include $A = 8.54 \times 10^{-6} \text{ cm}^2$, $f = 1.23 \text{ kHz}$, $\Delta E = 80 \text{ mV}$, $C_{\text{dl}} = 19.0 \text{ } \mu\text{F cm}^{-2}$, $D = 1.04 \times 10^{-8} \text{ cm}^2 \text{ s}^{-1}$, $v_{\text{DC}} = 0.0894 \text{ V s}^{-1}$, $E^0 = 0.2035 \text{ V vs. Fc}^{0/+}$, $R_u = 45000 \text{ ohm}$ $k^0 = 0.00072 \text{ cm s}^{-1}$, $\alpha = 0.50$ and $T = 293 \text{ K}$

6.3.8. AC voltammetry of F₄TCNQ in BMPYTFSI

BMPYTFSI is a lower viscosity ($\eta = 77$ cP) and more conducting ionic liquid than BMIMPF₆ or BMPIPTFSI. Reduction of 7.2 mM F₄TCNQ in this iL with $f = 1.23$ kHz enables 6-7 harmonics to be obtained at both carbon and platinum electrodes, which is ideal for quantitative electrode kinetics.

Simulation of the FT AC voltammetric data for the reduction of 7.24 mM F₄TCNQ at PT were undertaken by using $D = 3.9 \times 10^{-8}$ cm² s⁻¹. Comparison of experimental and simulated data is provided in Figure 18 using $A = 1.22 \times 10^{-4}$ cm², $k^0 = 0.016$ cm s⁻¹, $C_{dl}(c_0 = 10.6, c_1 = 4.5, c_2 = 4.1)$ μ F cm⁻² and $R_u = 8000$ ohm in simulations.

FT AC voltammogram obtained for the reduction of 7.24 mM F₄TCNQ at the carbon fiber electrode agree well with the simulation results shown in Figure 19 with $A = 8.54 \times 10^{-6}$ cm², $k^0 = 0.018$ cm s⁻¹, $C_{dl}(c_0 = 8.2, c_1 = 1.0, c_2 = 0.2)$ μ F cm⁻², $R = 45000$ ohm, $D = 3.9 \times 10^{-8}$ cm², $f = 1.23$ kHz and $\Delta E = 80$ mV. In contrast to the situation that prevails in BMIMPF₆ and BMPiPTFSI, k^0 values obtained in BMPyTFSI are similar at both carbon and platinum electrodes. However, the values 0.016 cm s⁻¹ and 0.018 cm s⁻¹ are close to the upper limit and so the differences are difficult to be observed under the given experimental conditions.

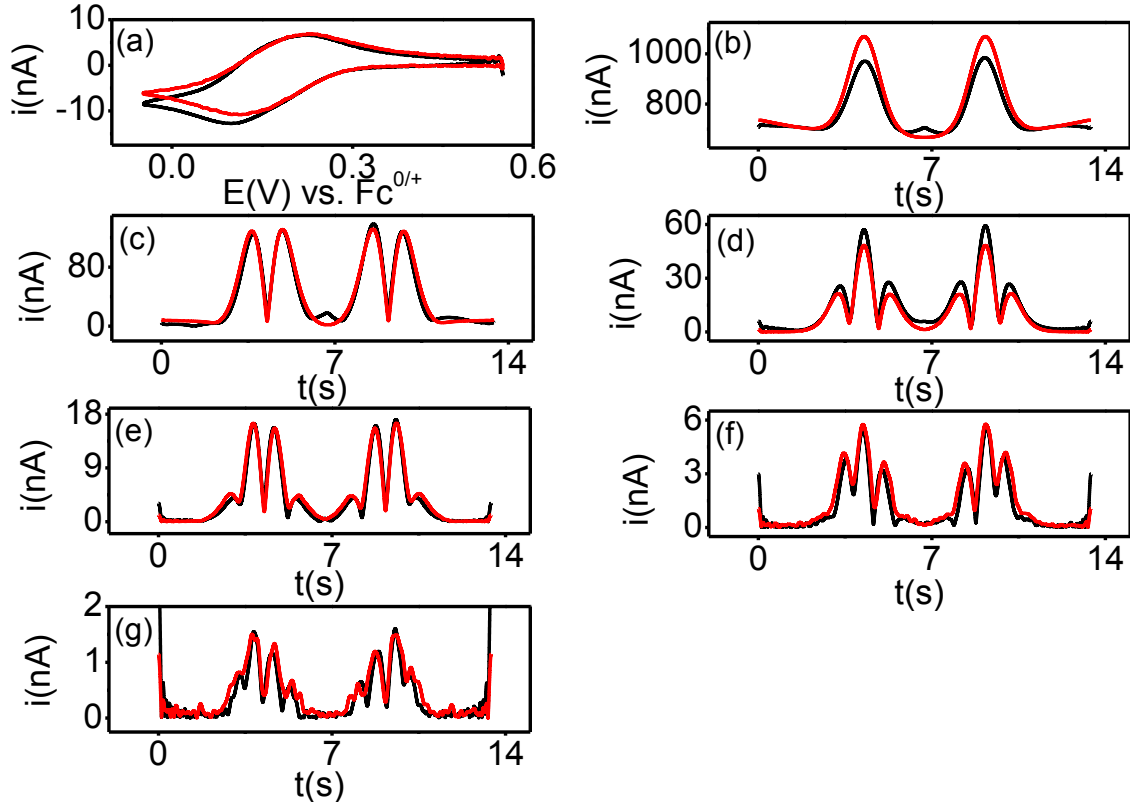


Figure 18: Comparison of experimental (—) and simulated (—) FT AC voltammograms for the reduction of 7.24 mM F_4TCNQ in BMPYTFSI at a platinum microdisk electrode (a) DC component (b-g) 1st to 6th harmonics, simulation and experimental parameters include $A = 8.54 \times 10^{-6} \text{ cm}^2$, $f = 1.23 \text{ kHz}$, $\Delta E = 80 \text{ mV}$, $C_{dl} (c_0 = 10.0, c_1 = 4.51, c_2 = 4.1) \mu\text{F cm}^{-2}$, $D = 3.9 \times 10^{-8} \text{ cm}^2 \text{ s}^{-1}$, $v_{DC} = 0.0894 \text{ V s}^{-1}$, $R_u = 8000 \text{ ohm}$, $k^0 = 0.018 \text{ cm s}^{-1}$, $E^0 = 0.153 \text{ V vs. Fc}^{0/+}$, $\alpha = 0.50$ and $T = 293 \text{ K}$

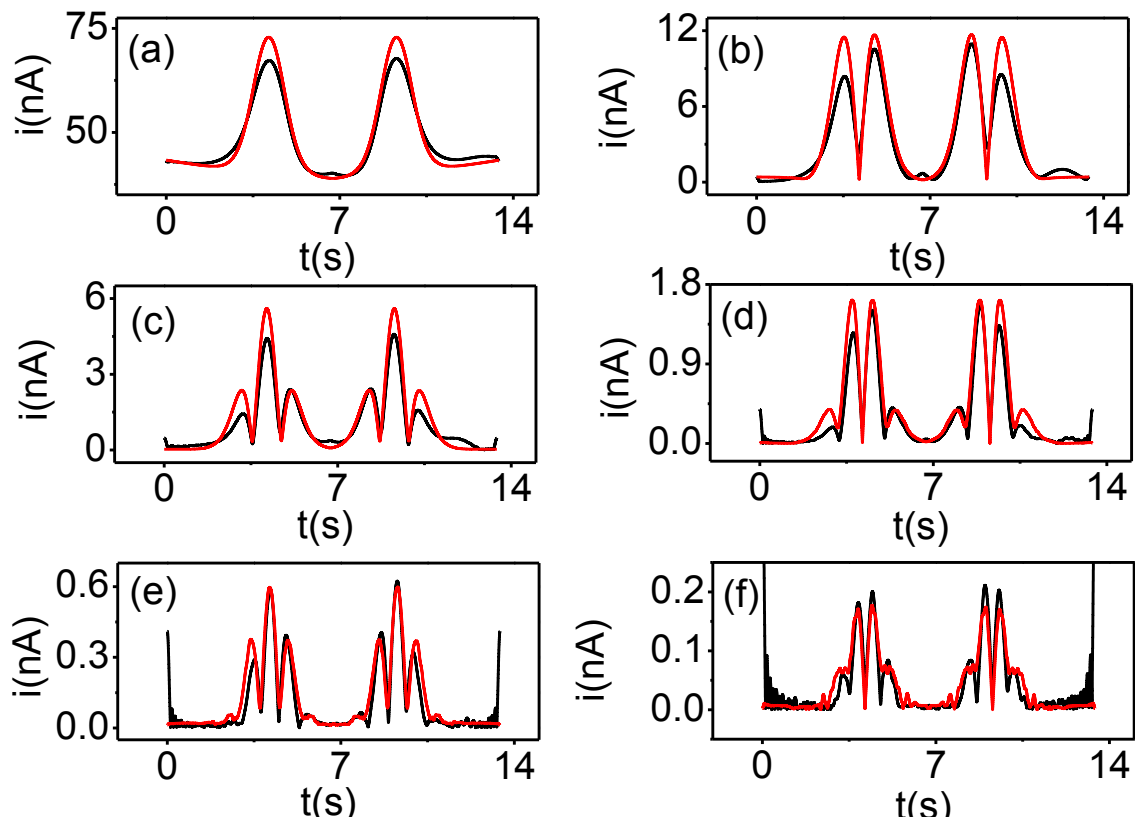


Figure 19: Comparison of experimental (—) and simulated (—) FT AC voltammograms for the reduction of 7.24 mM F_4TCNQ in BMPYTFSI at a carbon fiber microdisk electrode (a-f) 1st to 6th harmonics, simulation and experimental parameters include $A = 8.54 \times 10^{-6} \text{ cm}^2$, $f = 1.23 \text{ kHz}$, $\Delta E = 80 \text{ mV}$, C_{dl} ($c_0 = 8.2$, $c_1 = 1.0$, $c_2 = 0.20$) $\mu\text{F cm}^{-2}$, $D = 3.9 \times 10^{-8} \text{ cm}^2 \text{ s}^{-1}$, $v_{DC} = 0.0894 \text{ V s}^{-1}$, $E^0 = 0.1534 \text{ V vs. Fc}^{0/+}$, $R_u = 45000 \text{ ohm}$, $k^0 = 0.018 \text{ cm s}^{-1}$, $\alpha = 0.50$ and $T = 293 \text{ K}$

6.4. Discussion

Electron transfer kinetics of F_4TCNQ in molecular solvents is found close to the reversible limit and independent of the electrode material. However, the variation with the viscosity of the solvent can be observed from acetonitrile to $BMIMPF_6$ as summarized in Table 4. Slowest electron transfer rate constant was observed in $BMIMPF_6$, as its viscosity is highest of all solvents studied in this chapter. Slow kinetics obtained in $BMPIPTFSI$ can also be ascribed to the much higher viscosity of this iL as compared to acetonitrile. However, electron transfer kinetics in $BMPIPTFSI$ is also similar like the value obtained in $BMIMPF_6$, although they differ in viscosity. This suggests that some other factors rather than simple electrostatic interactions and viscosities of ionic liquids can operate to activate / deactivate the electron transfer processes⁴² in ionic liquids. Moreover, the stronger π - π interactions or H-bonding are possible with imidazolium cation and planar radical anion in addition to electrostatic ion pairing^{36,43,44}. Thus, the electron transfer kinetics in $BMPYTFSI$ lie near the reversible limit as is the case in MeCN (Bu_4NPF_6). Even though, piperidinium cation is also similar to the pyrrolidinium one, even slower kinetics were found in $BMPIPTFSI$ which may be attributed to modified solvent relaxation dynamics in the form of higher solvent reorganization or slower double-layer interface relaxation,³⁶ both of which can result in apparently slower heterogeneous kinetics in $BMPIPTFSI$. The rate of electron transfer in two solvents can be significantly different and slow electron transfer rate constant can be observed due to slow relaxation of the environment.²²⁻²⁴

Electrode kinetic of $F_4TCNQ^{0/\bullet-}$ redox process in $BMIMPF_6$ is observed to be electrode dependent as measured k^0 value at Pt is twice as high as observed on carbon fiber. This indicates that the electronic factor of the electrode is operating and causing the redox process of the electrode to become the electrode dependent. In this case, kinetics values obtained here can be considered real and measurable within the experimental uncertainties.⁴²

Moreover, structure of double layer is very complex in ionic liquids and there is no adequate model for electrode interface in these solvents that should allow the application of any double layer correction like in conventional solvents (Frumkin correction).¹² Our measured values are not corrected for double layer so need to be very careful, when the electron transfer rate constant at the electrode surface is measured in ionic liquids.

6.5. Conclusion

Large amplitude AC voltammetry at high frequency can be used to probe the fast electron transfer kinetics at microdisk electrodes. Electron transfer kinetics of $F_4TCNQ^{0/+}$ process in molecular solvents is near the reversible limit; however, use of microdisk electrodes in ionic liquids allows k^0 values to be estimated with more certainty for this process in ionic liquids.

Table 4: Summary of electrode kinetics parameters determined for $F_4TCNQ^{0/\bullet-}$ process in molecular solvents and ionic liquids

Solvents	Simulation parameters for F ₄ TCNQ ^{0/+−} process							
	Pt (d = 125 μm)				Carbon fiber (d = 33 μm)			
	<i>f</i> (kHz)	<i>R_u</i> (ohm)		<i>k</i> ⁰ (cm s ^{−1})	<i>f</i> (kHz)	<i>R_u</i> (ohm)		<i>k</i> ⁰ (cm s ^{−1})
BMIMPF₆ (<i>η</i> =371 cP)	1.23	4300		0.003	0.009	35000		0.0017
BMPIPTFSI (<i>η</i> =183 cP)	1.23	5000		0.0037	0.009	45000		0.00072
BMPYTFSI (<i>η</i> =71 cP)	1.23	8000		0.016	1.23	45000		0.018
	GC (<i>d</i> = 1.0 mm)		Pt (<i>d</i> = 1.0 mm)		BDD (<i>d</i> = 1.0 mm)		Au (<i>d</i> = 2.0 mm)	
	<i>R_u</i> (ohm)	<i>k</i> ⁰ (cm s ^{−1})	<i>R_u</i> (ohm)	<i>k</i> ⁰ (cm s ^{−1})	<i>R_u</i> (ohm)	<i>k</i> ⁰ (cm s ^{−1})	<i>R_u</i> (ohm)	<i>k</i> ⁰ (cm s ^{−1})
DMSO <i>η</i> =1.98 cP) (<i>f</i> =9.0 Hz)\	2650	0.07	2850	0.1	2200	0.06	1600	0.15
ACN (<i>η</i> =0.35 cP) (<i>f</i> =528 Hz)	590	0.9	525	1.0	546	1.0	360	0.6

References

- (1) Alden, J. A.; Hakoura, S.; Compton, R. G. *Anal. Chem.* **1999**, 71, 806.
- (2) Amatore, C.; Deakin, M. R.; Wightman, R. M. *J. Electroanal. Chem.* **1987**, 225, 49.
- (3) Bohinc, K.; Kralj-Iglič, V.; Iglič, A. *Electrochim. Acta* **2001**, 46, 3033.
- (4) Bond, A. M. *Broadening electrochemical horizons: principles and illustration of voltammetric and other techniques*; Oxford University press, **2002**.
- (5) Gewirth, A. A.; Niece, B. K. *Chem. Rev.* **1997**, 97, 1129.
- (6) Hallam, P. M.; Banks, C. E. *Electrochem. Commun.* **2011**, 13, 8.
- (7) Nicholson, R. S.; Shain, I. *Anal. Chem.* **1964**, 36, 706.
- (8) Rosvall, M. *Electrochem. Commun.* **2000**, 2, 791.
- (9) Wang, Y.; Velmurugan, J.; Mirkin, M. V. *Isr. J. Chem.* **2010**, 50, 291.
- (10) Wu, Y. H.; Hu, S. S. *Indian J. Chem. A* **2005**, 44, 891.
- (11) Zoski, C. G. *Handbook of electrochemistry*, **2007**.
- (12) Bard, A. J.; Faulkner, L. R. *Electrochemical methods: Fundamentals and Applications*; John Wiley: New York, **2001**.
- (13) Nicholson, R. S. *Anal. Chem.* **1965**, 37, 1351.
- (14) Nicholson, R. S.; Shain, I. *Anal. Chem.* **1964**, 36, 1212.
- (15) Rees, N. V.; Compton, R. G. *Russ. J. Electrochem.* **2008**, 44, 368.
- (16) Sun, P.; Mirkin, M. V. *Anal. Chem.* **2006**, 78, 6526.
- (17) Vijaikanth, V.; Li, G. C.; Swaddle, T. W. *Inorg. Chem.* **2013**, 52, 2757.

- (18) Wightman, R. M.; Wipf, D. O. In *Electroanalytical Chemistry*; Bard, A. J., Ed.; Marcel Dekker: New York, **1989**; Vol. 15, p 267.
- (19) Bano, K.; Kennedy, G. F.; Zhang, J.; Bond, A. M. *Phys. Chem. Chem. Phys.* **2012**, *14*, 4742.
- (20) Bano, K.; Nafady, A.; Zhang, J.; Bond, A. M.; Haque, I. U. *J. Phys. Chem. C* **2011**, *115*, 24153.
- (21) Bond, A. M.; Bano, K.; Adeel, S.; Martin, L. L.; Zhang, J. *ChemElectrochem.* **2013**, DOI: 10.1002/CELC.201300129.
- (22) Wipf, D. O.; Kristensen, E. W.; Deakin, R. M.; Wightman, R. M. *Anal. Chem.* **1988**, *60*, 306.
- (23) Andrieuz, C. P.; Garreau, D.; Hapiot, P.; Saveant, J.-M. *J. Electroanal. Chem.* **1988**, *248*, 447.
- (24) Andrieuz, C. P.; Garreau, D.; Hapiot, P.; Saveant, J.-M. *Chem. Rev.* **1990**, *90*, 723.
- (25) Forster, R. J.; Keyes, T. K. In *Handbook of electrochemistry*; Zoski, C. G., Ed.; Elsevier: **2006**.
- (26) Bowyer, W. J.; Engelman, E. E.; Evans, D. H. *J. Electroanal. Chem.* **1989**, *262*, 67.
- (27) Wightman, R. M.; Cockrell, J. R.; Murray, R. W.; Burnett, J. N.; Jones, S. B., *J. Am. Chem. Soc.* **1976**, *98*, 2562.
- (28) Oldham, K. B.; Zoski, C. G. *J. Electroanal. Chem.* **1988**, *11*, 256.
- (29) Aoki, K.; Tokuda, K.; Matsuda, H. *J. Electroanal. Chem.* **1985**, *195*, 229.
- (30) Bidwell, M. J.; Alden, J. A.; Compton, R. G. *J. Electroanal. Chem.* **1996**, *417*, 119.

- (31) Booth, J.; Compton, R. G.; Cooper, J. A.; Dryfe, R. A. W.; Fisher, A. C.; Davies, C. L.; Walters, M. K. *J. Phys. Chem.* **1995**, *99*, 10942.
- (32) Compton, R. G.; Unwin, P. R. *J. Electroanal. Chem.* **1986**, *205*, 1.
- (33) Compton, R. G.; Unwin, P. R. *J. Electroanal. Chem.* **1988**, *245*, 303.
- (34) Tokuda, K.; Aoki, K.; Matsuda, H. *J. Electroanal. Chem.* **1977**, *80*, 211.
- (35) Paddon, C. A.; Silvester, D. S.; Bhatti, F. L.; Donohoe, T. J.; Compton, R. G. *Electroanal.* **2007**, *19*, 11.
- (36) Hapiot, P.; Lagrost, C. *Chem. Rev.* **2008**, *108*, 2238.
- (37) Sher, A. A.; Bond, A. M.; Gavaghan, D. J.; Harriman, K.; Feldberg, S. W.; Duffy, N. W.; Guo, S. X.; Zhang, J. *Anal. Chem.* **2004**, *76*, 6214.
- (38) Feldberg, S. W. *J. Electroanal. Chem.* **1981**, *127*.
- (39) Feldberg, S. W.; Goldstein, C. I.; M. J. Rudolph, *J. Electroanal. Chem.* **1996**, *413*, 25.
- (40) Nagy, L.; Gyetvai, G.; Kollár, L.; Nagy, G. *J. Biochem. Biophys. Methods* **2006**, *69*, 121.
- (41) Tsierkezos, N. *J. Soln. Chem.* **2007**, *36*, 289.
- (42) Marcus, R. A. *J. Chem. Phys.* **1956**, *24*, 966.
- (43) Brooks, C. A.; Doherty, A. P. *J. Phys. Chem. B* **2005**, *109*, 6276.
- (44) Lagrost, C.; Preda, L.; Volanschi, E.; Hapiot, P. *J. Electroanal. Chem.* **2005**, *585*, 1.

CHAPTER 7

**ELECTRODE KINETICS STUDIES AT MICROELECTRODES UNDER
RADIAL DIFFUSION: HIGH FREQUENCY FT AC VOLTAMMETRY**

Monash University

Declaration for Thesis Chapter [7]

Declaration by candidate

In the case of Chapter [7], the nature and extent of my contribution to the work was the following:

Nature of contribution	Extent of contribution (%)
Initiation, key ideas, experimental work, writing up	80 %

The following co-authors contributed to the work. If co-authors are students at Monash University, the extent of their contribution in percentage terms must be stated:

Name	Nature of contribution	
Jie Zhang	Initiation, key ideas, writing up	
Alan M. Bond	Initiation, key ideas, writing up	

The undersigned hereby certify that the above declaration correctly reflects the nature and extent of the candidate's and co-authors' contributions to this work*.

Candidate's Signature  Date 28/11/2013

Name	
Jie Zhang	
Alan M. Bond	

Main Supervisor's Signature  Date 29/11/2013


*Note: Where the responsible author is not the candidate's main supervisor, the main supervisor should consult with the responsible author to agree on the respective contributions of the authors.

CHAPTER 7

ELECTRODE KINETIC MEASUREMENTS USING LARGE AMPLITUDE FOURIER TRANSFORMED AC VOLTAMMETRY AT MICROELECTRODES IN CONVENTIONAL SOLVENTS

Kiran Bano, Jie Zhang* and Alan M. Bond*

School of Chemistry, Monash University, Clayton, Victoria 3800, Australia

Corresponding Authors: 

Abstract

This chapter describes the applications of large amplitude FT AC voltammetry at microdisk electrodes under radial diffusion for kinetics measurement of $\text{TTF}^{0/+}$ process. Electrode kinetics values are estimated from the comparison of experiment and theory for the $\text{TTF}^{0/+}$ redox couple. Pros and cons of using very high frequency are discussed in detail for the extraction of kinetic and thermodynamic parameters under the experimental conditions employed. Simulation results at microelectrodes give electrode kinetics values for $\text{TTF}^{0/+}$ process as 2.5 cm s^{-1} , while $\text{TTF}^{+/2+}$ process is found to be slower ($k^0 = 0.4 \text{ cm s}^{-1}$) as determined previously.

7.1. Introduction

In DC Voltammetry, use of microelectrode is advantageous providing access to faster kinetics with less problems from iR_u drop and background current. However, AC voltammetry¹⁻⁴ has provided access to the measurement of the fast electron transfer kinetics even at macrodisk electrodes.^{5,6} Using large amplitude FT AC voltammetry electron transfer kinetics (up to 1.0 cm s^{-1}) can be determined if uncompensated resistance is accurately known. Likewise, for microdisk electrodes a higher AC frequency has further demonstrated the benefits of using FT AC voltammetry for electron transfer kinetics measurements in ionic liquids. However, in all these measurements linear diffusion was maintained.

In the current chapter, use of microelectrodes with FT AC voltammetric method is extended in conventional solvents to a large amplitude AC voltammetric study of TTF. Previously it has been established that for $\text{TTF}^{0/+}$ redox couple electron transfer rate constant ($k^0 \geq 1.0 \text{ cm s}^{-1}$) and so the value can not be precisely determined, whereas, kinetics of $\text{TTF}^{+/2+}$ redox couple are sufficiently slow and can be determined precisely ($k^0 = 0.35 \pm 0.05 \text{ cm s}^{-1}$). For a very fast process like the $\text{TTF}^{0/+}$ ones use of a microelectrode at high frequency provides enhanced kinetic sensitivity, so the electron transfer kinetics measurement is attempted under radial diffusion in this chapter.

7.2. Experimental

7.2.1. Chemicals.

Tetrathiafulvalene (TTF) 99% (Aldrich), ferrocene (Fc) $\geq 98 \%$ (Aldrich), *n*-tetrabutylammonium hexafluorophosphate (Bu_4NPF_6) 98%, (Wako) was recrystallised twice from ethanol and distilled acetonitrile (MeCN) 99.9%, (Sigma-Aldrich), dried and stored under nitrogen in a dry box.

7.2.2. Instrumentation and apparatus.

For DC voltammetric studies Bioanalytical Systems (BAS) model 100B electrochemical workstation and BASi Epsilon electrochemical workstation were used. Large amplitude FT AC voltammetric experiments were undertaken with home built instrumentation described elsewhere.⁸

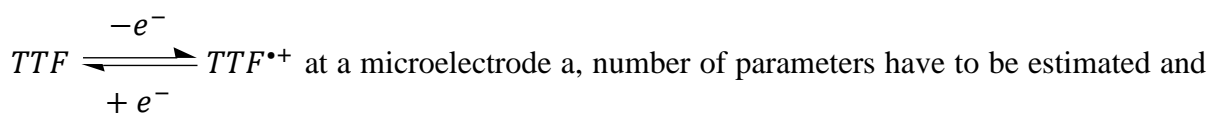
A conventional three electrode cell configuration was used for voltammetric experiments. The working electrode was a 12.0 μm diameter platinum (Pt) microdisk and 12 μm diameter carbon fiber electrode, the radii of the carbon fiber and platinum microdisk electrodes were calibrated using $\text{Fc}^{0/+}$ redox process in acetonitrile (0.1 M Bu_4NPF_6). A Pt wire in a glass capillary was used as a quasi-reference electrode and a Pt wire was used as the auxiliary electrode. Potentials derived from the Pt quasi reference electrode were calibrated against the Fc/Fc^+ external reference potential scale. Working electrodes were polished on 0.3 μm alumina followed by polishing on 0.05 μm alumina slurry on a polishing cloth (BAS), sonicated in deionised water, rinsed with water and acetone and then dried with nitrogen. All voltammetric experiments were undertaken under nitrogen at room temperature of 20 ± 2 °C.

Bulk electrolysis experiments were used to generate the one-electron oxidized specie TTF^{*+} by the method described elsewhere.⁹ Diffusion coefficients of TTF, TTF^{*+} and TTF^{2+} were used as described elsewhere.⁹ Uncompensated resistance was estimated in a potential region where no Faradaic current is present using the RC time constant method¹⁰ available with the BAS 100 instrument.

7.3. Results

7.3.1. Simulation Results

In order to extract kinetics information from AC voltammetric data for the



a theoretical model needs to be described. The total current data obtained with large amplitude FT AC voltammetry ($f = 1.23$ kHz and $\Delta E = 80$ mV) as a function of time was converted to the frequency domain using the FT algorithm. The power spectrum obtained in this way consisting of the DC aperiodic component and AC harmonic components for the $TTF^{0/+}$ redox couple is shown in Figure 1. The frequency domain data was then converted back to time domain data by a series of steps including Fourier transformation, band selection from the power spectrum and inverse Fourier transform. Theoretical analysis of experimental data was carried using radial diffusion at a microelectrode and Butler-Volmer theory¹⁰ was used for the estimation of electron transfer kinetics parameter. Simulations based on radial diffusion were carried out using DigiElch software package¹¹ for the total current versus time data obtained by large amplitude FT AC voltammetry. The same FT-inverse FT protocol as in experimental studies was then used to obtain the simulated DC component and AC harmonics. In the first instance it is assumed that the concentration (C), electrode area (A), uncompensated resistance (R_u), AC frequency (f), amplitude (ΔE), DC scan rate (v_{DC}) and temperature (T) are known or can be determined from an independent experiment. Parameters that need to be determined from comparison of experimental data and simulation include reversible potential (E^0), heterogeneous electron transfer rate constant (k^0), charge transfer coefficient (α), diffusion coefficients (D) and double layer capacitance (C_{dl}). A heuristic method of data analysis was used for evaluating the rate constants from theory-experiment comparisons. Charge transfer rate constants were extracted from the

kinetically more sensitive higher harmonics. Simulation parameters were varied until a satisfactory agreement with experimental data is achieved.

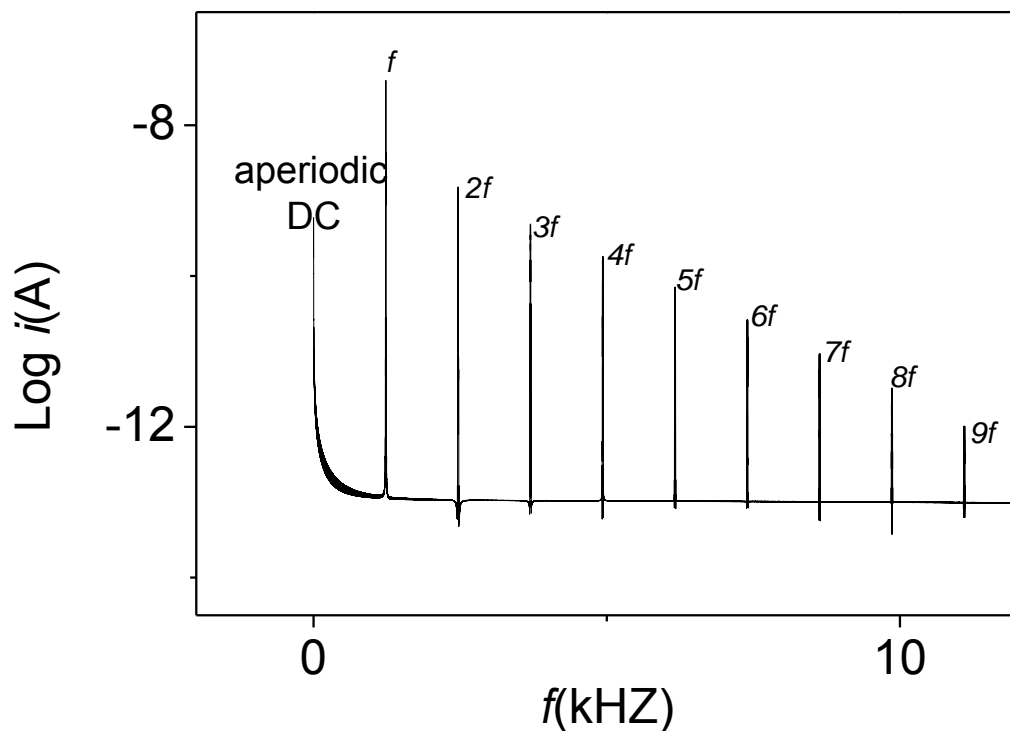


Figure 1: Microelectrode Log power spectrum obtained for a reversible one-electron reduction process using the following parameters: $C = 0.5 \text{ mM}$, $f = 1.23 \text{ kHz}$, $\Delta E = 80 \text{ mV}$, $v_{\text{DC}} = 0.600 \text{ V s}^{-1}$, $E^0 = 0.00 \text{ V}$, $D = 2.0 \times 10^{-5} \text{ cm}^2 \text{ s}^{-1}$, $r = 6.0 \text{ }\mu\text{m}$, $R_u = 35000 \text{ ohm}$

7.3.2. Diffusion coefficient measurement from limiting current of DC component

At a microelectrodes, the diffusion coefficient can be determined from limiting current of DC voltammogram using equation (1)

$$I_{\text{lim}} = 4nFDCr \quad (1)$$

If the AC sine wave perturbation doesn't affect the limiting current, then the DC component can be used to determine the diffusion coefficient. In order to validate this assumption, simulations were carried out in the absence of a sine wave perturbation (i.e. DC voltammetry) and with a sine wave perturbation of amplitude 80 mV, frequency 1.23 kHz. Analysis of the DC component for a reversible system shows that although the shape is altered by the AC perturbation, the limiting current is unaltered as shown in Figure 2. Furthermore, as expected, hysteresis is observed in the DC component in Figure 2 (a) when the scan rate v_{DC} is high (0.6 V s^{-1}) as compared to lower scan rate (0.02 V s^{-1}) where hysteresis is diminished (Figure 2(b)). Similar conclusions with respect to the limiting current are reached for the quasi-reversible case ($k^0 = 0.01 \text{ cm s}^{-1}$) where the data presented in Figure 3 shows that although the shape of the DC component is altered, the limiting current is not affected. It is concluded that the diffusion coefficient can be determined from the DC component of FT AC voltammetry at a microelectrode, provided the scan rate is sufficiently slow to achieve near steady-state condition in DC component.

7.3.3. $E_{1/2}$ measurement from AC voltammetric data at microelectrode

The half wave potential, $E_{1/2}$, is an important parameter in microelectrode voltammetry. It is related to E^0 and is affected by the magnitude of k^0 but R_u has a negligible effect in case of microelectrode. If a cyclic scan of the DC potential is used then $(E_{1/2})_{\text{m}}$ can be obtained as the average of $E_{1/2}$ found in the forward $(E_{1/2})_{\text{f}}$ and reverse $(E_{1/2})_{\text{b}}$ scan direction. In the case of

FT AC voltammetry at microelectrode, simulations were undertaken to ascertain the influence on $(E_{1/2})_m$ of the AC perturbation. For reversible and quasi-reversible systems, $(E_{1/2})_m$ is calculated from the DC component as $(E_{1/2})_m = (E_{1/2})_f + (E_{1/2})_b / 2$. Potentials derived from each AC harmonic are calculated from peak currents of (odd harmonics) and current minima (even harmonics) and compared their $E_{1/2}$. As shown in Table 1, for a reversible process, $E_{1/2}$ and AC potentials are similar. However, for quasi-reversible system ($k^0 = 0.1 \text{ cm s}^{-1}$ and 0.5 cm s^{-1}), higher harmonic AC potentials differ from $(E_{1/2})_m$, but 7th harmonic component gives a value close to E^0 , the value needed in the simulation. This is where the 7th harmonic is essentially equivalent to use of planar diffusion. For electrode processes with much slower kinetics $E_{1/2}$ can't be determined from any of the AC harmonics or DC components.

Table 1: $(E_{1/2})_m$ values and AC potential analogues for one-electron reduction process estimated from DC component and AC harmonics: simulations are based on parameters $C = 1.0 \text{ mM}$, $R_u = 35000 \text{ ohm}$, $f = 1.23 \text{ kHz}$, $\Delta E = 150 \text{ mV}$, $v_{DC} = 0.1 \text{ V s}^{-1}$, $D = 2.0 \times 10^{-5} \text{ cm}^2 \text{ s}^{-1}$, $r = 6.0 \text{ }\mu\text{m}$, $\alpha = 0.50$ and $E^0 = 0.00\text{V}$.

$E_{1/2}$ and AC potentials								
k^0	DC	1 st	2 nd	3 rd	4 th	5 th	6 th	7 th
Reversible	0.005	-0.0018	-0.0051	-0.0019	-0.00036	-0.0003	-0.00023	-0.0001
0.5	0.020	-0.0019	-0.0025	-0.0015	-0.00018	-0.0001	-0.00013	-0.0001
0.1	-0.025	-0.006	-0.007	-0.005	-0.006	-0.0009	-0.00092	-0.0004
0.001	-0.118	-0.228	-0.308	-0.302	-0.331	-0.317	-0.335	-0.330

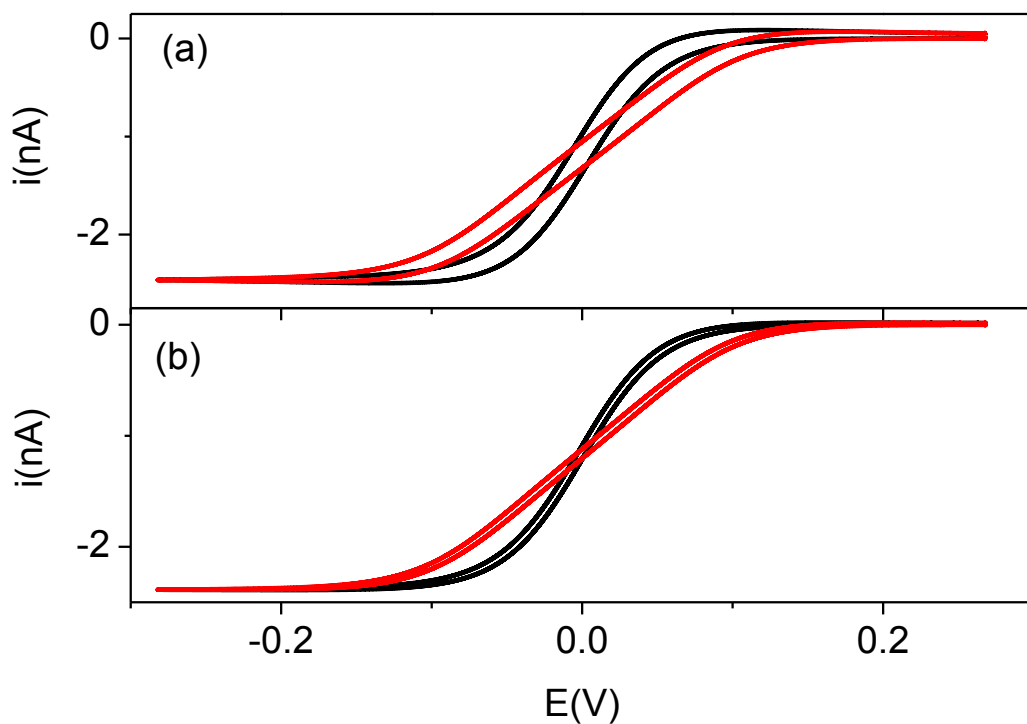


Figure 2. Comparison of simulated DC components (—) without and (—) with an AC perturbation of $f = 1.23$ kHz, $\Delta E = 80$ mV (a) $v_{DC} = 1.0$ V s⁻¹ and (b) $v_{DC} = 0.1$ V s⁻¹; Other simulation parameters are $C = 0.5$ mM, $k^0 = 2.0$ cm s⁻¹, $\alpha = 0.5$, $R_u = 0$, $D = 2.0 \times 10^{-5}$ cm² s⁻¹, $r = 6$ μ m, $T = 293$ K and $E^0 = 0$ V.

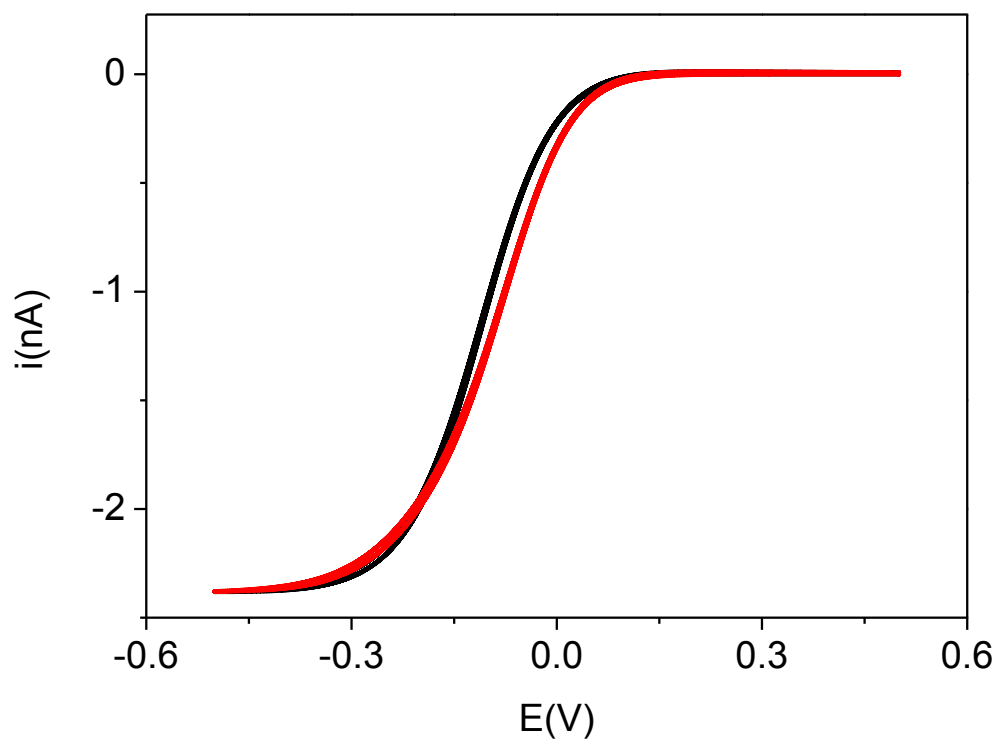


Figure 3. Comparison of simulated DC components (—) without and (—) with an AC perturbation of $f = 1.23$ kHz, $\Delta E = 80$ mV and $v_{\text{DC}} = 0.1$ V s⁻¹; Other simulation parameters and $C = 0.5$ mM, $k^0 = 0.01$ cm s⁻¹, $\alpha = 0.5$, $R_u = 0$, $D_O = 2.0 \times 10^{-5}$ cm² s⁻¹, $r = 6$ μ m T = 293 K and $E^0 = 0$ V.

7.3.4. Effect of uncompensated resistance

In order to examine the effect of iR drop, simulation of a redox system was performed with (a) $R_u = 0$ and (b) $R_u = 40000$ ohm along with other simulation parameters $f = 1.23$ kHz, $\Delta E = 80$ mV, $v_{DC} = 0.1$ V s⁻¹, $C^* = 1.0$ mM, $\alpha = 0.5$, $k^0 = 0.5$ cm s⁻¹, $D_O = 2.0 \times 10^{-5}$ cm² s⁻¹, $r = 6$ μ m and $E^0 = 0.00$ V. Simulation results showed that the 6th harmonic is barely affected in both cases either reversible or quasireversible, Figure 4 shows the reversible case.

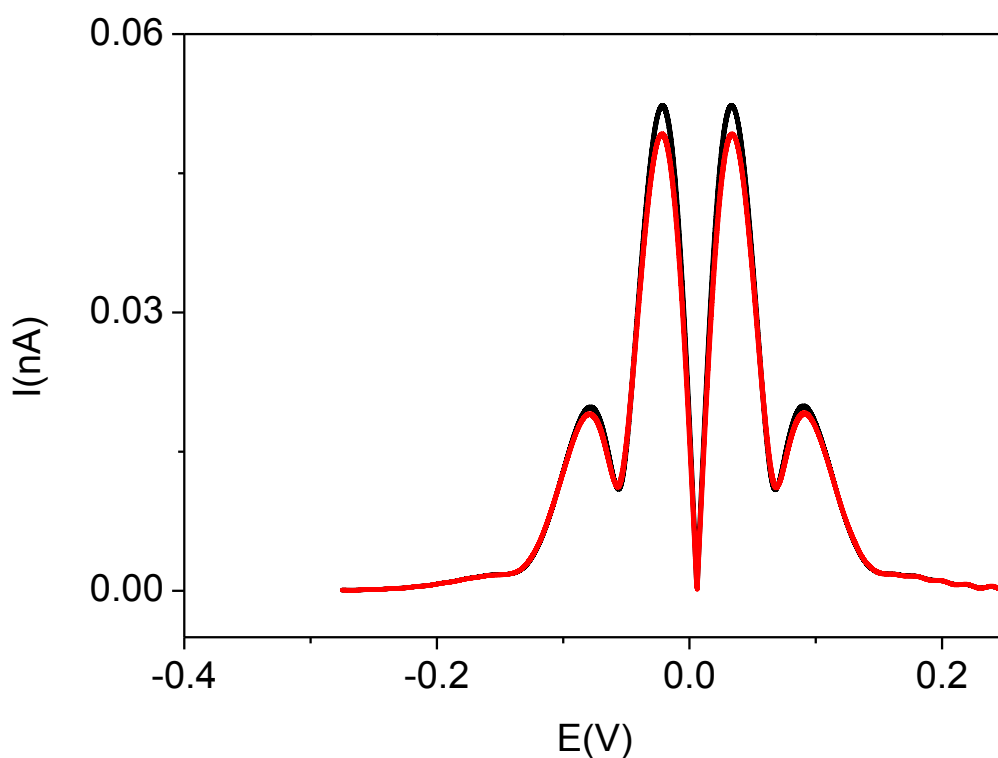


Figure 4: Comparison of the 6th harmonics of a simulated AC voltammograms for a reversible system with (—) $R_u = 0$ and (—) $R_u = 40000$ ohm, Other simulation parameters are $f = 1.23$ kHz, $\Delta E = 80$ mV, $v_{DC} = 0.1$ V s⁻¹; $C = 0.50$ mM, $k^0 = 0.50$ cm s⁻¹, $\alpha = 0.50$, $D = 2.0 \times 10^{-5}$ cm² s⁻¹, $r = 6$ μ m, $T = 293$ K and $E^0 = 0.00$ V.

7.3.5. Measurement of electrode kinetics at high frequency and upper limit of measurement

The upper limit for the measurement of the kinetics at micro electrode was determined at 9.0 Hz and 1.23 kHz frequency. According to this theoretical analysis k^0 electron transfer kinetics can be measured up to 1.0 cm s^{-1} from 6th harmonic peak current if low frequency ($f = 9.0 \text{ Hz}$) is used. However, by using high frequency 1.23 kHz as shown in Figure 5, sensitivity for the measurement of electron transfer kinetics can be enhanced up to 10 cm s^{-1} . For electron transfer kinetics lower than 0.1 cm s^{-1} larger amplitudes are required to get better voltammograms.

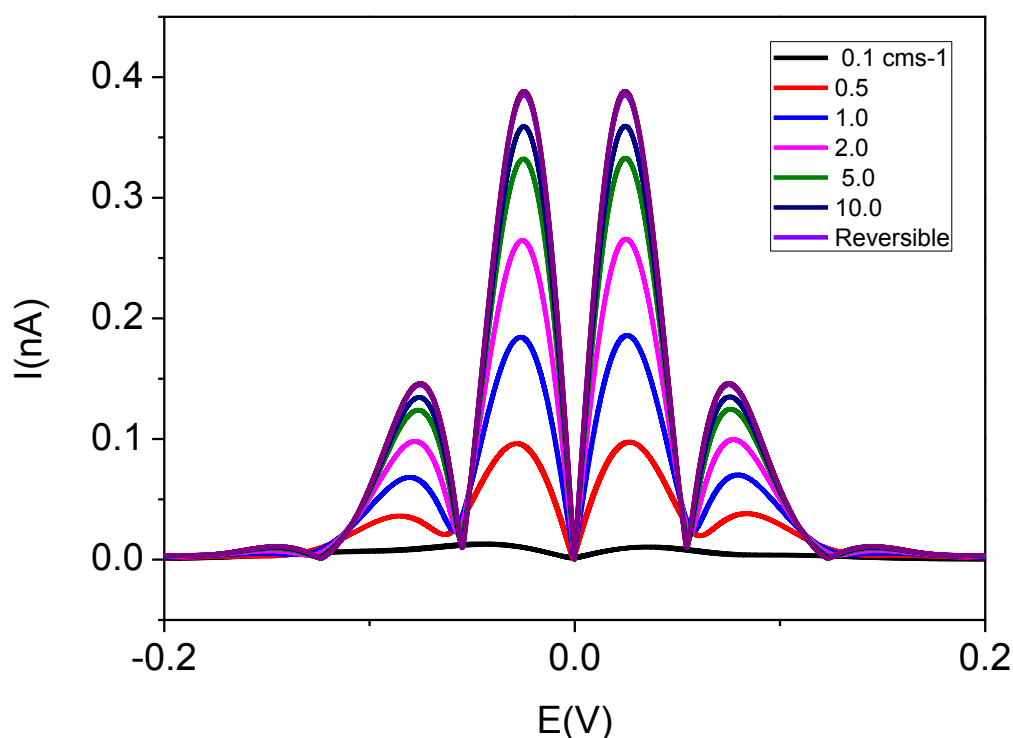


Figure 5: Simulated Fourier transformed large amplitude AC voltammograms 6th harmonic using various k^0 values $C = 1.0 \text{ mM}$, $f = 1.23 \text{ kHz}$, $\Delta E = 80 \text{ mV}$, $v_{\text{DC}} = 0.6 \text{ Vs}^{-1}$, $E^0 = -0.074 \text{ V}$, $\alpha = 0.50$, $D = 2.0 \times 10^{-5} \text{ cm}^2 \text{ s}^{-1}$, $r = 6.0 \text{ }\mu\text{m}$, $R_u = 35000$ and $C_{\text{dl}} = 10.0 \text{ }\mu\text{F cm}^{-2}$

7.3.6. Experimental results

Voltammetric experiments were carried out for the $\text{TTF}^{0/+}$ process at $f = 1.23$ kHz and $\Delta E = 80$ mV starting from either oxidation of TTF to TTF^{*+} or the reduction of TTF^{*+} to TTF. For the $\text{TTF}^{*+/0}$ redox system in acetonitrile (0.1 M Bu_4NPF_6), FT AC voltammetric studies at TTF^{*+} concentration of 0.46 mM were undertaken both at carbon and platinum microelectrodes. The D value used for simulations is $2.0 \times 10^{-5} \text{ cm}^2 \text{ s}^{-1}$ as deduced from peak currents of transient DC voltammograms at GC macrodisk electrode (1.0 mm) at 20 °C using Randle-Sevcik equation. Uncompensated resistance was measured to be 35000 ohm from the RC time constant. The first to sixth harmonics along with the DC component were compared with simulated data. Simulation parameters including uncompensated resistance of 35000 ohm, $(E_{1/2})_{\text{m}} = E^0 = -0.074 \text{ V vs. Fc}^{0/+}$, $v_{\text{DC}} = 0.655 \text{ V s}^{-1}$ and $D = 2.0 \times 10^{-5} \text{ cm}^2 \text{ s}^{-1}$ are used. Simulations of the DC component for reduction of 1.0 mM TTF^{*+} at a platinum microdisk electrodes are in excellent agreement with the experimental data with $k^0 = 2.5 \text{ cm s}^{-1}$ and $\alpha = 0.50$. Linear capacitance is assumed in the simulations with $C_{\text{dl}} = 12 \text{ } \mu\text{F cm}^{-2}$ to estimate the background capacitance current from fundamental harmonic. Experimental and simulated data for AC harmonic components 1 to 6 are found to be in superb agreement using the parameters given under Figure 6.

FT AC voltammetric data recorded at a platinum electrode for the reduction of 0.46 mM TTF^{*+} process were also simulated with the same R_{u} , D and α values as used for $\text{TTF}^{0/+}$ process at a carbon fiber electrode. In this case, k^0 value of 2.0 cm s^{-1} is used to model the $\text{TTF}^{*+/0}$ process. Other simulation parameters used are included in the caption of Figure 7 where a comparison of experimental and simulated voltammograms is provided for $\text{TTF}^{*+/0}$ process. Major contribution from background capacitance current is observed in DC component and fundamental harmonic. Simulation was conducted with parameters $R_{\text{u}} = 35000 \text{ ohms}$, $(E_{1/2})_{\text{m}} = E^0 = -0.074 \text{ V vs. Fc}^{0/+}$, $C_{\text{dl}} = 45 \text{ } \mu\text{F cm}^{-2}$, $D = 2.0 \times 10^{-5} \text{ cm}^2 \text{ s}^{-1}$ along

with $k^0 = 2.0 \text{ cm s}^{-1}$ and $\alpha = 0.5$. Experimental and simulated data for AC harmonic components 1 to 6 are also found to be in good agreement using the parameters given underneath the Figure 7.

Experimental results obtained for the oxidation of 1.0 mM TTF in acetonitrile (0.1 M Bu_4NPF_6) at platinum electrode were also simulated for two cases; (1) voltammetric scan over the potential range that includes only first oxidation process ($\text{TTF}^{0/+}$) (2) voltammetric scan over the potential range where two oxidation process are present simultaneously ($\text{TTF}^{0/+}/2+$). At first, simulation of experimental data with parameters including uncompensated resistance of 35000 ohm, $(E_{1/2})_m = E^0 = -0.074 \text{ V vs. Fc}^{0/+}$, $D = 2.0 \times 10^{-5} \text{ cm}^2 \text{ s}^{-1}$ were used. Electrode kinetic value $k^0 = 2.0 \text{ cm s}^{-1}$ along with $\alpha = 0.50$ is obtained from the 6th harmonic component by comparison of experimental and simulated data as shown in Figure 7. Huge capacitance affecting ($C_{dl} = 35 \text{ } \mu\text{F cm}^{-2}$) the DC component is observed along with enhanced hysteresis at 0.506 V s^{-1} , as compared to Figure 8 where $v_{\text{DC}} = 0.08196 \text{ V s}^{-1}$.

Electron transfer kinetics values $k_{\text{TTF}^{0/+}}^0$ and $k_{\text{TTF}^{0/+}/2+}^0$ associated with the $\text{TTF}^{0/+}$ and for $\text{TTF}^{0/+}/2+$ processes were also determined from the FT AC voltammograms for consecutive two electron oxidation $\text{TTF}^{0/+}/2+$ processes. Again, the hysteresis at high DC scan rate ($v_{\text{DC}} = 0.774 \text{ V s}^{-1}$) and high capacitance current ($C_{dl} = 40 \text{ } \mu\text{F cm}^{-2}$) at platinum affects the DC component. However, kinetic values can be obtained from the higher harmonic AC components using simulation parameters $D = 2.0 \times 10^{-5} \text{ cm}^2 \text{ s}^{-1}$, $R_u = 35000 \text{ ohm}$, $r = 6.0 \text{ } \mu\text{m}$, $v = 0.774 \text{ V s}^{-1}$, $E^0 = -0.074 \text{ V vs. Fc}^{0/+}$, $f = 1.23 \text{ kHz}$ and $\Delta E = 80 \text{ mV}$, $k_{\text{TTF}^{0/+}}^0 = 2.0 \text{ cm s}^{-1}$, $k_{\text{TTF}^{0/+}/2+}^0 = 0.40 \text{ cm s}^{-1}$ and $\alpha = 0.50$. Comparison of the experiment with theory is provided in Figure 9. Similar kinetics values are obtained from the oxidation of 1.0 mM TTF at the carbon fiber electrode.

7.4. Discussion

Electrode kinetics measurements described above don't include the effect of cross redox reaction as described in Chapter 5 as it doesn't affect the kinetics measurement when experiments are carried out from each redox levels.

Electron transfer kinetic associated with $\text{TTF}^{0/+}$ determined from each redox level TTF and TTF^{*+} by large amplitude FT AC voltammetry at microdisk electrode are in excellent agreement with the literature values.⁷ Utilizing the enhanced sensitivity of this method gives a more accurate value of k^0 value for the $\text{TTF}^{0/+}$ process that was considered close to the reversible limit with $k^0 \geq 1.0 \text{ cm s}^{-1}$ in chapter 5.

Results obtained for the second oxidation process $\text{TTF}^{*/2+}$ that has slower kinetic are also consistent with the chapter 5 results obtained at macrodisk electrode. Where the second process is considered as quasi-reversible with $k^0 = 0.35 \pm 0.05 \text{ cm s}^{-1}$ but measurement at macrodisk electrode for the k^0 value is also close to the upper limit of the measurement and it can be affected by the resistance value. However, in the case of microelectrode where the effect of R_u becomes negligible, more précised values of electrode kinetics are obtained.

Electrode kinetics values are found to be independent of the electrode material so the TTF redox processes can be considered adiabatic as per Marcus-Hush theory.¹² However, the effect of the double layer¹³ needs to be considered that is ignored in these measurements.

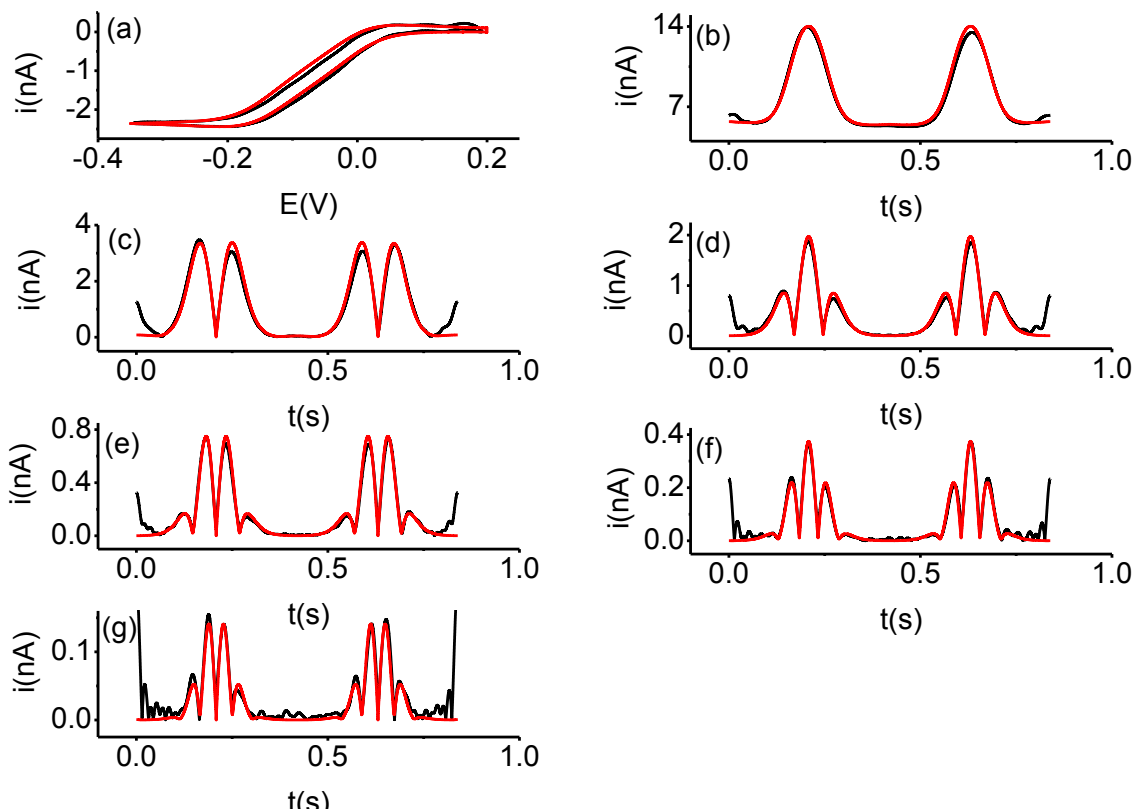


Figure 6: Comparison of experimental (—) FT AC voltammograms obtained for reduction of 0.46 mM $\text{TTF}^{+\bullet}$ in acetonitrile (0.1 M Bu_4NPF_6) at a carbon fiber microdisk electrode (a) 1st harmonic (b-g) 2nd - 6th harmonic and simulated ones (—) for a $\text{TTF}^{+\bullet/0}$ process obtained with $D = 2.0 \times 10^{-5} \text{ cm}^2 \text{ s}^{-1}$, $R_u = 35000 \text{ ohm}$, $r = 6.0 \text{ }\mu\text{m}$, $v_{\text{DC}} = 0.655 \text{ V s}^{-1}$, $E^0 = -0.074 \text{ V s}^{-1}$, $C_{\text{dl}} = 8.5 \text{ }\mu\text{F cm}^{-2}$, $f = 1.230 \text{ kHz}$ and $\Delta E = 80 \text{ mV}$, $k^0 = 2.5 \text{ cm s}^{-1}$, $\alpha = 0.5$

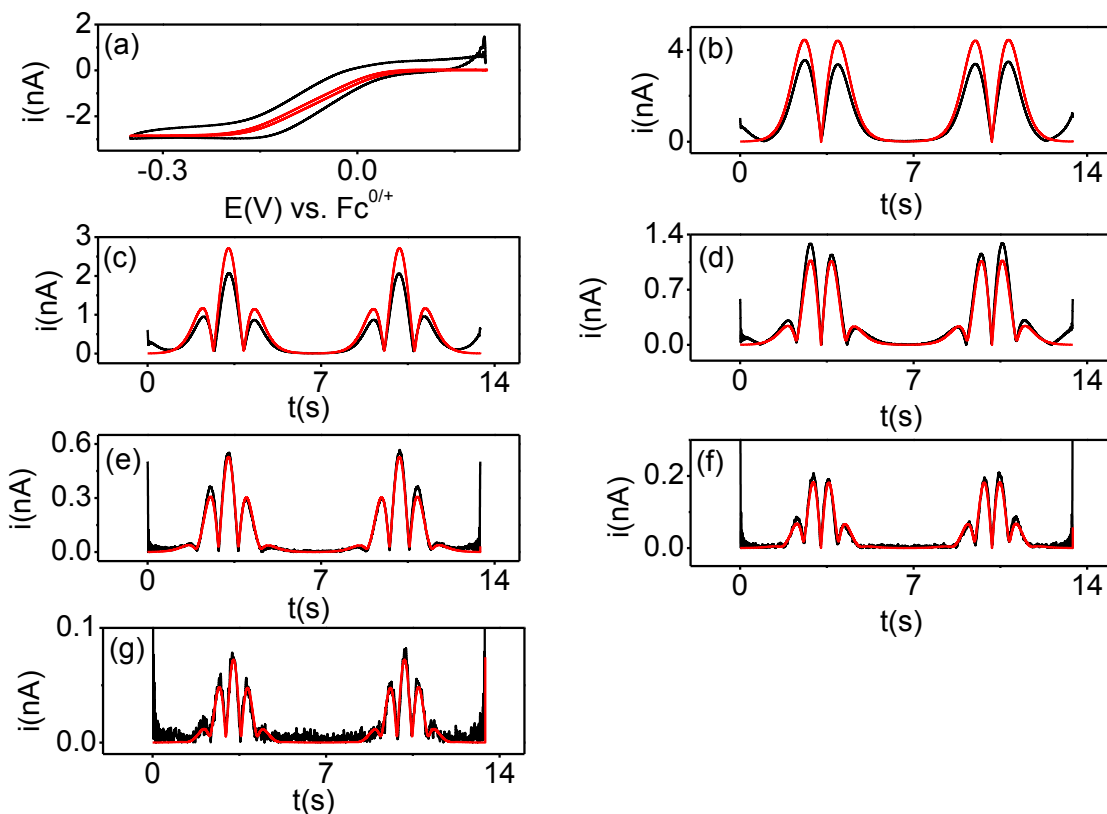


Figure 7: Comparison of experimental (—) FT AC voltammograms obtained for the reduction of 0.46 mM TTF^{*+} in acetonitrile (0.1 M Bu_4NPF_6) at a platinum electrode (a) 1st harmonic (b-g) 2nd - 6th harmonic and simulated ones (—) for a $\text{TTF}^{*+/0}$ process obtained with $D = 2.0 \times 10^{-5} \text{ cm}^2 \text{ s}^{-1}$, $R_u = 35000 \text{ ohm}$, $r = 6.0 \text{ }\mu\text{m}$, $v_{\text{DC}} = 0.08196 \text{ V s}^{-1}$, $E^0 = -0.074 \text{ V s}^{-1}$, $f = 1.23 \text{ kHz}$, $\Delta E = 80 \text{ mV}$, $k^0 = 2.0 \text{ cm s}^{-1}$ and $\alpha = 0.50$.

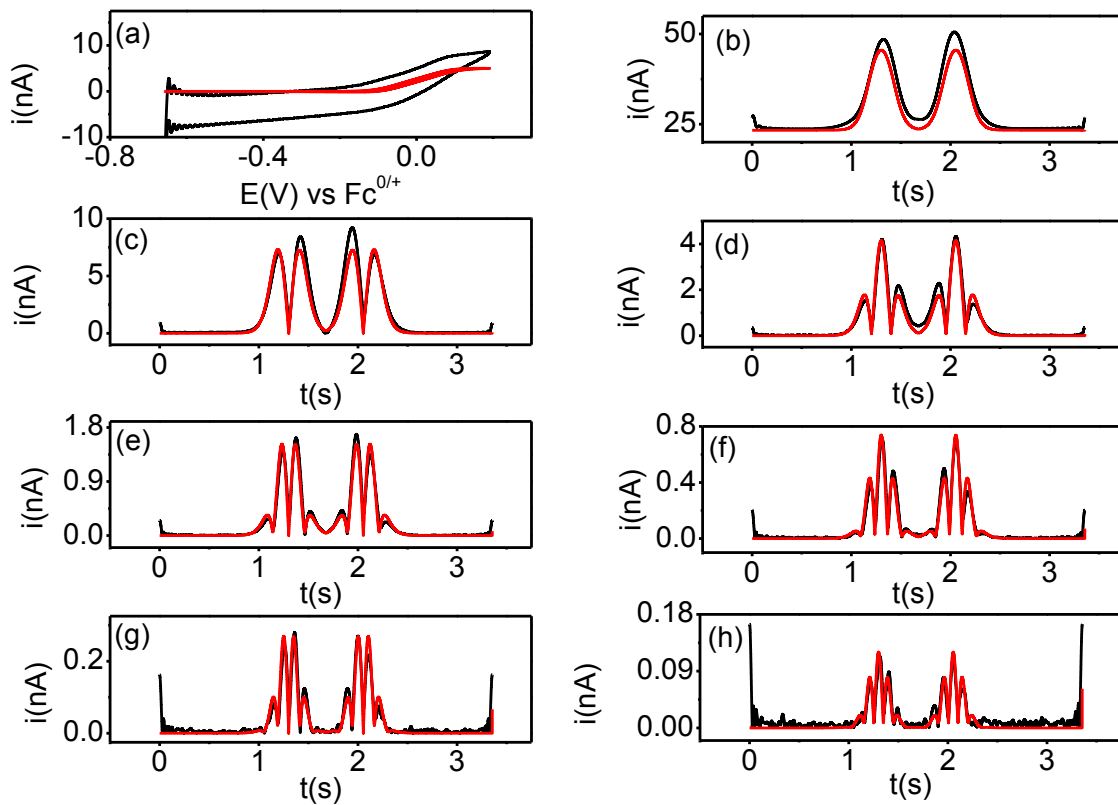


Figure 8: Comparison of experimental (—) FT AC voltammograms obtained for oxidation of 1.0 mM TTF in acetonitrile (0.1 M Bu_4NPF_6) at a platinum electrode (a) DC component (b-h) 2nd - 6th harmonic and simulated ones (—) for a $\text{TTF}^{0/+}$ process obtained with $D = 2.1 \times 10^{-5} \text{ cm}^2 \text{ s}^{-1}$, $R_u = 35000 \text{ ohm}$, $r = 6.0 \text{ } \mu\text{m}$, $v_{\text{DC}} = 0.506 \text{ V s}^{-1}$, $E^0 = -0.074 \text{ V vs. Fc}^{0/+}$, $f = 1.23 \text{ kHz}$ and $\Delta E = 80 \text{ mV}$, $k^0 = 2.0 \text{ cm s}^{-1}$ and $\alpha = 0.50$

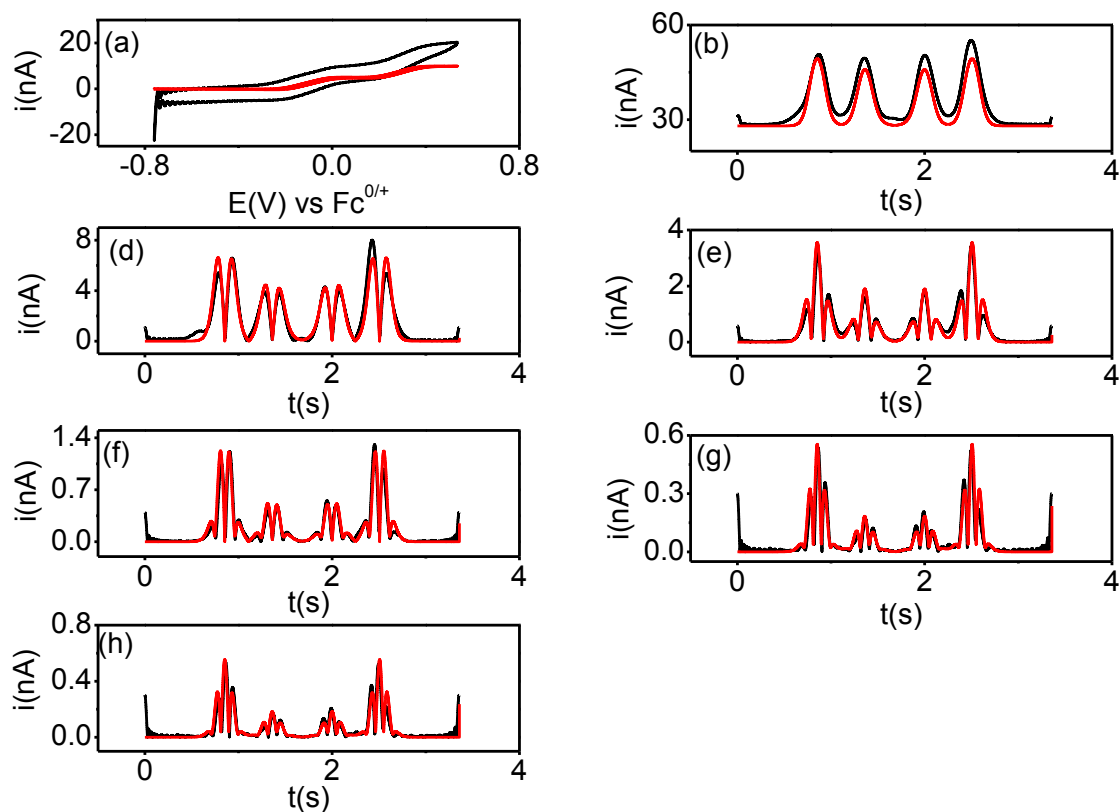


Figure 9: Comparison of experimental (—) FT AC voltammograms obtained for the oxidation of 1.0 mM TTF in acetonitrile (0.1 M Bu_4NPF_6) at a platinum electrode (a) DC component (b-g) 1st - 6th harmonic and simulated ones (—) for a $\text{TTF}^{0/+}/2+$ process obtained with $D = 2.0 \times 10^{-5} \text{ cm}^2 \text{ s}^{-1}$, $R_u = 35000 \text{ ohm}$, $r = 6.0 \text{ }\mu\text{m}$, $v_{\text{DC}} = 0.774 \text{ V s}^{-1}$, $E^0 = -0.074 \text{ V vs. Fc}^{0/+}$, $f = 1.23 \text{ kHz}$ and $\Delta E = 80 \text{ mV}$, $k_{\text{TTF}^{0/+}}^0 = 2.0 \text{ cm s}^{-1}$, $k_{\text{TTF}^{•+/2+}}^0 = 0.4 \text{ cm s}^{-1}$ and $\alpha = 0.50$.

7.5. Conclusion

It can be concluded that the high frequency regime of large amplitude FT AC voltammetry can be utilized to enhance the sensitivity of the method up to 10 cm^{-1} at microelectrodes. Very high frequency (1.23 kHz) sine wave imposed in fast scan AC voltammetry allowed to measure the kinetics of $\text{TTF}^{0/+}$ redox couple both at platinum and carbon fiber electrode.

References

- (1) Sher, A. A.; Bond, A. M.; Gavaghan, D. J.; Gillow, K.; Duffy, N. W.; Guo, S. X.; Zhang, J. *Electroanal.* **2005**, *17*, 1450.
- (2) Sher, A. A.; Bond, A. M.; Gavaghan, D. J.; Harriman, K.; Feldberg, S. W.; Duffy, N. W.; Guo, S. X.; Zhang, J. *Anal. Chem.* **2004**, *76*, 6214.
- (3) Zhang, J.; Guo, S. X.; Bond, A. M. *Anal. Chem.* **2007**, *79*, 2276.
- (4) Zhang, J.; Guo, S. X.; Bond, A. M.; Marken, F. *Anal. Chem.* **2004**, *76*, 3619.
- (5) Bano, K.; Kennedy, G. F.; Zhang, J.; Bond, A. M. *Phys. Chem. Chem. Phys.* **2012**, *14*, 4742.
- (6) Bano, K.; Nafady, A.; Zhang, J.; Bond, A. M.; Haque, I. U. *J. Phys. Chem. C* **2011**, *115*, 24153.
- (7) Grampp, G. K., A.; Jaenicke, W. *Ber. Bunsenges. Phys. Chem.* **1990**, *94*, 439.
- (8) Bond, A. M.; Duffy, N. W.; Elton, D. M.; Fleming, B. D. *Anal. Chem.* **2009**, *81*, 8801.
- (9) Bond, A. M.; Bano, K.; Adeel, S.; Martin, L. L.; Zhang, J. *ChemElectrochem.* **2013**, 10.1002/CELC.201300129.
- (10) Bard, A. J.; Faulkner, L. R. *Electrochemical methods: Fundamentals and Applications*; John Wiley: New York, **2001**.
- (11) <https://www.gamry.com/Products/DigiElch5.html>.
- (12) Marcus, R. A. *J. Chem. Phys.* **1956**, *24*, 966.

- (13) Frumkin, A. *Z. Physik. Chem.* **1933**, *A164*, 321.

CHAPTER 8

EFFECT OF DENSITY OF STATES AND ADIABATICITY IN ELECTRODE KINETICS STUDIES

Monash University

Declaration for Thesis Chapter [8]

Declaration by candidate

In the case of Chapter [8], the nature and extent of my contribution to the work was the following:

Nature of contribution	Extent of contribution (%)
Initiation, key ideas, experimental work, writing up	80 %

The following co-authors contributed to the work. If co-authors are students at Monash University, the extent of their contribution in percentage terms must be stated:

Name	Nature of contribution	
Jie Zhang	Initiation, key ideas, writing up	
Alan M. Bond	Initiation, key ideas, writing up	

The undersigned hereby certify that the above declaration correctly reflects the nature and extent of the candidate's and co-authors' contributions to this work*.

Candidate's Signature  Date 28/11/2013

Name	
Jie Zhang	
Alan M. Bond	

Main Supervisor's Signature  Date 29/11/2013

*Note: Where the responsible author is not the candidate's main supervisor, the main supervisor should consult with the responsible author to agree on the respective contributions of the authors.

CHAPTER 8

DEPENDENCE OF HETEROGENEOUS ELECTRON TRANSFER RATE CONSTANT ON ELECTRODE MATERIALS: THE EFFECT OF DENSITY OF STATES AND ADIABATICITY

Kiran Bano, Jie Zhang* and Alan M. Bond*

School of Chemistry, Monash University, Clayton, Victoria 3800, Australia

Corresponding authors:

Abstract

The effect of the density of states at the standard electrochemical rate constant of some outer-sphere electron transfer processes have been studied at boron doped diamond (BDD) electrode and compared with data at conventional GC and Pt electrodes. A comprehensive discussion is provided on the effect of the density of states on measurement of electrode kinetics and adiabaticity of the system. The effect of density of states is found with electron transfer kinetics for ruthenium hexamine $[(\text{Ru}(\text{NH}_3)_6)]^{3+}$ and silicone tungstate $[\alpha\text{-SiW}_{12}\text{O}_{40}]^{4-}$ reduction in aqueous medium where slower kinetics are observed at BDD. However, in case of 7,7,8,8-tetracyanoquinodimethane (TCNQ) and tetrathiofulvalene (TTF), their electrode processes appear to be adiabatic and independent of the low density of states of BDD.

8.1. Introduction

This chapter is concerned with the adiabaticity of electrode reactions and the effect of the electronic density of states (DOS) of electrode material on the charge transfer rate constant (k^0 value) of outer-sphere redox reactions.¹ Most of the outer-sphere electron transfers undergo rapid exchange of electrons at the surface of the electrodes. Electrode kinetic studies of such systems are of particular interest in fundamental electrochemistry and relate to the various factors as reorganization energies of the solvent in the vicinity of the electrodes, activation energies of the redox couple, electronic interactions of redox species with the electrodes, molecular properties of the system and to the density of states of the electrode materials.^{2,3} If a redox specie has strong electronic interaction with the electrode, electron transfer reaction follows an adiabatic pathway. For some organic compounds like quinones⁴⁻⁷ k^0 has been found essentially independent of the electrode substrates. In these cases, no significant dependence on the nature of the electrode material is witnessed and these reactions are regarded as adiabatic⁸ according to Marcus-Hush theory.³

Usually, the electronic density of states of the metal electrodes is higher than carbon due to the presence of a large number of atomic orbitals and conduction bands and doesn't vary with the potential. The rate constant of non-adiabatic heterogeneous electron transfer depends on the DOS of the electrode material, higher the DOS in the electrode at the E^0 of the redox system, higher will be the kinetics.⁹⁻¹⁶ Glassy carbon behaves like metals because they have a relatively even DOS distribution.¹⁷ The electron transfer mechanism at highly doped diamond electrodes also shows a metal-like behavior while relatively less doped electrodes are considered as semiconductors. However, the local density of states in GC and BDD at the Fermi level is generally lower than for metal electrodes.¹⁴ Various electrochemical methods^{7,18-20} have been employed to study electrochemical rate constants of electrode processes. Heterogeneous electron transfer rates relate quantitatively with the DOS in the

electrode material and can be used to authenticate the basic theories of adiabatic electron transfer.² The relation of the electron transfer rate with the density of states has been validated by measurement of a variety of electron transfer processes.^{17,21-23}

However, electrode kinetics measurements involving solution phase reactants are not only related to electrode material but may also to the double layer effect. The latter depends on the concentration of electrolyte, position of the redox potential with respect to the band gap region and charge of the participating species.^{24,25} It has been demonstrated for a series of quinine compounds at carbon and gold electrodes that the slower kinetics is observed at carbon if the potential of the redox couple lies close to the band gap region at carbon.⁷ Recent study reports the electron transfer kinetics measurement of ruthenium hexamine $[(\text{Ru}(\text{NH}_3)_6)]^{3+}$ and ferrocenylmethyl trimethylammonium (FcTMA^+) at boron doped diamond (BDD), where redox potential of the $[(\text{Ru}(\text{NH}_3)_6)]^{3+}$ lies in the region of band gap while redox potential of (FcTMA^+) is far away from the band gap region of BDD. In this case, kinetics is not determined by excess boron or sp^2 -hybridized carbon atom build-up at grain boundaries but by features of facets at BDD surfaces.¹⁴ On the contrary, for highly ordered pyrolytic graphite (HOPG) electrode kinetics on basal plane is usually considered slower than on edge plane due to lower density of state but recent studies using scanning electrochemical cell microscopy (SECCM) explains the deactivation or activation of kinetics on the freshly cleaved basal and edge plane graphite electrodes for $[\text{Fe}(\text{CN})_6]^{3-/4-}$ and $[\text{Ru}(\text{NH}_3)_6]^{3+/2+}$ processes.²⁶ When comparing electron transfer kinetics of carbon electrodes with other forms of carbon or metal electrode, various factors like surface functional groups at carbon electrodes, lower densities of states of the carbon as compared to metal electrodes and the variation in the local density of states with the potential at values close to the band gap may influence the kinetics.

Unfortunately, some of the above studies have been conducted by different groups using experimental conditions or electrode material may vary in each experiment. Many studies in the past predicting that the electron transfer rate is independent of the electrode material were later proved wrong due to less sensitivity of the technique. So whether k^0 values are independent of the electrode material or not often remains an open question and sensitivity of the technique is very important so that the observed independence is not due to insensitivity of technique.

Large amplitude FT AC voltammetry is promising for the kinetic determination of fast electrode processes because the effects of uncompensated resistance and slow kinetics can be distinguished by analysis of AC harmonic components.²⁷ This feature has been utilized in studies at macro electrodes^{4,5,28} where k^0 value can be measured up to 2.0 cm s^{-1} provided that the uncompensated resistance is accurately known. In this chapter FT AC voltammetry that has previously found its applications in k^0 measurements,^{29,30,4,5,27-29,31-35} is used for some classical electron transfer processes. The double layer effect³⁶ is predominantly present at disk electrodes used in this study that cannot be neglected in kinetics measurement and double layer correction cannot be as accurate as in the case of mercury electrodes. Double layer thickness can be minimized by the addition of a high electrolyte concentration. This is achieved by using large polyoxometallate ($\alpha\text{-SiW}_{12}\text{O}_{40}$) where the high electrolyte concentration ($1.0 \text{ M Na}_2\text{SO}_4 + 0.1 \text{ M H}_2\text{SO}_4$) is used to minimize the thickness of the double layer. This methodology facilitates measurement of the effect of DOS of electrode material on the electron transfer kinetics.

8.2. EXPERIMENTAL SECTION

CHEMICALS: Ruthenium hexamine trichloride ($[\text{Ru}(\text{NH}_3)_6]^{3+}$) 98% (Sigma-Aldrich), Tetrathiafulvalene (TTF) 99% (Aldrich), 7,7,8,8-tetracyanoquinodimethane (TCNQ) 98%

(Sigma-Aldrich), Silicotungstic acid $\text{H}_4[\alpha\text{-SiW}_{12}\text{O}_{40}]$ 98% (Aldrich), potassium chloride (KCl) 99% (Sigma-Aldrich), sulphuric Acid (H_2SO_4) 99% (Sigma-Aldrich), were used as obtained from the supplier tetrabutylammonium hexafluorophosphate (Bu_4NPF_6), 98% (Wako) was recrystallized twice from ethanol. Bu_4NPF_6 and acetonitrile (CH_3CN) 99.8 % (Sigma-Aldrich) were dried and stored under nitrogen in a dry box.

8.2.1. Instrumentation and procedure

All electrochemical experiments were carried out under a nitrogen atmosphere at room temperature (20 ± 2 °C). A standard electrochemical cell with three electrode configuration was used. Working electrodes were either macro disc platinum (Pt, $d = 1.0$ mm), glassy carbon (GC, $d = 1.0$ mm) and Boron doped diamond (BDD, $d = 1.0$ mm) (provided by Unwin's group, University of Warwick UK), Boron doped diamond (BDD, $d = 3.0$ mm) by Windsor. Uncompensated resistance was measured using the RC time constant method¹ available with the BAS 100 instrument in a potential region where no Faradaic current is present.

Working electrodes were polished using 3 μm and 0.05 μm alumina on a clean polishing cloth, washed and rinsed with water. Platinum wire was used as an auxiliary electrode and another platinum wire was used as a quasi-reference electrode in organic solvent, while Ag/AgCl, 3.0 M KCl was used in aqueous medium. DC cyclic voltammetric experiments were undertaken with CHI 400B DC potentiostat and large amplitude FT AC voltammetric experiments were carried out with home built instrumentation.³⁷ FT AC voltammetric experiments were carried out using a sine wave perturbation of amplitude (ΔE) = 80 mV with the desired frequencies from 9.0 Hz to 1228Hz.

8.2.2. Digital Simulations and AC Data Analysis

Simulations of experimental data were carried out with MECSim (Monash ElectroChemistry Simulator) written in Fortran. This software is based on expanding spatial grid formulation³⁸ and is based on the mathematical approach given by Rudolph³⁹ with minor corrections. Simulations were carried out for simple electron transfer process using Butler-Volmer theory¹ of electron transfer for the reaction given in equation eq. 1



where k^0 is the formal charge-transfer rate constant at potential E^0 vs. the reference electrode), E^0 is the reversible potential calculated as the average of the peak potentials for the reduction and oxidation components and α is an electron transfer coefficient that is independent of E^0 but varies with the value of k^0 , while O and R are oxidized and reduced species as a result of charge transfer.

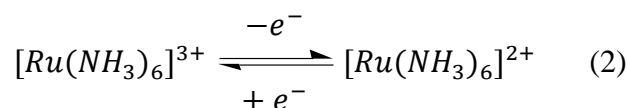
FT AC voltammetric data obtained experimentally or theoretically was then subjected to data analysis where time domain data (experimental raw data) were converted to frequency domain data using a FT algorithm to get power spectrum.²⁹ Selected frequencies corresponding to AC harmonics and aperiodic DC components from power spectrum were then subjected to band filtering and inverse Fourier transform to get desired DC or AC components as a function of time. Out of five unknown parameters R_u , E^0 , k^0 , α and C_{dl} (double layer capacitance), R_u was determined experimentally from the RC time constant where no faradiac current was present, E^0 was estimated from current minima of 2nd harmonic and C_{dl} was quantified from the background current in 1st harmonic.

A heuristic method of data analysis were used for evaluating the rate constants from theory-experiment comparisons. Charge transfer rate constants were extracted from the kinetically more sensitive higher harmonics where the current magnitudes are sensitive to the electron transfer rate constants.

8.3. Results

8.3.1. Electrode kinetics of $[\text{Ru}(\text{NH}_3)_6]^{3+}$

The $[\text{Ru}(\text{NH}_3)_6]^{3+}$ undergoes the electron transfer process shown in eq. 2 at GC and other metal electrodes⁴⁰



DC voltammogram of $[\text{Ru}(\text{NH}_3)_6]^{3+}$ shows one process at $E^0 = -0.168$ V with peak to peak separation between oxidation and reduction peaks close to 60 mV. The diffusion coefficient is determined to be $6.24 \times 10^{-6} \text{ cm}^2 \text{ s}^{-1}$ from the peak current of DC cyclic voltammogram as shown in Figure 1 for reduction of 0.47 mM $[\text{Ru}(\text{NH}_3)_6]^{3+}$ in 1.0 M KCl at GC electrode ($d = 1.0$ mm) using Randles-Sevcik equation (3)

$$I_p = 0.4463nFA \left(\frac{nFDv}{RT} \right)^{1/2} C \quad (3)$$

where I_p = peak current (A), n = number of electrons transferred in the redox event, A = electrode area (cm^2), F = The Faraday's Constant (C mol^{-1}), D = diffusion coefficient ($\text{cm}^2 \text{ s}^{-1}$), C = concentration (mol cm^{-3}) and v_{DC} = scan rate (V s^{-1}). In order to extract electrode kinetics parameters for $[\text{Ru}(\text{NH}_3)_6]^{3+/2+}$ process, AC cyclic voltametric studies are carried out at GC, Pt and BDD electrodes using a sine wave perturbation of $\Delta E = 80$ mV and $f = 9.0$ Hz and 1228 Hz. Comparison of higher harmonic peak currents at BDD, GC and platinum AC voltammetric data suggests that the electrode kinetics at BDD is significantly slower than at

GC or Pt. Resulting data are modelled by applying Butler-Volmer theory of electron transfer. Kinetic parameters are estimated in each case to probe the difference in the density of states of various electrode materials. $E^0 = -0.169$ V is measured from the minima of even harmonics and maxima of odd harmonics. C_{dl} is estimated from non-faradiac component of fundamental harmonic and C_{dl} values given in Table 1 show that capacitance is essentially non-linear at higher frequency. Concentration and diffusion coefficient values are checked by the fitting of DC component and 1st and 2nd harmonics, while, 3rd-6th harmonics are used to extract kinetics parameters by a detailed comparison of experiment and theory.

Experimental data at BDD are simulated using parameters $R_u = 30$ ohm, $E^0 = -0.169$ V and non-linear capacitance C_{dl} ($c_0 = 15$, $c_1 = 2.8$ and $c_2 = 1.3$) $\mu\text{F cm}^{-2}$, comparison of experiment versus theory is used to extract the electron transfer kinetics value $k^0 = 0.0105$ cm s^{-1} that readily lies in the limit of detection at 9.0 Hz. In case of BDD only low frequency (9.0 Hz) data are used for simulation and comparison of experimental data with theory is provided in Figure 1.

However, at GC and platinum electrodes current intensities of higher harmonics related to electron transfer kinetics are ten times higher than on BDD. In order to accurately measure the electron transfer kinetics $[\text{Ru}(\text{NH}_3)_6]^{3+/2+}$ process at GC and Pt electrode, study is extended to higher frequency (1228 Hz) to enhance the sensitivity of measurements, where six to seven harmonics are obtained by FT-inverse FT method. Platinum electrode data are simulated with $R_u = 37$ ohm, $E^0 = -0.178$ V and $c_0 = 36.5$ $\mu\text{F cm}^{-2}$. The k^0 value is obtained to be > 5.0 cm s^{-1} indicating that process at Pt electrode is essentially reversible. Similarly, GC electrode data are simulated to estimate the electrode kinetic parameter k^0 with $R_u = 53.0$ ohm, $E^0 = -0.166$ V and non-linear capacitance C_{dl} ($c_0 = 28.5$, $c_1 = 13.0$ and $c_2 = 8.8$) $\mu\text{F cm}^{-2}$. Electron transfer kinetics k^0 are obtained by comparison of theory and experiment and the estimated value (2.0 cm s^{-1}) is a bit lower as compared to PT electrode but this measured

value is very close to reversible limit. Comparison of experiment and theory for the reduction of $[\text{Ru}(\text{NH}_3)_6]^{3+}$ at GC is provided in Figure 2 while similar comparison of Pt data is provided in Figure 3.

Kinetic parameter obtained at BDD ($k^0 = 0.0105 \text{ cm s}^{-1}$), at GC ($k^0 = 2.0 \text{ cm s}^{-1}$) and at Pt ($k^0 > 5.0 \text{ cm s}^{-1}$) are in close agreement with literature values.^{26,41} However, $\alpha = 0.50$ in each case suggests that $[\text{Ru}(\text{NH}_3)_6]^{3+/2+}$ is an outer-sphere electron transfer process. Electron transfer kinetics at BDD electrode is strongly influenced by the amount of boron doping so these results are further validated by comparison of higher harmonic currents of GC and commercially available BDD electrode (Windsor) and it is concluded that $[\text{Ru}(\text{NH}_3)_6]^{3+/2+}$ process shows slower kinetics at BDD electrode as compared to the GC.

Table 1. Parameters used to simulate the reduction of 0.47 mM $[\text{Ru}(\text{NH}_3)_6]^{3+}$ in 1.0 M KCl

Electrode	F	$C_{dl}(c_0, c_1, c_2)$	R_u	k^0	E^0	α
	Hz	$\mu\text{F cm}^{-2}$	ohm	cm s^{-1}	V	
Pt	1228	36.5, 0.0, 0.0	37	> 5.0	-0.178	0.5
GC	1228	28.5, 13.0, 8.8	53	2.2	-0.168	0.5
BDD	9.0	15.7, 2.8, 1.5	30	0.015	-0.168	0.5

$A_{GC} = A_{BDD} = A_{Pt} = 0.00785 \text{ cm}^2$, $\Delta E = 80 \text{ mV}$, $D_{[\text{Ru}(\text{NH}_3)_6]^{3+}} = 6.24 \times 10^{-5} \text{ cm}^2 \text{ s}^{-1}$, E^0 vs. Ag/AgCl, 3.0 M KCl

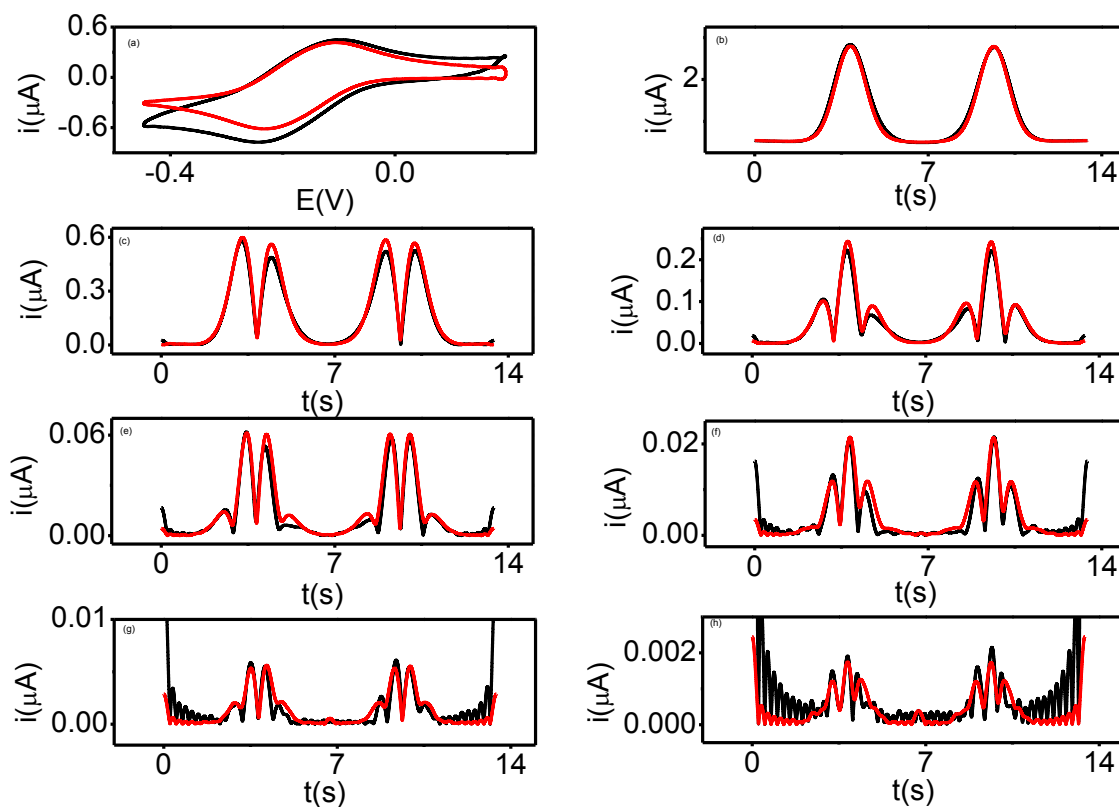


Figure 1. Comparison of simulated (—) and experimental (—) large amplitude FT AC voltammograms obtained for the reduction of 0.47 mM $[\text{Ru}(\text{NH}_3)_6]^{3+}$ solution in water (1.0 M KCl) at a BDD electrode (a) DC component (b-h) 1st - 7th harmonics, Other parameters are as defined in the text.

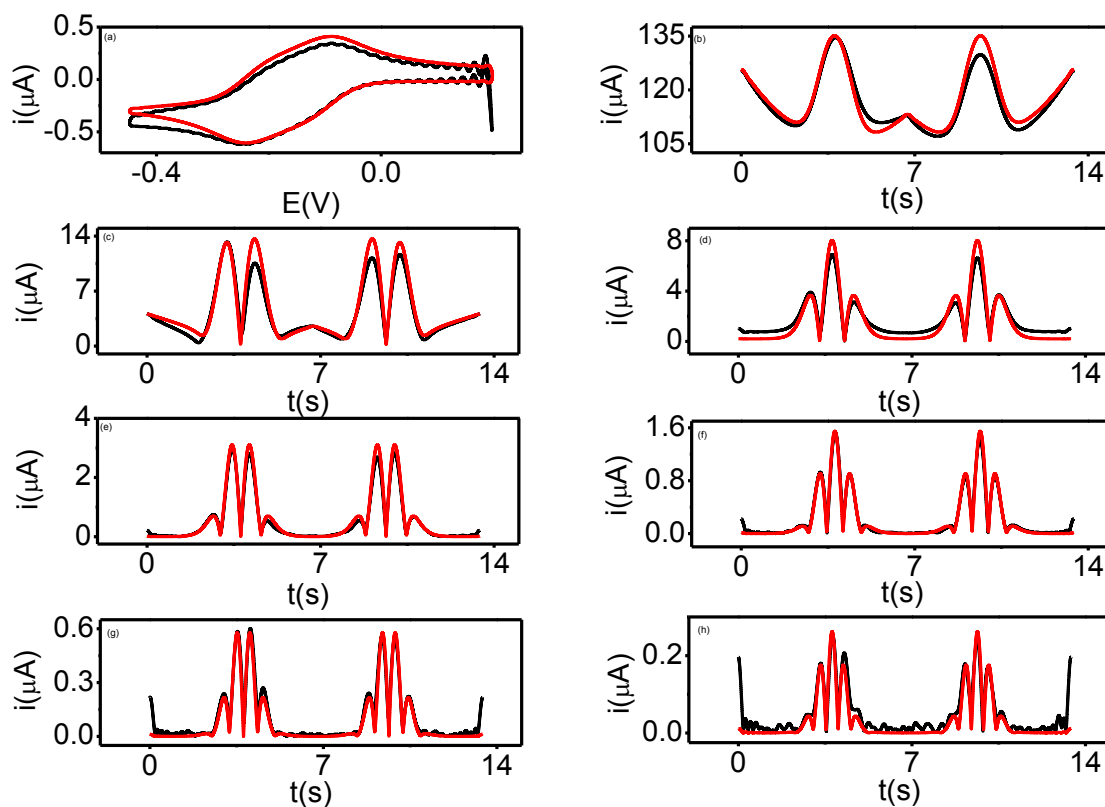


Figure 2. Comparison of simulated (—) and experimental (—) large amplitude FT AC voltammograms obtained for the reduction of 0.47 mM $[\text{Ru}(\text{NH}_3)_6]^{3+}$ solution in water (1.0 M KCl) at a GC electrode (a) DC component (b-h) 1st - 7th harmonics, Other parameters are as defined in the text.

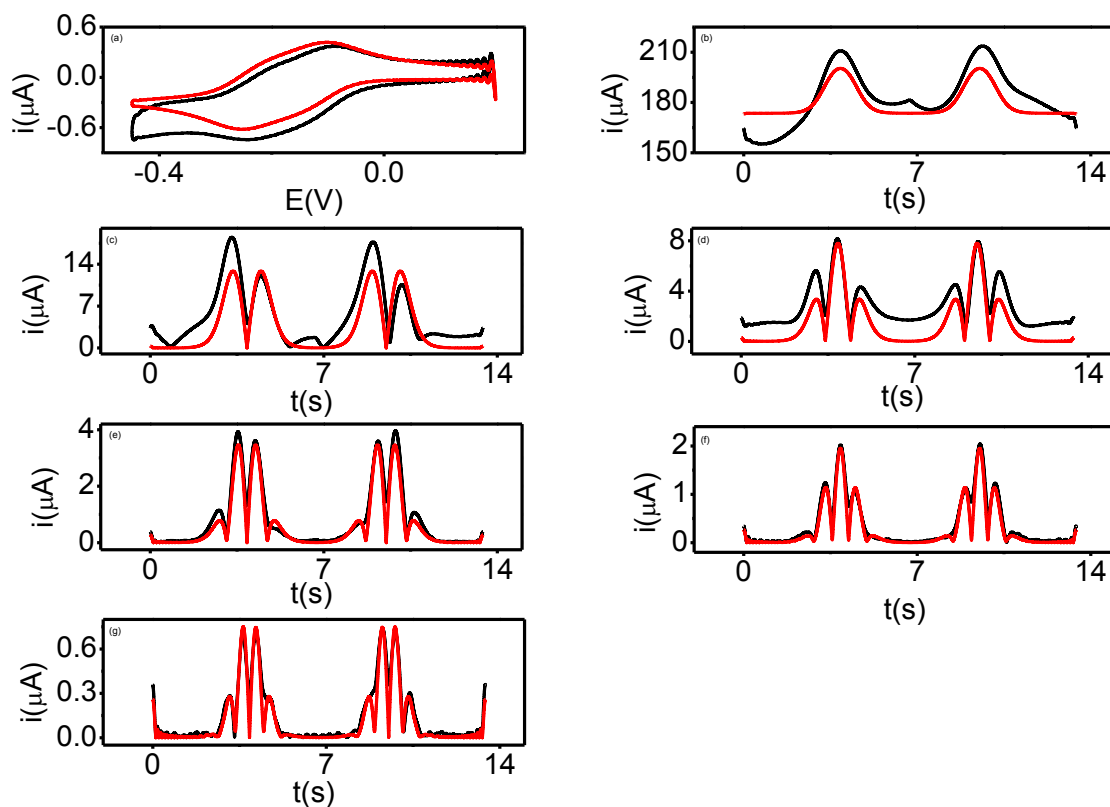
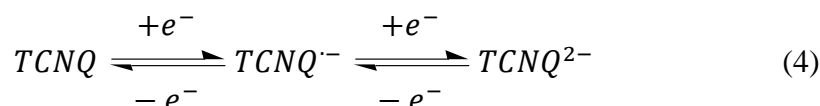


Figure 3. Comparison of simulated (—) and experimental (—) large amplitude FT AC voltammograms obtained for the reduction of 0.47 mM $[\text{Ru}(\text{NH}_3)_6]^{3+}$ solution in water (1.0 M KCl) at a Pt electrode (a) DC component (b-g) 1st - 6th harmonics, $f = 9.0$ Hz, $\Delta E = 80$ mV, Other parameters are as defined in the text.

8.3.2. Heterogeneous electron transfer kinetics of TCNQ

TCNQ is also considered a classical system that undergoes one electron transfer process to mono anion (TCNQ^{•-}) at $E^0 = -0.170$ V and second electron transfer to dianion (TCNQ²⁻) at $E^0 = -0.715$ V Fc^{0/+} as shown in eq. 4.



Previous large amplitude FT AC studies using $f = 9.0$ Hz show that both TCNQ^{0/+} and TCNQ^{•-/2-} processes have same $k^0 \sim 0.3$ cm s⁻¹ but this value is near the upper limit of detection under the experimental conditions.⁴² Here, we study the TCNQ^{0/+} at Pt, GC and BDD electrode using $f = 233$ Hz and $\Delta E = 80$ mV to see if the difference in the electrode density of states can be observed in case of BDD at high frequency. Diffusion coefficient (1.87×10^{-5} cm² s⁻¹) is calculated from the cyclic voltametric peak currents for the reduction of 2.0 mM TCNQ using Randles-Sevcik equation. AC voltametric data are further subjected to simulation using Butler-Volmer theory and kinetic parameters are extracted in each case by comparison of theory versus experiment.

For the reduction of TCNQ at BDD electrode, kinetic parameter k^0 is found to be 0.32 cm s⁻¹ when experimental data are simulated with the help of parameters like $R_u = 620$ ohm and C_{dl} ($c_0 = 5.5$ and $c_1 = 2.0$) $\mu\text{F cm}^{-2}$. Simulation results are compared with the experiment in Figure 4, whereas other experimental and simulation parameters are given in Table 2.

AC voltammetric data obtained at Pt electrode is simulated using parameters $R_u = 460$ ohm and non-linear capacitance C_{dl} ($c_0 = 20.5$, $c_1 = 5.0$ and $c_2 = 3.2$) $\mu\text{F cm}^{-2}$. Electron transfer kinetics are found to be 0.40 cm s⁻¹ at Pt electrode and simulated results in comparison with the experiment are shown in Figure 5. Similarly, kinetic parameter $k^0 = 0.39$ cm s⁻¹ is obtained at GC by using simulation parameters $R_u = 495$ ohm and non-linear capacitance C_{dl}

($c_0 = 20$, $c_1 = 5.0$ and $c_2 = 3.0$) $\mu\text{F cm}^{-2}$, while comparison of experiment and theory is shown in Figure 6.

Table 2. Parameters used to simulate the electro reduction of 2.0 mM TCNQ in 0.1 M Bu_4NPF_6 in acetonitrile

Electrode	$C_{\text{dl}}(c_0, c_1, c_2)$	R_u	k^0	E^0	α
	$\mu\text{F cm}^{-2}$	ohm	cm s^{-1}	V	
Pt	20.5, 5.0, 3.2	460	0.4	-0.164	0.5
GC	20.5, 5.0, 3.2	495	0.39	-0.164	0.5
BDD	5.5, 2.2, 0.0	620	0.32	-0.164	0.5

$A_{\text{GC}} = A_{\text{BDD}} = A_{\text{Pt}} = 0.00785 \text{ cm}^2$, $f = 233 \text{ Hz}$, $\Delta E = 80 \text{ mV}$, $D_{\text{TCNQ}} = 1.87 \times 10^{-5} \text{ cm}^2 \text{ s}^{-1}$

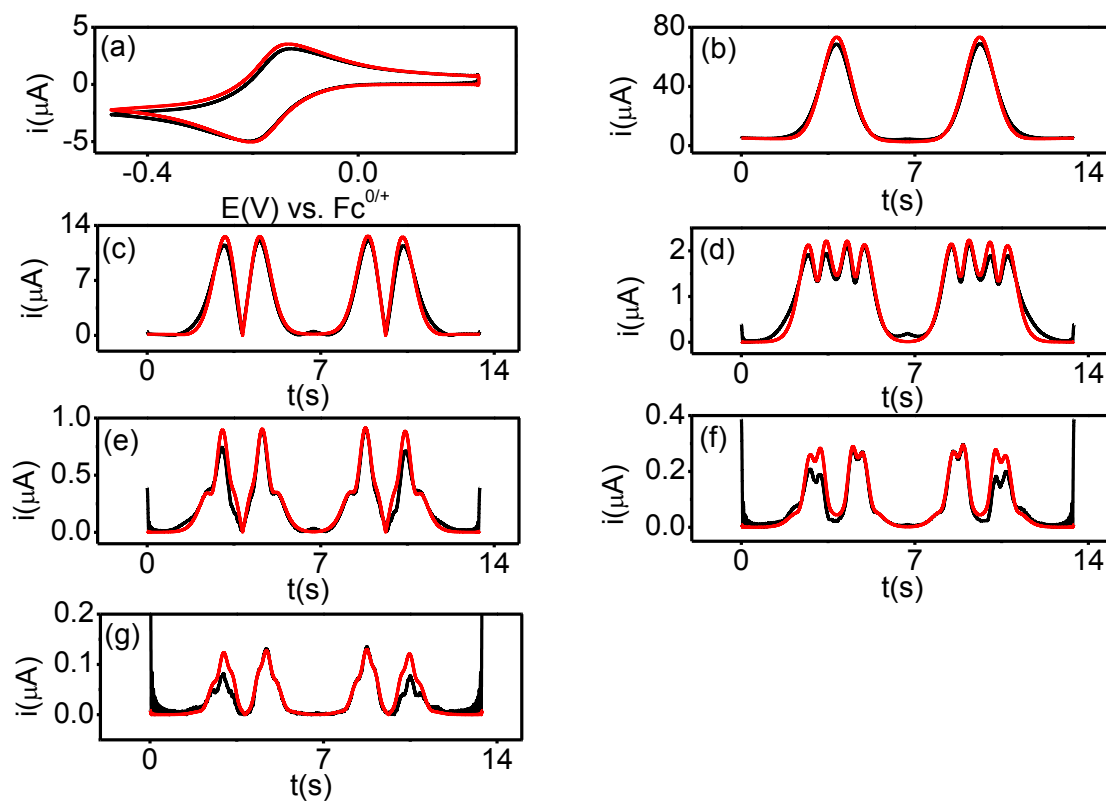


Figure 4. Comparison of simulated (—) and experimental (—) large amplitude FT AC voltammograms obtained for the one-electron TCNQ reduction of 2.0 mM TCNQ solution in acetonitrile (0.1 M Bu_4NPF_6) at a BDD electrode (a) DC component (b-g) 1st - 6th harmonics, $f = 233.0$ Hz, $\Delta E = 80$ mV, Other parameters are as defined in the Table 2.

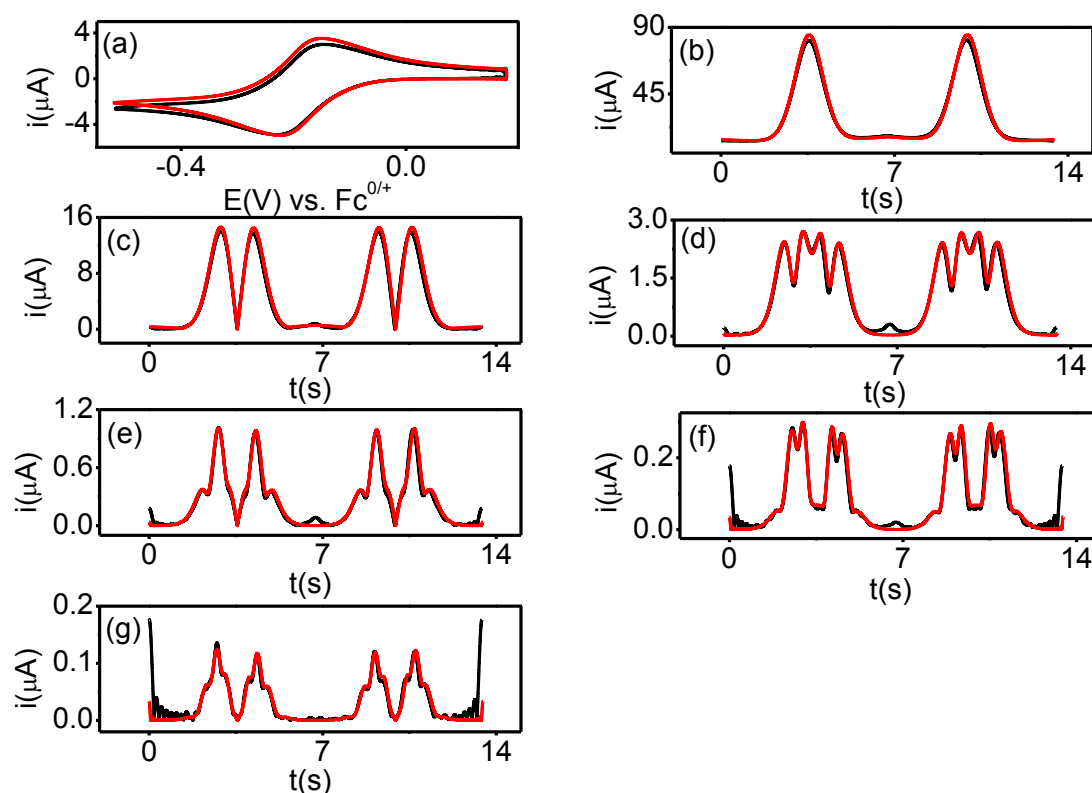


Figure 5. Comparison of simulated (—) and experimental (—) Large amplitude FT AC voltammograms obtained for the one-electron TCNQ reduction of 2.0 mM TCNQ solution in acetonitrile (0.1 M Bu_4NPF_6) at a Pt electrode (a) DC component (b-g) 1st- 6th harmonics, Other parameters are as defined in the text.

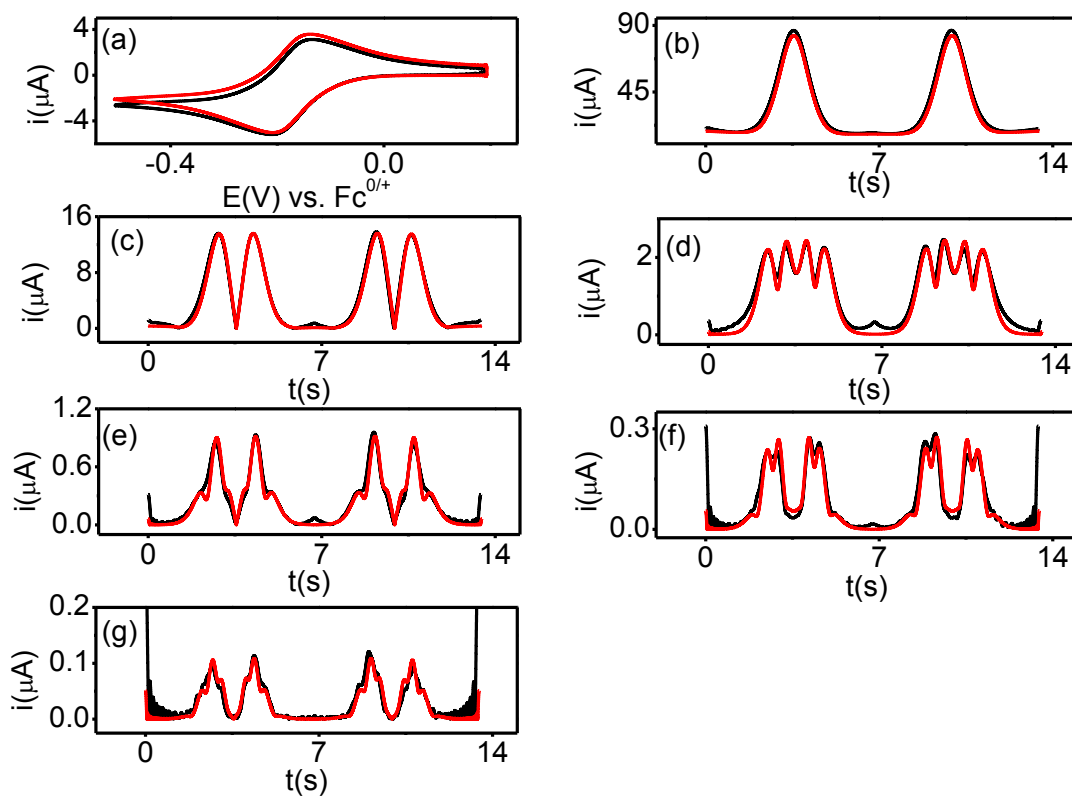
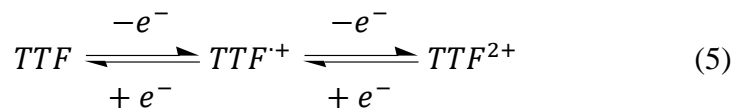


Figure 6. Comparison of simulated (—) and experimental (—) large amplitude FT AC voltammograms obtained for the one-electron TCNQ reduction of 2.0 mM TCNQ solution in acetonitrile (0.1 M Bu₄NPF₆) at a GC electrode (a) DC component (b-g) 1st-6th harmonics, Other parameters are as defined in the text.

8.3.2. Heterogeneous electron transfer kinetics of TTF

TTF undergoes two one electron oxidation processes i.e. $\text{TTF}^{0/+}$ at $E^0 = -0.074$ V and $\text{TTF}^{+/2+}$ at $E^0 = 0.311$ V vs. $\text{Fc}^{0/+}$ as shown in eq. 5.



Electrochemical oxidation of TTF is studied using large amplitude FT AC voltammetry ($f = 233$ Hz and $\Delta E = 80$ mV) and kinetics parameters are extracted by comparison of experiment and theory. The diffusion coefficient calculated ($D = 2.1 \times 10^{-5} \text{ cm}^2 \text{ s}^{-1}$) from the oxidation peak current of DC cyclic voltammogram of 1.0 mM TTF in acetonitrile (0.1M Bu_4NPF_6) using eq. 2 is used in simulations.

AC voltammetric studies have been carried out at GC, Pt and BDD electrodes when the electron transfer rate constants $k_{\text{TTF}^{0/+}}^0$ and $k_{\text{TTF}^{+/2+}}^0$ are assessed by simulation of AC voltammetric data for the $\text{TTF}^{0/+}$ oxidation process from the oxidation of 1.0 mM TTF solution at three electrodes.

For simulation of AC voltammogram for the oxidation of TTF at BDD electrode, at first, non-linear capacitance C_{dl} ($c_0 = 5.0$ and $c_2 = 0.55$) $\mu\text{F cm}^{-2}$ is extracted from fundamental harmonic. R_u is taken as 560 ohm in simulations to extract the $k^0 \sim 1.0 \text{ cm s}^{-1}$ from higher harmonic components of AC voltammograms corresponding to the $\text{TTF}^{0/+}$ process that is near the reversible limit. Similarly, k^0 value for $\text{TTF}^{+/2+}$ process is estimated as 0.4 cm s^{-1} in the similar comparison between theory and experiment; the rest of the parameters are described in Table 3. Comparison of experimental and simulated voltammograms at BDD is given in Figure 7.

Likewise, k^0 values obtained for GC and Pt electrodes as shown in Table 3 are independent of the electrode material. Comparison of experiment and theory for the oxidation of TTF at GC and Pt is given in Figure 8 and 9 while simulation parameters are given in Table 3. This observation suggests that TTF oxidation processes are adiabatic and difference in the density of states is not translated into the electrode kinetics. The charge transfer coefficient is found to be 0.50 at each electrode which indicates that $\text{TTF}^{0/\bullet+}$ and $\text{TTF}^{\bullet+/2+}$ processes are outer-sphere electron transfer processes.

Table 3. Parameters used to simulate the consecutive oxidation of TTF to $\text{TTF}^{\bullet+}$ and $\text{TTF}^{\bullet+}$ to TTF^{2+} .

Electrode	C (mM)	R_u (ohm)	$C_{dl} (c_0, c_1, c_2)$ ($\mu\text{F cm}^{-2}$)	$\text{TTF}^{0/\bullet+}$			$\text{TTF}^{\bullet+/2+}$		
				k^0 (cm s^{-1})	E^0 (V)	α	k^0 (cm s^{-1})	E^0 (V)	α
GC	1.0	510	10.0, 0.0, 5.5	1.0	-0.074	0.5	0.4	0.311	0.5
Pt	1.0	510	11, 0.0, 1.55	1.0	-0.074	0.5	0.32	0.311	0.5
BDD	1.0	560	4.0, 0.55, 0.00	1.0	-0.074	0.5	0.4	0.311	0.5

^[a] $A_{GC} = 0.019 \text{ cm}^2$, $A_{Pt} = 0.00785 \text{ cm}^2$, $f = 233 \text{ Hz}$, $\Delta E = 80 \text{ mV}$, $D_{TTF} = 2.1 \times 10^{-5} \text{ cm}^2 \text{ s}^{-1}$, $D_{TTF}^{\bullet+} = 2.0 \times 10^{-5} \text{ cm}^2 \text{ s}^{-1}$, $D_{TTF}^{2+} = 1.6 \times 10^{-5} \text{ cm}^2 \text{ s}^{-1}$, E^0 (V) vs. $\text{Fc}^{0/+}$ and $T = 293 \text{ K}$

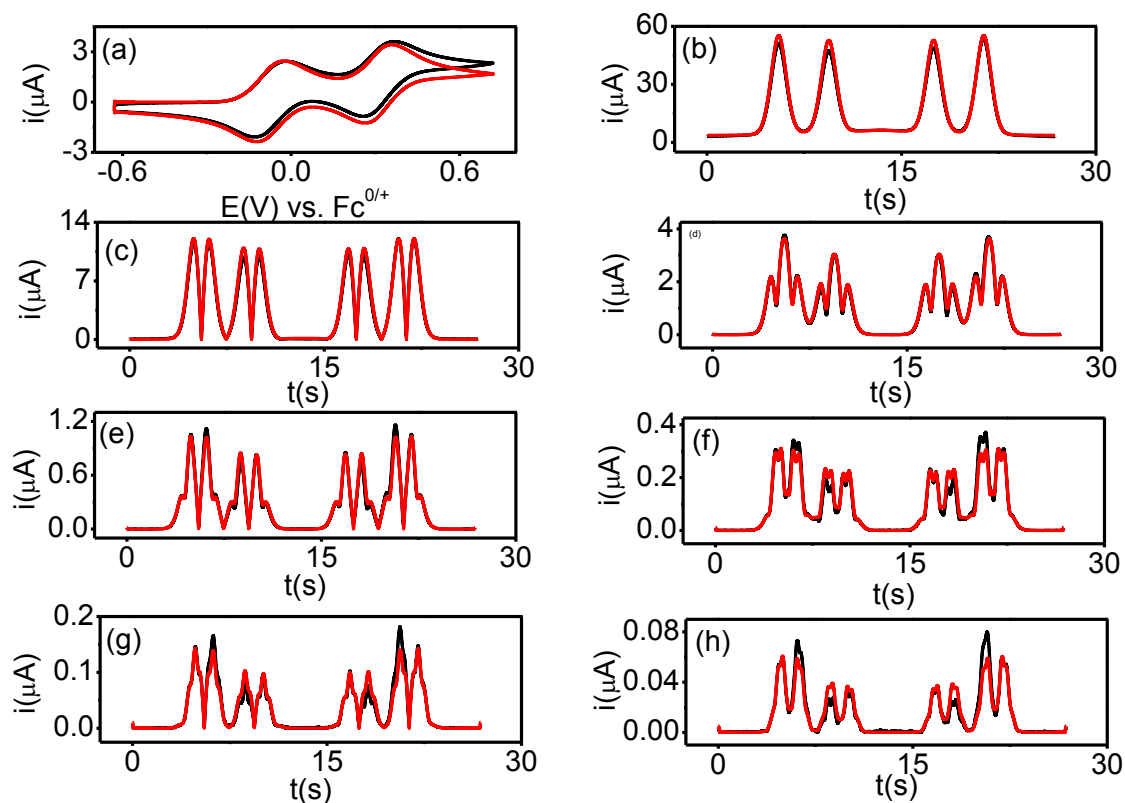


Figure 7. Comparison of simulated (—) and experimental (—) Large amplitude FT AC voltammograms obtained for the one-electron oxidation of 1.0 mM TTF in acetonitrile (0.1 M Bu_4NPF_6) at a BDD electrode (a) DC component (b-g) 1st – 6th harmonic, Other parameters are as defined in the Table 3.

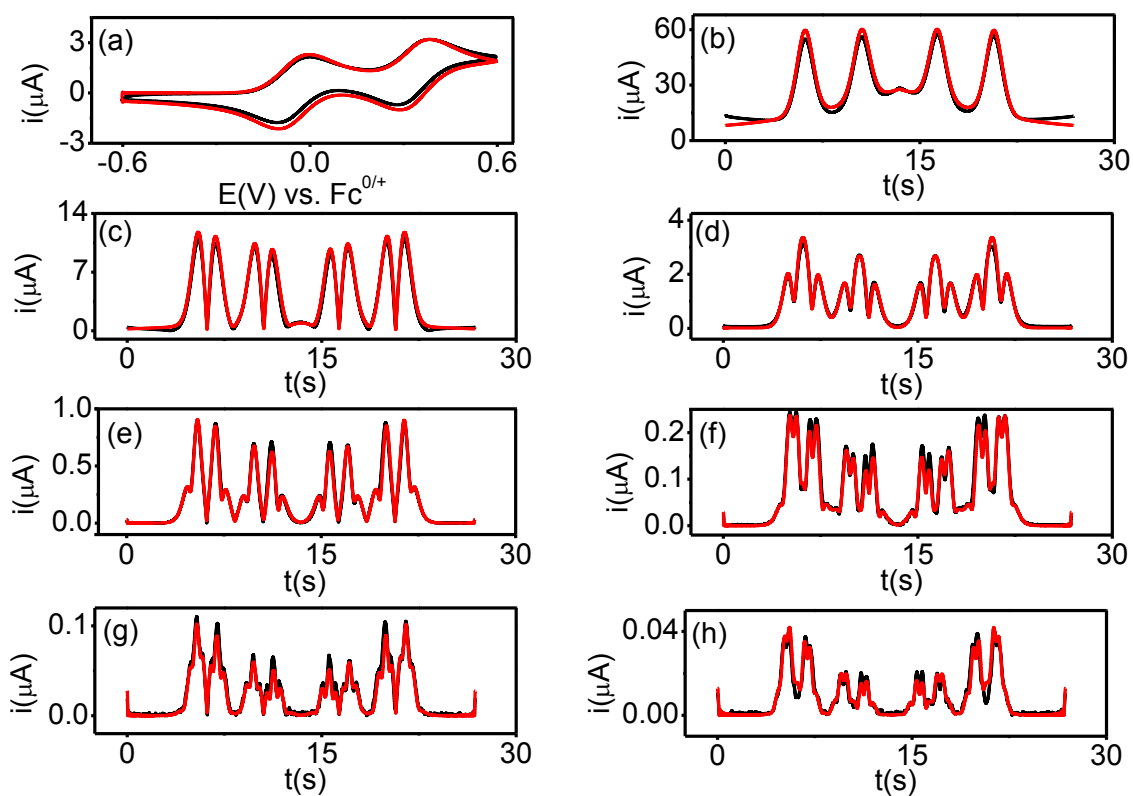


Figure 8: Comparison of simulated (—) and experimental (—) Large amplitude FT AC voltammograms obtained for the two-electron $\text{TTF}^{0/+2+}$ oxidation of 1.0 mM TTF in acetonitrile (0.1 M Bu_4NPF_6) at a GC electrode (a) DC component (b-g) 1st - 6th harmonics. Other parameters are as defined in the text.

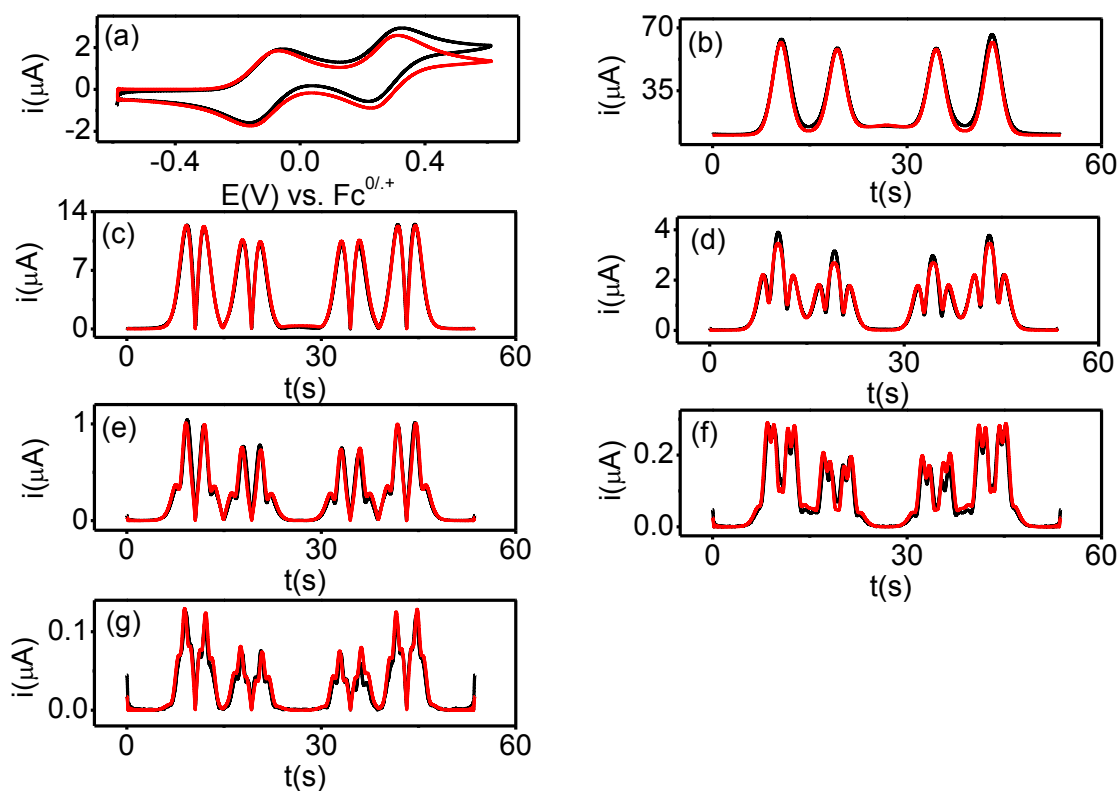


Figure 9: Comparison of simulated (—) and experimental (—) Large amplitude FT AC voltammograms obtained for the two-electron TTF^{0/+2+} oxidation of 1.0 mM TTF in acetonitrile (0.1 M Bu₄NPF₆) at a Pt electrode (a) DC component (b-g) 1st - 6th harmonics

8.3.3. Heterogeneous electron transfer kinetics of $\text{TTF}^{\bullet+}$

As electrode kinetics are also dependent on the reactant's charge,⁴³ further experiments have been conducted with $\text{TTF}^{\bullet+}$ rather than TTF or TTF^{2+} in the bulk solution that is positively charged species and is generated from bulk electrolysis of TTF by the method described elsewhere.⁴ Moreover uncertainties associated with C , D and A are essentially the same for studying $\text{TTF}^{\bullet+/2+}$ and $\text{TTF}^{\bullet+/0}$ processes so both redox processes can be well understood.

At first, the k^0 value related to the reduction of 0.1 mM $\text{TTF}^{\bullet+}$ at Au electrode is investigated by simulation of the experimental data obtained by using a sine wave with $\Delta E = 80$ mV and $f = 233.0$ Hz superimposed onto the DC ramp. Primarily, fully reversible k^0 for $\text{TTF}^{\bullet+/0}$ process was used to reassure the C and D values for DC components; simulations were then extended to fit various AC harmonics by varying the values of R_u , k^0 , and C_{dl} (double layer capacitance), the value of $E_{\text{TTF}^{\bullet+/0}}^0 = -0.074$ V vs. $\text{Fc}^{0/+}$ is estimated experimentally from the potential of minimum current between the two peaks in the second harmonic. The C_{dl} value as estimated from non-faradaic components of fundamental harmonic can be described in terms of nonlinear capacitive terms C_{dl} ($c_0 = 14.00$, $c_1 = 4.00$ and $c_2 = 4.00$) $\mu\text{F cm}^{-2}$. k^0 value has been assessed from “best” fits of simulated and experimental data derived from the higher harmonic components which are more sensitive to variation in kinetics. Excellent agreement is achieved between simulation and experiment (Figure 10) with $k^0 = 1.5 \text{ cm s}^{-1}$, $\alpha = 0.50$ and other experimental and simulation parameters described in Table 4

Voltammetric data for the oxidation of 0.1 mM $\text{TTF}^{\bullet+}$ at Au electrode is then subjected to the simulation using same theory experiment comparison methodology described above. For $\text{TTF}^{\bullet+/2+}$ process $E_{\text{TTF}^{\bullet+/2+}}^0 = 0.311$ V vs. $\text{Fc}^{0/+}$ derived from 2nd harmonic has been computed in the simulation to reassure the C and D . Nonlinear capacitive terms are anticipated as C_{dl} ($c_0 = 17.50$, $c_1 = 0.70$ and $c_2 = 0.70$) $\mu\text{F cm}^{-2}$ from fundamental harmonic. From higher AC

harmonics, electrode kinetics of $\text{TTF}^{\bullet+/2+}$ process appears to be quasi-reversible with $k^0 = 0.36 \text{ cm s}^{-1}$ and $\alpha = 0.50$ as compared to the $\text{TTF}^{\bullet+/0}$ process. A good fit of experimental data is obtained as shown in Figure 11; while $R_u = 265 \text{ ohm}$ is used along with other simulation parameters given in Table 4 for estimating k^0 value for $\text{TTF}^{\bullet+/2+}$ process.

From the initial observations, k^0 for $\text{TTF}^{\bullet+/2+}$ process is significantly slow as compared to $\text{TTF}^{\bullet+/2+}$ process and well calculable by large amplitude FT AC voltammetry. Simulation results (Table 4) of AC voltammetric studies at higher (1.0 M $\text{TTF}^{\bullet+}$) concentration further endorse the conclusions from previous section (6.3.2.). $\text{TTF}^{\bullet+/0}$ process, which in principle has a k^0 value of about 1.0 cm s^{-1} is very close to a value that produces reversible behavior and relatively low kinetics $k^0 \sim 0.3 \text{ cm s}^{-1}$ is revealed for $\text{TTF}^{\bullet+/2+}$ process. Kinetics values obtained above are in excellent agreement with previously reported values for $\text{TTF}^{\bullet+/0}$ process at GC and Pt electrodes⁴⁴. The effect of the electronic density of states could not be observed in this case as well.

Table 4: Parameters for the simulation of $\text{TTF}^{\bullet+}$ redox processes in MeCN (0.1M Bu_4NPF_6) at Au electrode; electrode kinetics estimation of $\text{TTF}^{\bullet+/2+}$ and $\text{TTF}^{\bullet+/0}$ processes, compared with the literature values obtained at GC and Pt electrode

<i>C</i> (mM)	Redox process	<i>R_u</i> (ohm)	<i>C_{dl}</i> (<i>c</i> ₀ , <i>c</i> ₁ , <i>c</i> ₂) ($\mu\text{F cm}^{-2}$)	α	<i>k</i> ⁰ at Au (cm s^{-1})	<i>k</i> ⁰ at Pt ^a (cm s^{-1})	<i>k</i> ⁰ at GC ^a (cm s^{-1})
0.1 mM	$\text{TTF}^{\bullet+/0}$	265	14.00, 4.00, 4.00	0.50	1.50	1.00	1.00
	$\text{TTF}^{\bullet+/2+}$	265	17.50, 0.70, 0.70	0.50	0.36	0.35	0.36
1.0 mM	$\text{TTF}^{\bullet+/0}$	320	15.50, 0.00, 0.00	0.50	1.00	1.00	1.00
	$\text{TTF}^{\bullet+/2+}$	320	15.00, 1.00, 0.00	0.50	0.30	0.35	0.36

$A = 0.019 \text{ cm}^2$, $f = 233 \text{ Hz}$, $\Delta E = 80 \text{ mV}$, $D_{\text{TTF}} = 2.1 \times 10^{-5} \text{ cm}^2 \text{ s}^{-1}$, $D_{\text{TTF}^{\bullet+}} = 2.0 \times 10^{-5} \text{ cm}^2 \text{ s}^{-1}$, $D_{\text{TTF}^{2+}} = 1.6 \times 10^{-5} \text{ cm}^2 \text{ s}^{-1}$, $E_{\text{TTF}^{\bullet+/0}}^0 = -0.074 \text{ V}$, $E_{\text{TTF}^{\bullet+/2+}}^0 = 0.311 \text{ V}$ vs. $\text{Fc}^{0/+}$ T = 293 K and a = Reference⁴⁴.

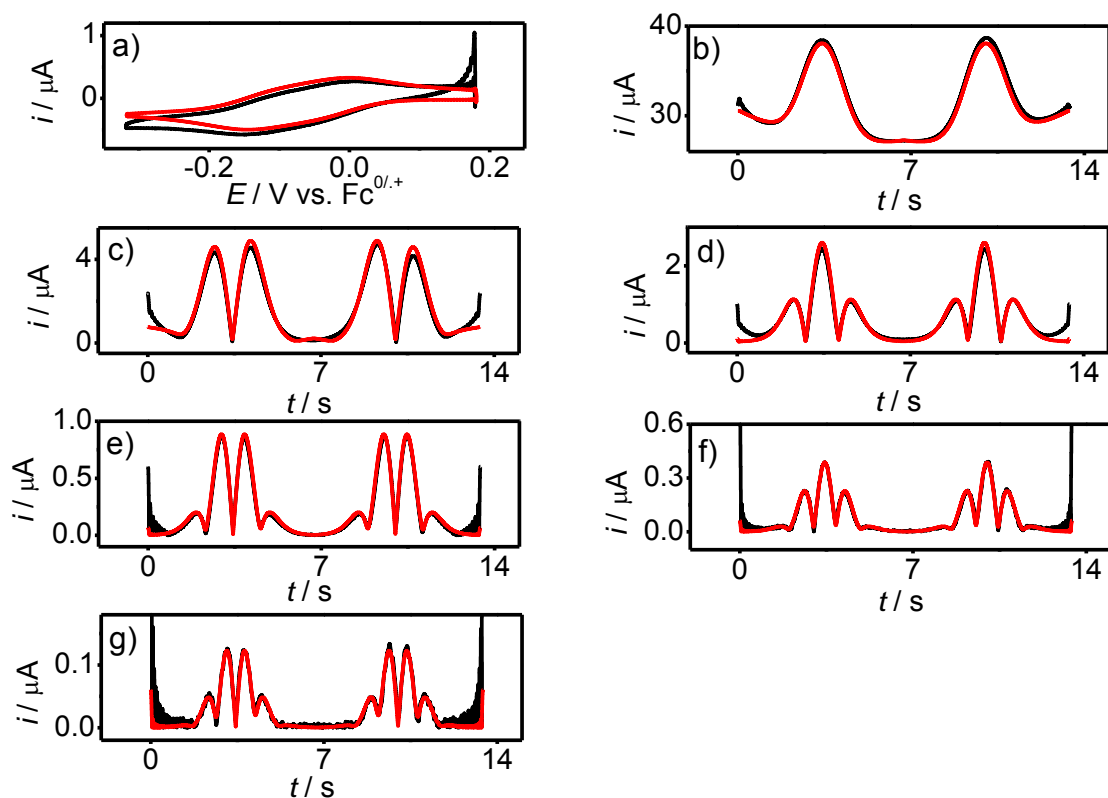


Figure 10: Comparison of simulated (—) and experimental (—) Large amplitude FT AC voltammograms for $\text{TTF}^{\bullet+/0}$ process obtained from the reduction of 0.1 mM $\text{TTF}^{\bullet+}$ in acetonitrile (0.1 M Bu_4NPF_6) at Au electrode (a) aperiodic DC component (b-g) 1st - 6th harmonics; $v_{\text{DC}} = 0.0789 \text{ V s}^{-1}$; simulation and other experimental parameters are described in Table 4.

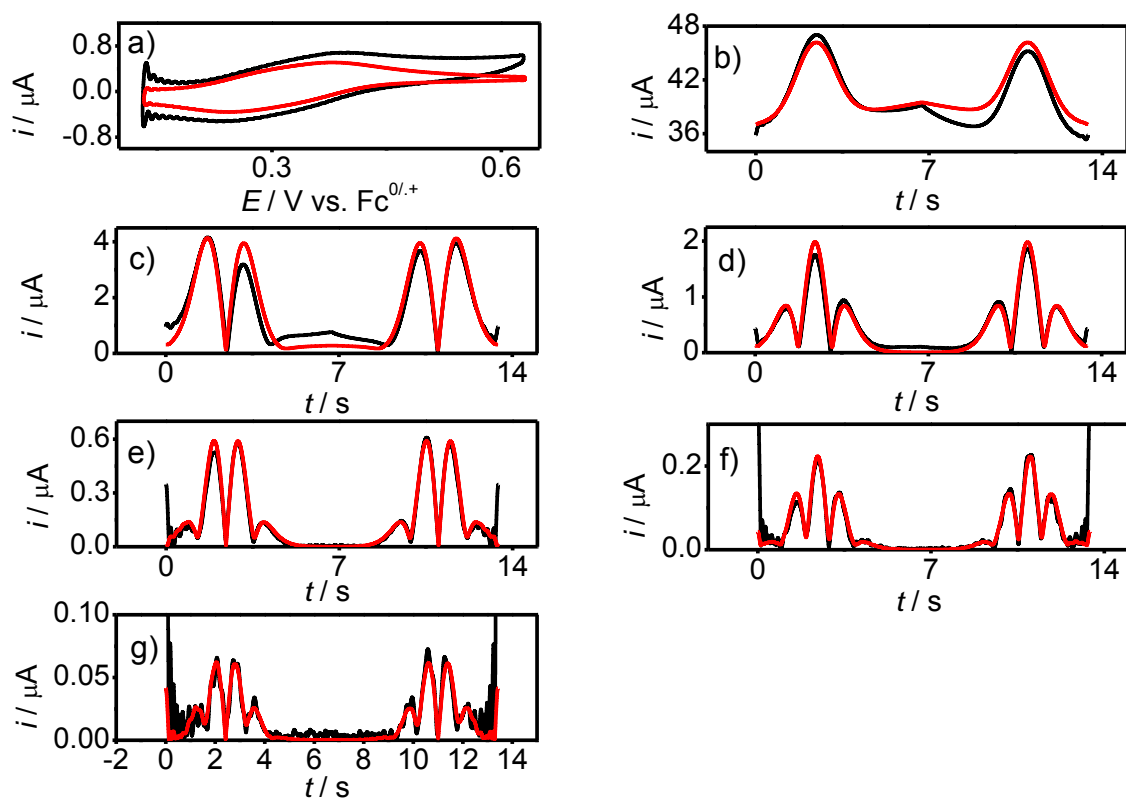
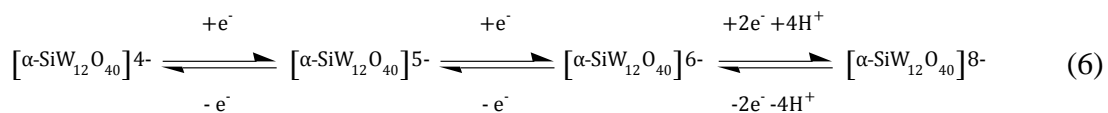


Figure 11: Comparison of simulated (—) and experimental (—) Large amplitude FT AC voltammograms for $\text{TTF}^{\bullet+}/2+$ process obtained from the oxidation of 0.1 mM $\text{TTF}^{\bullet+}$ in acetonitrile (0.1 M Bu_4NPF_6) at Au electrode (a) aperiodic DC component (b-g) 1st - 6th harmonics; $v_{\text{DC}} = 0.07749 \text{ V s}^{-1}$; simulation and other experimental parameters as described in Table 4.

8.3.4. Heterogeneous electron transfer kinetics of silicotungstate

Voltammetric study is then extended to a commonly used polyoxometallate $[\alpha\text{-SiW}_{12}\text{O}_{40}]^{4-}$ in 0.1M $\text{H}_2\text{SO}_4 + 1.0 \text{ M Na}_2\text{SO}_4$. High electrolyte concentration provides a situation which suppresses the Frumkin double layer effect.⁴⁵ $[\alpha\text{-SiW}_{12}\text{O}_{40}]^{4-}$ undergoes three reduction processes in 0.1M $\text{H}_2\text{SO}_4 + 1.0 \text{ M Na}_2\text{SO}_4$; DC voltammograms shown in Figure 12 consist of three processes. First and the second corresponding to the $[\alpha\text{-SiW}_{12}\text{O}_{40}]^{4-/5-}$ and $[\alpha\text{-SiW}_{12}\text{O}_{40}]^{5-/6-}$ processes, whereas the third has a significantly larger current and corresponds to proton coupled two-electron reaction as reported previously and shown in eq. 6.^{46,47}



The diffusion coefficient of $[\alpha\text{-SiW}_{12}\text{O}_{40}]^{4-}$ ($D = 2.76 \times 10^{-6} \text{ cm}^2 \text{ s}^{-1}$) as calculated from the peak current of first reduction process $[\alpha\text{-SiW}_{12}\text{O}_{40}]^{4-/5-}$ (Figure 12) at GC electrode using Randles-Sevcik equation is used in simulations. In this study we focus on the first two reduction processes that are very close to the reversible limit and don't involve any complex chemical reaction.

Initially, AC voltammetric data of 1.0 mM $[\alpha\text{-SiW}_{12}\text{O}_{40}]^{4-}$ in 0.1 M $\text{H}_2\text{SO}_4 + 1.0 \text{ M Na}_2\text{SO}_4$ obtained for $[\alpha\text{-SiW}_{12}\text{O}_{40}]^{4-/5-}$ process is used for simulation to extract the electrode kinetics parameters at GC, BDD and Au electrodes.

At first, AC voltammetric data for the reduction of $[\alpha\text{-SiW}_{12}\text{O}_{40}]^{4-}$ in 0.1 M $\text{H}_2\text{SO}_4 + 1.0 \text{ M Na}_2\text{SO}_4$ at BDD electrode is simulated. Highly non-linear capacitance C_{dl} ($c_0 = 22$, $c_1 = 35$ and $c_2 = 80$) $\mu\text{F cm}^{-2}$ is observed for the $[\alpha\text{-SiW}_{12}\text{O}_{40}]^{4-/5-}$ process. Experimentally determined $R_u = 80 \text{ ohm}$ is used to extract the k^0 value of 0.04 cm s^{-1} from and $\alpha = 0.50$ indicates that electron transfer is an outer-sphere reaction at BDD electrode. A similar exercise is extended

over the potential range where two consecutive reduction processes are simultaneously present. Simulations are then extended to extract the electrode kinetic parameters for the $[\alpha\text{-SiW}_{12}\text{O}_{40}]^{4-/5-}$ and $[\alpha\text{-SiW}_{12}\text{O}_{40}]^{5-/6-}$ processes from their respective reduction peaks in AC voltammogram showing $[\alpha\text{-SiW}_{12}\text{O}_{40}]^{4-/5-/6-}$ reduction process. After the initial confirmation of D and C from DC component, the capacitance is then estimated as C_{dl} ($c_0 = 15.0, c_1 = 10.0$ and $c_2 = 45.0$) $\mu\text{F cm}^{-2}$ from the background capacitance current of fundamental harmonic. Kinetic parameter k^0 for $[\alpha\text{-SiW}_{12}\text{O}_{40}]^{4-/5-}$ is found to be 0.05 cm s^{-1} , same as obtained in the case when it was measured alone for this process. The k^0 value for $[\alpha\text{-SiW}_{12}\text{O}_{40}]^{5-/6-}$ process is found to be 0.068 cm s^{-1} from second reduction peak, comparison of theory with experimental data is shown in Figure 13

As compared to the BDD electrode, kinetics studies for studies $[\alpha\text{-SiW}_{12}\text{O}_{40}]^{4-/5-}$ and $[\alpha\text{-SiW}_{12}\text{O}_{40}]^{5-/6-}$ processes on GC and Au electrodes shows close to the reversible behaviour for the $[\alpha\text{-SiW}_{12}\text{O}_{40}]^{4-/5-}$ and $[\alpha\text{-SiW}_{12}\text{O}_{40}]^{5-/6-}$ processes. At these electrodes E^{0i} s found to be less negative as compared to that on BDD and $\alpha = 0.50$ is characteristic of outer-sphere electron transfer. Electrode kinetics parameters at each electrode are shown in Table 4 and 5 along with other simulation and experimental parameters. Comparison of experimental and theoretical data at GC and Au electrode is given in Figures 14- 17.

Table 5: Simulation and experimental parameters for the $[\alpha\text{-SiW}_{12}\text{O}_{40}]^{4-/5-}$ process in 0.1M $\text{H}_2\text{SO}_4 + 1.0 \text{ M Na}_2\text{SO}_4$

Electrode	C	R_u	$C_{dl} (c_0, c_1, c_2)$	k^0	E^0	A
	(mM)	(ohm)	$\mu\text{F cm}^{-2}$	cm s^{-1}	V	
BDD	1.00	80	22.0, 35.0, 80.0	0.045	-0.146	0.5
	0.23	120	28.0, 7.0, 25.0	0.045	-0.146	0.5
GC	1.00	120	22.0, 35.0, 80.0	≥ 2.0	-0.139	0.50
	0.23	120	22.0, 7.0, 25.0	≥ 2.0	-0.139	0.50
Au	1.00	120	75.0, 35.0, 56.0	≥ 2.0	-0.138	0.50
	0.23	120	70.0, 0.0, 30.0	≥ 2.0	-0.138	0.50

^[a] $A_{Au} = 0.019 \text{ cm}^2$, $A_{GC} = A_{BDD} = 0.00785 \text{ cm}^2$, $f = 9.0 \text{ Hz}$, $\Delta E = 80 \text{ mV}$, $D = 2.76 \times 10^{-6} \text{ cm}^2 \text{ s}^{-1}$, and $T = 293 \text{ K}$

Table 6. Simulation and parameters for the $[\alpha\text{-SiW}_{12}\text{O}_{40}]^{4-/5-/6-}$ process in 0.1M $\text{H}_2\text{SO}_4 + 1.0 \text{ M Na}_2\text{SO}_4$

Electrode	C	R_u	$C_{dl} (c_0, c_1, c_2)$	$[\alpha\text{-SiW}_{12}\text{O}_{40}]^{4-/5-}$			$[\alpha\text{-SiW}_{12}\text{O}_{40}]^{5-/6-}$		
				k^0	E^0	α	k^0	E^0	α
	(mM)	(ohm)	($\mu\text{F cm}^{-2}$)	(cm s^{-1})	(V)		(cm s^{-1})	(V)	
BDD	1.0	80	15.0, 10.0, 45.0	0.04	-0.146	0.50	0.06	-0.401	0.50
	0.23	120	11.0, 0.0, 25.0	0.048	-0.146	0.50	0.055	-0.401	0.50
GC	1.0	120	20.0, 10.0, 65.0	≥ 2.0	-0.139	0.50	≥ 2.0	-0.392	0.5
	0.23	120	30.0, 0.00, 45.0	≥ 2.0	-0.139	0.50	≥ 2.0	-0.392	0.5

^[a] $A_{GC} = A_{BDD} = 0.00785 \text{ cm}^2$, $f = 9.0 \text{ Hz}$, $\Delta E = 80 \text{ mV}$, $D = 2.76 \times 10^{-6} \text{ cm}^2 \text{ s}^{-1}$, and $T = 293 \text{ K}$

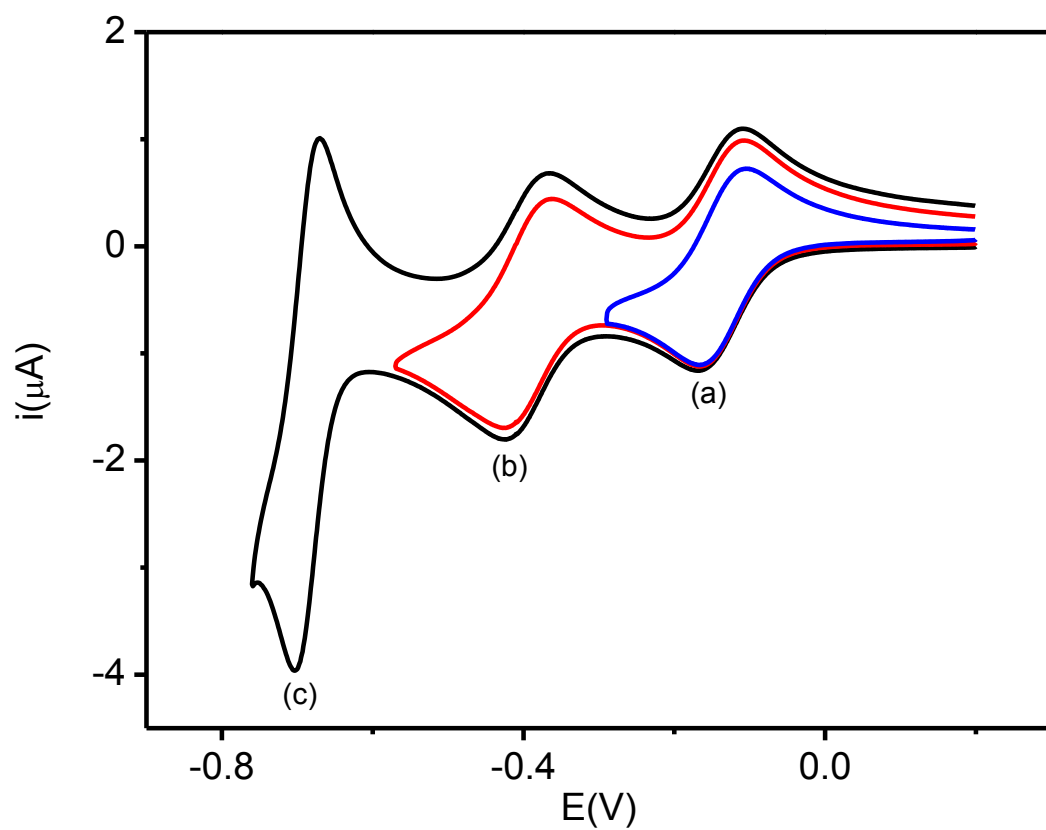


Figure 12: DC voltammograms obtained for the reduction of 1.0 mM $(\alpha\text{-SiW}_{12}\text{O}_{40})^{4-}$ in (0.1 M H_2SO_4 + 1.0 M Na_2SO_4) at a 1.0 mm GC electrode with different switching potentials 0.75 V (—), 0.50 V (—) and 0.3 V (—) at a scan rate $\nu_{\text{DC}} = 0.1 \text{ V s}^{-1}$,

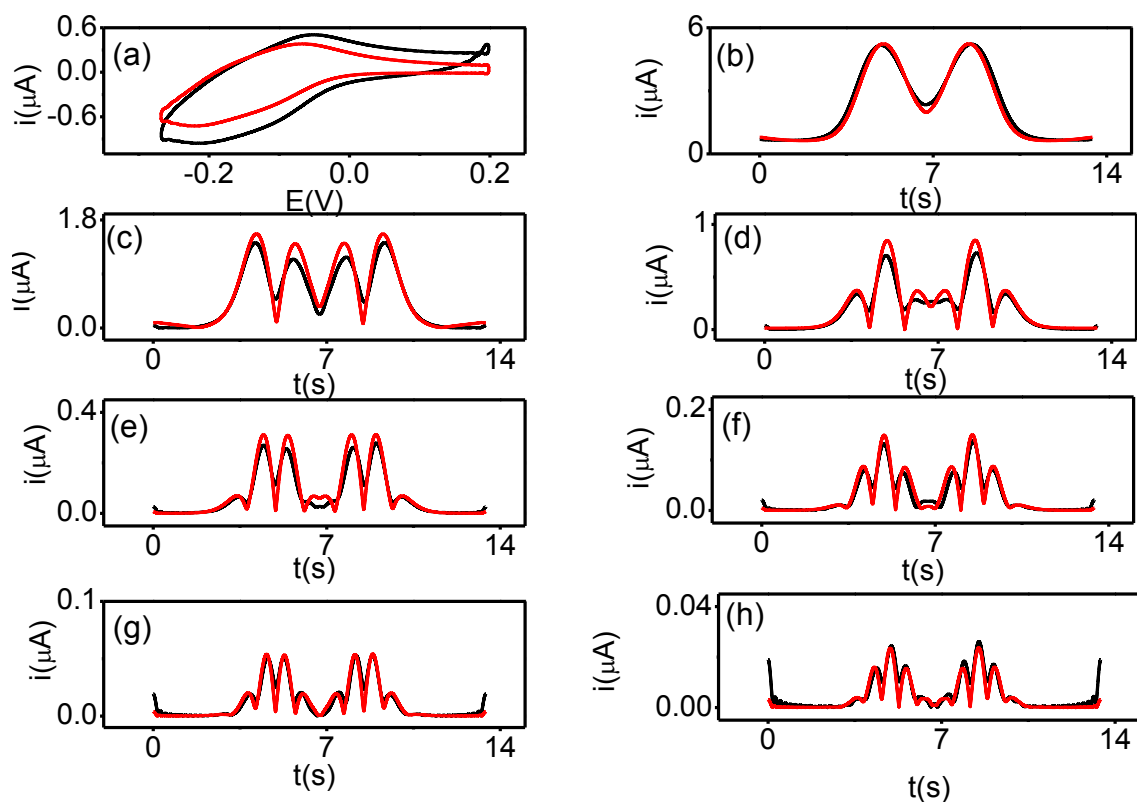


Figure 13. Comparison of simulated (—) and experimental (—) large amplitude FT AC voltammograms obtained for the one-electron reduction of 1.0 mM $(\text{SiW}_{12}\text{O}_{40})^{4-}$ in 0.1 M $\text{H}_2\text{SO}_4 + 1.0$ M Na_2SO_4 at a BDD electrode (a) DC component (b-h) 1st -7th harmonics, Other parameters are as defined in the Table 5.

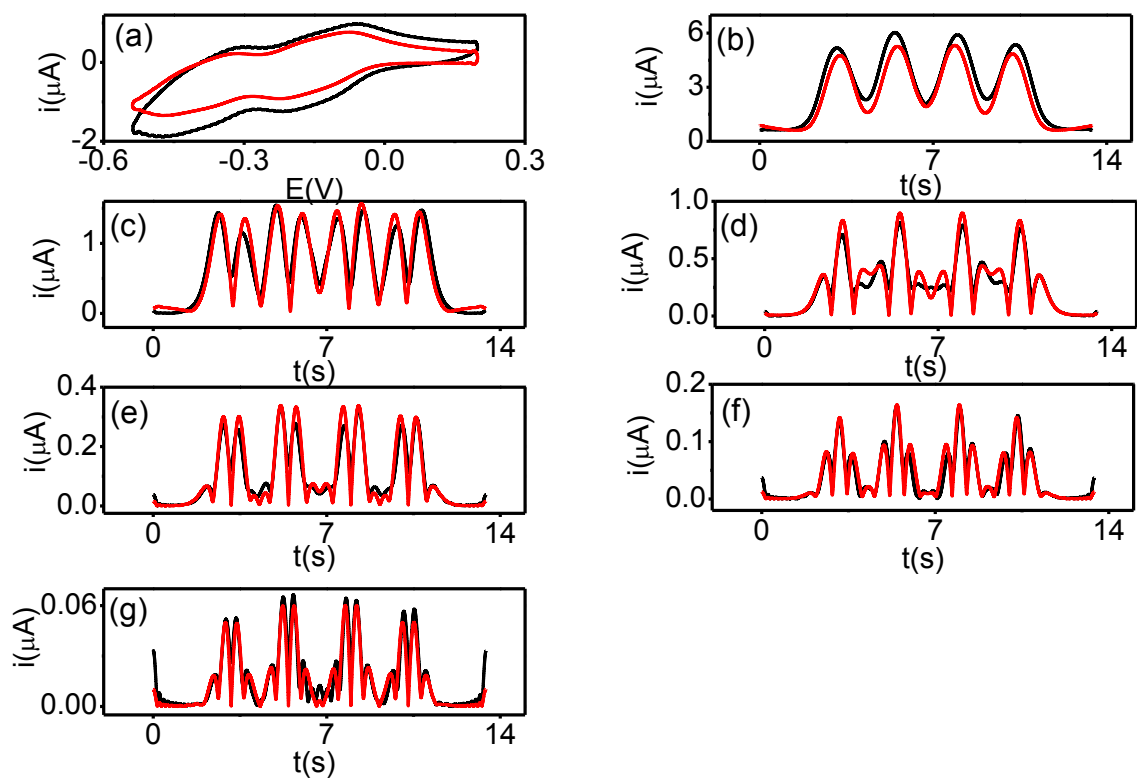


Figure 14: Comparison of simulated (—) and experimental (—) large amplitude FT AC voltammograms obtained for the two electron reduction 1.0 mM $(\alpha\text{-SiW}_{12}\text{O}_{40})^{4-}$ in (0.1 M H_2SO_4 + 1.0 M Na_2SO_4) at a GC electrode (a) DC component (b-g) 1st - 6th harmonics; Other parameters are as defined in the Table 6

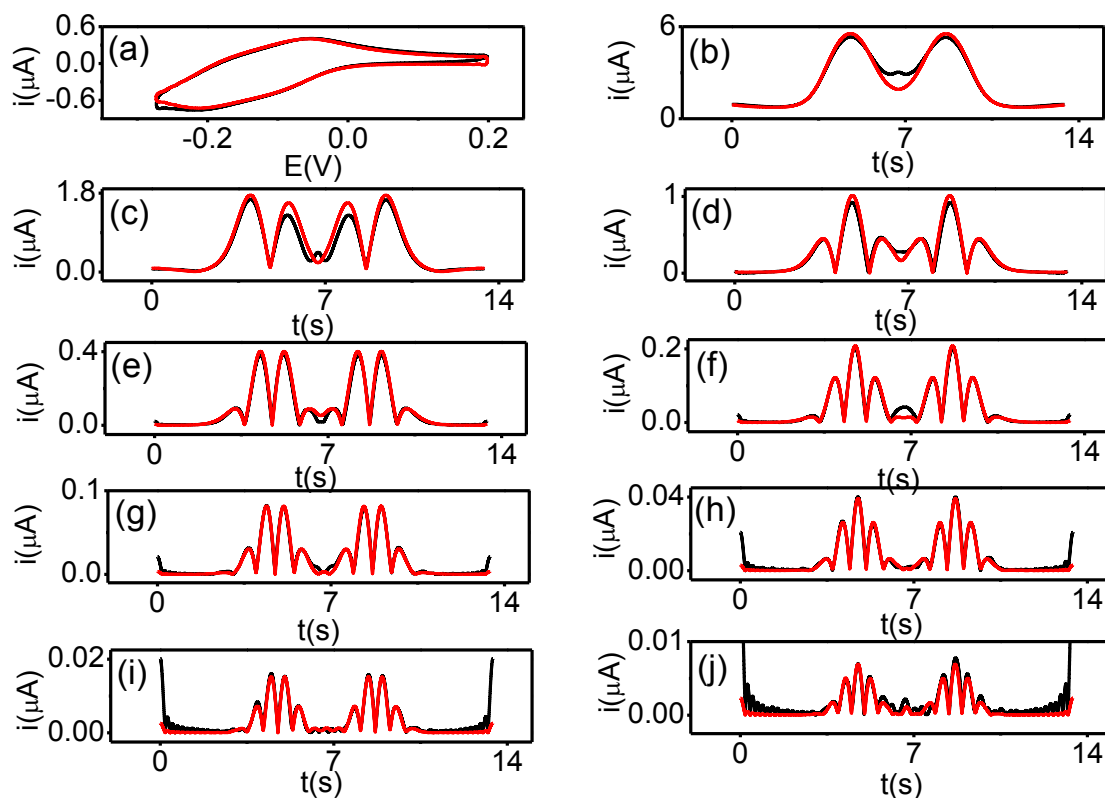


Figure 15: Comparison of simulated (—) and experimental (—) large amplitude FT AC voltammograms obtained for the of 1.0 mM $(\text{SiW}_{12}\text{O}_{40})^{4-}$ in (0.1 M H_2SO_4 + 1.0 M Na_2SO_4) at a GC electrode (a) DC component (b-J) 1st - 9th harmonics; Other parameters are as defined in the Table 5

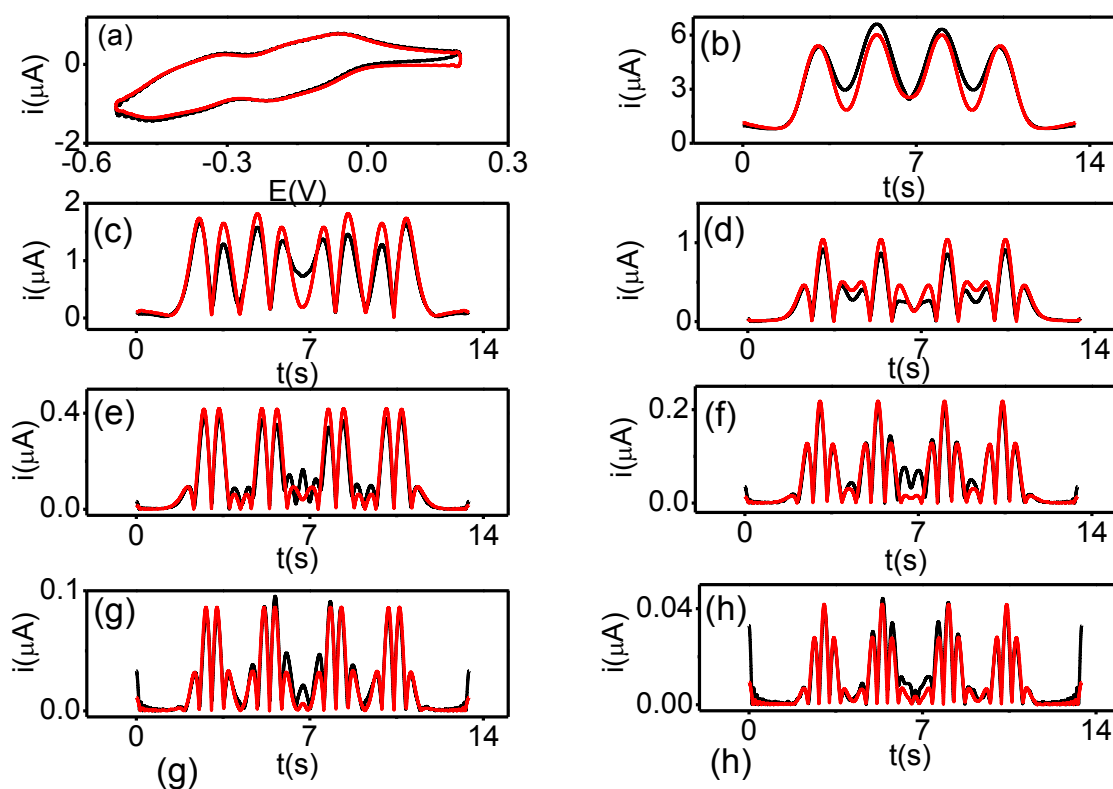


Figure 16: Comparison of simulated (—) and experimental (—) large amplitude FT AC voltammograms obtained for the of two electron reduction 1.0 mM $(\text{SiW}_{12}\text{O}_{40})^{4-}$ in (0.1 M H_2SO_4 + 1.0 M Na_2SO_4) at a GC electrode (a) DC component (b-h) 1st - 7th harmonics ; Other parameters are as defined in the Table 6

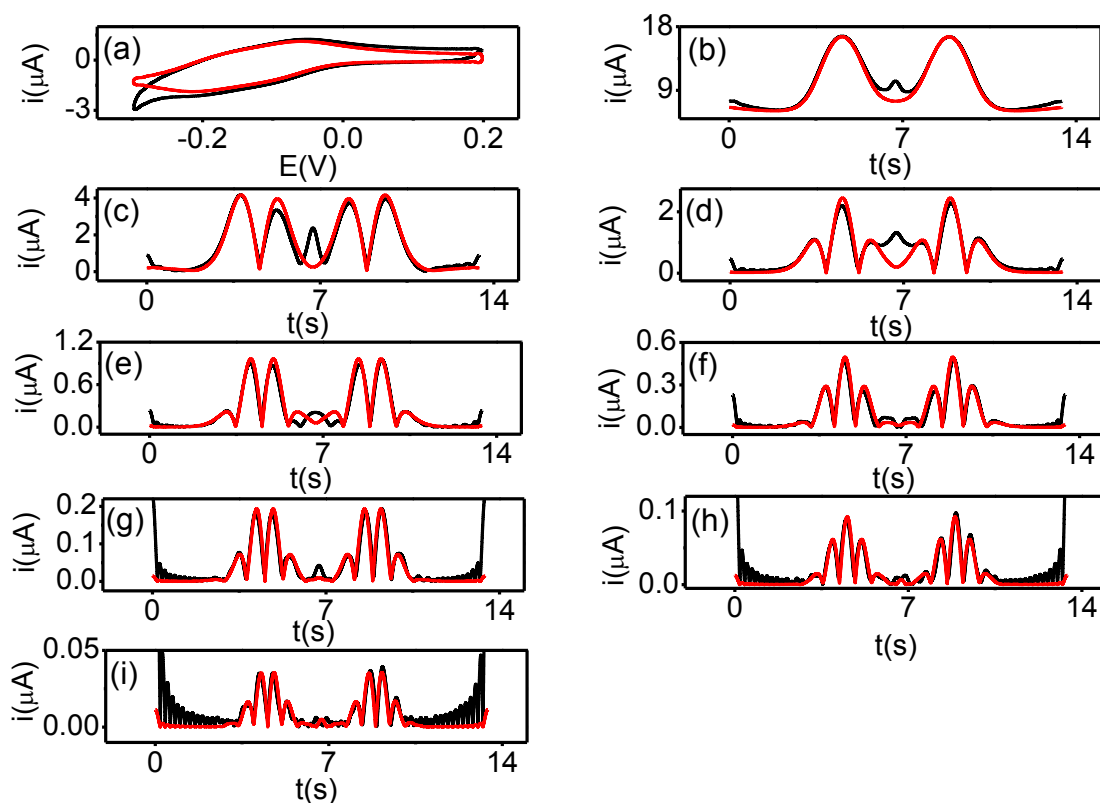


Figure 17: Comparison of simulated (—) and experimental (—) large amplitude FT AC voltammograms obtained for the of 1.0 mM $(\alpha\text{-SiW}_{12}\text{O}_{40})^{4-}$ in (0.1 M H_2SO_4 + 1.0 M Na_2SO_4) at a Au electrode (a) DC component (b-i) 1st - 8th harmonics; Other parameters are as defined in the Table 5.

8.4. Discussion

In this study, redox systems with E^0 over a range of potential are selected. The $[\text{Ru}(\text{NH}_3)_6]^{3+/2+}$ reaction is an outer-sphere electron transfer process¹ and is known to have an electrode kinetics value close to the reversible limit on a variety of metal electrodes⁴⁸ and carbon nanotubes.⁷ The electrode kinetics at GC and metal electrodes is observed to be very fast as compared to those obtained at other carbon electrodes. GC electrode behaves more like a metal electrode in the presence of abundant surface functional groups³⁶ so when compared with other metal electrodes, redox processes studied in this chapter appear to be adiabatic. Results obtained for the reduction of $[\text{Ru}(\text{NH}_3)_6]^{3+}$ in 1.0 M KCl show that the k^0 values are consistent with those obtained at BDD and CNTs by SECCM studies.^{7,49,50} The reversible potential of $[\text{Ru}(\text{NH}_3)_6]^{3+/2+}$ process is known to lie in the band gap region so it leads to slower kinetics at BDD. However, for the $\text{TTF}^{*+}/2+$ process, the kinetics are found to be independent of the electrode material. $[\text{Ru}(\text{NH}_3)_6]^{3+}$ and TTF^{*+} are charged species to be studied and contribution from surface functional groups at carbon electrodes cannot be ignored as they can catalyze or inhibit the electron transfer processes. Kinetics results obtained for the TCNQ (neutral species) are therefore compared to above two examples. In this case, k^0 value at BDD are comparable to those obtained at GC and Pt. Although, if the effect of surface functional groups is expected, it should catalyze one redox process and inhibit the other (i.e. TCNQ , $\text{TCNQ}^{\cdot-}$ or TTF^{*+}). From these outer-sphere reactions, k^0 is essentially independent of the electrode; these results raise further issues about the controlling factors in the electrode kinetics determination at BDD. For carbon electrodes, kinetics may depend on surface functional groups, electrode DOS and activation energies of redox couples. This type of behavior cannot be explained in terms of Dogonadze theory where the DOS of carbon electrode is more important. Such type of reactions are usually described by Hush theory that assumes stronger interactions between electrode and redox couples and their

reaction rates are affected by activation energies of redox couples, reorganization energies of solvent in the vicinity of the electrodes and molecular properties of the system.³

However in these standard examples, neither double layer corrections nor work terms are considered. Electrode kinetic data obtained for the reduction of $[\alpha\text{-SiW}_{12}\text{O}_{40}]^{4-}$ studied high electrolyte concentration has a minimum contribution of the work terms for transfer of ions into Frumkin double layer. In this case the most dominant factor affecting the electrode kinetics may be the density of states. Redox potential of negatively charged $[\alpha\text{-SiW}_{12}\text{O}_{40}]^{4-}$ and positively charged $[\text{Ru}(\text{NH}_3)_6]^{3+}$ both lie very close and so should be on the same side of the band gap region at BDD. Thus, if a double layer effect⁵¹ is influencing the electrode kinetics parameters, it should accelerate one and retard the other. However, slower kinetics were observed at BDD electrode for both redox systems so it can be argued that the effect of density states of BDD dominates as in the case with $[\text{FcTMA}]^+$ that has slower kinetics at BDD as compared to conventional metal or GC electrode, although the reversible potential in that case is well apart from the band gap of BDD.¹⁴

This work proposes the hypothesis that the effect of the density of states influences the electrode kinetics of some redox couples, so that, the concept of adiabaticity need not necessarily be observed for many outer-sphere redox processes. Although, for some redox couples the effect of the density of states is observed.

8.5. Conclusion

Density of states effects or adiabaticity in electron transfer kinetics has been found. In some electron transfer processes, solvent properties dominate in the electron transfer process and in some cases electrode properties govern the electron transfer rates. BDD electrodes provide a key method to distinguish the two cases.

References

- (1) Bard, A. J.; Faulkner, L. R. *Electrochemical methods: Fundamentals and Applications*; John Wiley: New York, **2001**.
- (2) Marcus, R. A. *J. Chem. Phys.* **1956**, *24*, 966.
- (3) Hush, N. S. *Reactions of molecules at electrodes*; Wiley-Interscience: Chichester, **1971**.
- (4) Bond, A. M.; Bano, K.; Adeel, S.; Martin, L. L.; Zhang, J. *ChemElectrochem.* **2013**, DOI: 10.1002/CELC.201300129.
- (5) Bano, K.; Nafady, A.; Zhang, J.; Bond, A. M.; Haque, I. U. *J. Phys. Chem. C* **2011**, *115*, 24153.
- (6) Samuelson, R.; Sharp, M. *Electrochim. Acta* **1977**, *23*, 315.
- (7) Nissim, R.; Batchelor-McAuley, C.; Henstridge, M. C.; Compton, R. G. *Chem. Commun.* **2012**, *48*, 3294.
- (8) Schmickler, W. *J. Electroanal. Chem. Interfac. Electrochem.* **1986**, *204*, 31.
- (9) Forster, R. J.; Loughman, P.; Keyes, T. E. *J. Am. Chem. Soc.* **2000**, *122*, 11948.
- (10) Grado-Caffaro, M. A.; Grado-Caffaro, M. *Physica. A* **2008**, *387*, 445.
- (11) Han, K. S.; Kim, S. S.; Kang, K. H.; Mean, B. J.; Choi, H. H.; Han, O. H.; Lee, M. *Electrochem. Commun.* **2009**, *11*, 466.
- (12) Ifuku, R.; Nagashio, K.; Nishimura, T.; Toriumi, A. *Appl. Phys. Lett.* **2013**, *103*, 033514.
- (13) Lascovich, J. C.; Santoni, A. *Appl. Surf. Sci.* **1996**, *103*, 245.
- (14) Patten, H. V.; Meadows, K. E.; Hutton, L. A.; Iacobini, J. G.; Battistel, D.; McKelvey, K.; Colburn, A. W.; Newton, M. E.; Macpherson, J. V.; Unwin, P. R. *Angew. Chem. Int. Edit.* **2012**, *51*, 7002.
- (15) Paul, S. *IEEE Trans. Electron. Dev.* **2006**, *53*, 1775.

- (16) Sasaki, K.; Sato, K.; Saito, R.; Jiang, J. *Phys. Rev. B* **2007**, 75, 035405.
- (17) Kozub, B. R.; Henstridge, M. C.; Batchelor-McAuley, C.; Compton, R. G. *Int. J. Electrochem. Sci.* **2011**, 6, 6047.
- (18) Mirkin, M. V.; Richards, T. C.; Bard, A. J. *J. Phys. Chem.* **1993**, 97, 7672.
- (19) Nicholson, R. S. *Anal. Chem.* **1965**, 37, 1351.
- (20) Wightman, R. M.; Wipf, D. O. in *Electroanalytical Chemistry*; Bard, A. J., Ed.; Marcel Dekker: New York, **1989**; Vol. 15, p 267.
- (21) Cline, K. K.; McDermott, M. T.; McCreery, R. L. *J. Phys. Chem. A* **1994**, 98, 5314.
- (22) Dimov, I. B.; McAuley, C.B.; Aldous, L.; Compton, R. G. *Phys. Chem. Chem. Phys.*, **2012**, 14, 2375.
- (23) Ernst, S. A., L.; Compton, R. G. *J. Electroanal. Chem.* **2011**, 663, 108.
- (24) Alden, J. A.; Hakoura, S.; Compton, R. G. *Anal. Chem.* **1999**, 71, 806.
- (25) Booth, J.; Compton, R. G.; Cooper, J. A.; Dryfe, R. A. W.; Fisher, A. C.; Davies, C. L.; Walters, M. K. *J. Phys. Chem.* **1995**, 99, 10942.
- (26) Lai, S. C. S.; Patel, A. N.; McKelvey, K.; Unwin, P. R. *Angew. Chem. Int. Ed.* **2012**, 51, 5405.
- (27) Zhang, J.; Guo, S. X.; Bond, A. M. *Anal. Chem.* **2007**, 79, 2276.
- (28) Bano, K.; Kennedy, G. F.; Zhang, J.; Bond, A. M. *Phys. Chem. Chem. Phys.* **2012**, 14, 4742.
- (29) Sher, A. A.; Bond, A. M.; Gavaghan, D. J.; Gillow, K.; Duffy, N. W.; Guo, S. X.; Zhang, J. *Electroanal.* **2005**, 17, 1450.
- (30) Fleming, B. D.; Barlow, N. L.; Zhang, J.; Bond, A. M.; Armstrong, F. A. *Anal. Chem.* **2006**, 78, 2948.
- (31) Lee, C. Y.; Bond, A. M. *Langmuir* **2010**, 26, 16155.

- (32) Lee, C. Y.; Bullock, J. P.; Kennedy, G. F.; Bond, A. M. *J. Phys. Chem. A* **2010**, *114*, 10122.
- (33) Matthews, S. M.; Shiddiky, M. J. A.; Yunus, K.; Elton, D. M.; Duffy, N. W.; Gu, Y. F.; Fisher, A. C.; Bond, A. M. *Anal. Chem.* **2012**, *84*, 6686.
- (34) Sher, A. A.; Bond, A. M.; Gavaghan, D. J.; Harriman, K.; Feldberg, S. W.; Duffy, N. W.; Guo, S. X.; Zhang, J. *Anal. Chem.* **2004**, *76*, 6214.
- (35) Zhang, J.; Guo, S. X.; Bond, A. M.; Marken, F. *Anal. Chem.* **2004**, *76*, 3619.
- (36) Mikkelesen, S. R.; Purdy, W. C. *Electroanal.* **1989**, *1*, 235.
- (37) Melnikova, N. V.; Egorushkin, V. E.; Bobenko, N. G.; Ponomarev, A. I. *Russ. Phys. J.* **2013**, *55*, 1266.
- (38) Feldberg, S. W. *J. Electroanal. Chem.* **1981**, *127*, 1.
- (39) Mao, X. W.; Simeon, F.; Rutledge, G. C.; Hatton, T. A. *Adv. Mater.* **2013**, *25*, 1309.
- (40) Hallam, P. M.; Banks, C. E. *Electrochem. Commun.* **2011**, *13*, 8.
- (41) Safar, G. A. M.; Malachias, A.; Magalhaes-Paniago, R.; Marinho, M. V.; Stumpf, H. *J. Phys. Chem. C* **2012**, *116*, 25611.
- (42) Bano, K.; Nafady, A.; Zhang, J.; Bond, A. M. *J. Phys. Chem. C* **2011**, *115*, 24153.
- (43) Gennett, T.; Weaver, M. J. *J. Electroanal. Chem.* **1985**, *186*, 179.
- (44) Bond, A. M.; Bano, K.; Adeel, S.; Martin, L. L.; Zhang, J. *ChemElectrochem.* **2013**, DOI: 10.1002/CELC.201300129.
- (45) Frumkin, A. Z. *Physik. Chem.* **1933**, *A164*, 321.
- (46) Zhang, J.; Ting, B. P.; Koh, Y. T.; Ying, J. Y. *Chem. Mater.* **2011**, *23*, 4688.
- (47) Zhang, J. G., J. K.; Tan, W. T.; Bond, A. M. *Inorg. Chem.* **2006**, *45*, 3732.
- (48) Fathalian, A. *Semiconduct.* **2012**, *46*, 769.

- (49) Zhang, Z. H.; Peng, J. C.; Chen, X. H.; Wang, J. X. *J. Mater. Sci. Technol.* **2003**, *19*, 110.
- (50) Hallam, P. M.; Banks, C. E. *Electrochem. Commun.* **2011**, *13*, 8.
- (51) Frumkin, A. *Adv. Electrochem. Electrochem. Eng.* **1961**, *1*, 65.

CHAPTER 9

CONCLUSIONS AND FUTURE WORKS

CHAPTER 9

CONCLUSIONS AND FUTURE WORKS

9.1. Conclusions

The main conclusion of the thesis is that large amplitude FT AC voltammetry can be utilized to determine the electron transfer kinetics of fast processes. Low frequency (9.0 Hz) large amplitude FT AC voltammetry at stationary macrodisk electrode can be used to measure the electrode kinetics parameter up to 0.5 cm s^{-1} when the D value is of the order of $10^{-5} \text{ cm}^2 \text{ s}^{-1}$ and upper limit of measurement in aqueous media is 2.0 cm s^{-1} provided that the resistance was accurately measured and capacitance is modelled well within the simulation. The use of kinetically sensitive higher harmonics of large amplitude FT AC cyclic voltammetry for the determination of electrode kinetics associated with $\text{TCNQ}^{0/\bullet-}$ and $\text{TCNQ}^{\bullet-/2-}$ processes in acetonitrile produce an estimate of k^0 values of about $0.30 \pm 0.05 \text{ cm s}^{-1}$ at both GC and Pt electrodes. This electrode independence is consistent with TCNQ electron transfer processes being fully adiabatic, although since the kinetic evaluation occurs very near to the limit of the ability to distinguish from a reversible process, the absolute values contain significant uncertainty arising from systematic error.

Large amplitude FT AC voltammetric method of rotating disk electrodes was also introduced that can resolve the voltammograms into DC and AC harmonic components; the hydrodynamics can be analyzed from the DC component and flow rate independent higher harmonics provides the kinetics information. Thus, all parameters related to mass transport and electrode kinetics are available from a single experiment. The theory of the technique has been described and applied to analysis of the reversible $[\text{Ru}(\text{NH}_3)_6]^{3+/2+}$ and quasi-reversible

$[\text{Fe}(\text{CN})_6]^{3-/4-}$ processes. Excellent agreement between theoretical and experimental data is obtained over a wide range of electrode rotation rates.

Difficulties observed in kinetics measurement are overcome by the application of high frequency AC perturbations, that is very useful in improving the accuracy of the measurement of fast kinetics. Use of the kinetically sensitive higher harmonics available from large amplitude FT AC voltammetry with a frequency of 233 Hz frequency allows the electrode kinetics associated with $\text{TTF}^{0/+}$ and $\text{TTF}^{+/2+}$ processes in acetonitrile to be estimated at Pt and GC electrodes. Via heuristic forms of data analysis, the electrode kinetics for the $\text{TTF}^{0/+}$ process is concluded to be very fast ($k_{\text{TTF}^{0/+}}^0 \geq 1.0 \text{ cm s}^{-1}$) implying that the process is either at or close to the reversible limit. In contrast $k_{\text{TTF}^{+/2+}}^0 \sim 0.35 \text{ cm s}^{-1}$ could be reliably estimated for the quasi-reversible $\text{TTF}^{+/2+}$ process. The fact that kinetic parameters for the $\text{TTF}^{+/2+}$ were found to be similar to GC and PT electrodes, suggests that this electron transfer process is adiabatic.

The electrode kinetics measurement at macrodisk electrodes is always challenging due to systematic errors. Therefore, in order to increase the sensitivity of a method for reliable quantitative determination of electrode kinetics, microelectrode method was introduced. Microdisk electrodes provide the excellent means to determine the electron transfer kinetics with negligible effect from iR_u drop. At microelectrodes, the high frequency regime of large amplitude FT AC Voltammetry can be utilized to enhance the sensitivity of the method up to 10 cm s^{-1} in conventional solvent. This method is demonstrated very well by studying TTF redox system.

In case of ionic liquids where D is of the order of $10^{-8} \text{ cm}^2 \text{ s}^{-1}$, by using microelectrodes, electron transfer kinetics can be determined up to 0.01 cm s^{-1} at 9.0 Hz. Whereas, the use of high frequencies can lead to measurement of electron transfer kinetics upto 0.1 cm s^{-1} . By

adopting these methodologies, the effect of the electrode materials is investigated on the electron transfer kinetics. Electron transfer kinetics of some outer-sphere electron transfer processes studied in this thesis show the effect of the density of states at boron doped diamond. In the detailed study considering all the factors affecting the electrode kinetics, the predominance of the adiabaticity of the electrode reactions or the effect of the density of states is discussed in detail.

9.2. Future Works

In the future, it is envisaged that applications of large amplitude FT AC Voltammetry will be extended to the use of ultra-microelectrodes in the determination of the kinetics of fast process and to further enhance the sensitivity of the method. The internal standard method described in the appendix will be further utilized to give a general internal reference concept for the kinetics determination in electrochemistry.

In this thesis electron transfer kinetics has been measured using heuristic methods of comparison between theory and experiment and kinetics values are derived based on the best fit. In the future, this heuristic approach of the data analysis will be used along with Bayesian type of statistical analysis.

Fast electron transfer reactions coupled with chemical, catalytic or enzymatic catalysis reactions will be studied to find the applications of methods employed in this thesis.

APPENDIX

INTERNAL REFERENCE CONCEPT FOR THE RELIABLE DETERMINATION OF ELECTRON TRANSFER KINETICS

Monash University

Declaration for Thesis Appendix

Declaration by candidate

In the case of Appendix, the nature and extent of my contribution to the work was the following:

Nature of contribution	Extent of contribution (%)
Initiation, key ideas, experimental work, writing up	70 %

The following co-authors contributed to the work. If co-authors are students at Monash University, the extent of their contribution in percentage terms must be stated:

Name	Nature of contribution	
Jie Zhang	Initiation, key ideas, writing up	
Alan M. Bond	Initiation, key ideas, writing up	

The undersigned hereby certify that the above declaration correctly reflects the nature and extent of the candidate's and co-authors' contributions to this work*.

Candidate's Signature  Date 28/11/2013

Name	Signatures
Jie Zhang	
Alan M. Bond	

Main Supervisor's Signature  Date 29/11/2013

*Note: Where the responsible author is not the candidate's main supervisor, the main supervisor should consult with the responsible author to agree on the respective contributions of the authors.

APPENDIX

APPLICATION OF AN INTERNAL REFERENCE CONCEPT FOR THE RELIABLE DETERMINATION OF THE KINETICS OF FAST ELECTRON TRANSFER PROCESSES USING LARGE AMPLITUDE FOURIER TRANSFORMED AC VOLTAMMETRY

Kiran Bano, Jie Zhang* and Alan M. Bond*

School of Chemistry, Monash University, Clayton, Victoria 3800, Australia

Corresponding authors:

Abstract

The concept of using an internal standard for improving the reliability for determining the electron transfer rate constant of a fast heterogeneous electron transfer process using large amplitude FT AC voltammetry has been developed. Detailed simulations are provided to demonstrate that when a reversible process is present as an internal reference, the impact of systematic errors (electrode area, concentration and uncompensated resistance) associated with the measurement of electrode kinetics for rapid quasi-reversible processes are significantly diminished. This method significantly enhances the precision for the reliable determination of electrode kinetic data that are close to the upper limit of detection. The key ideas and a practical application of this new method are demonstrated experimentally by measuring the kinetics of the quasi-reversible $\text{Cc}^{+/0}$ (Cc^+ = cobaltocenium) process using the $\text{Fc}^{0/+}$ (Fc = ferrocene) reversible process as the internal reference. By this strategy, a heterogeneous electron transfer rate constant is estimated to be 0.5 cm s^{-1} at a glassy carbon electrode based on the analysis of higher order AC harmonics available in large amplitude FT AC voltammetry from the reduction of Cc^+ in acetonitrile (0.1 M Bu_4NPF_6).

Introduction

The quest to push the upper limit of the detection in the measurements of the kinetics of heterogeneous charge transfer reactions has been a constant driving force for electrochemists. To date, techniques that have been commonly employed for electrode kinetic measurements, include polarography¹ at a dropping mercury electrode and cyclic voltammetry² at stationary macrodisk electrode where the applied potential varies linearly with time. In the case of cyclic voltammetry, the theory developed by Nicholson³ has allowed electrode kinetic information to be acquired from the difference in the reduction (E_p^{red}) and oxidation (E_p^{ox}) peak potentials as a function of scan rate. In practice, use of the method with high scan rates, allows the kinetics of fairly rapid electron transfer reactions to be. However, significant limitations arise at high scan rates due to increasingly large influence of double layer charging and iR_u or ohmic drop.^{2b} In order to minimize the double layer and iR_u effect microelectrodes and nanoelectrodes have been used under either voltammetric⁴ or scanning electrochemical microscopic conditions.⁵ These techniques offer significant advantages and allow access to higher scan rate/mass transport rate regimes but they have more strict experimental requirements. Since the construction and characterization of small interfaces and electrodes are challenging and often introduce uncertainty into the measurements.

Large amplitude FT AC voltammetry provides significant advantages⁶ over DC methods, since the background current rejected higher harmonic components are highly sensitive to k^0 . Furthermore, unlike the case with DC voltammetry,^{2a} slow kinetics and iR_u influence the characteristics of each higher harmonics in a distinctly different manner.^{6h} With this method, kinetics of fast electron transfer processes can be measured as seen using macro disc electrodes,^{6a, 6h, 7} with k^0 of up to 2 cm s^{-1} having been determined.^{6a} However, due to the systematic errors associated with concentration (C), diffusion coefficient (D), electrode area

(A) and uncompensated resistance (R_u) kinetic values still can contain significant uncertainty.^{6a}

In this paper, we introduced a new internal reference concept for the measurements of k^0 of fast processes with improved reliability. Although, internal reference methods have been widely used when reporting the reversible potential data in non-aqueous media when a conventional reference electrode is not available,^{6d,8} this approach has not been used for the quantitative determination of kinetics. Initially, the advantage of using a reversible process as an internal reference in the measurements of the kinetics of rapid quasi-reversible processes are examined. Thus, key ideas and applications of this new method are then demonstrated experimentally by measuring the electrode kinetics for the quasi-reversible $Cc^{+/0}$ process using the $Fc^{0/+}$ process as the internal reversible reference process.

Experimental

Chemicals. Cobaltocenium hexafluorophosphate (Cc) 98% (Aldrich), ferrocene (Fc) $\geq 98\%$ (Aldrich) were used as received from the manufacturer. *n*-tetrabutylammonium hexafluorophosphate (Bu_4NPF_6) 98%, (Wako) was recrystallised twice from ethanol. This supporting electrolyte and distilled acetonitrile (MeCN) 99.9%, (Sigma-Aldrich) were dried and stored under nitrogen in a dry box.

Instrumentation and procedures. In DC voltammetric studies, a CHI 400B electrochemical work station was used. Fourier transformed large amplitude AC voltammetric experiments were undertaken with home built instrumentation described elsewhere.⁹

All electrochemical experiments were carried out in a glove box under a nitrogen atmosphere at room temperature ($T = 20 \pm 2\text{ }^\circ\text{C}$). A conventional electrochemical cell with three electrode cell configuration was used for all voltammetric experiments. A macrodisk GC ($d = 1.0\text{ mm}$) was used as a working electrode. A Pt wire in a glass capillary was used as a quasi-reference

electrode and a Pt wire placed in the solvent (supporting electrolyte) as an auxiliary electrode. Working electrodes were polished with aqueous 0.3 μm alumina slurry, followed by polishing on 0.05 μm alumina slurry on a polishing cloth (BAS), sonicated in deionised water, rinsed with water and acetone and then dried under nitrogen.

Results:

Theoretical estimation of the upper limit of k^0 that can be detected: As large amplitude AC voltammetry requires estimation of kinetics parameters k^0 from the peak currents of higher harmonic AC components so simulation were initially undertaken to investigate the effect of k^0 value approaching the limit of reversibility on the characteristics of the voltammetric responses using other parameters frequency (f) = 228 Hz, amplitude (ΔE) = 80 mV, charge transfer coefficient (α) = 0.5, DC scan rate (v_{DC}) = 0.1 V s^{-1} , R_u = 510 ohm, C = 1.0 mM, D = $2.0 \times 10^{-5} \text{ cm}^2 \text{ s}^{-1}$, double layer capacitance (C_{dl}) = 20 $\mu\text{F cm}^{-2}$, Electrode Area (A) = 0.00785 cm^2 . The 6th harmonics obtained by simulation as a function of k^0 are shown in Figure 1. Resulting data reveals that processes with k^0 values up to 2.0 cm s^{-1} can be measured under these conditions since the characteristics of the sixth harmonic, particularly the current magnitude are clearly distinguishable from the reversible one. However, the peak current magnitude, a key factor in a kinetic determination by FT AC voltammetry is influenced by other parameters such as R_u , C , D and A . Therefore, the upper limit of detection of 2.0 cm s^{-1} is convenient for the processes having known values of these parameter. In the presence of any of these uncertainties, any k^0 value $> 0.5 \text{ cm s}^{-1}$ may be regarded as reversible.^{6a}

It is now proposed that if a reversible process can be introduced as an internal reference, systematic errors in R_u , C , D and A , if present, should be identical for internal standard and the process of interest and calibration becomes possible. In the context of the internal

standard, electrode kinetics do not play a role in determining the voltammetric characteristics. Consequently, the reversible limit can be defined for the quasi-reversible process of interest and electrode kinetics becomes normalized to this value, allowing contribution from systematic errors to be significantly minimized. This should be especially significant when analysis of data takes place close to the upper limit of detection of k^0 where current values are not very sensitive to the electrode kinetics.

To test the significance of this concept simulation were undertaken with a model reversible system (process $A^{0/+}$) and a quasi-reversible system ($B^{+/0}$ process) with $k_{B^{+/0}}^0 = 0.50 \text{ cm s}^{-1}$ assuming R_u and other parameters such as A , C and D , are precisely known or are accurate using simulation parameters (taken as the true values) within experimental error: $a^*(f = 228 \text{ Hz}, \Delta E = 80 \text{ mV}, v = 0.1 \text{ V s}^{-1}, (C)_A = (C)_B = 0.5 \text{ mM}, D_A = D_B = 2.0 \times 10^{-5} \text{ cm}^2 \text{ s}^{-1}, C_{dl} = 20 \text{ } \mu\text{F cm}^{-2}, A = 0.005 \text{ cm}^2, k_{B^{+/0}}^0 = 0.50 \text{ cm s}^{-1}, E_{B^{+/0}}^0 = -0.300 \text{ V and } \alpha_{B^{0/+}} = 0.50)$.

In the practical applications it is always desirable to accurately know each of the above parameters. However, during the course of experiment most probable uncertainties may arise due to error in the measurement of uncompensated resistance, change in C due to solvent losses or because of change in the electrode area due to some surface blocking phenomenon during the experiment.

Uncertainties arising due to electrode area and uncompensated resistance has similar effect on both processes in a single measurement. Concentrations of A and B can be different but their ratio stays constant within the experimental error so concentration changes due to evaporation of solvent will have similar effect on both species. Changes in the diffusion coefficient caused by any variation in temperature during the experiment will also influence the both processes in a same way as in case of C .

Three cases were considered to understand the importance of internal standard to account the effect of systematic errors in kinetics measurement by theory and experiment comparison.

Case I: All parameters are accurately known

If values of each parameter in a certain experiment are considered correct. Simulations are carried out assuming reversible kinetics for both processes ($A^{0/+}$ and $B^{+/0}$) and then electrode kinetics value for the quasi reversible process $B^{+/0}$ can be determined independently without the requirement of an internal standard

Case II: One of the parameters is uncertain

In this case simulation data obtained by a^* parameters was taken as a model system and 6th harmonic of the simulation results with a^* parameters was considered as an experimental result. At first 10% uncertainty was assumed in one of the parameters such as resistance, simulations were then performed to match the peak current magnitude of 6th harmonic of a^* data. Due to the presence of a reversible process ($A^{0/+}$) for any given R_u (with a deviation of 10% from its true value) as shown in Table 1, there is always a value for the other parameters like C , D and A with which the best agreement between the theory and experiment for the reversible $A^{0/+}$ process can be attained. Then $k_{B^{+/0}}^0$ value was calibrated with respect to $A^{0/+}$ process and $k_{B^{+/0}}^0$ value obtained from 6th harmonic were in the range of 0.4 - 0.65 cm s⁻¹, which is close enough to the true value of 0.50 cm s⁻¹.

It should be noted that one of the major advantages of FT AC voltammetry, in contrast to the DC voltammetry, is that DC and harmonic components, which provide the information of the system in different timescale, is obtained under identical experimental conditions from a single measurements.^{6d,13} Therefore, theory-experiment comparison exercise is generally undertaken using both DC and AC components from the same set of parameters. The results

in Figures 2- Figure 4 show that even though a good theory-experiment agreement for 6th harmonic can be acquired using sets of parameters deviating from the true values (Table 1), DC and other harmonics show clear differences between theory and experiment. Therefore, practically the $k_{B^{+/0}}^0$ can be determined from 6th harmonic peak current when two parameters are uncertain and should be considerably close to the true value than those given in Table 1.

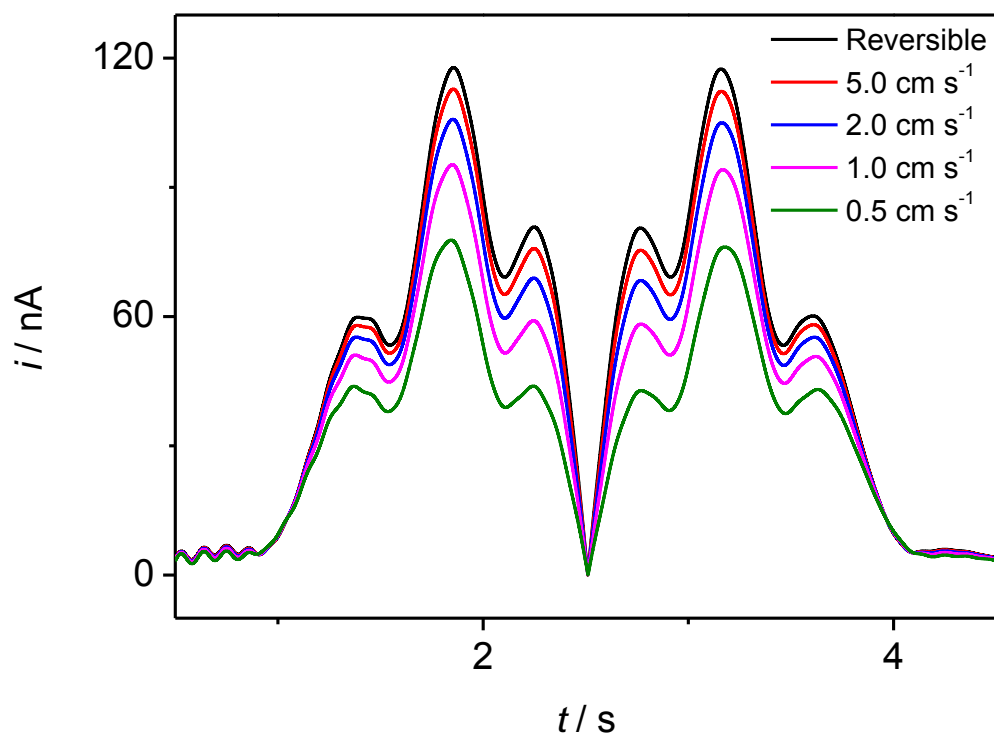


Figure 1: Simulated large amplitude FT AC voltammograms (6th harmonic) obtained for $A^{0/+}$ electrode process using parameters $R_u = 510$ ohm, $D = 2.1 \times 10^{-5} \text{ cm}^2 \text{ s}^{-1}$, $C_{dl} = 20 \text{ } \mu\text{F cm}^{-2}$, $A = 0.00785 \text{ cm}^2$, $C = 1.0 \text{ mM}$.

Table 1: $k_{B^{+}/0}^0$ obtained from theory-experiment comparison using 6th harmonic when uncertainties are associated with R_u (10% deviation from its true value) and A , C or D .

	Simulation parameters compensating R_u error	Case I ($R_u = 450$ ohm)	Case II ($R_u = 550$ ohm)
(a)	A (cm ²)	0.002	0.003
	$k_{B^{+}/0}^0$ (cm s ⁻¹)	0.55	0.55
(b)	C (mM)	0.26	0.90
	$k_{B^{+}/0}^0$ (cm s ⁻¹)	0.55	0.4
(c)	$D \times 10^5$ (cm ² s ⁻¹)	0.50	6.50
	$k_{B^{+}/0}^0$ (cm s ⁻¹)	0.28	0.70

(a*) $f = 228$ Hz, $\Delta E = 80$ mV, $v_{DC} = 0.1$ V s⁻¹, $C = 0.5$ mM, $D_A = D_B = 2.0 \times 10^{-5}$ cm² s⁻¹, $C_{dl} = 20$ μ F cm⁻², $R_u = 500$ ohm, $A = 0.005$ cm², $E_{A^{0/+}}^0 = 0.30$ V, $k_{B^{+}/0}^0 = 0.50$ cm s⁻¹, $E_{B^{+}/0}^0 = -0.30$ V and $\alpha_{B^{0/+}} = 0.50$.

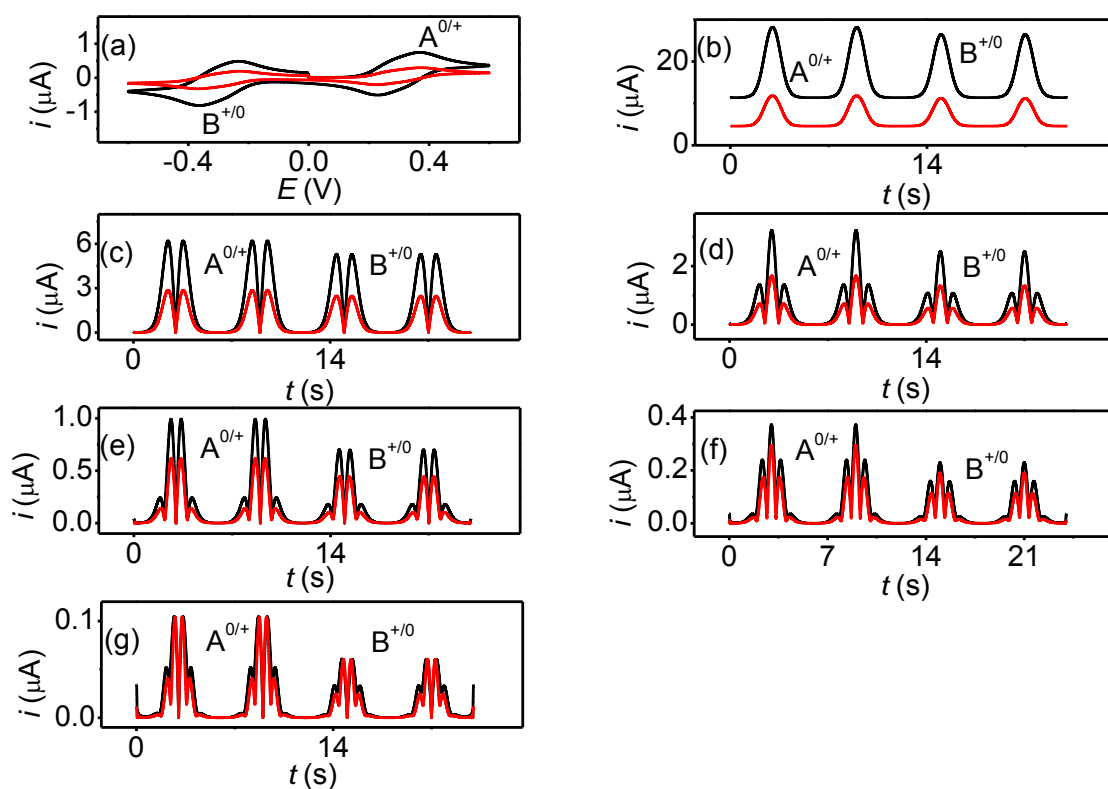


Figure 2: Comparison of simulation data for case I (—) with “a*” parameters to (—) with “a” parameters where $A = 0.002 \text{ cm}^2$ and $R_u = 450 \text{ ohm}$ (a) DC component (b-g) 2nd to 6th AC harmonics; (a* and a) are described in Table 1

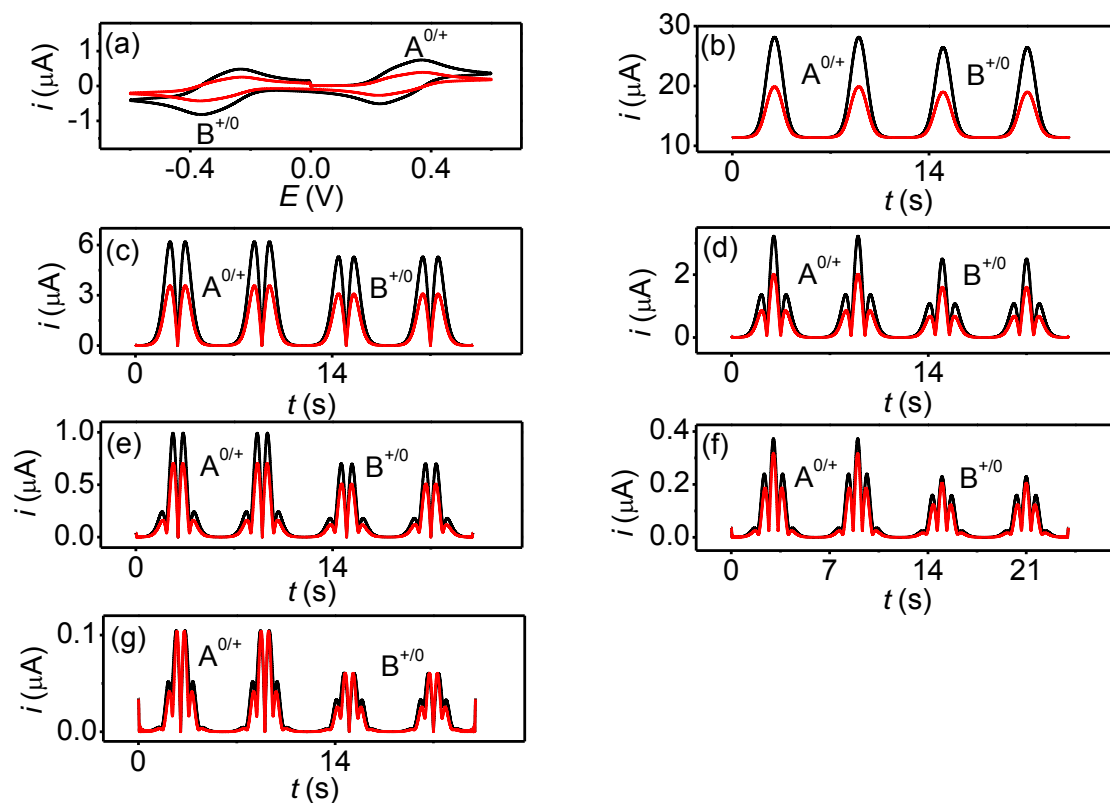


Figure 3: Comparison of simulation data for case I (—) with “a*” parameters to (—) with “b” parameters where $C = 0.26$ mM and $R_u = 450$ ohm (a) DC component (b-g) 2nd to 6th AC harmonics; (a* and b) are described in Table 1

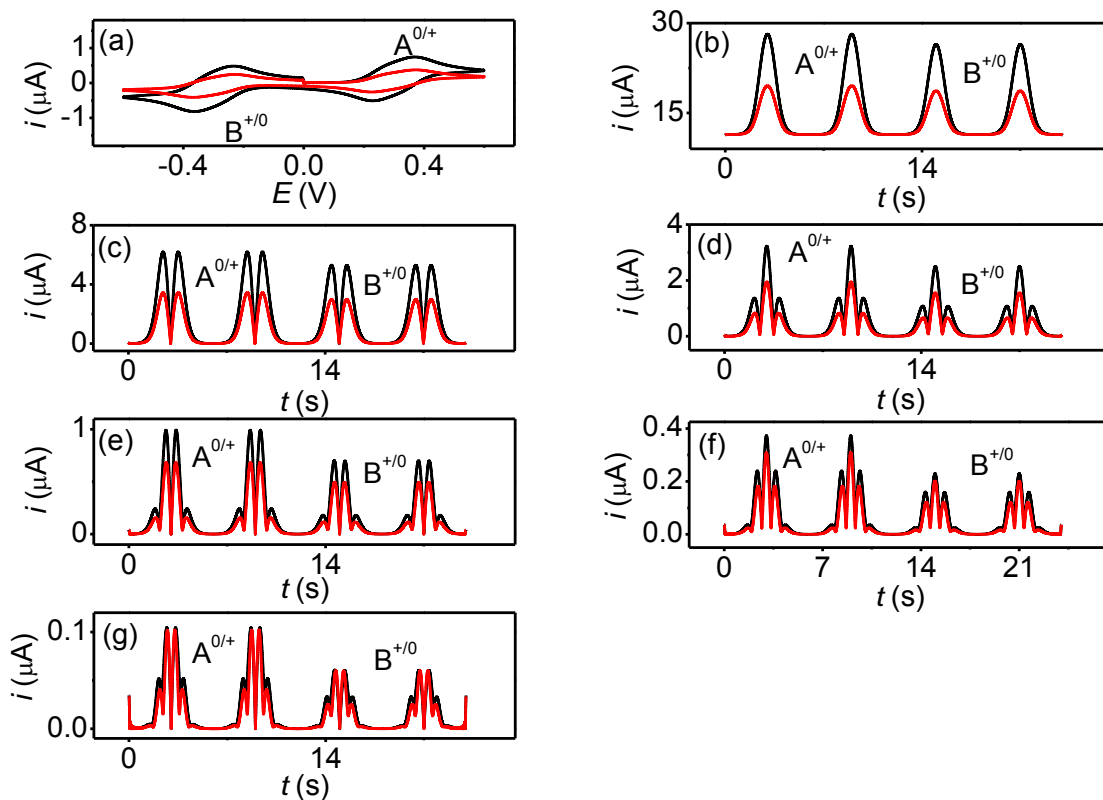


Figure 4: Comparison of simulation data for case I (—) with “a*” parameters to (—) with “b” parameters where $D = 0.5 \text{ cm}^2 \text{ s}^{-1}$ and $R_u = 450 \text{ ohm}$ (a) DC component (b-g) 2nd to 6th AC harmonics; (a* and c) are described in Table 1

Measurement of the kinetics of $Cc^{+/0}$ process using the reversible $Fc^{0/+}$ process as an internal standard. To demonstrate the application of the internal reference method, the kinetics of the quasi-reversible $Cc^{+/0}$ process was measured in the presence of the reversible $Fc^{0/+}$ process as an internal reference. DC voltammetry of 1.25 mM Fc and 1.30 mM Cc^+ was first carried out when both of them were simultaneously present in acetonitrile (0.1 M Bu_4NPF_6). Each of the Fc and Cc^+ give rise to one chemically reversible one-electron transfer process at GC electrode in the potential region investigated as shown in Figure 5. The magnitudes of the relevant peak currents were used to determine the diffusion coefficients using Randles-Sevcik equation (2).

$$I_p = 0.4463nFA \left(\frac{nFDv}{RT} \right)^{1/2} C \quad (2)$$

D_{Cc^+} was calculated to be $2.21 \times 10^{-6} \text{ cm}^2 \text{ s}^{-1}$ from the peak currents of the reduction CVs of Cc^+ as shown in Figures 5a and is close to those reported in literature.¹⁴ $D_{Fc} = 2.4 \times 10^{-5} \text{ cm}^2 \text{ s}^{-1}$ was calculated from the peak currents of the oxidation CVs of Fc at GC (Figure 5b) and is consistent with the literature values.¹⁵ Thermodynamic parameter $E_{Cc^{+/0}}^0$ for $Cc^{+/0}$ redox couple was calculated as -1.326 V vs. $Fc^{0/+}$ at GC electrode from the cyclic voltammograms shown in Figure 5, again consistent with the literature value.^{15a, 16}

Primary experiments were focusing on the evaluation of electrode kinetics of Cc^+ with reference to Fc was carried out at GC electrode using AC sine wave frequency of 228 Hz and amplitude 80 mV over the DC ramp of scan rate 154 mV s^{-1} . AC voltammetric experiments were conducted over the potential region where $Fc^{0/+}$ oxidation and $Cc^{+/0}$ reduction were simultaneously present. Under these conditions, excellent signal to noise ratios were obtained for all seven AC harmonics. Experimental data were then subjected to simulation for

extraction of the kinetic parameters using Butler-Volmer theory by the heuristic form of data analysis.

The best fit to the aperiodic DC components were obtained with $D_{Fc} = 2.4 \times 10^{-5} \text{ cm}^2 \text{ s}^{-1}$ for 1.25 mM Fc and $D_{Cc^+} = 2.2 \times 10^{-5} \text{ cm}^2 \text{ s}^{-1}$ for 1.30 mM Cc^+ in acetonitrile (0.1 M Bu_4NPF_6) under the conditions that reversibility of the two processes was certain. After the concentration and diffusion coefficients were reassured by fitting the aperiodic DC component, attention was then concentrated to the extraction of C_{dl} from 1st harmonic. Polynomial fitting of C_{dl} was obtained by varying the non-linear capacitance terms c_n until a good fit was obtained between experiment and theory. Non-linear capacitance terms were estimated as ($c_0 = 24.5$, $c_1 = c_2 = 0.0$, $c_3 = 0.5$ and $c_4 = 1.30$) $\mu\text{F cm}^{-2}$ by fitting of the non-Faradaic component of 1st harmonic. Originally measured $R_u = 490 \text{ ohm}$ was used in the simulation along with $E_{Cc^{+/0}}^0 = -1.326 \text{ V vs Fc}^{0/+}$. Initially, $k_{Fc^{0/+}}^0$ and $k_{Cc^{+/0}}^0$ were assumed fully reversible, however, higher harmonic peak current magnitude for $Cc^{+/0}$ process was lower than the $Fc^{0/+}$ process. This suggested that $k_{Cc^{+/0}}^0$ was significantly lower as compared to $k_{Fc^{0/+}}^0$. Values of $k_{Fc^{0/+}}^0$ and $k_{Cc^{+/0}}^0$ were then refined to match the peak current magnitudes of 6th and 7th harmonics of experimental FT AC voltammogram. Comparison of the experiment and theory is given in Figure 6 where DC component is shown in the potential domain while all AC harmonics are shown in time domain. An excellent agreement between theory and experiment was obtained with $k_{Cc^{+/0}}^0 = 0.50 \text{ cm s}^{-1}$ and α was considered 0.50 for both redox processes.

Experimental FT AC cyclic voltammetric results were also obtained from the concentration solution containing 0.105 mM Fc and 0.106 mM Cc^+ . The data was then subjected to simulation to see the effect of varying the iR_u drop from higher to lower on the electrode

kinetic measurement of $Cc^{+/0}$. Non-Faradaic capacitance was modelled in capacitive terms $c_0 = 20.00 \text{ } \mu\text{F cm}^{-2}$, $c_4 = 1.50 \text{ } \mu\text{F cm}^{-2}$, $c_6 = 1.5 \text{ } \mu\text{F cm}^{-2}$ from fundamental harmonic. Simulations were then refined to match all the DC and AC harmonics of experimental data with simulation parameters $R_u = 500 \text{ ohm}$ and $\alpha = 0.50$. Kinetic parameter was extracted to be $k_{Cc^{+/0}}^0 = 0.5 \text{ cm s}^{-1}$ by simulations to match the peak current magnitudes of higher harmonics by making the theory and experiment comparison (Figure 7); the rest of the simulation and experimental parameters are described in Figure 7.

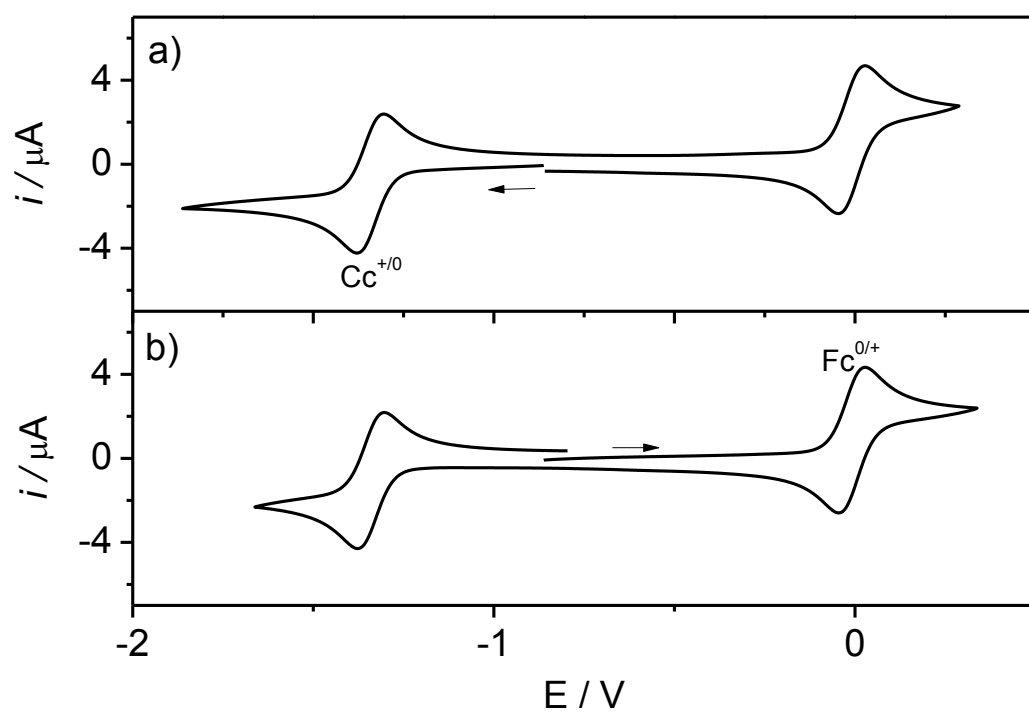


Figure 5. DC Voltammograms obtained at a GC macro-disk electrode ($d = 1.0$ mm) starting from (a) reduction of 1.3 mM Cc^{+} and (b) oxidation of 1.25 mM Fc in acetonitrile (0.1 M Bu_4NPF_6), $v_{\text{DC}} = 100 \text{ mV s}^{-1}$

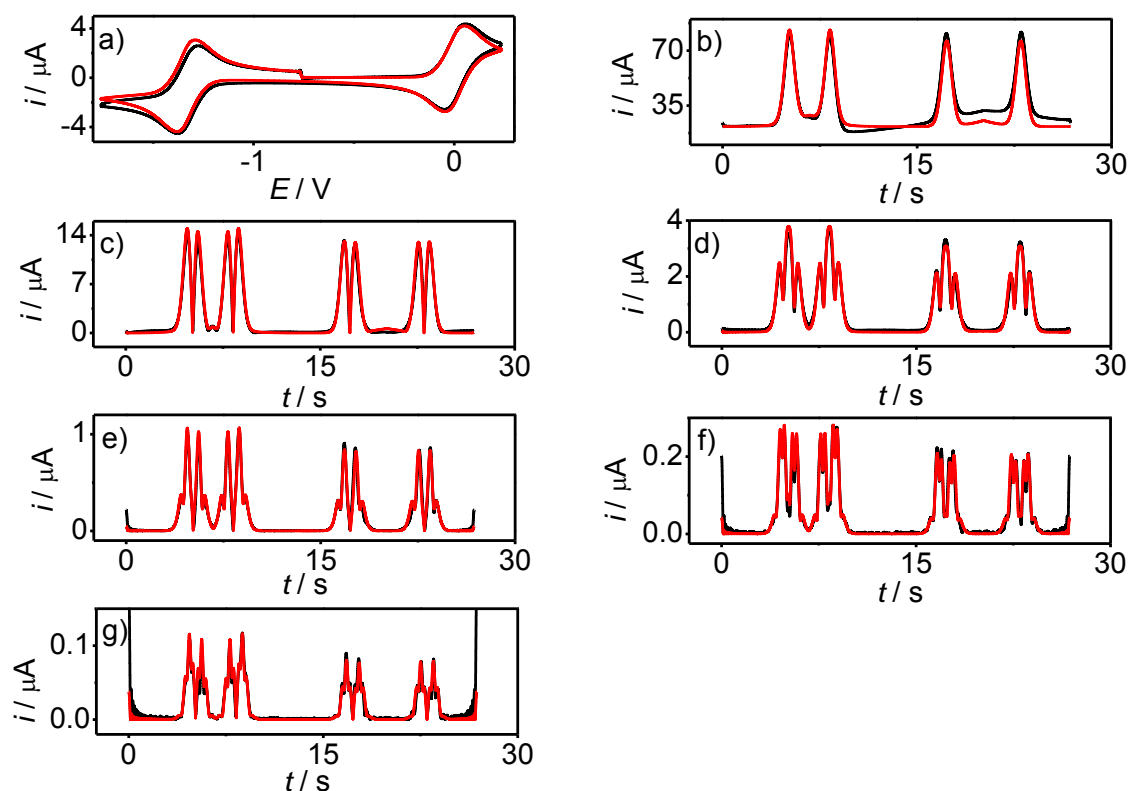


Figure 6. Comparison of simulated (—) and experimental (—) FT large amplitude AC voltammograms obtained from 1.25 mM Fc and 1.30 mM Cc^+ in acetonitrile (0.1 M Bu_4NPF_6) at GC electrode (a) aperiodic DC component (b-h) 1st - 7th harmonics; $v_{DC} = 0.149 \text{ V s}^{-1}$, $A = 0.00785 \text{ cm}^2$, $f = 228 \text{ Hz}$, $\Delta E = 80 \text{ mV}$, $D_{Fc} = 2.4 \times 10^{-5} \text{ cm}^2 \text{ s}^{-1}$, $D_{Cc^+} = 2.2 \times 10^{-5} \text{ cm}^2 \text{ s}^{-1}$, $R_u = 490 \text{ ohm}$, $k_{Cc^+}^0 = 0.5 \text{ cm s}^{-1}$, $C_{dl}(c_0 = 24.5, c_3 = 0.5, c_2 = 0.0 \text{ and } c_4 = 1.30 \text{ } \mu\text{F cm}^{-2})$ and $T = 293\text{K}$.

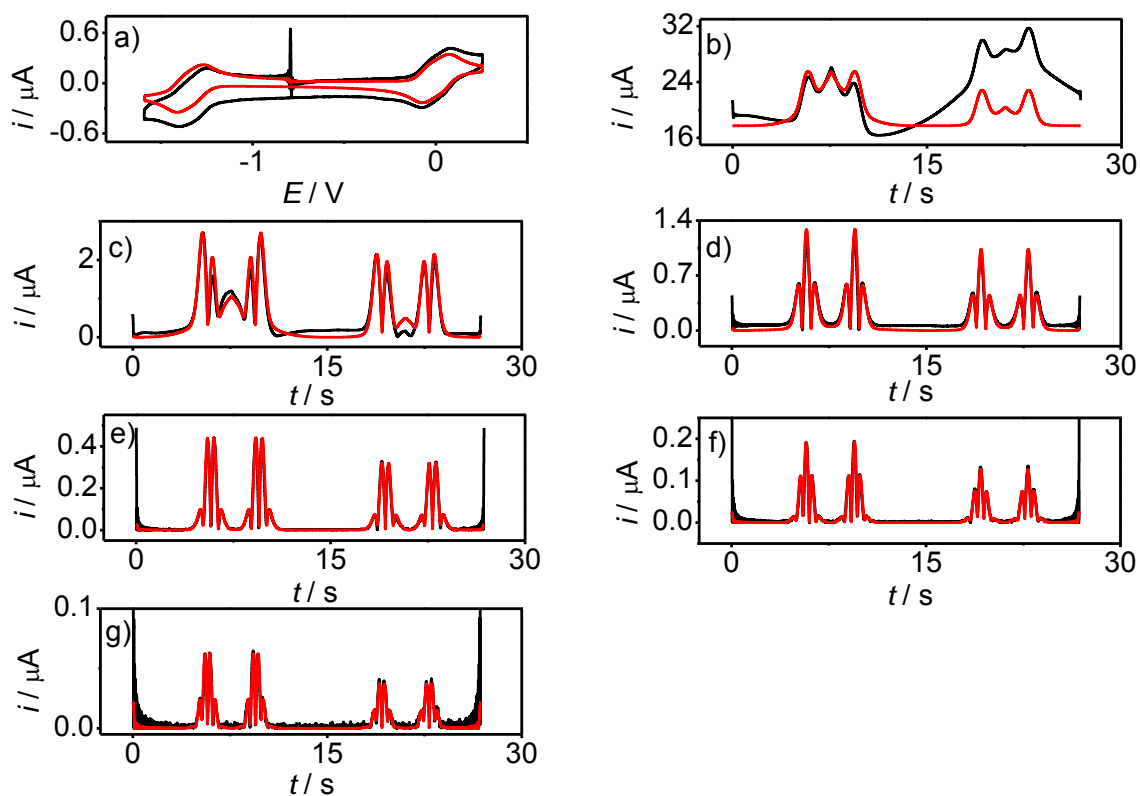


Figure 7. Comparison of simulated (—) and experimental (—) FT large amplitude AC voltammograms obtained from 0.105 mM Fc and 0.1068 mM Cc^+ in acetonitrile (0.1 M Bu_4NPF_6) at GC electrode (a) aperiodic DC component (b-g) 1st - 6th harmonics; $v_{DC} = 0.152$ $V s^{-1}$, $A = 0.00785$ cm^2 , $f = 228$ Hz, $\Delta E = 80$ mV, $D_{Fc} = 2.40 \times 10^{-5} cm^2 s^{-1}$, $D_{Cc^+} = 2.20 \times 10^{-5} cm^2 s^{-1}$, $R_u = 500$ ohm, $k_{Cc^+}^0 = 0.5$ $cm s^{-1}$, C_{dl} ($c_0 = 20.0$ $\mu F cm^{-2}$, $c_4 = 1.50$ $\mu F cm^{-2}$, $c_6 = 1.5$ $\mu F cm^{-2}$) and $T = 293K$.

Discussion:

In FT AC voltammetric method described above, peak current magnitudes were used to measure the electrode kinetic parameter and usual heuristic method for the computation of k^0 was applied in experiment versus theory comparison of voltammetric data. The peak current magnitudes of AC harmonics are affected by errors in various parameters and can lead to uncertainties in kinetic measurement. As established in the theoretical section, major contributing errors from R_u , C , D and A have least effect on the measurement of kinetics in the presence of a reversible redox couple. In this case, $\text{Fc}^{0/+}$ was selected as an internal standard for the kinetic measurement as per criteria¹⁷ described for the measurement of E^0 . Its redox potential is at a sufficient distance from the $\text{Cc}^{+/0}$ process, has no reaction or cross reaction with Cc^+ redox couple and most importantly it undergoes a reversible electron transfer reaction. $k_{\text{Cc}^{+/0}}^0$ for the $\text{Cc}^{+/0}$ process was estimated as 0.50 cm s^{-1} which can be considered as more accurate and precise as compared to the situation involving individual kinetic measurement.¹⁸ Inherently slower kinetics observed for $\text{Cc}^{+/0}$ process as compared to Fc can be explained in terms of Marcus theory; where reorganization energies play a vital role in qualitative prediction of electrode kinetics. Probably, higher reorganization energies for cobaltocenium¹⁸⁻¹⁹ as compared to those for Fc lead to the slower kinetics for $\text{Cc}^{+/0}$ process. Another possible explanation is provided in terms of strong ion-pairing between Cc^+ and PF_6^- anion and resulting double layer effect.¹⁹ While Fc being the neutral molecule is less probable to have ion pairing so reversible behaviour was observed for its oxidation. The observed $k_{\text{Cc}^{+/0}}^0$ values for $\text{Cc}^{+/0}$ process in this study by internal reference method are more reliable and authenticates $\text{Fc}^{0/+}$ is an ideal internal reference for electrode kinetics measurement. Uncertainties associated with the electrode kinetics are well accounted by this method, compared to the situation, that exists in other methods for the fast ET kinetic measurement.

Conclusion:

This paper ascertains a general method which allows $\text{Fc}^{0/+}$ redox process to be used as an internal reversible standard to determine the electrode kinetics of $\text{Cc}^{+/0}$ redox process using large amplitude FT AC voltammetry. The method reduces systematic errors that result from the electrochemical measurement conditions including C , D , A and R_u . Therefore, this should be particularly useful for reliable quantitative determination of electrode kinetics by any voltammetric method as now they have been tested for the precise measurement by AC method.

Acknowledgement: Authors greatly acknowledge the financial support from Australian Research Council. KB acknowledges the awards of Monash University Science Faculty Dean's Postgraduate Research Scholarship.

References

1. (a) Bond, A. M. *Modern Polarographic Methods in Analytical Chemistry*. Marcel Dekker: New York, **1980**; (b) Delahay, P. *New Instrumental Methods in Electrochemistry*. Wiley-Interscience: New York, **1954**.
2. (a) Nicholson, R.S. *Anal. Chem.* **1965**, 37, 1351; (b) Bard, A. J.; Faulkner, L. R. *Electrochemical methods: Fundamentals and Applications*. John Wiley: New York, **2001**.
3. Nicholson, R. S.; Shain, I. *Anal. Chem.* **1964**, 36, 706.
4. (a) Wightman, R. M.; Wipf, D. O. in *Electroanalytical Chemistry*, ed. A. J. Bard. Marcel Dekker: New York, **1989**, vol. 15, p 267; (b) Girault, H. H. in *Modern Aspects of Electrochemistry*, ed. Bockris, J. O.; Conway, B. E.; White, R. E. Plenum Press: New York, **1993**, vol. 25; (c) Wang, Y.; Velmurugan, J.; Mirkin, M. V. *Isr. J. Chem.* **2010**, 50, 291.

5. (a) Amemiya, S.; Bard, A. J.; Fan, F. R. F.; Mirkin, M. V.; Unwin, P. R. *Ann. Rev. Anal. Chem.* **2008**, *1*, 95; (b) Mirkin, M. V.; Richards, T. C.; Bard, A. J. *J. Phys. Chem.* **1993**, *97*, 7672; (c) Patten, H. V.; Lai, S. C. S.; Macpherson, J. V.; Unwin, P. R. *Anal. Chem.* **2012**, *84*, 5427; (d) Shen, M.; Arroyo-Curras, N.; Bard, A. J. *Anal. Chem.* **2011**, *83*, 9082.

6. (a) Bano, K.; Nafady, A.; Zhang, J.; Bond, A. M.; Haque, I. U. *J. Phys. Chem. C* **2011**, *115*, 241533 (b) Fleming, B. D.; Barlow, N. L.; Zhang, J.; Bond, A. M.; Armstrong, F. A. *Anal. Chem.* **2006**, *78*, 2948; (c) O'Mullane, A. P.; Zhang, J.; Brajter-Toth, A.; Bond, A. M. *Anal. Chem.* **2008**, *80*, 4614; (d) Sher, A. A.; Bond, A. M.; Gavaghan, D. J.; Harriman, K.; Feldberg, S. W.; Duffy, N. W.; Guo, S. X.; Zhang, J. *Anal. Chem.* **2004**, *76*, 6214; (e) Shiddiky, M. J. A.; O'Mullane, A. P.; Zhang, J.; Burke, L. D.; Bond, A. M. *Langmuir* **2011**, *27*, 10302; (f) Shiddiky, M. J. A.; Torriero, A. A. J.; Reyna-Gonzalez, J. M.; Bond, A. M. *Anal. Chem.* **2010**, *82*, 1680; (g) Zhang, J.; Bond, A. M. *J. Electroanal. Chem.* **2007**, *600*, 23; (h) Zhang, J.; Guo, S. X.; Bond, A. M. *Anal. Chem.* **2007**, *79*, 2276; (i) Zhang, J.; Guo, S. X. Bond, A. M.; Marken, F. *Anal. Chem.* **2004**, *76*, 3619.

7. (a) Bano, K.; Kennedy, G. F.; Zhang, J.; Bond, A. M. *Phys. Chem. Chem. Phys.* **2012**, *14*, 4742; (b) Bond, A. M.; Bano, K.; Adeel, S.; Martin, L. L.; Zhang, J. *ChemElectrochem.* **2013**, DOI: 10.1002/celc.201300129.

8. (a) Gritzner, G.; Kuta, J. *Pure & Appl. Chem.*, **1984**, *56*, 461; (b) Torriero, A. A. J.; Sunarso, J.; Forsyth, M.; Pozo-Gonzalo, C. *Phys. Chem. Chem. Phys.* **2013**, *15*, 2547.

9. Bond, A. M.; Duffy, N. W.; Elton, D. M.; Fleming, B. D. *Anal. Chem.* **2009**, *81*, 8801.

10. Feldberg, S. W. *J. Electroanal. Chem.* **1981**, *127*, 1.

11. Rudolph, M.; Reddy, D. P.; Feldberg, S. W. *Anal. Chem.* **1994**, *66*, 589A.

12. (a) Feldberg, S. W. *J. electroanal. Chem.* **1981**, *127*, 1; (b) Feldberg, S. W.; Goldstein, C. I.; Rudolph, M. *J. Electroanal. Chem.* **1996**, *413*, 25.
13. Sher, A. A.; Bond, A. M.; Gavaghan, D. J.; Gillow, K.; Duffy, N. W.; Guo, S. X.; Zhang, J. *Electroanal.* **2005**, *17*, 1450.
14. Mirkin, M. V.; Richards, T. C.; Bard, A. J. *J. Phy. Chem.* **1993**, *97*, 7672.
15. (a) Bond, A. M.; Oldham, K. B.; Snook, G. A. *Anal. Chem.* **2000**, *72*, 3492; (b) Wang, Y.; Rogers, E. I.; Compton, R. G. *J. Electroanal. Chem.* **2010**, *648*, 15.
16. Stojanovic, R. S.; Bond, A. M. *Anal. Chem.* **1993**, *65*, 56.
17. Torriero, A. J.; Feldberg, S.; Zhang, J.; Simonov, A.; Bond, A. M. *J. Solid State Electrochem.*, DOI: 10.1007/s10008-013-2183-3
18. Tsierkezos, N. G. *J. Mol. Liq.* **2008**, *138*, 1.
19. Fawcett, W. R.; Opallo, M. *J. Phys. Chem. A* **1992**, *96*, 2920.

